UNIVERSITY OF SOUTHAMPTON

FACULTY OF ENGINEERING, SCIENCE AND MATHEMATICS

School of Ocean and Earth Science

Failure processes in submarine landslides: A geomorphological approach.

by

Aaron Micallef

Thesis for the degree of Doctor of Philosophy

July 2007

Graduate School of the
National Oceanography Centre, Southampton

This PhD dissertation by

Aaron Micallef

has been produced under the supervision of the following persons

Supervisor/s

Prof. Douglas G. Masson
Dr. Christian Berndt
Prof. Dorrik A.V. Stow

Chair of Advisory Panel

Prof. Carl L. Amos _____

Member/s of Advisory Panel

Dr. Christian Berndt _____

Prof. Douglas G. Masson _____

Prof. Dorrik A.V. Stow _____

UNIVERSITY OF SOUTHAMPTON

ABSTRACT

FACULTY OF ENGINEERING, SCIENCE & MATHEMATICS
SCHOOL OF OCEAN & EARTH SCIENCE

Doctor of Philosophy

FAILURE PROCESSES IN SUBMARINE LANDSLIDES: A GEOMORPHOLOGICAL APPROACH.

by Aaron Micallef

This thesis presents a novel technique for the quantitative characterisation of bathymetric data sets. The technique integrates three main geomorphometric methods: morphometric attributes and their statistical analyses, feature-based quantitative representation, and automated topographic classification. These methods allow useful morphological information to be extracted from bathymetric data and can significantly enhance submarine geomorphological investigations. The methods are applied to bathymetric data from the Storegga Slide, one of the largest known submarine landslides, to investigate three aspects of submarine mass movements: spreading, fractal statistics and morphology and slide development.

The morphological signature of spreading, in the form of a repetitive pattern of ridges and troughs, covers at least 25% of the Storegga Slide scar. Two modes of failure can be identified for submarine spreading. The first involves retrogressive slide development via the unloading of the headwall. The second entails the extension of a thin coherent slab of semi-consolidated material downslope by gravity. Both modes of failure involve the break up of surface sediment units into coherent blocks and their displacement along planar slip surfaces. The block movement pattern entails an exponential increase of displacement, and thinning of the failing sediment, with distance downslope. Loss of support and seismic loading are the main potential triggering mechanisms of submarine spreading.

Analysis of headwall morphologies within the Storegga Slide reveals the occurrence of spatial scale invariance. One explanation for this scale invariance is that the Storegga Slide is a geomorphological system that may exhibit self-organised criticality. Spatial scale invariance may also be linked to the retrogressive nature of the Storegga Slide. The shape and fractal dimension of headwalls, on the other hand, can be used as a proxy for the type and number of the formative mass movements.

A detailed reconstruction of the development of the north-eastern Storegga Slide shows that after the initial evacuation of the surface sediment as turbidity currents, the area failed as an extensive spread. The spreading blocks subsequently underwent higher displacement and remoulding, and were partly removed by debris flows and turbidity currents. The renewed instability within the spreading areas may have been related to gas hydrate dissociation and pore pressure increases due in response to the changing overburden, and the distribution of contourite drift deposits within underlying palaeoslide scars.

Dedicated to:

Lucienne and my family

Contents

List of tables

List of figures

DECLARATION OF AUTHORSHIP

I, ... AARON MICALLEF ....., [please print name]

declare that the thesis entitled [enter title]

FAILURE PROCESSES IN SUBMARINE LANDSLIDES: A GEOMORPHOLOGICAL APPROACH.

and the work presented in the thesis are both my own, and have been generated by me as the result of my own original research. I confirm that:

- this work was done wholly or mainly while in candidature for a research degree at this University;
- where any part of this thesis has previously been submitted for a degree or any other qualification at this University or any other institution, this has been clearly stated;
- where I have consulted the published work of others, this is always clearly attributed;
- where I have quoted from the work of others, the source is always given. With the exception of such quotations, this thesis is entirely my own work;
- I have acknowledged all main sources of help;
- where the thesis is based on work done by myself jointly with others, I have made clear exactly what was done by others and what I have contributed myself;
- none of this work has been published before submission, **or** [delete as appropriate] parts of this work have been published as: [please list references]

Micallef, A., C. Berndt, D.G. Masson, and D.A.V. Stow (2007a), A technique for the morphological characterization of submarine landscapes as exemplified by debris flows of the Storegga Slide, *Journal of Geophysical Research*, *112*, F02001.

Micallef, A., D.G. Masson, C. Berndt, and D.A.V. Stow (i2007b), Morphology and mechanics of submarine spreading: A case study from the Storegga Slide, *Journal of Geophysical Research*, *112*, F03023.

A. Micallef

31st July 2007

Acknowledgements

My greatest debt is to Prof. Douglas G. Masson, Dr. Christian Berndt and Prof. Dorrik A. Stow, who were my supervisors for this PhD project. There are many things I have to thank them for: the fact that they believed in me since the first time we met; the freedom they granted me throughout my PhD, in particular with regard to the research routes I wanted to pursue; their constant support towards attending conferences, courses and cruises; their constructive criticism and insightful comments; their flexibility to fulfil all my requests; their availability even when they were very busy; their patience and their enthusiasm; the list is endless! I feel that I have progressed a lot as a scientist thanks to their help, and I feel extremely lucky to have had them as my supervisors.

I would like to acknowledge a debt of gratitude to Lucienne, my family, and my friends in Southampton, Malta and abroad, for their tremendous support and patience during the past three years.

I express my grateful thanks to the members of Geology and Geophysics Research group for their support and technical assistance, in particular to Dr. Tim Le Bas, Ms. Rebecca Bell, Prof. Jonathan Bull, Dr. Aurelien Gay, Dr. Aggeliki Georgiopoulou, Ms. Sally Hunter, Mr. Veit Hühnerbach, Dr. Veerle Huvenne and Ms. Magda Szuman. Special thanks to my office mates Ms. Raquel Arzola, Mr. Cedric Boulart and Ms. Kirsty Edgar, and my housemate Mr. Xi Pan for putting up with me for such a long time!

I would like to thank a number of institutions for contributing their data to this project: Norsk Hydro A.S.A. for the multibeam bathymetry and 2D seismic data sets, B.P. Norway for the 3D seismic data and European North Atlantic Margin (ENAM) II Programme for the sidescan sonar imagery. I am grateful to Dr. Robin S. Snow and Dr. Stefan Bünz for sharing the FORTRAN code for the divider method (Chapter 7) and the BSR depth data (Chapter 8), respectively.

The National Oceanography Centre, University of Southampton and HERMES project (EC contract no. GOCE-CT-2005-511234, funded by the European Commission's Sixth Framework Programme under the priority 'Sustainable Development, Global Change and Ecosystems') are acknowledged for my research studentship and for funding this project.

Chapter 1:

INTRODUCTION

1.1 INTRODUCTION TO THESIS

1.1.1 THE GEOMORPHOLOGICAL APPROACH

The Earth's surface is not chaotic; it consists of a range of individual landforms of different shapes and sizes, which are structured by interacting processes operating on a variety of spatio-temporal scales [*DeBoer*, 1992]. Geomorphology is a field of research of the geosciences where the shape of the Earth is used to interpret the nature of the geological processes that contributed to its formation [*Hutchinson and Gallant*, 2000; *Jamieson et al.*, 2004]. The core of the geomorphological approach is therefore the understanding of the interaction between form and process. The importance of the study of landforms is related to two important properties: landforms are the outcome of past geomorphic and geological processes, and they are a boundary condition for current/future geomorphic processes [*Dehn et al.*, 2001].

The foundations of geomorphology were laid in Europe in the first half of the nineteenth century (e.g. work by Hutton, Lyell), although the conceptual structure of modern geomorphology owes its origin to work by American geologists in the second half of the 19th century (e.g. Davis, Gilbert, Penck) [*Summerfield*, 1991]. Traditional geomorphology started as a fieldwork-based discipline. It involved describing landforms and placing them into the framework of an evolutionary model. The modern development of geomorphology, particularly in the last 60 years, has entailed a growing emphasis on the quantitative analysis of the land surface, investigation of material properties, measurement of geomorphic processes and predictive modelling [e.g. *Beven and Kirkby*, 1979; *Horton*, 1945; *Richards*, 1982]. The character of geomorphological research has become more applied and numerical.

The quantitative characterisation of terrain, known as geomorphometry, has become a field of research in its own right. In geomorphometry, mathematical and statistical processing techniques are employed to quantify aspects of the land surface and improve the mapping, modelling and understanding of the formative geological processes. The application of geomorphometry has assisted and improved the geomorphological analyses of a wide range of environmental settings: e.g. soil studies [*Irvin et al.*, 1997;

Oliver, 1987], fault morphology [*Florinsky*, 1996; *Gelabert et al.*, 2005]; mountain geomorphology [*Chase*, 1992; *Ouchi and Matsushita*, 1992]; fluvial systems [*Chang et al.*, 1998; *Gardner et al.*, 1990]; hillslopes [*Giles and Franklin*, 1998]. In comparison to the traditional approach, geomorphometric techniques enable the comparison between landscapes, facilitate the extraction of quantitative morphological information, and avoid problems of subjectivity.

1.1.2 SUBMARINE LANDSLIDES

In the 1960s, the growing interest of the oil industry in the ocean basins triggered an active programme of drilling and surveying of the ocean floor. Since then, a remarkable effort has been made by both industrial and academic institutions to generate a wealth of information about submarine landscapes, and to better understand the geologic processes that shaped them. The more geologists have learnt about the ocean floor, the clearer it became that submarine landslides are ubiquitous features of submarine slopes [*Canals et al.*, 2004; *Hühnerbach and Masson*, 2004; *Masson et al.*, 2006; *Prior and Coleman*, 1979]. During the last decade, the effort made to characterise submarine landslides along the European margins has significantly increased our understanding of these geological phenomena [*Locat and Mienert*, 2003; *Mienert and Weaver*, 2002 + references therein]. Submarine landslides have been shown to be comon on both active and passive margins, and to occur in a wide range of geological settings and depths [*Hampton et al.*, 1996; *Mienert et al.*, 2002]. From a geological point of view, submarine landslides are important processes because they are the most effective agents through which sediments are transferred across the continental slope to the abyssal plains [*De Blasio et al.*, 2004; *Masson et al.*, 2006; *Prior et al.*, 1982]. Sediment and rock transport in submarine landslides is mainly gravity-driven and occurs on very low slopes [*Mulder and Cochonat*, 1996]. A range of submarine mass movement processes have been recognised, although slides, debris flows and turbidity currents are the most widespread [*Masson et al.*, 2006; *Weaver et al.*, 2000]. Submarine landslides can be complex events, which vary largely in size and features, depending on the amount of the disintegration that the mobilised sediment or rock undergoes. They can be up to three orders of magnitude bigger than the largest known subaerial landslide [*Guthrie and Evans*, 2007; *Haflidason et al.*, 2004]. Slide deposits can measure hundreds of metres

in thickness, and displacement of sediment can be in the range of hundreds of kilometres [*Canals et al.*, 2004; *Lykousis et al.*, 2002; *Masson et al.*, 1998]. The triggers of submarine landslides are both intrinsic (e.g. loading and underconsolidation of slope sediments, and the associated development of excess pore pressure; presence of 'weak layers' due to the alternating deposition of sediments with different geotechnical characteristics) and extrinsic (e.g. earthquakes; eustatic changes in sea-level; storms; volcanic activity; gas hydrate phase changes) [*Locat and Lee*, 2002; *Masson et al.*, 2006].

1.1.3 THE STOREGGA SLIDE

A number of submarine landslides are known to occur along the Norwegian continental margin [*Evans et al.*, 2005; *Owen et al.*, 2007]. The largest of these is the Storegga Slide, located 120 km offshore Norway. The Storegga Slide is perhaps the best studied submarine landslide in the world. Most of the interest in this region, both industrial and academic, has been linked to the Ormen Lange gas field, Norway's second-largest gas reservoir. Discovered in 1997, Ormen Lange is located within the scar created by the Storegga Slide, some 3000 m below sea-level [*Solheim et al.*, 2005b]. Since the first survey was carried out, state-of-the-art acoustic data acquisition systems and geotechnical techniques have been employed to survey the slide scar seafloor and assess the risk associated with the gas field development and subsequent hydrocarbon extraction. Today the database includes multibeam sonar images, 2D and 3D seismic data, sidescan sonar imagery, sub-bottom profiles, remotely operated vehicle images, piston cores, gravity cores and geotechnical/geological drillings. The analyses of these data have resulted in numerous academic publications and industrial reports that have addressed various aspects of the Storegga Slide: stratigraphical and geological development [*Berg et al.*, 2005; *Forsberg and Locat*, 2005; *Hjelstuen et al.*, 2005; *Nygård et al.*, 2005; *Rise et al.*, 2005], slide triggers [*Atakan and Ojeda*, 2005; *Bouriak et al.*, 2000; *Bouriak et al.*, 2003; *Bungum et al.*, 2005; *Lindholm et al.*, 2005; *Mienert et al.*, 2005; *Strout and Tjelta*, 2005], chronology [*Haflidason et al.*, 2005], palaeoslides [*Solheim et al.*, 2005a], slide dynamics [*Bryn et al.*, 2005a; *Bünz et al.*, 2005; *De Blasio et al.*, 2005; *Gauer et al.*, 2005; *Haflidason et al.*, 2004; *Kvalstad et al.*, 2005a] and specific geological features [*Bryn et al.*, 2005b; *Riis et al.*, 2005].

1.2 OBJECTIVE OF THE THESIS

The general objective of this thesis is to achieve a deeper understanding of submarine mass movements by applying a quantitative geomorphological approach to the study of the Storegga Slide.

1.3 OVERVIEW OF THE THESIS

The study is organised as follows:

In **Chapter 2**, the research context of the thesis is outlined and the specific research questions that will be addressed in the thesis are identified. **Chapter 3** is a general overview of the geological setting of the Storegga Slide and a summary of the most recent published information about the slide morphology and development.

The study is based on three high-resolution acoustic data sets from the Storegga Slide: multibeam bathymetry, sidescan sonar imagery and 2D/3D seismic data. **Chapter 4** presents information about the acquisition, quality and coverage of these data sets.

Chapters 5 to 8 comprise the method, results and discussion sections of the thesis. These sections are presented as four research articles that have been either published by, or submitted to, international peer-reviewed journals.

Chapter 5 is the method section. In this chapter, a geomorphometric technique for the investigation of bathymetric data is proposed. The technique, consisting of an adaptation and integration of three analytical methods used in subaerial geomorphology, is shown to enable the extraction of useful morphological information from the bathymetric data set and to improve the interpretation of debris flow lobes within the Storegga Slide.

In **Chapters 6 to 8** I employ the method described in **Chapter 5** to investigate three aspects of submarine mass movements within the Storegga Slide: spreading, fractal statistics and morphology, and slide development.

Chapter 6 is the first part of the results section. Ridge characterisation and geomorphometric mapping are applied to the entire Storegga Slide bathymetric data set to demonstrate that spreading is a widespread type of mass movement, and to characterise its morphological signature. These results are combined with the sidescan sonar imagery and seismic data to understand the mode of failure. Limit-equilibrium and mechanical modelling are used to identify the potential triggers of spreading and to explain the physical boundary conditions that control the development of a spread and the associated style of sediment displacement.

Chapter 7 is the second part of the results section. In this chapter, the geomorphometric technique is employed to automatically extract quantitative information about the shape and dimensions of one hundred and fifteen mass movements, and their associated headwalls. This information is used to demonstrate that the Storegga Slide exhibits scale invariance in terms of the statistics and morphology of its constituent mass movements. An attempt is then made to identify the origin of this scale invariance in terms of system dynamics and geological processes, and to understand its implications.

Chapter 8 is the discussion section. A geomorphometric analysis of the seafloor is carried out in the north-eastern part of the Storegga Slide scar. Submarine mass movements are mapped in detail, and the geological factors and processes responsible for these mass movements are identified. These results are then used to derive a development model of the north-eastern Storegga Slide that improves the interpretation of *Haflidason et al.* [2004] based on visual interpretation.

A synthesis of the main conclusions of this study, and a discussion of the broader implications, are provided in **Chapter 9**.

The study demonstrates how the application of the geomorphological approach to the study of the Storegga Slide significantly improves our understanding of submarine mass movements.

1.4 RATIONALE

1.4.1 WHY ADOPT A QUANTITATIVE GEOMORPHOLOGICAL APPROACH?

(a) As explained in chapter 2, the application of geomorphometry has generally been very successful in the study of subaerial landscapes. Attempts have also been made to employ these techniques in the investigation of the submarine environment. However, the quality and spatial coverage of submarine elevation data has generally been low. Acoustic data sets of adequate resolution for a meaningful geomorphometric analysis have only become available recently. This fact, combined with the difficulty in transferring some subaerial geomorphometric techniques directly to the submarine environment, has prompted marine geologists to favour the qualitative interpretation of their bathymetric data sets. In comparison to subaerial landscapes, the application of geomorphometric techniques in the study of submarine environments has been less common and the methods are less sophisticated.

(b) I believe that high-resolution bathymetric data sets, such as the one available for the Storegga Slide, contain a wealth of information that is not currently being exploited by the marine geologist. The information can be extracted using geomorphometric techniques, which, in comparison to qualitative interpretation, are rapid and accurate, and avoid problems of subjectivity. The techniques are effective in capturing the morphology of the landscape and representing it mathematically. All of this allows a thorough investigation of the landscape to be carried out. Today, the increasing availability of high-resolution acoustic data sets and the rapid development of computing power make the application of geomorphometric techniques in the submarine environment feasible. The development of geomorphometric techniques for submarine landscapes is an important research route to pursue

also because often the only data that a marine geologist has at his disposal is bathymetry.

(c) In this study an attempt is made at integrating different geomorphometric techniques as well as different acoustic data sets. This is interesting for two reasons: (i) as explained in chapter 2, most geomorphometric analyses of subaerial landscapes are based on one technique; (ii) the majority of studies characterising the geology of the seafloor involve the use of one acoustic data set [*Mitchell and Clarke*, 1994].

1.4.2 WHY STUDY SUBMARINE LANDSLIDES?

A deeper understanding of submarine landslides is important for a number of reasons:

(a) Submarine landslides are significant from a geological point of view:

- Submarine landslides are important submarine geological processes in terms of their widespread occurrence, their size and the volume of sediment they displace [*Canals et al.*, 2004].
- Submarine landslides are a major factor shaping continental margins, e.g. modifying the distribution pattern of canyon-channel systems and levées [*Lastras et al.*, 2006].
- The study of submarine landslides can provide an important insight into the evolution of continental margins. For example, slope sediments offshore Norway have the potential to record the timing, extent and activity of past glaciations. Thus, knowledge of past sediment displacement is essential to understand the stratigraphic sequences and derive reliable dates.
- Submarine geomorphology, together with the study of planetary surfaces, is the new research frontier in geomorphology. In comparison to geomorphological research carried out so far, submarine geomorphology is different in terms of the environmental setting and the spatiotemporal scales being considered.

(b) Submarine mass movement processes are still not very well-understood:

- Significant advances in the characterisation and explanation of submarine landslides have been made in recent years. However, there are still many gaps in our understanding of submarine mass movements. For example, the causes and triggers of slope failures, and the mode of failure and mechanisms that characterise submarine landslides are poorly understood [*Bünz et al.*, 2005; *Locat*, 2001; *Masson et al.*, 2006]. This is mainly due to the fact that submarine landslides are largely inaccessible, and their products occupy extensive areas that often cannot be surveyed and analysed in their entirety [*Lastras et al.*, 2006].
- On the other hand, some data sets from submarine landslides may provide information that is not usually available for subaerial landslides, e.g. representation of the internal structure. The study of some submarine landslides can thus provide insights into the dynamics of subaerial mass movements.

(c) Submarine landslides are a geohazard to humans and their infrastructures:

- An increasing proportion of the world's oil and gas is now recovered from deep-water areas offshore, where submarine slope instability can be a major geohazard to offshore seabed infrastructures. In addition, changes made by humans to the seafloor and the immediate substructure can trigger localised slope failures.
- Submarine landslides are known to affect the coastal zones by triggering land subsidence [e.g. *Assier-Rzadkiewicz et al.*, 2000] and generating tsunamis [e.g. *Gracia et al.*, 2003]. Tsunamis, in particular, have a strong social and economical impact on the affected populations.
- Gas hydrates, located underneath the surface of many slide scars (including the Storegga Slide), constitute a main source of greenhouse gas. If released during a landslide, this gas could potential contribute to the "Greenhouse effect" [*Kennett et al.*, 2003; *Nisbet and Piper*, 1998; *Paull et al.*, 1991].
- In consideration of the above, the prediction of submarine landslides and the assessment of the risk they pose are important. However, the

modelling and forecasting of submarine landslides are still problematic [*Masson et al.*, 2006].

1.4.3 WHY STUDY THE STOREGGA SLIDE?

(a) The large 'state-of-the-art' data sets from the Storegga Slide, with data quality and resolution equal or higher than available for slides elsewhere, allows a detailed quantitative analysis of different types of mass movements on different scales. This analysis is also backed up by substantial geological and geophysical background information that is found in the literature.

(b) The Storegga Slide is a geologically recent event [*Haflidason et al.*, 2005]. One of the major advantages of studying recent mass movements is that they can be much better constrained than older events in terms of resulting morphologies, deposits, dynamics, impacts and ages.

(c) Most of the Storegga Slide studies, particularly the identification of individual mass movements and the description of the slide evolution history, have been based entirely on a qualitative investigation [*Haflidason et al.*, 2004]. Only two studies of the Storegga Slide employ basic geomorphometric techniques [*Haflidason et al.*, 2005; *Issler et al.*, 2005].

(d) The study of the Storegga Slide may help understand the other submarine landslides located along the Norwegian margin because the geological setting in which they occur is similar.

1.4.4 REASONS FOR FOCUSING ON SPREADING, FRACTAL STATISTICS AND MORPHOLOGY AND SLIDE DEVELOPMENT.

(a) Spreading: Spreading is a type of mass movement that has received considerable attention in terrestrial environments, but its occurrence has hardly been documented in submarine environments. As a result, knowledge about the characteristic morphology and geological processes responsible for submarine spreading is not available. A detailed study of submarine spreading is important because the spreading morphology can be identified

in the proximity of areas in the Ormen Lange region where infrastructural work is taking place. Spreading morphology can also be observed in numerous submarine landslide scars from around the world.

(b) Fractal statistics and morphology: The fractal model is a powerful approach to the representation of geoscientific data [*Burrough*, 1981]. In particular, the statistical properties of terrestrial landslide populations have become a recent focus of study [e.g. *Guzzetti et al.*, 2002]. Such studies have important implications that relate to the aggregate behaviour of landslide systems, extrapolation of morphology and processes between scales, and the assessment of hazard risk associated with landslides. In comparison, marine geologists have seldom applied the fractal concept to the study of submarine landslides.

(c) Slide development: The resolution of the bathymetric data set available for the Storegga Slide is very high, making this submarine landslide ideal for detailed geomorphometric analyses. Yet, the reconstruction of the development of the Storegga Slide is entirely based on visual interpretation [*Haflidason et al.*, 2004]. A more detailed understanding of the development of the Storegga Slide is achieved if geomorphometric techniques are applied to the bathymetric data. This is important because it provides a more profound understanding of the formative submarine mass movements, the associated geological processes and controls and the way in which submarine mass movements are spatially interrelated. The highest resolution and density of acoustic data are found in the Ormen Lange region. As a result, most of the studies on mass movement mapping and dynamics within the Storegga Slide concentrated on this part of the Storegga Slide [e.g. *De Blasio et al.*, 2004; *Gauer et al.*, 2005; *Kvalstad et al.*, 2005a]. Much less attention has been paid to mass movements in the north-eastern Storegga Slide, where the development model is not as detailed and well constrained as in the Ormen Lange region [*Haflidason et al.*, 2004]. Chapter 8 therefore focuses on data from the north-eastern Storegga Slide. The north-eastern Storegga Slide is also the focus of multiple proposed IODP drill sites and will thus be an area of interest in the near future [*Brown et al.*, 2006].

1.5 NOMENCLATURE

Several authors have noted that there is a submarine mass movement terminology problem; the nomenclature is complex, not standardised and often used imprecisely [*Canals et al.*, 2004; *Hampton et al.*, 1996; *Masson et al.*, 2006]. The landslide terminology that will be used in the rest of thesis is defined below:

- Landslide: The downward and outward movement of slope-forming materials under the influence of gravity when a slope fails [*Schuster*, 1978].
- Mass movement: The mode of slope failure; landslides are classified into mass movement types according to morphology, material mobilised and the mechanics of movement.
- Topple: A forward rotation of a detached mass of rock or sediment about a pivot on the slope.
- Spreading: Extensional downslope displacement of a surficial mass of rock or sediment on gently sloping ground.
- Slide: Movement of a rigid, internally undeformed, mass of rock or sediment along a discrete shear surface. In a translational slide, the movement of the slide mass occurs along a near-planar slip surface, whereas in a rotational slide, the movement occurs around an axis.
- Debris flow: Moving laminar flows of agglomerated particles held together by a cohesive sediment matrix.
- Turbidity current: A flow of sediment that is supported by the upward component of fluid turbulence in a current.

Chapter 2:

RESEARCH CONTEXT

2.1 INTRODUCTION

This chapter provides a research context for the work presented in the thesis. Published studies on three fields of research – geomorphometry (Section 2.2), spreading (Section 2.3), and fractal concepts and their application in the geosciences (Section 2.4) – are reviewed, discussed and critically analysed. The object of this chapter is to provide a background to my studies, identify the research questions that need addressing in each of the above fields of research, and place my work into the context of this research.

2.2 GEOMORPHOMETRY

2.2.1 INTRODUCTION

Geomorphometry is a subdiscipline of geomorphology. Its objective is the quantitative description and measurements of topography and landforms [*Dehn et al.*, 2001; *Pike and Dikau*, 1995]. The study of surface form, and more particularly, the taking of surface measurements from maps or models, has a long history that can be traced back to the mid-nineteenth century [*Cayley*, 1859; *Chorley and Pogorzelsi*, 1957; *Maxwell*, 1870]. An overview of the history of geomorphometry can be found in *Pike* [2000]. During the last 20 years, the study of geomorphometry has been rejuvenated and its scope broadened. This has gone hand in hand with the technical advances in computing and the increasing use of Digital Elevation Models (DEMs) [*Mark*, 1978]. A DEM stores elevation values at regularly distributed points in the form of grids, from which the characterisation of the form of the land surface is carried out. The geomorphometric study of DEMs has been carried out in a wide range of subaerial geological settings. A detailed study of the use of DEMs in landscape investigation was carried out by *Florinsky* [1998]. Today, geomorphometric research is stimulated by the need to explore inaccessible landscapes, in particular planet surfaces [*Aharonson et al.*, 2001; *Blair*, 1986; *Greeley*, 1994; *Miliaresis and Argialas*, 1999].

The objectives of this sub-chapter are to review the standard techniques in geomorphometry, provide examples of their application in subaerial geomorphology, and critically evaluate them. I will then discuss the application of geomorphometry in the study of submarine landscapes and derive the research questions that need to be addressed.

2.2.2 BASIC CONCEPTS

Evans [1972] distinguishes between general and specific geomorphometry. General morphometry, as applied in this thesis, is "the measurement and analysis of those characteristics of landform which are applicable to any continuous rough surface"

[*Evans*, 1972, p. 18]. Specific geomorphometry, in comparison, is the measurement and analysis of specific landforms. The basic assumptions in general geomorphometry are: (i) there is a close relationship between surface processes and topographic characteristics [*Moore et al.*, 1991] and (ii) the study of elevation differences, and their variation as a function of distance, yields relevant geological information [*Bolongaro-Crevanna et al.*, 2004; *Székely and Karátson*, 2004]. The morphology of the land surface can be quantified in terms of geometric attributes of the terrain, known as morphometric attributes. General geomorphometry relies heavily on DEMs as the basic data from which morphometric attributes are extracted [*Bolongaro-Crevanna et al.*, 2004]. These attributes have mainly been used to garner information about the formative processes of the landscape and to compare terrains quantitatively [*Hutchinson and Gallant*, 2000; *Onorati and Poscolieri*, 1988; *Onorati et al.*, 1992]. Morphometric attributes can also be combined to classify the continuous surface of the landscape into topographic regions/elements [*Etzelmüller and Sulebak*, 2000]. General geomorphometry has been applied successfully in a wide range of geological settings and environmental applications: e.g. soil studies [*Irvin et al.*, 1997; *Oliver*, 1987], fault morphology and orientation [*Florinsky*, 1996; *Gelabert et al.*, 2005], mountain geomorphology [*Chase*, 1992; *Ouchi and Matsushita*, 1992], drainage basins [*Chang et al.*, 1998; *Gardner et al.*, 1990] and hillslopes [*Giles and Franklin*, 1998].

2.2.3 GEOMORPHOMETRIC TECHNIQUES

The techniques used in general geomorphometry can be grouped into four main categories.

I. MORPHOMETRIC ATTRIBUTES AND STATISTICS

This is the simplest and most established method in general geomorphometry. It involves the study of the statistical, spatial characteristics and relationships of point attributes [*Evans*, 1972, 1980]. Analysis of elevation data generally starts with describing every point in a DEM by its primary derivatives (slope gradient and slope aspect) and its secondary derivatives (profile and plan curvature). These derivatives are measured directly from the DEM and are thus called primary morphometric attributes.

Slope gradient is the most widely used of these attributes. More recently, specific measures called secondary morphometric attributes have been developed, consisting of one or more primary morphometric attribute combined into an empirical measure (e.g. aggradation and degradation index [*Moore et al.*, 1993]). The analysis proceeds with the statistical characterisation of the frequency distributions of the morphometric attributes and the calculation of their moment statistics. Moment statistics have been shown to represent several aspects of surface roughness [*Evans*, 1990, 1998]. The calculation of morphometric attributes and statistics has already been demonstrated to provide a thorough insight into the nature of the terrain and the spatial distribution of morphological features, and to provide good alternatives to geomorphological mapping beyond the traditional field surveying and photo interpretation [*Atkinson et al.*, 1998; *Florinsky*, 1998; *Luoto and Seppälä*, 2002; *Rowbotham and Dudycha*, 1998; *Walsh et al.*, 1998; *Wolinsky and Pratson*, 2005]. The importance of morphometric attributes and their statistical analyses to landscape analysis was recognised by *Curtis et al.* [1965], *Speight* [1974] and *Anhert* [1970], although it was I.S. Evans who systematised these geomorphometric techniques into a unified analytical framework [*Evans*, 1972, 1975, 1977, 1979, 1980, 1984, 1990]. Numerous other related techniques, such as bivariate and multivariate analysis [*Jordan*, 2003], have also been developed.

II. FEATURE-BASED QUANTITATIVE REPRESENTATION

The premise behind feature-based quantitative representation is that morphometric attributes can be used to classify the continuous surface of a landscape into discrete landscape elements/units. These elements/units are assumed to represent areas with a predominance of certain surface processes. This method encompasses a wide range of techniques.

GEOMORPHOMETRIC SIGNATURES

This is the most basic form of feature-based quantitative representation. It involves the extraction of patterns in the landscape from morphometric attributes according to geomorphometric signatures. The boundaries of landscape units can be identified as groups of aggregated pixels sharing similar geomorphometric characteristics [*Giles and*

Franklin, 1998]. Signatures of particular landscape units are calibrated either via the use of Geographic Information Systems (GIS) queries or decision-tree classifications, which subdivide the terrain according to simple mathematical criteria or conditional statements. The process is both interactive and interpretive, requiring repeated visualisation of the resulting classification maps and adjustment of classification parameters. Examples of its use include *Pike* [1988] and *Giles* [1998].

FEATURE EXTRACTION ALGORITHMS

This is an evolution of the previous technique. Landscape units in a map are identified using computer code based on physical and mathematical formulae [e.g. *Bolongaro-Crevanna et al.*, 2004; e.g. *Chang et al.*, 1998; *Dymond et al.*, 1995; *Giles and Franklin*, 1998; *Jenson and Domingue*, 1988; *Wood*, 1996]. Individual or groups of algorithms are utilised to classify morphometric attributes as a number of classes of simple landscape units defined either by the form or the relationship of the form with neighbouring features. Numerous automatic line extraction processes have been developed in recent years that are applicable to several kinds of two-dimensional data. Examples include utilisation in digital image editing [*Koike et al.*, 1995], in the skeletonisation of seismic data [*Lu and Cheng*, 1990], and in drainage network analysis [*Chorowicz et al.*, 1992].

AUTOMATED PATTERN RECOGNITION

This technique entails the derivation of patterns from the landscape surface or extracted features in order to identify landforms. The main forms of pattern-recognition analyse the spatial properties of structures that are composed of straight or curved lines, and they attempt to identify a pattern within the image frame [*Baxes*, 1984]. A typical pattern-recognition routine involves elements of image processing and the geometry-based comparison of image segments with sets of target images. The technique has been principally applied to (i) the extraction of drainage networks and watersheds [*Band*, 1986; *Chorowicz et al.*, 1992; *Collins*, 1975; *Fairfield and Leymarie*, 1991; *Haralick*, 1983; *Jenson and Domingue*, 1988; *Riazanoff et al.*, 1988; *Tribe*, 1991]; (ii) the identification of linear or circular features from satellite imagery [*Cross*, 1999;

Miliaresis, 2001; *Raghavan et al.*, 1995; *Wadge and Cross*, 1989]; (iii) the characterisation of hillslope forms [*Chorowicz et al.*, 1989; *Pavlidis*, 1977].

IMAGE PROCESSING

DEMs and derived morphometric attribute maps can be viewed as raster images and hence be processed using digital image processing procedures [*Jordan et al.*, 2005]. Image processing procedures, such as contrast enhancement, density slicing and edge detection, increase the apparent contrast between features within the image and extract lineaments [*Koike et al.*, 1998; *Miliaresis and Argialas*, 1999; *Raghavan et al.*, 1993; *Sagar et al.*, 2003]. They are particularly useful for analysing and synthesising complex spatial structures of the terrain [*Medler and Yool*, 1998].

III. TOPOGRAPHIC CLASSIFICATION

In the past, physiographic analysis was a standard practice of landscape investigation based on fieldwork and visual interpretation of topographic maps [*Fenneman*, 1931]. The objective of this practice was to partition the terrain into functional physiographic units by taking into account the form and spatial distribution of the component features. Physiographic units represent areas with homogenous and continuous terrain geometry where common geological and geomorphological processes operate [*Bolongaro-Crevanna et al.*, 2004].

Today, physiographic analysis has been replaced by topographic classification. This is an automated technique that segments the surface of a DEM into classes. There is a low degree of variability of morphometric attributes within individual classes, and a high degree of variability between classes [*Etzelmüller and Sulebak*, 2000]. Numerous classification procedures have been developed, among which are cluster analysis and aggregation techniques [e.g. *Dikau*, 1994; *Sulebak et al.*, 2000]. Compared to the methods described in section 2.2.3 - II, the emphasis of topographic classification is on the extraction of homogenous terrain units rather than on distinct morphological features. The assumption is that these terrain units of homogenous relief represent areas with a predominance of certain surface processes. Classification is accomplished

through an iterative process in which individual data points are allocated class memberships using simple statistical measures of distance in attribute space [*Ward et al.*, 1992].

CLUSTER ANALYSIS

Clustering procedures are used to describe multivariate data in terms of clusters or groups of data points that possess strong internal similarities [*Duda and Hart*, 1973]. These techniques are often used for digital and satellite image interpretation and can be either supervised or unsupervised.

One of the most widely used unsupervised clustering algorithms is ISODATA, which stands for Iterative Self-Organising Data Analysis Technique, and is also known as ISOCLUSTER or migrating means technique. This technique defines natural groupings of data in attribute space. The ISODATA method uses the Euclidean distance between each pair of data points in a *k*-dimensional attribute space to form clusters, beginning with either arbitrary cluster means or means of an existing signature set. The algorithm is iterative and based upon assignment of cells into candidate clusters, and then moving them from one cluster to another in such a way that the sum of squared error measure is minimised. The ISODATA utility repeats the clustering of the image until either a maximum number of iterations have been performed, or a maximum percentage of unchanged cells have been reached between two iterations. The output of the classification is presented as a digital thematic map where each generated cluster is represented by a different class. Unsupervised classification methods are useful because they may identify classes that do not correspond to preconceived notions of the make-up of the landscape [*Irvin et al.*, 1997]. Examples of its use in the geosciences include *Medler and Yool* [1998], *Sulebak et al.* [1997], *Romstad* [2001] and *Adediran et al.* [2004]. In these examples, the authors employ morphometric attributes as input layers for ISODATA to improve the classification of landscapes and extract morpho-units.

A number of limitations characterise the application of unsupervised classifications. Knowledge of the landforms in the study area is necessary to evaluate the thematic map generated by the technique. The attributes used in the classification need to be selected

with care in order to reflect the nature of the landscape being studied. Unsupervised classifications lack information about transition zones or adjacent elements, which may be a serious limitation in the classification of spatial data [*Weibel and DeLotto*, 1988]. The method also requires specification of the exact number of classes to be detected. If the number of classes is too high or too low, the quality of the result is reduced [*Massons et al.*, 1996].

FUZZY CLASSIFICATION

Clustering methods assign each data point to a particular class. In fuzzy classification techniques, however, data points can be assigned partial membership in many classes. Fuzzy classification is based on fuzzy set concepts [*Zadeh*, 1965], which provide a different mathematical method of dealing with continuous data. This classification procedure has been used to classify natural resource phenomena such as geologic data [*Bezdek et al.*, 1984] and soils data [*McBratney and De Gruijter*, 1992]. Although it provides additional information about each point in a DEM, fuzzy classification is time-consuming and the results it generates are difficult to interpret.

IV. GEOSTATISTICAL AND SPATIAL ANALYSIS

Geostatistics is a collection of statistical methods, based on the theory of regionalised variables, which are applied widely to describe the spatial relationships of geoscientific data [*Matheron*, 1963]. The experimental variogram is central to many geostatistical techniques [*Chappell et al.*, 2003] and is based upon the idea that the statistical variation in the data is a function of distance or sampling lag [*Bishop et al.*, 1998]. The application of geostatistics has been successful in revealing spatial patterns in numerous environmental applications, e.g. remote sensing [*Atkinson et al.*, 1994] and DEMs [*Chappell*, 1996].

Other common methods of spatial analysis of landscapes include spectral, trend, autocorrelation and network analyses [*Jordan*, 2003]. Spectral analysis, in particular, is useful in revealing periodicity and anisotropy in a DEM [*Jordan*, 2003; *Pike and*

Rozema, 1975]. However, this technique only expresses a few aspects of landform geometry. It cannot describe properties such as skewness of elevation or slope curvature, particularly when the spectrum used is one-dimensional. Pre-processing operations are necessary, most of which involve the use of arbitrary thresholds. Spectral analysis alone is thus not adequate for a thorough analysis of a topographic surface.

2.2.4 GENERAL CONSIDERATIONS

I. BENEFITS OF GEOMORPHOMETRIC TECHNIQUES

The use of geomorphometry in the interpretation and investigation of subaerial terrain surfaces has proven to be a very valuable technique [*Irvin et al.*, 1997]. Central to this success is the fact that geomorphometric techniques are effective in capturing the morphology of both discrete landforms and continuous surfaces [*Pike*, 2000]. In comparison to visual interpretation, techniques of general geomorphometry avoid problems of subjectivity, operator variance and landform delimitation prior to analysis [*Evans*, 1990]. Geomorphometric techniques are rapid, accurate, reproducible and transparent [*Drăgut and Blaschke*, 2006]. They quantify landform components and provide detailed information about them. This enables a thorough investigation of the landscapes and facilitates comparison between them [*Irvin et al.*, 1997]. Most of the techniques are available within widely used GIS packages and the results are easily integrated with other forms of digital environmental data. The techniques represent landscapes mathematically, which facilitates input into physically-based models.

II. LIMITATIONS OF GEOMORPHOMETRIC TECHNIQUES

In order to exploit the full potential of geomorphometric techniques, a deep understanding of their limitations is also required. This section lists the general weaknesses of various aspects of the geomorphometric method and the studies that have employed them.

(a) General geomorphometry is a non-systematic set of methods that are not standardised and that consists of a large diversity of non-strictly defined,

sometimes interdependent, techniques [*Shary et al.*, 2002]. Methodological approaches formalising a GIS-based geomorphological classification system are still missing [*Drăgut and Blaschke*, 2006] and some geomorphometric attributes are not well defined [*Wood*, 1996]. All of this complicates the comparison of results between different studies.

(b) In many geomorphometric techniques it is necessary to employ user-defined thresholds. In most cases these are selected arbitrarily. The selection should be based as much as possible on field data or observations [*Giles and Franklin*, 1998].

(c) Most studies use a single method for landscape description and feature recognition [*Jordan et al.*, 2005]. The landscape is a complex surface and no single morphometric attribute can fully describe it [*Evans*, 1984]. Individual results from different techniques need to be combined to produce a final result [*Dehn et al.*, 2001]. The latter reduces the inaccuracy that accompanies the initial selection of morphometric attributes for a particular study area [*Florinsky*, 1998; *Sulebak et al.*, 1997]. There is seldom any integration of the techniques.

(d) Scale is the term used to describe the geographic level of detail [*Etzelmüller and Sulebak*, 2000]. In geomorphometry, any calculation varies with scale in a way that is hard to predict [*Shary et al.*, 2002]. One of the major problems with geomorphometric techniques is the dependence of the results on the data resolution and sampling pattern [*Jamieson et al.*, 2004]. The accuracy of the DEM in the vertical and horizontal, for example, was shown to contribute to variations in the calculation of slope gradient [*Evans*, 1975, 1979].

(e) A DEM consists of discrete elevation measurements and is thus undifferentiable. The surface of the Earth, on the other hand, is a mathematically continuous surface that is differentiable. DEMs can thus only be considered a representation of real landscapes. Morphometric attributes obtained by differentiation have no objective value without being related to the scale of the DEM [*Dehn et al.*, 2001; *Shary et al.*, 2002].

(f) Since the terrain surfaces have been shown to be fractal-like and infinitely complex [*Burrough*, 1981], there will always be a level of detail that cannot

be captured or analysed whatever the resolution of the DEM. This consideration is particularly important in scale-independent modelling.

(g) Relative errors in the compilation of a DEM can become very large during the derivation of morphometric attributes, according to the error propagation laws by *Burrough and McDonald* [1998]. Secondary derivatives are particularly sensitive to error.

(h) The issue of equifinality, where the same morphology may be explained by a variety of processes, is also relevant to geomorphology in general. This hinders the interpretation of process from form, particularly in topographic classification.

2.2.5 GEOMORPHOMETRY AND SUBMARINE LANDSCAPES

When geomorphometric techniques were first applied to terrestrial environments in the 1960s, attempts were made to transfer these techniques to the submarine environments. The results of such studies were, however, limited by the one-dimensionality and the low resolution of the bathymetric data that were available at the time [e.g. *Krause and Menard*, 1965; *Neidell*, 1966]. In the last two decades, improvements in the resolution of the acoustic data acquisition techniques have resulted in a renewed interest in employing geomorphometric techniques to study seafloor morphology. High-resolution bathymetric data sets and the derived DEMs have allowed an in depth quantitative analysis to be carried out. A list of some works that have utilised geomorphometric techniques in their study of bathymetric data is provided in Table 2.1. Similar techniques have also been utilised in the interpretation of sidescan sonar data [e.g. *Blondel et al.*, 1998; *Carmichael et al.*, 1996; *Huvenne et al.*, 2002; *Mitchell and Somers*, 1989].

Table 2.1: List of studies carried out in the last two decades that applied geomorphometric techniques to submarine landscapes.

Technique	Reference
General geomorphometry	
Morphometric attributes/basic geometrical analysis	[*Adams and Schlager*, 2000] [*De Moustier and Matsumoto*, 1993] [*Teide Group*, 1997]
Morphometric attributes and their statistical analyses	[*Berkson and Matthews*, 1983] [*Booth and O'Leary*, 1991] [*Chakraborty et al.*, 2001] [*Goff and Jordan*, 1988] [*Mitchell et al.*, 2000] [*Mitchell et al.*, 2002] [*Mitchell et al.*, 2003] [*Mitchell*, 2003] [*Smith and Shaw*, 1989]
Spectral analysis	[*Fox and Hayes*, 1985] [*Fox*, 1996] [*Gilbert and Malinverno*, 1988] [*Goff and Tucholke*, 1997]
Geostatistical methods	[*Herzfeld*, 1989] [*Herzfeld and Higginson*, 1996]
Feature-based quantitative representation	[*Mitchell and Clarke*, 1994] [*Pratson and Ryan*, 1996]
Neural networks	[*Jiang et al.*, 1993]
Numerous techniques	[*Preston et al.*, 2001]
Specific geomorphometry	[*Gee et al.*, 2001] [*Haflidason et al.*, 2005] [*Hühnerbach and Masson*, 2004] [*Issler et al.*, 2005] [*McAdoo et al.*, 2000] [*Mitchell and Searle*, 1998] [*Mitchell et al.*, 2002] [*Mitchell*, 2003] [*Mitchell*, 2004] [*Mitchell*, 2005] [*Mitchell*, 2007] [*Stretch et al.*, 2006]

Geomorphometric techniques have generally performed well in submarine environments. The use of specific geomorphometric techniques, where features of interest are identified prior to analysis, has involved examining how different morphological parameters change spatially and with each other. They have been amongst the most successful techniques, particularly with regard to the study of submarine mass movements. Their success is attributed to the fact that they are well-suited to identify processes and controls that operate on inaccessible landforms where the process cannot be measured and the controlling variables are not apparent [*Jarvis and Clifford*, 1990]. The application of specific geomorphometric techniques in submarine environments has been characterised by a preference for simple univariate shape indices.

The techniques of general geomorphometry used in the study of submarine landscapes are less numerous and varied than those used in the study of subaerial landscapes. The majority of studies where geomorphometry is applied to the study of submarine landscapes have involved either spectral analyses of the bathymetric data or the statistical analysis of morphometric attributes. Studies employing general geomorphometry in submarine environments are also significantly less numerous than those applying general geomorphometry in subaerial landscapes. This may be due to the fact that, in contrast to specific geomorphometric techniques, studies of general geomorphometry require higher resolution acoustic data, and also due to the fact that not all the techniques can be transferred directly to submarine landscapes. The reasons for the latter are provided in Chapter 5. The approach to analysing bathymetric data has commonly been the visual interpretation of charts of contoured bathymetry or shaded relief maps [e.g. *Clouard and Bonneville*, 2001; *Imbo et al.*, 2003; *Laberg and Vorren*, 2000; *Lastras*, 2002; *Lykousis et al.*, 2002]. Geophysical surveys are usually the first step in the investigation of submarine landscapes because, in comparison to the sampling of the seafloor, they are easier to carry out and require less time. Most of the time, acoustic data are also the only information available. The analysis of submarine topographic data generally involves the use of different charts that display different shapes, textures and tones. The interpretation is thus carried out across several dimensions and depends on the experience of the interpreter [*Mitchell and Clarke*, 1994]. A quantitative investigation of acoustic data using general geomorphometric techniques would be very useful in investigating the geology of the seafloor because the

analytical procedure is standardised, subjectivity is reduced and landform delimitation is not required. DEMs also contain additional morphological information that is not captured by either visual interpretation or specific geomorphometric techniques. This morphological information can be very useful in the automated classification of submarine topographic surfaces. I therefore believe that general geomorphometric techniques have a huge potential in the study of submarine environments that has not been fully taken advantage of.

2.2.6 QUESTIONS FOR THIS THESIS

(a) Can general geomorphometric techniques, devised for the study of subaerial landscapes, also be applied to submarine environments? If not, can these techniques be modified, or a new set of techniques developed, for submarine landscapes?

(b) How does the application of general geomorphometric techniques in the study of submarine landscapes improve the interpretation of bathymetric data sets?

(c) A flaw of most subaerial geomorphometric studies is the use of a single technique to investigate the landscape. Does the integration of a number of geomorphometric techniques in the study of submarine landscapes yield a more accurate and reliable result?

2.3 SPREADING

2.3.1 INTRODUCTION

The term 'spreading' or 'lateral spreading' describes lateral extensional movements in a surficial mass of rock or sediment [*Varnes*, 1978]. This mass movement type entails the finite and downslope displacement of rock/sediment on gently sloping ground, and the fracturing of the rock/sediment mass into coherent blocks (Figure 2.1). Displacement may occur along a shear zone [*Rohn et al.*, 2004], and the deformation may involve subsidence, translation, rotation and disintegration of the upper coherent units [*Cruden and Varnes*, 1996; *Dikau et al.*, 1996; *Varnes*, 1978]. Spreading can take place in rigid rock overlying ductile material (termed rock spreading [*Pasuto and Soldati*, 1996]), or in sensitive soils (termed soil spreading [*Buma and van Asch*, 1996]). Spreading has been described as the most pervasive type of liquefaction-induced ground failure [*Bartlett and Youd*, 1995], because this type of slope failure has generally been associated with the build up of pore pressure or liquefaction in a shallow underlying deposit during an earthquake. Spreading is generally regarded as an initial form of mass movement that evolves into more advanced forms such as translational sliding, rotational sliding and toppling [*Crosta*, 1996; *Dikau et al.*, 1996; *Rohn et al.*, 2004]. Spreading is a potential source of damage to structures and transport routes during earthquakes [*Kanibir et al.*, 2006]. It occurs on gentle slopes that appear stable, and it has been identified in numerous countries and geological settings: e.g. deltaic plains in Venezuela [*Gonzáles et al.*, 2004]; calcareous mountains in Austria [*Rohn et al.*, 2004]; interfingering unconsolidated sediments in California [*Holzer et al.*, 2004].

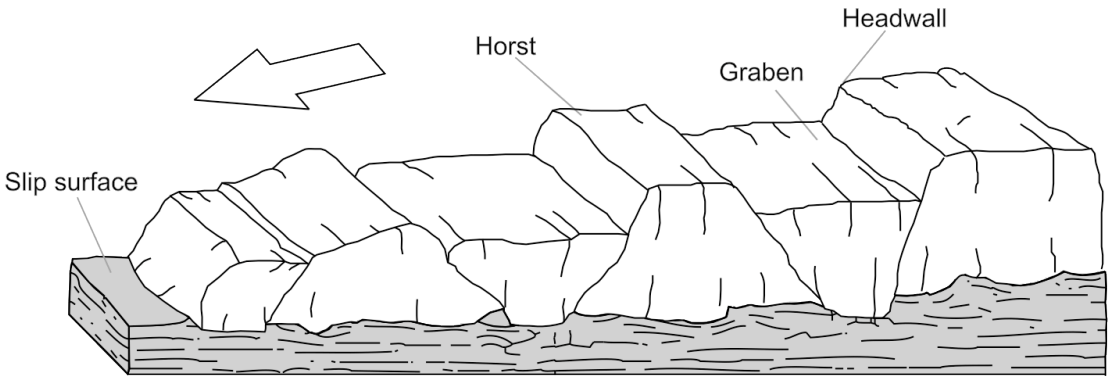

Figure 2.1: Schematic illustration of a spread in a subaerial setting.

The literature on spreading is not as extensive and exhaustive as for other types of mass movement. Everything we know about spreading comes from studies carried out in subaerial environments. Spreading is mainly discussed in journals of engineering geology and geotechnics, whilst only one text book covers spreading in detail.

What follows is a synthesis and assessment of the major findings and trends in the literature on spreading. I will explain the principal methods of investigation of this mass movement and then discuss the current knowledge about the morphology, causes, mechanisms and controls of spreading. Finally I will analyse the investigations of spreading in the submarine realm, and conclude with the research questions that need to be addressed.

2.3.2 METHODS OF INVESTIGATION

Spreading has been investigated by two principal methods. The first method is fieldwork based on surveying, mapping, aerial photography interpretation and sampling. Such studies are either descriptive or they take into consideration the consequences of spreading. The magnitude and direction of the displacement of the failing ground is estimated from the offset of known reference points (e.g. trees, kerbs), and from stereographic diagrams of fracture distribution [e.g. *Conti and Tosatti*, 1994; *Kanibir et al.*, 2006]. Geological maps are then used to relate the observed displacement to lithology. Recently, the use of geotechnical techniques has also increased, e.g. use of

inclinometers, penetration tests and shear-wave velocity measurements [*Boulanger et al.*, 1997; *Cetin et al.*, 2004; *Chu et al.*, 2003].

The main tool of investigation of spreading, however, is modelling. This is because of our difficulty in understanding what occurs beneath the surface and our poor knowledge of how spreading occurs. Modelling of spreading has two purposes: the prediction of ground displacement and experimental simulation.

I. PREDICTION OF GROUND DISPLACEMENT

The prediction of ground displacement is achieved using three methods of numerical modelling.

EMPIRICAL MODELLING

The main trend in the modelling of spreading has been empirical modelling (Table 2.2). In empirical modelling, one does not consider the mechanics of the spreading process, but investigates the relationship between horizontal displacement and a set of parameters based on a number of field observations. These parameters can be of a topographic, seismological and/or geotechnical nature. If it is based on the careful selection of parameters and the compilation of an extensive database, empirical modelling is a simple and reliable technique that is easy to implement at the site-specific level. The main drawback of empirical modelling is that it is a black-box model, and the underlying mechanics of spreading are not identified. This method oversimplifies geotechnical data and lacks support from formal probabilistic analysis.

Table 2.2: Information about the most influential empirical models of subaerial spreading.

Reference	Information
[*Hamada et al.*, 1986; *Hamada et al.*, 1987]	One of the first models, this is a simple empirical model of horizontal displacement associated with spreading in Japan and California. Slope gradient of the ground surface and liquefied soil thickness are the main parameters. The model is applicable to a narrow range of site conditions and ignores seismic and geotechnical parameters.
[*Youd and Perkins*, 1987]	This model is based on case-studies from the western USA and Alaska. Ground deformation is related to a number of earthquake source parameters, such as distance to seismic source and moment magnitude of earthquake. This model is good for mapping and it provides a conservative, upper-bound estimate of deformation. On the other hand, it is very site-specific.
[*Bartlett and Youd*, 1992a1992b, 1995; *Youd et al.*, 2002]	This model has become widely used in the geotechnical community. Multilinear regression, using a modified stepwise procedure, is fitted to a case history of 467 displacement vectors and 267 borings from Japan and USA. The parameters used are moment magnitude of earthquake, nearest horizontal distance to seismic energy source, thickness of saturated cohensionless soils, average fine content and average grain size. A second model also takes into consideration the slope gradient of the ground surface. These models are applicable to a range of soil types and grain sizes, and they do provide a good fit to the data. On the other hand, the accuracy of the model is limited by the use of data from sites where boundary effects have influenced ground displacement. Data from borings is interpolated across large distances, so that the values of some soil parameters may not be representative. Additionally, the parameters of slide mass and distance to boundary margins are not taken into consideration. The model works best when liquefaction has taken place over widespread areas rather than isolated regions. Some of these short-comings have been addressed in a later version of the model that takes into consideration 6 parameters [*Youd et al.*, 2002].
[*Shamoto et al.*, 1998]	The authors employed laboratory based estimates of the limiting shear strains in liquefied soil prior to the onset of dilation to estimate spread displacements. They coupled these estimates with the limiting shear strains observed in the field using a semi-empirical adjustment factor.
[*Bardet et al.*, 1999]	This is a model developed using a multilinear regression approach similar to that of *Bartlett and Youd* [1995]. It is based on the review of existing empirical models and employs six-parameters derived from topographical, borehole and seismological data.
[*Hamada*, 1999]	In this study, the horizontal displacements of the ground in a number of case studies are predicted by applying the similitude law obtained from an experiment of flow tests of model ground.
[*Rauch and Martin*, 2000]	EPOLLS (Empirical Prediction Of Liquefaction-induced Spreading) is an empirical model based on statistical regression techniques applied to a database of historical spreads, and takes into consideration seismological, topographical and geological parameters. This model allows the prediction of the magnitude of potential surface deformation, even if the site conditions are not well known.

Table 2.2 is a list of the most influential work in empirical modelling of spreading during the last 20 years. Some of the above empirical models have been assessed by inputting the parameters measured at a study area and comparing the displacement predicted by the model with that measured at the site. For example, *Cetin et al.* [2004] tested the accuracy of the models by *Hamada et al.* [1986], *Shamoto et al.* [1998] and *Youd et al.* [2002] in predicting ground displacement in Ismit Bay, Turkey. The models of *Hamada et al.* [1986] and *Shamoto et al.* [1998] tended to overpredict or underpredict ground displacement significantly. The model by *Youd et al.* [2002] overpredicted ground displacements. In *Kanibir et al.* [2006], liquefaction-induced ground deformations were measured from aerial photographs and compared with those predicted from the empirical models of *Bardet et al.* [1999], *Hamada et al.* [1986], *Hamada et al.* [1999] and *Youd et al.* [2002]. The best agreement was shown by *Bardet et al.* [1999], whereas the other methods overpredicted ground displacements.

The lack of agreement observed between the displacement measured in the field and that predicted by empirical models is due to a number of factors:

- Uncertainties in the estimation of predictive model parameters due to limited available data and unknown spatial variations of properties. Where no data is available, a mathematical scheme is used to interpolate data between boreholes. This results in the predicted displacements tending to be more accurate in the vicinity of boreholes [*Kanibir et al.*, 2006].
- Underreporting of ground displacement due to either inaccurate mapping procedures or limiting the measurement of ground displacement to that observed in ground fissures.
- Some empirical models ignore seismic and geotechnical parameters altogether [e.g. *Hamada et al.*, 1986].
- Near-field peak ground accelerations are sometimes smaller than those predicted by standard attenuation relationships, resulting in overprediction of ground displacements [*Cetin et al.*, 2004].
- The estimation of predictive parameters prior to deformation by spreading is difficult [*Youd et al.*, 2002]. This applies in particular to free face ratio, ground slope and variable shear stresses that arise from edge of slope geometries prior to displacement [*Hamada et al.*, 1986].

- Selection of parameters during motion, such as residual shear strength properties and pore pressure variation, is problematic.
- Difficulty in identifying liquefiable layers and their contribution to overall ground displacement.
- Bias towards the study area from where data for the parameterisation of the original model was collected; most of the time emphasis is made on the larger slides, which explains the overprediction of ground displacement.

SLIDING BLOCK ANALYSIS

Sliding block analysis is a mechanistic method, originally proposed by *Newmark* [1965] and based on the analogy of the sliding block. It estimates the rigid body motion of the liquefied layer through the consideration of input-waves and shear strength mobilised along the sliding plane [*Dobry and Baziar*, 1992]. The main difficulty with this method is in selecting the residual shear strength properties and pore pressure variation during ground motion [*Kanibir et al.*, 2006].

FINITE ELEMENT MODELLING

Finite element modelling is well suited to modelling the relevant mechanics and boundary conditions of a spread. A comprehensive model would need to simulate seismic excitation, soil softening, loss of shear strength, distortion of liquefied deposits, distribution of pore water, progressive failure, deformation and changes in pore pressure after dynamic loading ends, among others. It is very difficult to model all these aspects of spreading processes thoroughly. As a result, such numerical models are rarely attempted. Also, since it is difficult to assign appropriate models for the solid and liquid phases of the ground during liquefaction, a single-phase approach is preferred. Perhaps the most sophisticated of these finite element models for spreading is the one by *Finn et al.* [1994].

II. SCALE MODEL SIMULATIONS

Another principal method of investigating spreading is the use of laboratory scale models where the failure process is studied under controlled conditions. This technique is useful to study the onset of liquefaction, although it is not possible to simulate all relevant aspects of the spreading process.

SHAKE TABLE MODELS

A technique that has been pioneered by Japanese researchers (e.g. *Tokida et al.* [1993]; *Towhata et al.* [1991]; *Towhata et al.* [1989]), it involves the construction of scale models on a shake table to study the behaviour of liquefaction-induced spreads. Because of size and density limitations, the boundary effects of the rigid walls of the container and the effects of capillary rise, shake table models cannot simulate every aspect of the spread. They are, however, considered as a good qualitative tool.

CENTRIFUGE MODELS

These models are rotated at high speed to produce a centrifugal acceleration and simulate the stress conditions of soil structures during spreading [e.g. *Fiegel and Kutter*, 1994; *Kutter et al.*, 2004; *Sharp et al.*, 2003; *Taboada and Dobry*, 1998]. They are considered more accurate than shake tables, although it is difficult to determine the prototype displacements precisely.

2.3.3 MORPHOLOGY

The ground deformation associated with spreading comprises the extensional fissuring of the surface units in the form of alternating non-tectonic horst and graben structures [*Dikau et al.*, 1996]. The fissures are oriented perpendicular to the direction of mass movement, and the horsts are generally sharp crested [*Hutchinson*, 1988]. The fissures are crescentic and concave-downslope in the head area of the failing mass, and they gradually transform into a convex-downslope fissure pattern in the distal part of the spread. The extension in the head area may result in subsidence of the unit and the formation of a graben, whereas compression of the failing unit may occur at the toe of the spread [*Bartlett and Youd*, 1995]. Along the lateral margins of the spread, shear

deformation takes place. Sand boils and sand venting features occasionally develop in the lower part of the spread and are a surface expression of soil liquefaction in the underlying layers [*Chu et al.*, 2003; *Kanibir et al.*, 2006].

Spreads generally occur on mild slopes (between 0.3% and 5%) [*Bartlett and Youd*, 1992b]. Horizontal displacements can range between 1 cm and 10 m, although the average displacement for spreading in soils is in the order of 2.5 m [*Dikau et al.*, 1996; *Rauch and Martin*, 2000]. Rock spreading can extend over several kilometres, and the displacement rate may range between 10^{-4} to 10^{-1} m yr^{-1} [*Dikau et al.*, 1996]. The associated vertical displacements are relatively smaller; for example, a displacement of 0.3 m was measured for spreading on the shores of a Turkish lake [*Kanibir et al.*, 2006].

2.3.4 MECHANICS OF SPREADING

The fact that the principal method of analysis of spreading is empirical modelling is indicative of the fact that little is known about the mechanics of the failure process. Deformation in a spread is known to be driven by a combination of transient and static shear stresses, attributed to a loss of shear strength of the underlying saturated soils. A liquefied underlying soil allows the overlying unsaturated rock/soil to slide downslope as intact blocks. Scale model simulations show that spreading does not always occurs along a well-defined shear surface, but may involve shear distortions across a thickness of the liquefied deposit [*Fiegel and Kutter*, 1994; *Towhata et al.*, 1991]. Both field and laboratory observations show that horizontal displacements are highest near the surface of the spread [*Doi and Hamada*, 1992]. The horizontal displacement of the unbroken blocks at the surface is coupled with their vertical displacement and tilting. The horizontal displacements are considerably larger than the vertical. The distance between the blocks tends to increase with distance from the centre of failing slab, and the ongoing extension leads to the widening of the fractures [*Rohn et al.*, 2004]. The blocks are subject to tilting, internal fracturing, subsidence, heaving and overthrusting, but they may also remain relatively undeformed [*Dikau et al.*, 1996].

2.3.5 CAUSES AND CONTROLS OF SPREADING

The geological conditions conducive to spreading are usually those where consolidated rocks or sediments overlie a ductile substratum [*Dikau et al.*, 1996; *Rohn et al.*, 2004], or where slopes have been subjected to mass movements resulting in disturbed drainage and high water contents. Spreading is inextricably linked with liquefaction, which is taken to mean the substantial loss of shear strength in saturated, cohesionless soils due to excess pore water pressures. In subaerial environments, earthquakes have been shown to be the most common trigger of liquefaction [*Boulanger et al.*, 1997; *Cetin et al.*, 2004; *Chu et al.*, 2003; *Kanibir et al.*, 2006]. Spreading is also frequently observed along stream banks, in recent alluvial and deltaic deposits, and in loosely packed, saturated sandy fills [*Youd and Hoose*, 1976]. Changes in the height of the water-table can thus be another trigger of this mass movement [*Dikau et al.*, 1996]. Rock spreading, on the other hand, appears to be particularly sensitive to seismic loading [*Sorriso-Valvo et al.*, 1999].

The magnitude of spreading deformation is affected by a complex interaction of many factors:

(a) Slope gradient: Shake table model studies have shown a positive correlation between surface slope and displacement [*Sasaki et al.*, 1991]. However, in the field such a correlation cannot be observed [*O'Rourke and Pease*, 1997]. Rather than the displacement, the direction [*Youd and Kiehl*, 1996] and the velocity [*Doi and Hamada*, 1992] of the spread are correlated with the surface slope.

(b) Pore water: The upward migration of pore water in partially drained soils was shown to have an impact on the magnitude of spreading displacements [*Stark and Mesri*, 1992].

(c) Thickness of liquefied layer: Both in the lab and in the field, a positive correlation was observed between surface displacement and the thickness of the liquefied soil deposit [*Bartlett and Youd*, 1992b; *Hamada et al.*, 1987; *O'Rourke and Pease*, 1997; *Tokida et al.*, 1993; *Yasuda et al.*, 1992].

(d) Sediment size: *Bartlett and Youd* [1995] observed a positive correlation between the percentage of fine sediment and the extent of surface displacement. This may be attributed to the effect of fine sediments on the dissipation of the excess pore pressure [*Toyota and Towhata*, 1994]. Coarse-

grained sediments, on the other hand, increase the resistance of the soil to liquefaction [*Finn et al.*, 1994].

(e) Boundary conditions: A free face in the distal part of a spread results in greater displacement [*Youd and Kiehl*, 1996], whereas the boundaries and underlying morphology have an effect on the magnitude and direction of displacement [*O'Rourke and Lane*, 1989].

2.3.6 SUBMARINE SPREADING

In comparison to subaerial spreading, submarine spreading has received very little attention. This mass movement has been identified recently within the Storegga Slide and investigated in two papers: *Kvalstad et al.* [2005] and *Gauer et al.* [2005]. The only examples of a study of a submarine spread outside of the Storegga Slide are from offshore California by *Field et al.* [1982] and *Field and Hall* [1982]. The Storegga Slide studies provide an interesting perspective into the modelling of the submarine spreading process, although the seismic lines on which the observations are based are of low resolution due to the rugged seabed. These studies also do not provide information about the associated morphology. *Kvalstad et al.* [2005] use infinite slope modelling, retrogressive slide modelling and the dynamic wedge model based on the energy approach, combined with soil strength parameters from the site investigations. The main conclusion of the study is that strain softening plays an important role in spreading, and that spreading develops via retrogressive failure. *Gauer et al.* [2005] use computational fluid dynamics and a rheological model based on a Bingham fluid to reproduce depositional patterns similar to the observed morphology within the Storegga Slide. In this paper, the model that best reproduces this morphology is also a retrogressive sliding process based on strain softening.

2.3.7 QUESTIONS FOR THIS THESIS

It is clear that our knowledge on spreading comes prevalently from the investigation of subaerial environments. As a result, there is a number of research questions related to submarine spreading that still need to be answered:

(a) Is spreading a widespread type of mass movement in submarine environments?

(b) How do the morphological characteristics of subaerial spreading compare with those of submarine spreading? What are the dimensions and extent of failure in a submarine spread? There is the need for a preliminary investigation of spreading in a submarine environment.

(c) Subaerial spreading is often modelled empirically because several gaps still remain in our understanding of the mechanics of the spreading process. As shown in section 2.3.2 - I, empirical models provide relatively inconsistent predictions of the observed ground displacements. In submarine environments there is neither the variety nor the quantity of geotechnical data that is required to model the slope failure empirically. However, we do have high resolution seismic data that reveal the internal architecture of a spread. Such data is generally not available for subaerial environments. Investigation of these acoustic data sets can provide new insights into the failure process that would allow us to constrain the failure mode of submarine spreads. This information may potentially be useful in understanding the mechanics of subaerial spreading as well. Better understanding of the mode of failure will allow us to model the spreading process physically rather than empirically, and to attempt to improve the prediction of the ground displacement associated with spreading.

(d) If we can model the spreading process more accurately, it would then be possible to relate it to the observed morphology and obtain a better understanding of the causes and controls of submarine spreading, which have not been identified yet.

(e) The main problem with applying models of subaerial spreading to the submarine environment relates to the consideration of liquefaction of the slip layer as playing a fundamental role in triggering and enabling spreading. We are still unable to determine the association between liquefaction and spreading in submarine environments.

2.4 FRACTAL CONCEPTS AND THEIR APPLICATION IN THE GEOSCIENCES

2.4.2 THEORETICAL BACKGROUND

I. BASIC CONCEPTS

The fractal concept, introduced by Benoit Mandelbrot in 1967 [*Mandelbrot*, 1967], represents one of the most profound changes to the ways in which scientists look at natural phenomena. A fractal is defined as a set or function for which the Hausdorff-Besicovitch dimension exceeds the topological dimension [*Mandelbrot*, 1967]. Fractal shapes are characterised by the following two properties [*Tricot*, 1995]:

a) Fractals are non-rectifiable: Referred to as the Steinhaus Paradox or the property of indeterminate measurable geometry, the measurement of the length of a fractal shape increases with improving accuracy [*Steinhaus*, 1960].
b) Fractals are self-similar: A fractal shape possesses symmetry across scales, so that it is made of parts similar to the whole [*Mandelbrot*, 1983]. Fractal objects are thus scale-invariant, and the scaling may be discrete, multiple or continuous. Self-similarity can be either deterministic, where a mathematical function is applied recursively over a range of scales, or statistical, where only measurable statistical parameters of the object (or process) are repeated over a range of scales [*Goodchild and Mark*, 1987]. The fractal is termed self-similar if the copies of the object are identical bar isotropic scaling and rotation [*Mandelbrot*, 1983] (e.g. topographic contours [*Gilbert*, 1989]). If the scaling is anisotropic, the fractal is called self-affine (e.g. vertical topographic relief [*Turcotte*, 1992]). Statistically self-similar objects are isotropic by definition.

A fundamental property of fractals is the fractal dimension (or similarity dimension, D), which is a single, non-integer, power-law exponent based on iterative measurements between measure and measuring unit across at least one order of magnitude [*Baas*, 2002; *Mandelbrot*, 1983]. The fractal dimension gives a useful measure of the complexity of a spatial pattern [*Lathrop and Peterson*, 1992]. Statistically self-similar objects are described by a single fractal dimension across the whole range of scales for which the fractal dimension is physically meaningful [*Beauvais and Montgomery*,

1997]. When more than one fractal dimension is required to describe the scaling relationship, the object is termed multifractal [*Cheng*, 1999; *Gao and Xia*, 1996].

II. METHODS

Numerous methods have been put forward to estimate the fractal dimension of shapes (see *Gao and Xia* [1996] and *Klinkenberg and Goodchild* [1992] for a review). Table 2.3 lists the most popular techniques used to calculate the fractal dimension in the geosciences. The theoretical bases for these methods can be found in *Turcotte* [1992].

Table 2.3: Methods used to estimate the fractal dimension in the geosciences.

Method	Application	Examples
Divider method	Tidal channels; faults; coastlines.	[*Andrle*, 1992; *Angeles et al.*, 2004; *Aviles et al.*, 1987; *Richardson*, 1961]
Box-counting method	Channel networks; vegetation.	[*Beauvais and Montgomery*, 1997; *Morse et al.*, 1985]
Spectral analysis	Terrain surface form; seafloor roughness.	[*Burrough*, 1981; *Fox and Hayes*, 1985; *Tate*, 1998a]
Fuzzy morphological coverings	Terrain surface form and profiles	[*Huang et al.*, 1997]
Area-perimeter scaling	Terrain surface form	[*Goodchild*, 1982]
Variogram method	Terrain surface form	[*Burrough*, 1981; *Klinkenberg*, 1992]
Line-scaling method	Terrain surface form	[*Ouchi and Matsushita*, 1992]
Frequency-magnitude relations	Coastlines	[*Kent and Wong*, 1982]

No single method appears to be the best to determine the fractal dimension [*Klinkenberg*, 1994]. In comparison to the other methods, the divider method is one of the most widely used, has a breadth of application, and is easy to implement [*Angeles et al.*, 2004].

Multifractal measures, on the other hand, replace the constant dimension with a function of the dimension, and they are aimed at disentangling spatially intertwined fractals [*Agterberg*, 1984; *Schertzer and Lovejoy*, 1991]. Methods used to estimate the

multifractal dimension include the continuous spectrum [*Everts and Mandelbrot*, 1992] and the co-dimensional function [*Lavallé et al.*, 1993].

The frequency-magnitude method has mostly been used to investigate the fractal properties of data populations. Frequency-magnitude histograms represent scale-invariance with a power law distribution [*Turcotte*, 1999]. In a power law distribution, when comparing the number of events of size M or greater with the number of events of size αM or greater (where α is an arbitrary factor), the number always differs by the same factor of $\alpha^{-\gamma}$, regardless of the absolute size of the events [*Hergarten*, 2003]. For this reason, a power law distribution may be replaced with other measures of magnitude of an object/event. Such a distribution is free of characteristic scale and is thus termed a fractal distribution.

III. SELF-ORGANISED CRITICALITY

In the past 20 years, the fractal characteristics of frequency-magnitude distributions have been interpreted in terms of self-organised criticality (SOC) [*Baas*, 2002; *Bak et al.*, 1988; *Turcotte*, 1999]. The concept was first introduced in statistical physics, but it has been applied in many fields, including economics and sociology [*Bak et al.*, 1987]. Self-organisation refers to the emergence of order in a system through its internal dynamics and feedback mechanisms [*Baas*, 2002]. In self-organised criticality, the system is in, or tends to move towards, a quasi-stationary, critical state [*Hergarten and Neugebauer*, 1998]. There is a nearly constant "input" into the system, and the "output" is comprised of a series of events that follow a fractal distribution. The simplest mathematical (and physical) model of self-organised criticality is the 'sandpile' model [*Bak et al.*, 1988; *Turcotte*, 1992]. In this model there is a grid of boxes (Figure 2.2). A particle is dropped into a randomly selected box at each time step. When the total number of particles in a box reaches a threshold value, the particles are redistributed amongst the adjacent boxes. Such a redistribution of particles can lead to an 'avalanche' of redistributions, with the area of the boxes participating in the redistribution defining the size of the avalanche. In this model, the non-cumulative number of 'avalanches' is a function of the area according to a power law distribution.

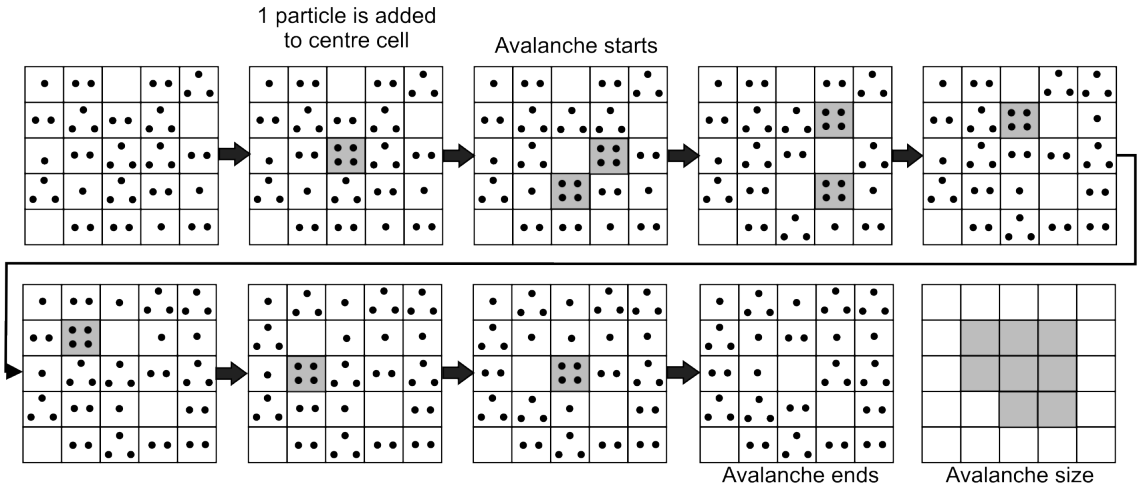

Figure 2.2: The theoretical 'sandpile' model based on a 5 × 5 grid. The dots indicate the number of particles within each cell of the grid. When a particle is added to the centre cell in this example, an avalanche of a size of 8 cells is triggered. In the 'sandpile' model, the frequency-magnitude distribution of these avalanches is power law.

2.4.3 APPLICATION OF FRACTAL CONCEPTS IN THE GEOSCIENCES

Since Mandelbrot's treatise on fractals [*Mandelbrot*, 1967], fractal geometry has proved to be a powerful approach in the representation of natural phenomena [*Herzfeld and Overbeck*, 1999]. The fractal model provides a good application to a range of landscape features and environmental data [*Burrough*, 1981; *Goodchild and Mark*, 1987; *Pelletier*, 1999; *Shih et al.*, 1999; *Southgate and Möller*, 2000; *Sung and Chen*, 2004; *Turcotte*, 1992; *Xu et al.*, 1993]. Unlike mathematical fractals, however, landscapes only display statistical self-similarity over a limited range of spatial/temporal scales [*Cheng et al.*, 1999]. The use of fractal analyses in the geosciences varies from: (i) testing whether a feature is fractal or not, (ii) delineating geomorphic regions, (iii) determining the single/multiple formative processes and the scales over which they occur, and (iv) as a means of descriptive parameterisation of topography [*Baas*, 2002; *Cox and Wang*, 1993; *Huang and Turcotte*, 1989]. In comparison to traditional morphometric measures, fractal geometry allows a deeper insight into the geological features being investigated [*Angeles et al.*, 2004; *Klinkenberg*, 1992].

The identification of fractal statistics in landscapes implies that the formative geological processes are scale-invariant. This goes against the widely-held principle that landforms are scale-dependent [*Gao and Xia*, 1996; *Schumm and Lichty*, 1965]. Most empirical work, in fact, suggests that landscapes do not possess a single fractal dimension. Self-similarity is observed over finite bandwidths and at some point self-similarity breaks down [*Aviles et al.*, 1987; *Mandelbrot*, 1983]. Some geographic entities, in particular topographic surfaces, are thus better represented and analysed using multifractals [*Beauvais and Montgomery*, 1997; *Dodds and Rothman*, 2000; *Rouai and Jaaidi*, 2003]. The scale at which the fractal dimension changes is indicative of a change in the dominant geomorphic process [*Mark and Aronson*, 1984]. The traditional monofractal analyses, commonly employed in the geosciences, are appropriate to model the planform topographic patterns, but they are unsuitable for modelling the multifractal character of continuous elevation [*Lovejoy and Schertzer*, 1995; *Outcalt et al.*, 1994].

Despite the success of the fractal model, there are still some problems as regards its application in the geosciences:

(a) Estimates of fractal dimensions tend to differ with the choice of method and details of estimation [*Andrle*, 1992; *Cox and Wang*, 1993; *Lakhtakia et al.*, 1986; *Tate*, 1998a].

(b) It is difficult to relate the fractal dimension to a geological process [*Tate*, 1998b] or to interpret what the fractal dimension stands for [*Gao and Xia*, 1996]. Fractals do not necessarily constrain the formative mechanism [*Turcotte*, 1992].

(c) The fractal model provides a good fit for some land surfaces and an imperfect fit for others [*Klinkenberg and Goodchild*, 1992], which means that it is not a universal model.

(d) The similarity dimension is the most popular dimension in fractal geometry, yet it is not the only one. Other dimensions, which include parameters derived from Fourier series and anisotropy coefficients [*Herzfeld and Overbeck*, 1999], may be more suited for the study of certain aspects of the terrain, such as surface roughness.

(e) Research on fractal geometry and scaling in terrain surfaces has been so active that many results have not been well resolved, and some of them are contradictory [*Xia and Clarke*, 1997].

The statistical characteristics of large populations of landslides have become a recent focus of study in geology and geomorphology. There is accumulating evidence that the frequency-magnitude distributions of landslides and other natural phenomena exhibit fractal statistics despite large differences in the geological settings and triggering mechanisms (e.g. landslides [*Chien-Yuan et al.*, 2007; *Dai and Lee*, 2002; *Dussauge et al.*, 2003; *Fuyii*, 1969; *Guzzetti et al.*, 2002; *Hovius et al.*, 1997; *Hovius et al.*, 2000; *Iwahashi et al.*, 2003; *Katz and Aharonov*, 2006; *Malamud et al.*, 2004; *Noever*, 1993; *Ohmori and Hirano*, 1988; *Sugai et al.*, 1994; *Van Den Eeckhaut et al.*, 2007; *Whitehouse and Griffiths*, 1983; *Yokoi et al.*, 1995]; earthquakes [*Gutenberg and Richter*, 1954; *Matsuzaki and Takayasu*, 1991]; forest fires [*Malamud et al.*, 1998]). Understanding the origin of power laws is difficult. Self-organised criticality has become established as a strong candidate for explaining the emergence of fractal statistics [*Hergarten*, 2003; *Turcotte et al.*, 2006] because this concept explains how a broad range of complex phenomena exhibits similar behaviour under very broad conditions [*Turcotte*, 2001]. The application of the self-organising concept to landsliding has been useful in quantifying risk and carrying out hazard analyses [*Brardinoni and Church*, 2004; *Guzzetti et al.*, 2005; *Hungr et al.*, 1999], extrapolating incomplete landslide inventories [*Gilbert*, 1989; *Malamud et al.*, 2004], modelling the long-term evolution of landscapes [*Benda and Dunne*, 1997] and quantifying erosion by landsliding [*Hovius et al.*, 1997; *Malamud et al.*, 2004]. Self-organised criticality has proved to be a promising concept in understanding landsliding because it provides a statistical insight into the behaviour of the sliding process and a unifying concept in which landslide processes operate. It also has important implications for modelling and the emergence of macroscopic behaviour.

The application of the self-organising criticality concept has not, however, gone unchallenged. Not all the models of natural phenomena exhibit the necessary critical states [*Sapozhnikov and Foufoula-Georgiou*, 1996]. The definitions and interpretations of self-organised criticality in the literature are not standardised, which hinders comparison of results [*Baas*, 2002]. In the case of landslides, a large extrapolation is

needed when comparing the mathematical 'sandpile' model with real physical settings. The exponent of the power law of landslide distributions is generally higher than the value of 1 obtained from the mathematical 'sandpile' model [*Malamud et al.*, 2004]. Large amounts of data are required to investigate the spatial and temporal scales of landslides. The quantity and quality of field data, however, is generally not good enough to reveal a fractal distribution [*Hergarten and Neugebauer*, 1998]. Other models of self-organised criticality, such as the forest-fire model and the Olami-Feder-Christensen model, use laws that are inconsistent with natural physical processes, or fail on a quantitative level [*Hergarten*, 2003]. The origin of power law scaling can also be attributed to inherent heterogeneity in geology, soil-moisture and structure, for example [*Hergarten*, 2003; *Pelletier et al.*, 1997]. Thus more work is required to explain the power law behaviour of natural phenomena comprehensively.

2.4.4 FRACTALS AND THE STUDY OF SUMBARINE LANDSCAPES

There are few studies that apply the fractal concept to submarine landscapes. Most of these investigate the roughness of seafloor topography using the variogram method, spectral or autocorrelation functions [e.g. *Berkson and Matthews*, 1983; *Fox and Hayes*, 1985; *Goff et al.*, 1991; *Herzfeld*, 1989; *Herzfeld et al.*, 1995]. These authors have shown that the seafloor is neither self-similar nor self-affine. However, they do conclude that seafloor topography may be fractal in the sense of the definition involving the Hausdorff-Besicovitch dimension, and that it is best described by fractal geometry due to different and increasingly detailed features appearing at increasing resolution. There is only one study addressing the fractal characteristics of 2D features [*Goff and Tucholke*, 1997]. There are only two studies that investigate frequency-magnitude distributions of submarine landslides [*Issler et al.*, 2005; *ten Brink et al.*, 2006]. These studies reveal that, like their subaerial counterparts, submarine landslide populations exhibit a power law distribution. However, they do not attempt to understand the origin of this behaviour. There are no studies that investigate whether landslide morphology exhibits scale invariance and/or fractal characteristics. The dearth of studies applying fractal concepts to the submarine environment is due to the lack of high-resolution bathymetric data sets and the few, small and incomplete inventories of submarine

landslides that can be derived. Fractal analyses need high-resolution databases, which have only recently become available for submarine landscapes.

2.4.5 QUESTIONS FOR THIS THESIS

(a) The Storegga Slide has perhaps the best inventory of mass movements of any submarine landslide. Do these mass movements exhibit a power law frequency distribution? If they do, how does the distribution compare to that of subaerial mass movements? What is the origin of this power law behaviour? Can the concept of self-organised criticality explain this behaviour?

(b) Can the concepts of fractal geometry and scale invariance be applied to submarine features in 2D? Can these concepts be applied to submarine mass movement morphology?

(c) How does the application of the fractal concept improve our understanding and/or modelling of submarine landslides?

Chapter 3:

STUDY AREA

3.1 LOCATION AND GEOLOGICAL SETTING

The Norwegian margin is a passive continental margin that developed during the continental break-up between Fennoscandia and Laurentia about 54 Ma ago [*Saunders et al.*, 1997]. The geological evolution of the Norwegian margin has principally been controlled by tectonics, slope instabilities and glaciations [*Rise et al.*, 2005]. The Norwegian margin today is characterised by an up to 200 km wide continental shelf (Figures 3.1; 3.2). The shelf is a result of westerly sediment outbuilding since Pliocene times and is comprised of Plio-Pleistocene prograding wedges composed of glacigenic debris flows interbedded with hemipelagic sediments [*Rise et al.*, 2005]. The shelf is intersected by numerous glacial troughs, the largest and deepest of which is the Norwegian Channel (Figure 3.2). The depth of the continental shelf ranges from less than 150 m to 450 m within the deepest glacial troughs. From the continental shelf, the seabed slopes gently into the abyssal plain of the Norway and Lofoten Basin. The continental slope, which has a maximum slope gradient of 5°, has been characterised by a number of large-scale slope failures that have transferred sediment to the deep basin areas (Figure 3.1; Table 3.1) [*Owen et al.*, 2007]. The best-studied examples are the Storegga, Trænadjupet, Andøya and Nyk Slides [*Haflidason et al.*, 2004; *Laberg and Vorren*, 2000; *Laberg et al.*, 2000; *Lindberg et al.*, 2004]. These slope failures have taken place on slopes as gentle as 1° and they left behind an erosive scar which is partly filled with failed material. They are characterised by steep headwalls and sidewalls, and irregular and locally-steep seafloor topography within the chaotic slide deposits [*Owen et al.*, 2007]. The major slides have occurred soon after a glaciation, which may suggest a tendency for post-glacial timing of movements. Earthquakes are the most commonly quoted trigger on the Norwegian margin, although it is generally recognised that weaknesses in the sedimentary column also facilitate movement if a major earthquake took place [*Canals et al.*, 2004]. The presence of numerous buried slides (e.g. Sklinnadjupet Slide [*Evans et al.*, 2002]) attest to the repetitive slope instability in the Norwegian margin.

The mid-Norwegian margin consists, from south to north, of the Møre, Vøring and Lofoten-Vesterâlen margins. Most of the mid-Norwegian margin is formed by the architecture of the Møre and Vøring margins, which are major sedimentary depocentres

subdivided by structural highs into several sub-basins. The Storegga Slide is situated in the Møre Basin, about 120 km off Kristiansund, western coast of Norway (Figures 3.1; 3.2). The Møre Basin developed as a result of repeated rifting episodes that began in the Late Jurassic (Figure 3.3). These episodes continued in three phases until the Late Palaeocene/Early Eocene continental break-up. Subsequent thermal subsidence resulted in a 10 km thick sedimentary basin [*Brekke*, 2000]. The Møre Basin is separated from the Vøring Plateau to the north by the Jan Mayen Lineament, which is the continental continuation of the oceanic Jan Mayen Fracture Zone. The mid-Norwegian margin also features a number of north-south oriented dome structures, of which Ormen Lange is an example (Figure 3.4). These structures are the result of episodic moderate compression phases between the Late Eocene and the Mid-Miocene [*Brekke and Riis*, 1987; *Vågnes et al.*, 1998].

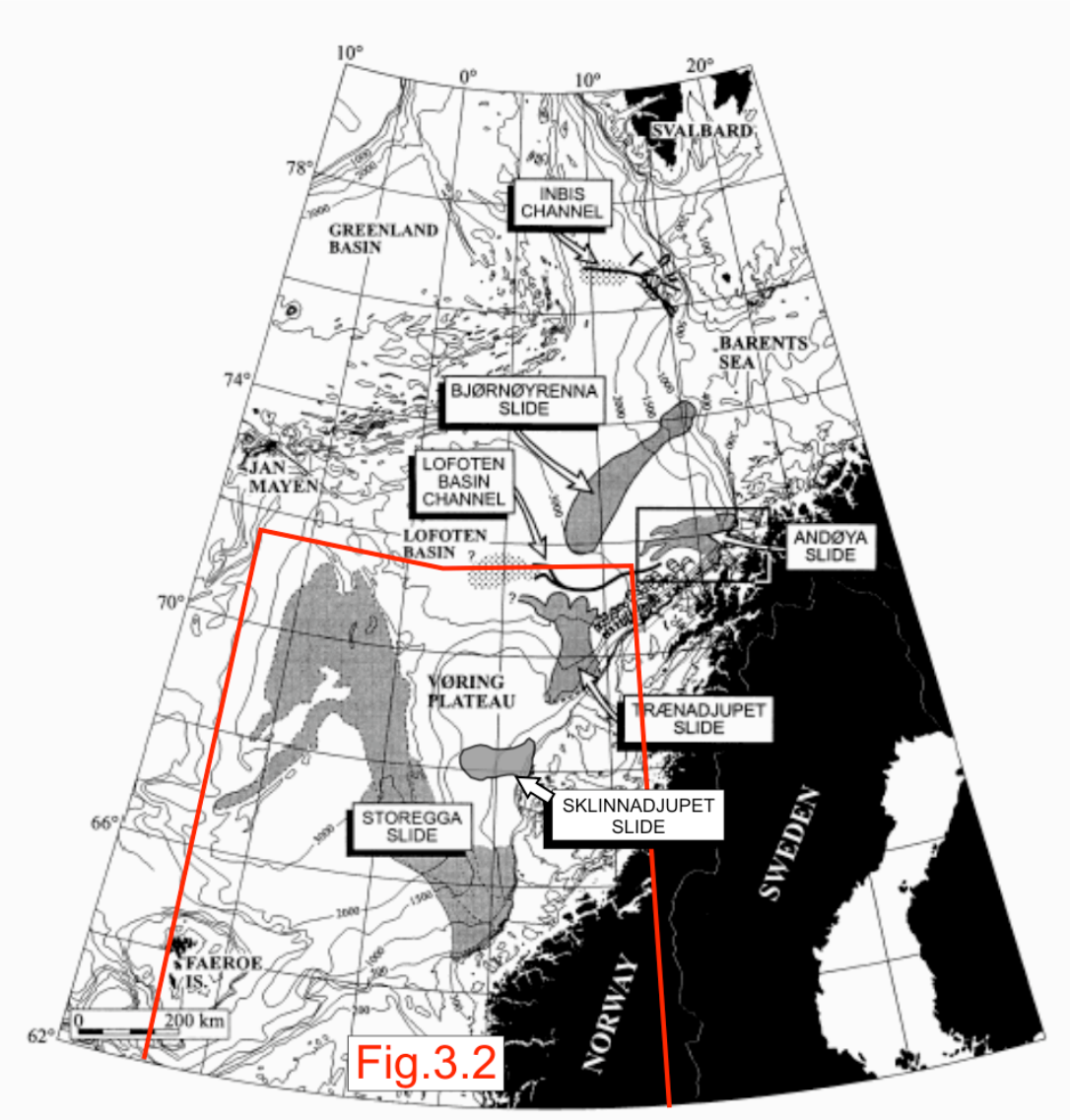

Figure 3.1: Bathymetric map of the Norwegian Margin (contours at 100 m intervals) showing the main submarine landslides and channels.
Source: Adapted from *Laberg et al.* [2000].

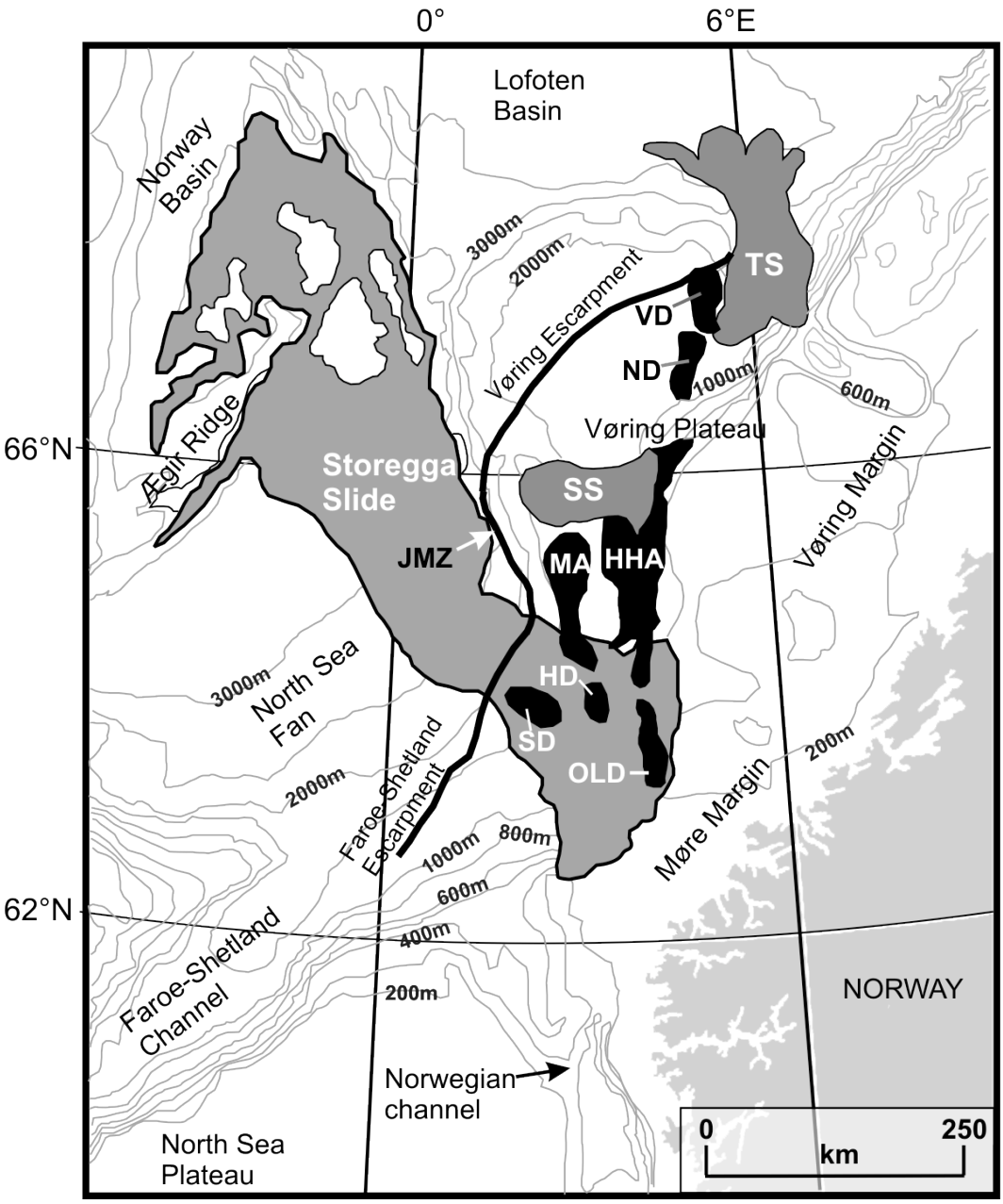

Figure 3.2: Physiography and geology of the mid-Norwegian margin. The limits of the Storegga Slide, the Trændjupet Slide (TS) and Sklinnadjupet Slide (SS) are indicated by a solid black line and shaded in grey. The Ormen Lange Dome (OLD), Solsikke Dome (SD), Havsule Dome (HD), Modgunn Arch (MA), Helland-Hansen Arch (HHA), Naglfar Dome (ND), Vema Dome (VD) and Jan Mayen Fracture Zone (JMZ) are labelled. The shelf break is found between 280 m and 410 m of depth, and represents the western limit of the Norwegian continental shelf.
Source: Adapted from Norsk Hydro A.S.A.

Table 3.1: Dimensions and ages of selected submarine instabilities along the Norwegian Margin.

Slide	Area (km^2)	Volume (km^3)	Run-out distance (km)	Age (cal yrs B.P.)	Reference
Andøya	9700	180	190	10 000	[*Laberg et al.*, 2000]
Hinlopen	10 000	1350	300	Pre-Last Glacial Maximum	[*Vanneste et al.*, 2006]
Nyk	> 2200	?	?	16 300	[*Lindberg et al.*, 2004]
Storegga	95 000	2400 - 3200	770	8100	[*Haflidason et al.*, 2004; *Haflidason et al.*, 2005]
Trænadjupet	14 100	900	200	4000	[*Laberg and Vorren*, 2000; *Laberg et al.*, 2002a]

3.2 STRATIGRAPHIC FRAMEWORK

Between 54 and 2.6 Ma, sedimentation within the Storegga Slide region was dominated by the fine-grained oozes and shales of the Brygge and Kai formations [*Roekoengen et al.*, 1995] (Figure 3.3). On the top of these formations is the Naust formation, which encompasses a thick, low-angle wedge of clastic sediments and sheet-like units of the Plio-Pleistocene. The thickness of the Naust formation exceeds 1000 m over extensive areas [*Rise et al.*, 2005]. The development of the Naust sedimentary sequences was controlled by the Fennoscandian ice sheet growth and retreat patterns [*Laberg et al.*, 2002b]. The first major glaciation of Fennoscandia is thought to have occurred at 2.6 Ma [*Jansen and Sjøholm*, 1991], although repeated ice sheet advance across the mid-Norwegian continental shelf has only been documented since about 0.5 Ma [*Dahlgren et al.*, 2002; *Sejrup et al.*, 2000]. During peak glaciation, the grounding line of the ice-sheets was pushed forward to the continental shelf edge. Sediment, primarily consisting of glacial diamictons, was transported by fast flowing ice streams in the form of deformable till beds [*Dahlgren et al.*, 2002; *Dimakis et al.*, 2000; *Dowdeswell et al.*, 1996]. Sediments deposited at the shelf break were remobilised and transported downslope as debris flows. In the Ormen Lange area, depositional rates during peak glaciation reached values of 1.5 – 2 m kyr^{-1} [*Berg et al.*, 2005]. During interglacials and

periods of retreated ice cover, the depositional rate declined to 0.02 – 0.1 m kyr^{-1} [*Berg et al.*, 2005]. The sediment deposited during this period consisted of fine-grained normal marine and glacimarine clays, which were transported and deposited by ocean currents and hemipelagic sedimentation [*Berg et al.*, 2005]. The Naust formation is therefore characterised by pronounced changes in lithology, comprising stacked accumulations of debris-flow deposits interbedded with hemipelagic and contouritic sediment units. The formation is further subdivided into five sequences (W, U, S, R and O in stratigraphic order) that are linked to the main glaciations [*Berg et al.*, 2005] (Figure 3.3). The boundaries of these sequences are usually regional and vary considerably in thickness [*Sejrup et al.*, 2004]. The Naust O unit is further subdivided into the O1 – O7 sub-units (Figure 3.3).

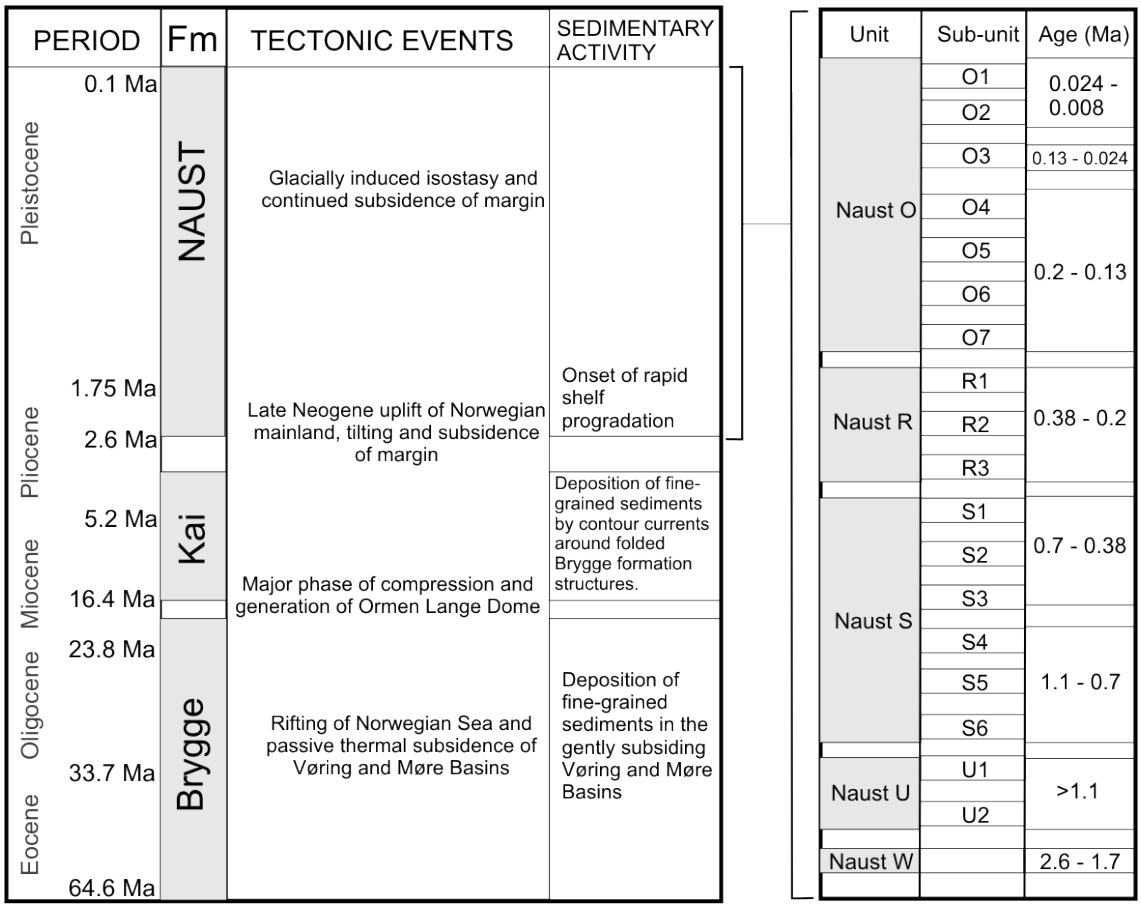

Figure 3.3: Stratigraphic framework, main tectonic events and sedimentary activity that characterised the mid-Norwegian margin during the last 65 Ma.
Source: Adapted from Norsk Hydro A.S. and *Berg et al.* [2005].

The material mobilised during the Storegga Slide comprised the youngest stratigraphic units of the Naust formation, consisting of normally consolidated stratified fine-grained sediment [*Canals et al.*, 2004; *Haflidason et al.*, 2004; *Hjelstuen et al.*, 2005]. The individual mass movements that comprised the Storegga Slide involved the mobilisation of glacial diamicton above a slip surface comprised of marine clay. More consolidated sediments, as well as older sediments, were also incorporated locally [*Bouriak et al.*, 2000]. The slide has cut deepest into the Naust formation sediments in the Ormen Lange region, removing 450 m of sediment [*Bünz et al.*, 2005].

Currently the slide scar is being infilled by soft marine clays deposited under the influence of bottom currents [*Bryn et al.*, 2005b; *Canals et al.*, 2004], which have reduced the slope gradient and deposited contourites of up to 30 m in thickness in the vicinity of the main headwall during the Holocene [*Sejrup et al.*, 2004]. Distribution and thickness of post-slide sediment is heavily influenced by the present surface ocean circulation, as the eastern branch of the northward flowing Atlantic water passes over the Ormen Lange and upper Storegga Slide [*Haflidason et al.*, 2004]. Sediment is supplied from the erosion of the North Sea Fan and areas to the south [*Bryn et al.*, 2003].The deposition rate in the areas surrounding the slide has been much lower, in the order of 0.2 m kyr^{-1} [*Hjelstuen et al.*, 2004].

3.3 THE STOREGGA SLIDE

3.3.1 GENERAL MORPHOLOGY

The Storegga Slide , first described by *Bugge* [1983], is marked by a bathymetric depression that leads into the Norwegian basin (Figure 3.2). The shape of the depression is controlled by the Vøring Plateau to the north, the North Sea Fan to the south, and the deeper structural features of the Jan Mayen Fracture Zone and the Faroe-Shetland Escarpment. The depression has been accentuated by recurring downslope-oriented sediment movements that have dominated this part of the mid-Norwegian margin in the last 3 Ma.

The Storegga Slide is 770 km long and has a maximum width of 255 km. It has a total area of 95 000 km^2, with the slide scar comprising 30% of this area [*Bryn et al.*, 2005a; *Canals et al.*, 2004]. The most recent studies suggest a maximum estimated volume of 2400 - 3200 km^3 for the slide, a value which is considerably lower than the 5580 km^3 originally estimated by *Bugge et al.* [1987]. This still makes the Storegga Slide one of the largest submarine mass movements known, and it is an order of magnitude larger than other high latitude submarine slides (Table 3.1) [*Haflidason et al.*, 2004]. The main slide headwall is situated along the shelf break, in water depths of 150 – 400 m. The headwall is 320 km long and forms a scarp having slope gradients of 10º - 45º, and reaching heights of up to 160 m. The headwall is composed of stable overconsolidated glacial clays, and is commonly disrupted by features such as pockmarks and iceberg ploughmarks [*Evans et al.*, 1996; *Gauer et al.*, 2005].

The Storegga Slide scar corresponds to a vast bathymetric depression that is located downslope of the shelf break (Figure 3.4). This zone is bounded by a 120 km long northern sidewall, which is up to 100 m high, rugged and interrupted by smaller slope failures, and a smooth and pronounced 200 km long southern sidewall. The slide scar area is wide, cauliflower-shaped and roughly semi-circular. The seafloor is characterised by a number of extensive and gentle terraces separated by long and steep headwalls and scarps (Figure 3.3). The distance between the headwalls and scarps varies from 10 km along the northern sidewall to 50 km in the deeper part of the slide [*Kvalstad et al.*, 2005]. At these headwalls and scarps the slide stepped from one slip surface to the next. The names given to the headwalls are therefore taken from the Naust units that have been cut by the slides (Figure 3.5). Only the O and R headwalls are from the Holocene Storegga Slide (Figure 3.5), whereas the Lower and S headwalls are older features [*Bryn et al.*, 2005a; *Riis et al.*, 2005; *Solheim et al.*, 2005]. The mean slope gradient of the seafloor in the slide scar is in the order of 0.7°. The slide scar area narrows downslope into a ~60 km wide corridor bounded by the steep flanks of the Møre and Vøring volcanic highs, which opens into a low-relief broad depositional area [*Canals et al.*, 2004]. The slide scar covers a distance of 300 km from the continental shelf down to the abyssal floor, which is located in the Norwegian Basin at a depth of 2800 – 3000 m. The largest fraction of the sediment mobilised during the Storegga Slide is thought to have been transported in the form of giant turbidity currents and

deposited in the remaining ~500 km downslope of the slide scar, with the most distal deposits being located northwest of the Aegir Ridge.

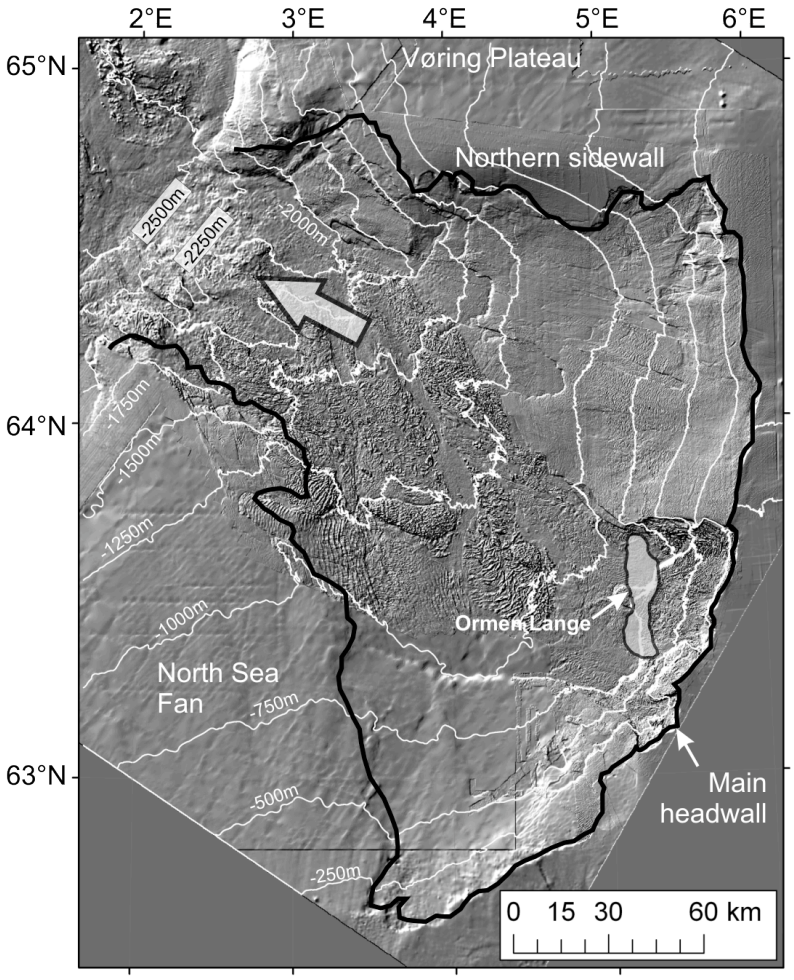

Figure 3.4: Shaded relief map of the Storegga Slide scar. The solid black line indicates the boundary of the Storegga Slide scar. The white lines represent bathymetric contours at 250 m intervals. The block arrow denotes the direction of sediment movement.

3.3.2 SLOPE FAILURE PROCESSES AND SLIDE DEVELOPMENT

The slide scar today includes a variety of surface forms that are indicative of the main types of mass movement processes that have shaped the Storegga Slide seafloor (Figure 3.4). These forms vary from the well represented debris flow deposits, to turbidity current pathways, debris slide scars, ridge systems and block detachment zones. The majority of the slide debris has been transported across the deeper part of the slide in the form of gravity flows. The morphology of the central part of the slide scar is dominated by blocky debris flow deposits, whereas ridge and trough patterns are concentrated

along the shallower parts of the scar. A more pronounced and continuous ridge and trough pattern is observed in the south-western part of the slide scar. This is a compression zone formed at some stage in the development of the Storegga Slide. The compression zone is most likely the result of the collapse of the Saalian glacial fan, built out in the Ormen Lange region, and its impact with the southern sidewall [*Bryn et al.*, 2005a].

Originally three distinct Storegga Slide events were identified [*Bugge et al.*, 1987; *Jansen*, 1987; *Kenyon*, 1987]. According to these studies, the First Slide comprised the entire area of the slide scar and had a very smooth morphology. The Second Slide was located in the central part of the slide scar of the former slide and involved a deeper glide plane and more consolidated sediments, which have moved the farthest. The Third Slide had an effect on the central and upper part of the slide, with the mobilisation of sediments of the same consistency as those in the Second Slide. Tephrachronology was used to date the first event to >30 000 ka [*Bugge et al.*, 1987].

The main failure event is now dated to ca. 7250±250 ^{14}C yr BP (8100±250 cal. yr BP) [*Haflidason et al.*, 2005]. The slide is believed to have been a quasi-simultaneous multi-phase event, and to have started in the mid- to lower slope [*Bryn et al.*, 2003; *Haflidason et al.*, 2004]. There is still no clear evidence of the location where the slide was initiated. The most recent results obtained from seafloor surveying combined with high resolution seismic surveys, sediment coring and drilling, published in *Canals et al.* [2004] and *Haflidason et al.* [2004], present five partially superimposed debris flow lobes (lobes 1 – 5) (Figure 3.5). These lobes are interpreted to represent more than 99% of the total volume of sediments released during the Storegga Slide [*Haflidason et al.*, 2005]. The thickest of these lobes was lobe 2, which generated a tsunami up to 12 m high that swept the Norwegian coast and resulted in tsunami deposits on land [*Bondevik et al.*, 1997; *Bondevik et al.*, 2005; *Harbitz*, 1992]. In addition to these five major lobes, there are lobes identified from 58 smaller individual slide events. The dimensions of the lobes range from 2400 km^3 and a run-out distance of 450 km for first major phase, to a volume of 0.01 km^3 for the minor slides located close the headwall [*De Blasio et al.*, 2003; *Haflidason et al.*, 2004]. There are also a few minor slides identified along the northern sidewall, occurring at a later date of 2200 - 5700 cal. yr BP [*Brown et al.*, 2006; *Canals et al.*, 2004; *Haflidason et al.*, 2005]. All of these lobes have been grouped into

six major phases of retrogressive processes, with the size of the slide diminishing upslope from one phase to the next [*Haflidason et al.*, 2004; *Issler et al.*, 2003]. The last stages of the slide involved a slowing down of the retrogressive processes as the sediments became stronger close to the shelf, where they had been influenced by glacial compaction.

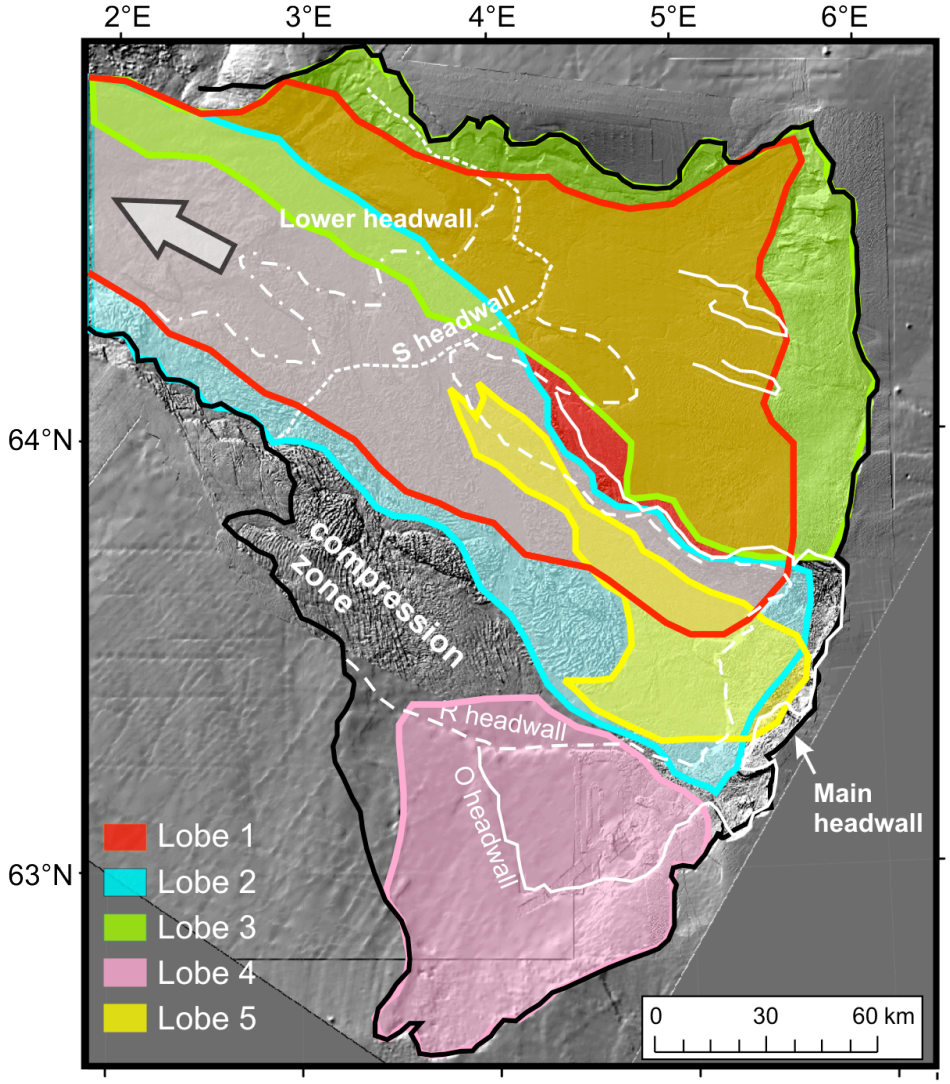

Figure 3.5: Reconstruction of the Holocene Storegga Slide into five large slide lobes. Failure was initiated in the distal part of the slide and developed retrogressively upslope. Most of the sediment from lobes 1 and 3 has been transported as turbidity currents, whereas the deeper, more lithified sediment in lobe 2 has been mobilised as debris flows. The volume of sediment released by lobe 2 was responsible for generating the tsunami and compression zones in the western part of the scar [*Bryn et al.*, 2005a]. The location of the main headwalls is also shown. The Lower and S headwalls predate the Storegga Slide. The arrow indicates the direction of sediment movement.
Source: Adapted from *Haflidason et al.* [2004] and *Bryn et al.* [2005a].

3.3.3 PALAEOSLIDES

Analyses of the internal architecture of the Storegga Slide depression and the surrounding areas point to the intermittent occurrence of a number of large palaeoslides since late Pliocene times [*Evans et al.*, 1996; *Evans et al.*, 2005; *King et al.*, 1996; *Solheim et al.*, 2005]. For instance, the south-western part of the Storegga Slide cuts into the northern part of the North Sea Fan, an important zone of high sedimentation during the Plio-Pleistocene. This depocentre consists of a number of large palaeoslides that occurred in the Naust Succession, including the Vigra Slide, the Møre Slide, and the Tampen Slide [*Evans et al.*, 2005]. The sediments mobilised by these slides consisted of mixed debris flow and laminated suspension-settled hemipelagic and distal glaciomarine sediments. The deposits from these palaeoslides were later disturbed by the Storegga Slide event [*King et al.*, 1996].

In the Storegga bathymetric depression itself, seven slides, ranging from 2400 km^2 to 27 100 km^2 in area, predate the Holocene Storegga Slide, with five of them partly underlying the latest Storegga Slide [*Bryn et al.*, 2003; *Canals et al.*, 2004; *Nygård et al.*, 2003]. The slides occurred at semi-regular intervals during the last 0.5 Ma, in good agreement with the main continental shelf glaciations [*Haflidason et al.*, 2004; *Haflidason et al.*, 2005; *Sejrup et al.*, 2000]. The majority of the slides are found within the glacigenic sediment sequences and follow key seismic horizons [*Solheim et al.*, 2005]. Due to subsequent erosion, the volumes of the older slides are difficult to establish, but it seems likely that some were at least as large as the Holocene Storegga Slide, and that the oldest of these events is found within the lowest unit of the Naust formation, dating to the late Pliocene and early Pleistocene [*Evans et al.*, 2005]. *Solheim et al.* [2005] list some common properties that these palaeoslides seem to share: stability of headwall during slide scar infill, bedding-parallel slip surfaces located in seismically stratified marine clays, and rotated blocks with little internal remoulding and minor displacement located near the headwalls.

3.3.4 CAUSES OF INSTABILITY

The primary cause of instability in the Storegga Slide region is related to the stratigraphic framework outlined in section 3.2. Recent studies with seismic reflection data indicate that the slip surfaces of the Storegga Slide are bedding-parallel, and that slide deposits are bound by the same seismostratigraphic reflectors over long distances [*Berg et al.*, 2005; *Bryn et al.*, 2005a; *Haflidason et al.*, 2003; *Kvalstad et al.*, 2005]. For example, the shallow parts of the slide scar are thought to have failed along the Naust O3 sediment sub-unit, whereas failure in the deeper parts of the Ormen Lange region follows the R2 layer [*Bryn et al.*, 2005a]. Hemipelagic fine-grained sediment and distal glacial marine clay layers are thus the preferred layer for the formation of slip surfaces [*Solheim et al.*, 2005]. This behaviour is a result of the fact that marine clays are more geotechnically sensitive than the glacial clays at the same consolidation stress due to high water content, overpressures, clay content and plasticity, and low unit weight [*Berg et al.*, 2005]. Such a framework can be observed in other submarine landslides along the Norwegian margin (e.g. Trændjupet Slide [*Laberg et al.*, 2002b] and Nyk Slide [*Lindberg et al.*, 2004] (Figure 3.1)).

During peak glaciations, the proximal parts of the Storegga Slide have been affected by rapid deposition of glacial sediment. The last glacial cycle, for example, deposited up to 600 m of sediments within the Storegga Slide region. Underconsolidation due to rapid sedimentation is considered as an additional destabilising factor [*Bryn et al.*, 2003], because the rapid loading of sediment with low permeability causes the development of excess pore water pressure [*Strout and Tjelta*, 2005]. Pore overpressures were created in the contouritic marine clays and the Kai and Brygge formations, reaching values in the order of 20 – 30% in excess of hydrostatic pressure at the shelf edge [*Kvalstad et al.*, 2005]. The Storegga Slide region is particularly predisposed to the lateral transfer of excess pore pressure because it is located between the two shelf edge glacial lobes of the North Sea Fan and Skjoldryggen depocentres [*Canals et al.*, 2004]. Also, the Brygge formation contains compressible material with a higher permeability than the overlying sediment, which allows pore pressures to be transmitted laterally to areas with less overburden.

Sliding is, however, unlikely to occur without the application of external triggers. Earthquake activity is put forward as the most likely of these triggers [*Bryn et al.*, 2005a; *Bugge et al.*, 1988; *Bungum et al.*, 2005]. The distribution of the slides in the north-eastern Atlantic shows clustering around major tectonic lineations [*Evans et al.*, 2005]. The Storegga Slide lies along the line of the most important Norwegian Sea oceanic fracture zone, the Jan Mayen Fracture Zone (Figure 3.2), where frequent and significant modern seismicity is known to have occurred [*Atakan and Ojeda*, 2005; *Bungum et al.*, 2005; *Lindholm et al.*, 2005]. *Dawson et al.* [1988] put forward three likely causes of the Early Holocene seismicity in this region. The first is the widespread loading on the continental shelf by Late Weichselian glaciation and glaciomarine sediments. The second is neotectonic activity induced by glacial unloading and the return of subcrustal material producing post-glacial rebound consequent to the Late Weichselian deglaciation of Fennoscandia. The third is the hydro-isostatic crustal deformation due to rapid sea level change. Seismic activity in Scandinavia is thus thought to have been at its highest between 10 ka and 7 ka [*Bryn et al.*, 2003; *Canals et al.*, 2004; *Gudmundsson*, 1999].

The Storegga Slide region forms a regional embayment in the strike of the margin. This embayment is bordered by bedrock highs formed by the volcanic rocks of the Faroe-Shetland Escarpment and the Vøring Escarpment to the north, and by the glacigenic deposits of the North Sea Fan to the south [*Berndt et al.*, 2001]. Such a structural setting may thus have played a role in trapping seismic energy, amplifying ground motions and maximising the effects of earthquake activity [*Lindholm et al.*, 2005].

In the Storegga Slide, bottom simulating reflectors (BSRs) have been identified north of the slide that extend into the eastern part of the slide scar area [*Bouriak et al.*, 2000; *Bouriak et al.*, 2003; *Bünz et al.*, 2003; *Bünz and Mienert*, 2004; *Nouzé et al.*, 2004; *Paull et al.*, 2007; *Sultan et al.*, 2004]. A BSR consists of a continuous reflection of medium to high amplitudes and reversed polarity relative to the seafloor reflection, and is used as an indicator for the presence of gas hydrates and associated free gas. *Bugge et al.* [1987] observed the existence of gas hydrates at the same depth as the glide plane on the northern sidewall of the Storegga Slide. There is little indication of gas or gas hydrates on the North Sea Fan, but an abundance of gas-related features has been revealed by acoustic surveys on the northern sidewall of the slide [*Bünz et al.*, 2003;

Gay and Berndt, 2007; *Mienert et al.*, 2005]. Gas hydrate dissociation was dismissed as the major trigger of the Storegga Slide because hydrate stability modelling indicates that the critical hydrate stability conditions, and therefore the maximum potential pore pressure build up, occur in the shallower parts of the slide close to the main headwall [*Mienert et al.*, 2005]. This does not fit into the retrogressive model proposed for the Storegga Slide [*Haflidason et al.*, 2004]. However, it is still being debated whether gas hydrate dissociation may have played a secondary role by weakening the soil and extending the unstable area.

Chapter 4:

DATABASE

The thesis is based on three types of high-resolution acoustic data sets. These data sets were acquired by the Seabed Project (1996 – 1998) and the Ormen Lange Project (1998 – 2002) industry and academic consortia as a part of the Norwegian Deepwater Program.

4.1 MULTIBEAM BATHYMETRY

The bathymetric data set comprises the Storegga Slide seafloor from the main slide headwall at the continental shelf edge (~200 m depth) down to a water depth of 2700 m. The horizontal resolution varies from 5 m grids in the Ormen Lange area, to 9 km grids in the southern part of the slide scar (ETOPO5 data), although most of the area is covered by data of 25 m resolution or better (Figure 4.1). The vertical precision varies from ± 10 cm to 2 m at depths of up to 800 m, to ±10 m at 2000 m depths or more (E. Sletten-Andersen, pers. comm.). The data consist of integrated multibeam sonar and 3D seismic data that were collected from various systems, including industry-owned near-bottom vehicles. The acquired sonar data were manually edited to remove spurious altitude (edited for gyro, heave, pitch and roll), navigation (edited for speed and distance between fixes) and bathymetric data. In the case of the latter, a mild filter was used to initially limit bathymetry data points. The data were then geographically registered on a UTM Zone 31 (WGS84) grid and viewed in colour relief. This was carried out to identify and remove points where obvious problem bathymetry data were seen. The bathymetric surveys are considered to be very geographically precise because they were carried out using a state-of-the-art satellite navigation system.

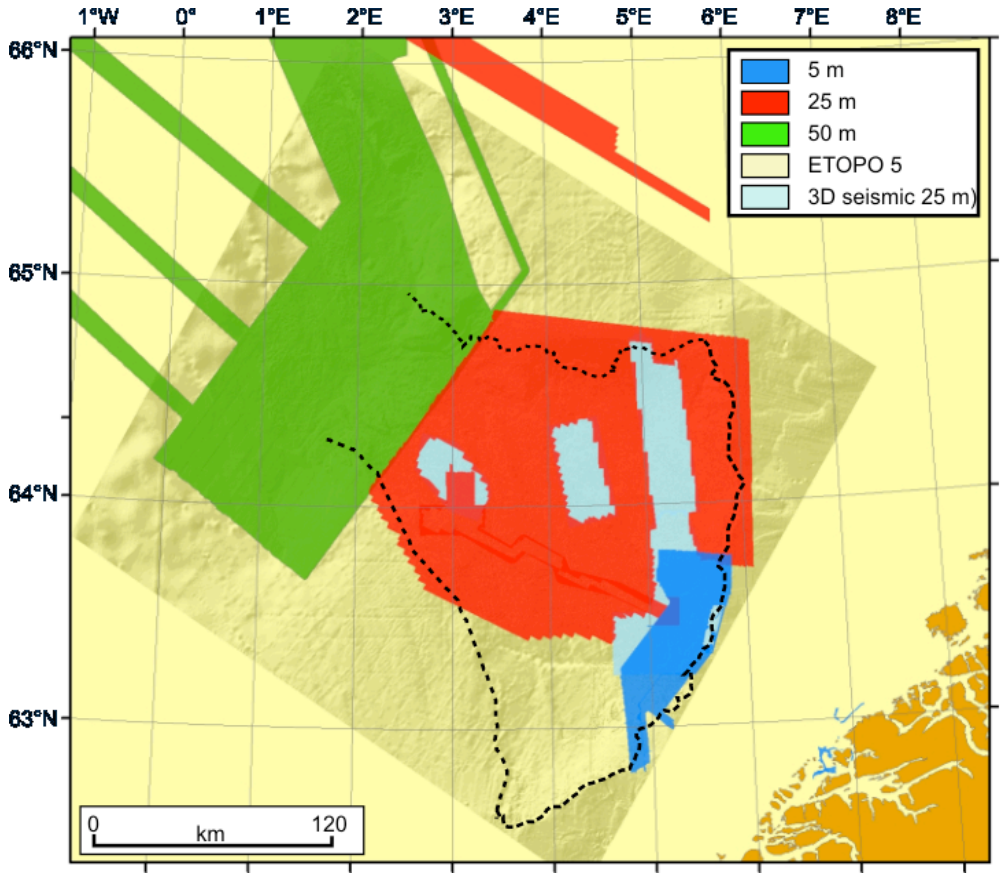

Figure 4.1: Coverage and spatial resolution of the Storegga Slide bathymetric data. The black dotted line denotes the Storegga Slide scar boundary.

4.2 TOWED OCEAN BOTTOM INSTRUMENT (TOBI) SIDESCAN SONAR IMAGERY

The TOBI sidescan sonar system operates at a frequency of 30 kHz and 32 kHz on starboard and port side, respectively. This results in a swath width of up to 3000 m on each side, which produces an acoustic footprint that varies from about 4 m along-track by 7 m across-track close to the vehicle track, to about 40 m along-track by 2 m across-track at far range [*Le Bas*, 1995]. 20 000 km^2 of TOBI sidescan sonar imagery were compiled from surveys of the Storegga Slide scar (Figure 4.2). These images have a nominal resolution of 6 m. TOBI imagery was processed, digitally mosaiced and geographically corrected at the National Oceanography Centre, Southampton, using PRISM (Processing of Remotely-sensed Imagery for Seafloor Mapping) software package. Processing of the TOBI sidescan sonar data comprised the following procedures:

- Smoothing of the altitude of TOBI above seafloor by a median filter
- Merging of ship navigation and cable data with the imagery, and calculation of the TOBI position using an inertial navigation algorithm
- Smoothing of the TOBI gyro heading values using a one minute smoothing filter
- Slant-range correction assuming a flat bottom
- Correlation of port and starboard sides to search for interference noise
- Application of a median filter to remove high or bright speckle noise
- Dropout removal for large imagery dropouts
- Across-track equalisation of illumination on an equal range basis

The sidescan sonar surveys were carried out using the same navigation system as for the bathymetric surveys. However, the geographical precision of the TOBI imagery is lower because the TOBI vehicle is towed a few kilometres behind the vessel. Significant errors in the accuracy of the geographical position are introduced because the TOBI vehicle is assumed to lie on the ship track and its position is corrected for layback delay [*Haflidason et al.*, 2004]. As a result, the inaccuracy of TOBI imagery position may be up to 100 m, particularly at turning points.

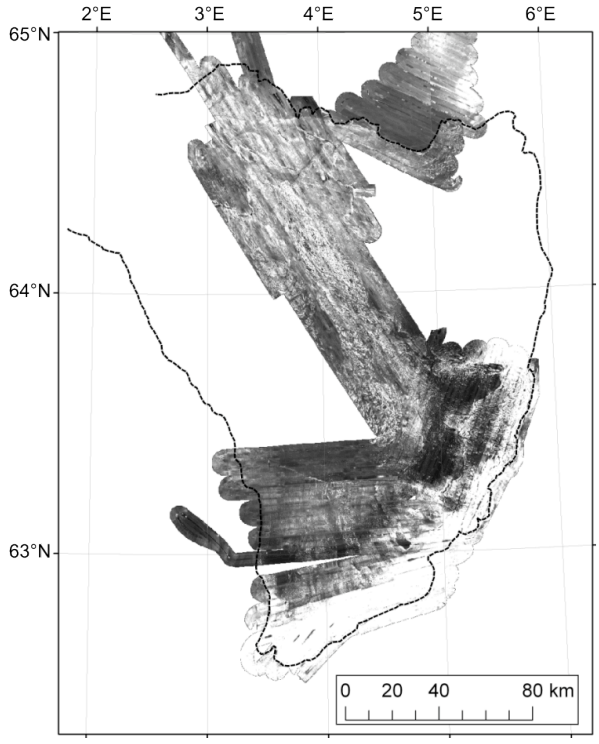

Figure 4.2: Coverage of the TOBI sidescan sonar imagery. The black dotted line denotes the Storegga Slide scar boundary.

4.3 SEISMIC DATA

Both 2D and 3D seismic data sets are available for this study (Figure 4.3).

The 2D seismic data comprise a series of high-resolution seismic profiles located across the main Storegga Slide headwall and the northern sidewall. These have a horizontal sampling density of 6.25 m and a vertical resolution of ~2 m. The surveys were carried out using a source that consisted of two mini-GI air guns immersed at 1.5 m, which enabled the production of an acoustic frequency ranging between 20 and 300 Hz. The data were geometrically attenuated and migrated, and processed using a low-pass filter.

The industry-type 3D seismic data were shot during September 2001 with a dual source Bolt 1900 LLX T airgun array, in a 10 streamers configuration. Processing of the data included source signature deconvolution, surface consistent multiple suppression, binning to a 25 m grid and Kirchhoff pre-stack time migration. The 3D seismic data set covers a 2000 km^2 area across the northern sidewall. The data have a 25 m bin spacing and ~5 m vertical resolution near the surface.

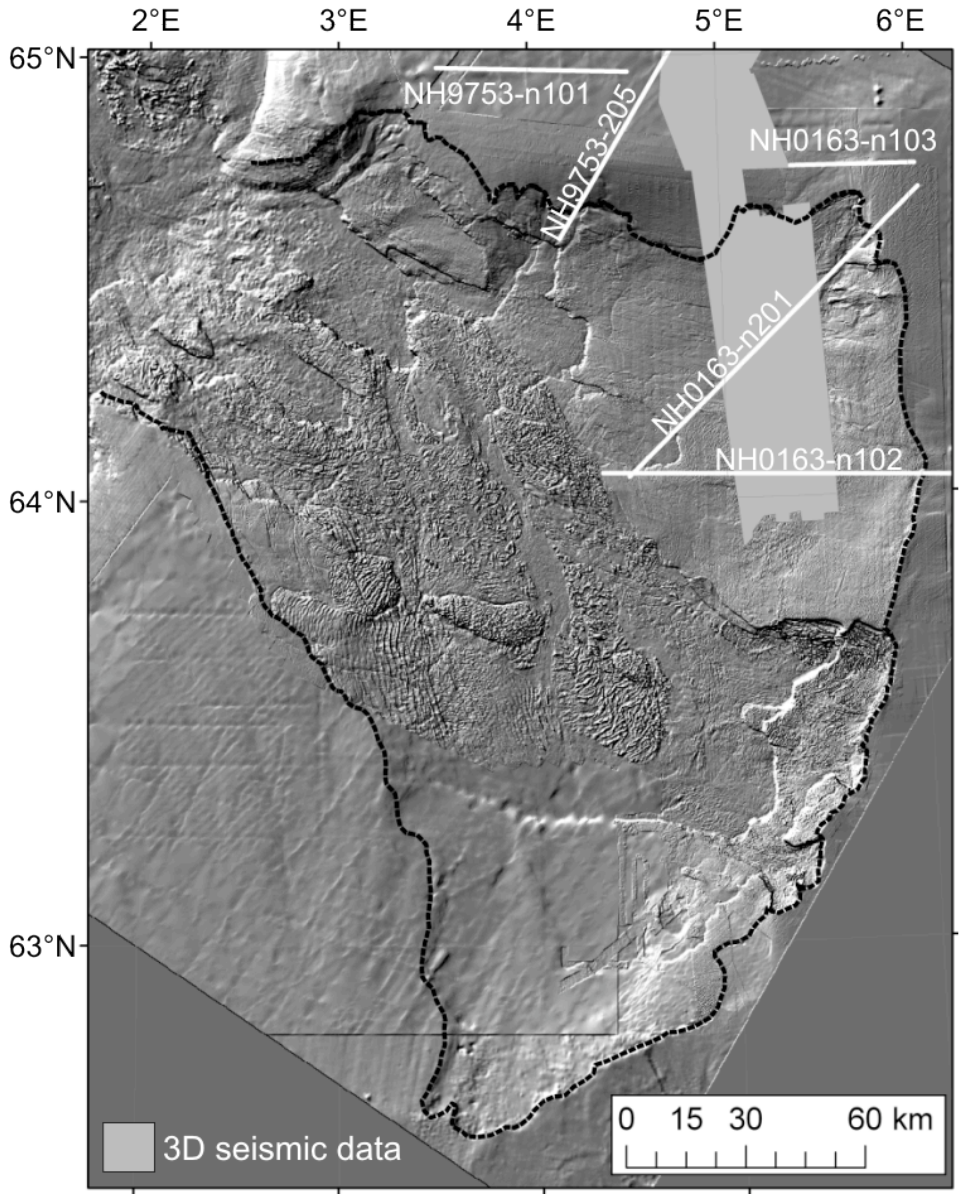

Figure 4.3: 2D seismic lines (solid white lines) and the 3D seismic polygon (in grey) located on a shaded relief bathymetric map of the Storegga Slide scar. The solid black line denotes the Storegga Slide scar boundary.

4.4 DATA VISUALISATION AND ANALYSIS SOFTWARE

Eleven geospatial analysis software packages were reviewed and tested using sample bathymetric and sidescan sonar data sets. This was carried out to understand which software package worked best for acoustic data visualisation and the analysis procedures described in chapters 5 – 8. The tested software packages were:

(a) ArcGIS 9.1 (ESRI)
(b) DiGEM (http://member.aol.com/oconrad/dgm/dgm_main.htm)
(c) ER Mapper Professional
(d) ERDAS Imagine 8.7 (Leica Geosystems)
(e) GMT [*Wessel and Smith*, 1991]
(f) GRASS (http://www.baylor.edu/~grass/index2.html)
(g) IDRISI (Clark Labs)
(h) LandSerf (http://www.geog.le.ac.uk/jwo/research/LandSerf/index.html)
(i) MicroDEM (http://www.nadn.navy.mil/Users/oceano/pguth/website/microdem.htm)
(j) Surfer 8 (Golden Software)
(k) Terrain Analysis System [*Lindsay*, 2005]

The criteria for the selection of the best software package were simple and rapid visualisation of spatial data in 2D and 3D, the availability a wide range of geospatial and statistical analytical techniques, and the potential for software development. After the tests were carried out, it was concluded that ArcGIS and ERDAS Imagine best satisfied these criteria. As a result, all data visualisations and analyses presented in this thesis were carried out using these two software packages.

The visualisation and interpretation of the seismic data were carried out using Kingdom Suite software (Seismic Micro-Technology).

Chapter 5:

METHOD

A technique for the morphological characterisation of submarine landscapes as exemplified by debris flows of the Storegga Slide.

Aaron Micallef, Christian Berndt, Douglas G. Masson and Dorrik A.V. Stow

This chapter is a research article that has been published in the Journal of Geophysical Research – Earth Surface, Volume 112, Page F02001, doi:10.1029/2006JF000505. The manuscript was submitted on the 23rd March 2006, accepted on the 15th of November 2006 and published on the 3rd of April 2007.

5.1 INTRODUCTION

Geomorphometry is the quantitative description of landscapes [*Pike and Dikau*, 1995]. It is based on the assumption that there is a close quantitative relationship between surface processes and topographic characteristics [*Moore et al.*, 1991], and that these characteristics contain geological information that can be extracted by numerical analysis. Since the 1970s geomorphometry has increasingly been based on Digital Elevation Models (DEMs). DEM analyses generally involve the process of taking derivatives of altitude to compute morphometric attributes, and the summarisation of these attributes using moment statistics [*Evans*, 1998]. A more thorough investigation is achieved by using spatial derivatives of these initial attributes (e.g. topographic wetness [*Moore and Neiber*, 1989]). An overview of the history and state of the art in geomorphometry can be found in *Pike* [2000]. Compared to traditional geomorphological methods, techniques used in general geomorphometry have the benefits of avoiding problems of subjective interpretation and of landform definition prior to analysis. The present challenge in geomorphometry is to delineate landforms from a continuous grid of terrain attributes. This has been dealt with by employing a variety of techniques, among which are feature-extraction and automated pattern recognition algorithms [e.g. *Chang et al.*, 1998; *Chorowicz et al.*, 1989]. On the whole, however, geomorphometry has remained a non-systematic set of techniques, and no standardised methodology for the quantitative study of landscapes and the extraction of landforms is available.

Geomorphometry has been applied successfully in a variety of subaerial settings: e.g. fault morphology [*Florinsky*, 1996], drainage basins [*Gardner et al.*, 1990] and deep-seated landsliding [*Roering et al.*, 2005]. Today the discipline is stimulated by the need to explain inaccessible or enigmatic landscapes. Whereas geomorphometric techniques have become a standard tool in the investigation of planetary landscapes [e.g. *Aharonson et al.*, 2001], their application to submarine environments has been more infrequent. Some examples of the latter include the use of spectral models to classify ridge-crest terrains [*Fox*, 1996] and the automated extraction of submarine drainage systems [*Pratson and Ryan*, 1996]. In general, the geological interpretation of submarine landscapes tends to be relatively more subjective, with shaded relief maps

being one of the standard tools of bathymetric data representation. Submarine landscapes and bathymetric data have a number of characteristics that makes the application of traditional geomorphometric techniques problematic. First, in comparison to terrestrial landscapes, submarine topographies are generally smoother and changes in elevation occur over more extensive areas [*Shepard*, 1963]. The features of interest are also larger and extend over considerable depth ranges [*Hühnerbach and Masson*, 2004; *Masson et al.*, 2006]. This means that the range of morphometric attributes and their statistics, over which changes in the landscape can be observed, are in general much narrower than for subaerial terrains. Capturing submarine terrain variability using traditional geomorphometric techniques is therefore more difficult. Secondly, whereas there exists the possibility of ground-truthing subaerial DEMs and satellite images, this is very hard to achieve in submarine environments. As a result, geomorphometric techniques for the study of submarine landscapes need to be very robust, combining results from a variety of methods to ensure that the outcome is a genuine representation of the topographic variability. Thirdly, since submarine DEMs cover more extensive areas than subaerial DEMs, they are bound to include data sets of different resolutions. The resolution of the same data set is also bound to change with depth [*De Moustier and Matsumoto*, 1993]. The outcomes of geomorphometric techniques depend very much on data resolution [*Evans*, 1975]. Thus, integrating results from different techniques should help overcome the sensitivity of the individual techniques to different resolutions.

In this paper we adapt a number of geomorphometric techniques to the submarine environment and propose a methodology for the study of bathymetric data sets. We apply these techniques to a high-resolution bathymetry data set from the Storegga Slide (Figure 5.1), the largest documented submarine landslide on glacially-influenced margins [*Bugge et al.*, 1987; *Canals et al.*, 2004]. Bathymetry data sets contain a wealth of information that is generally not fully exploited by the marine geologist. The very high resolution of our data set, combined with the diversity of topographic features encompassed, makes the Storegga Slide an ideal site for the development of submarine geomorphometric techniques.

The objectives of this study are to: (1) adapt established geomorphometric techniques and develop a methodology for the improved quantitative analysis of submarine elevation data and (2) to test the applicability of this methodology by applying it to the morphological interpretation of debris flow deposits.

5.2 METHODOLOGY AND OBSERVATIONS *

In this section we will describe the data set available for this project and the techniques used to analyse it. The methods in sections 5.2.2 and 5.2.4 - I involve an adaptation of techniques used in subaerial geomorphometry, whereas the methods in sections 5.2.3 and 5.2.4 – II are new techniques developed during this Ph.D.

5.2.1 DATA SET INFORMATION

The Storegga Slide lies 70 – 150 km off the western coast of Norway, in the Norwegian Sea (Figure 5.1), and covers an area of ~95 000 km^2, including 27 000 km^2 of slide scar [*Bryn et al.*, 2003; *Canals et al.*, 2004]. The most recent studies have shown that the Holocene Storegga slide was a multi-phase retrogressive event with an estimated volume of 2400 – 3200 km^3 [*Canals et al.*, 2004; *Haflidason et al.*, 2005]. The slide scar consists of a vast bathymetric depression that includes a variety of mass movement forms, ranging from spreads to turbidity currents.

*(Note: the methods described in section 5.2 are explained in more detail as a series of procedures in ArcGIS 9.1 in the DVD accompanying this thesis).

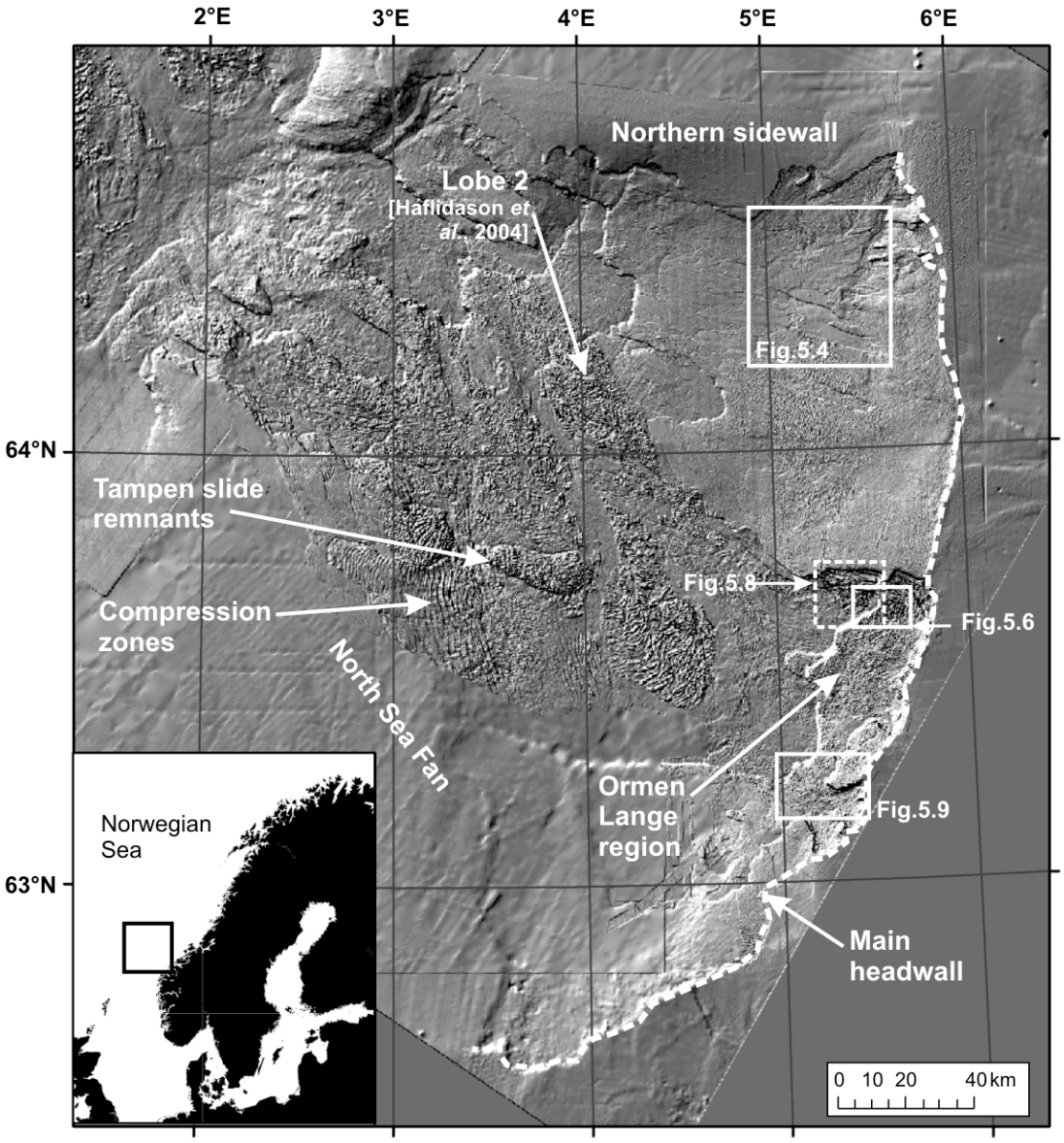

Figure 5.1: Shaded relief map of the study area and the major topographical features. Boxes indicate the location of Figures 5.4, 5.6, 5.8 and 5.9.

Our investigation of the Storegga Slide is based on high-quality bathymetry data that comprise the Storegga Slide seafloor from the slide headwall at the continental shelf edge down to a water depth of 2700 m. The horizontal resolution varies from 5 m grids in the Ormen Lange area, to 9 km grids in the southern part of the study area (ETOPO5 data), although most of the area is covered by data of 25 m resolution or better. The vertical precision varies from ± 10 cm to 2 m at depths of up to 800 m, to ±10 m at 2000 m depths or more (E. Sletten-Andersen, pers. comm.).

For this study, we selected an area that includes the main scar of the Storegga Slide, extracting 53 million elevation data points that are represented in a DEM with a cell size of 25 m × 25 m. This was done by interpolation in areas of coarser resolution and aggregation using means in higher resolution areas. The selected resolution of the DEM was found adequate for subaerial slope analysis by *Nogami* [1995]. All techniques are tested in areas where the original data had a resolution of 25 m or better.

5.2.2 MORPHOMETRIC ATTRIBUTES AND STATISTICS

The process of calculating derivatives to obtain morphometric attributes, and of summarising their frequency distributions by taking moment statistics, has been at the basis of altitudinal data analyses since the 1970s [*Evans*, 1980]. The importance of altitude and its primary and secondary derivatives (slope and curvature) to geomorphological studies was recognised by *Curtis et al.* [1965] and *Anhert* [1970] in pedological and slope morphology studies, respectively. The technique was incorporated into geomorphometric systems by *Evans* [1972]. Since then, frequency distribution-based characterisations of a range of different settings have been carried out (e.g. slope instability [*Carrara et al.*, 1977] and hillslope mapping [*Evans*, 1979]).

We started our investigation of the Storegga Slide by computing the following digital morphometric maps of the study area using the Geographic Information System (GIS) ArcGIS: (a) Shaded relief map (using 3× exaggeration and NW illumination); (b) Slope gradient map (in °); (c) Slope aspect map (in °); (d) Profile curvature map (in ° m^{-1}); (e) Plan curvature map (in ° m^{-1}). The attributes were extracted for 3 × 3 cell neighbourhoods using the equations in Table 5.1. The frequency distributions of the morphometric attribute data are presented in Figure 5.2. The frequency distribution of slope gradient data is unimodal and highly positively skewed (Figure 5.2a). This results from the fact that the Storegga Slide is located in a gently dipping depositional environment on a continental slope. The cumulative frequency distribution for the slope gradient shows that, for 90% of the area, the slope gradient is < 4º, while almost 57% of the terrain has a slope gradient < 1º. The point of inflection in this curve is positioned at a slope gradient of 5º (Figure 5.2a). This separates lower relief and gentler terrain from more prominent geomorphological features such as headwalls and blocks in the Ormen

Lange region, Lobe 2, Tampen slide remnants, compression zones, and downslope headwalls. This slope angle is considered an important threshold in the slope angle distribution. When analysed on a circular scale, the mean and standard deviation of slope aspect were determined to be 290.36º and 70.04º, respectively (Figure 5.2b). The slope aspect frequency distribution maxima occur at the NW (315º), W (270º) and SW (225º) directions, with N (0º) having the highest frequency. The graph is characterised by peaks occurring at 45º intervals. The frequency distributions for the curvatures are unimodal and almost symmetrical, and as such do not provide much additional information.

Table 5.1: Formulae used to derive the morphometric attributes.

Attribute	**Formula**
Slope gradient	$\arctan(p^2 + q^2)^{1/2}$
Slope aspect	$-90[1 - \text{sign}(q)](1 - \lvert\text{sign}(p)\rvert) + 180[1 + \text{sign}(p) - 180\text{sign}(p)\arccos[-q/(p^2 + q^2)^{1/2}]/\pi$
Profile curvature	$-(p^2 r + 2pqs + q^2 t)/[(p^2 + q^2)(1 + p^2 + q^2)^{3/2}]$
Plan curvature	$-(q^2 r - 2pqs + p^2 t)/(p^2 + q^2)^{3/2}$

where $p = \frac{\partial z}{\partial x}$; $q = \frac{\partial z}{\partial y}$; $r = \frac{\partial^2 z}{\partial x^2}$; $s = \frac{\partial^2 z}{\partial x \partial y}$; $t = \frac{\partial^2 z}{\partial y^2}$

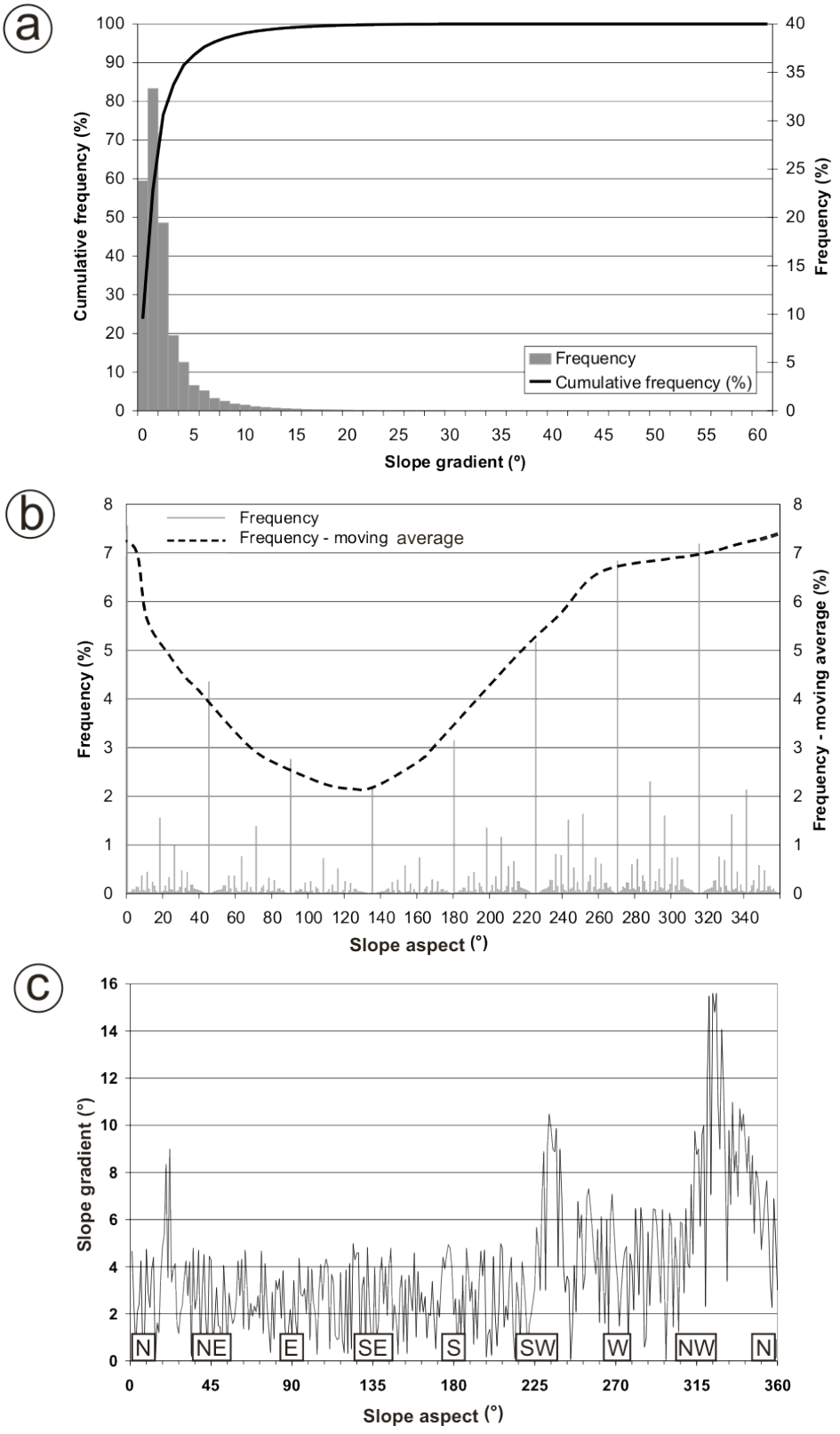

Figure 5.2: Frequency and cumulative frequency distribution for (a) slope gradient and (b) slope aspect, with moving average; (c) Plot of slope gradient against slope aspect for a 2% sample of the bathymetric data from the Storegga Slide.

Bivariate analysis extracts relationships between pairs of morphometric attributes across a DEM. As an example, slope gradient is plotted against slope aspect in Figure 5.2c. Due to the very large number of data points in the study area, data were resampled at 2%, resulting in ~1 million values for each morphometric attribute. The resulting plot is dominated by three peaks. It shows that slopes tend to be steeper than average if they face NNE, SW or NW. When the peaks were displayed on a combined slope gradient-slope aspect map and a shaded relief map, they were found to correspond to the major headwalls in the Storegga Slide. The highest peak displayed is for the NW direction and corresponds to the main slide headwall.

5.2.3 FEATURE-BASED QUANTITATIVE REPRESENTATION

Feature-based quantitative representation describes the morphology of an area through the geometric attributes of individual landforms. Individual or groups of algorithms are applied to classify relief or morphometric attributes into a number of classes of simple forms. Examples of this technique include the extraction of fluvial networks [*Chorowicz et al.*, 1992] and the identification of linear and circular features from satellite imagery [*Raghavan et al.*, 1995].

I GEOMORPHOMETRIC MAPPING

Geomorphometric mapping is a technique developed during this Ph.D. to delineate the boundaries of finite geomorphometric objects from the continuous grid of morphometric attributes. A geomorphometric map is a parametric representation of the general morphology of a landscape. The process entails the identification of morphometric attributes, computational slicing of the domain of each attribute into intervals, and mapping of these intervals. This approach of topographic parameterisation, particularly the use of breaks of slope to identify the boundaries of slope units, is inspired by techniques used in subaerial geomorphological mapping [e.g. *Gardiner and Dackombe*, 1983; *Parsons*, 1988]. A virtual field study was carried out, using a 3D visualisation of bathymetry, to identify the elementary morphological units of the landscape. The four fundamental features recognised were: (a) Break of slope: A change in slope gradient between adjacent cells that is higher than 10º. This feature was

divided into three groups: Low (10° - 20°), medium (20° - 30°) and high (>30°). (b) Change of slope: A change in slope gradient that is > 5º and < 10º. Changes of slope can be either convex or concave. (c) Sloping surface: An area, larger than 1 km^2, with a constant slope aspect and gradient, the latter being < 5°. (d) Blocks and ridges: features of positive relief that occur either in isolation or in a repetitive pattern.

A dendrogram (Figure 5.3), which attributes a range of morphometric attribute values to the first three features, was constructed. The extraction of blocks and ridges is described in detail in section 5.2.4. The choice of the thresholds of the ranges for each morphometric attribute was based on observations of the morphometric attribute maps, on their frequency distributions and moment statistics. As an example, the lower limit for changes of slope is based on the turning point identified in the cumulative frequency curve of slope gradient occurring at 5° (Figures 5.2a and 5.3). We simplified the technique by restricting the use of attributes as discriminating variables to profile curvature, slope gradient, slope aspect and elevation differences, which have previously been shown to be effective in describing subaerial landforms [e.g. *Giles*, 1998; e.g. *Graff and Usery*, 1993]. We then extracted each feature based on the dendrogram. To extract the breaks and changes of slope, the profile curvature raster image was reclassified into the five classes of profile curvature specified in the dendrogram (Figure 5.3). In this way, a range of profile curvature values was flagged to a class, which made it possible to contour each class separately. The height of the break of slope was calculated for 200 points using trigonometry. The sloping surfaces were extracted by first generating a slope aspect map of the study area with a cell size of 1 km × 1 km. Then a contour map of slope gradient for the range 0º - 5º was produced at 0.5º intervals, displaying regions of constant slope gradient. The two maps were combined, and slope arrows were manually drawn in areas of constant slope aspect bounded by a slope contour. The slope direction was read from the aspect map while the slope gradient was derived from the slope contour map.

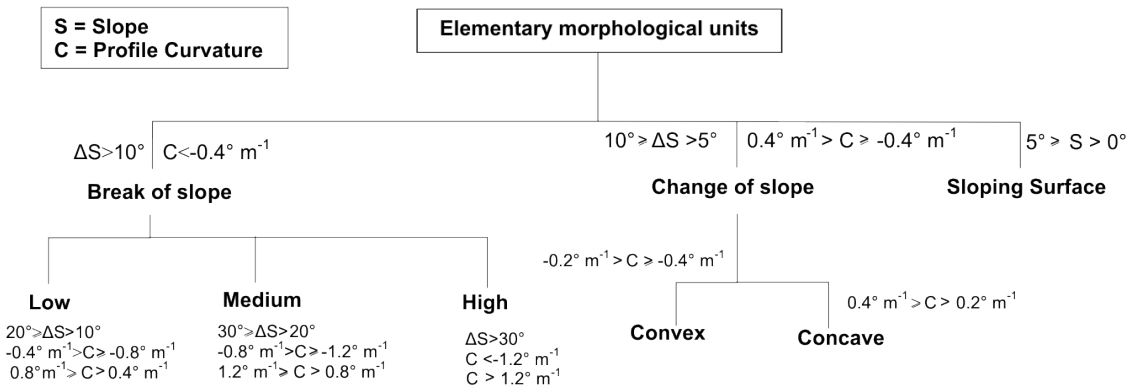

Figure 5.3: Dendrogram of the elementary morphological units based on the survey of ten testing areas within the Storegga Slide.

Figure 5.4 shows a geomorphometric map displaying the above fundamental morphometric features for a part of the Storegga Slide. Interpretation of the geomorphometric map is best carried out using all geological knowledge available for the area. The extracted lineaments mainly correspond to boundaries of geomorphological features. For instance, the breaks of slope shaped in a Z-form in the south-central part of the map correspond to the flanks of two debris slides. The height of the sidewalls ranges between 32 m and 39 m. In the northeastern part of the map are located two elliptical features and an extensive void area. These represent two mounds located upslope of the exposed failure plane of Lobe 1 [*Haflidason et al.*, 2004]. In order to verify whether the extracted lineaments do correspond to actual morphological features, the geomorphometric map from a different part of the Storegga Slide was draped over a 3D visualisation of the bathymetry, as shown in Figure 5.5. A low break of slope is located at the top of the 150 m high headwall where the terrain suddenly becomes steeper, whereas a concave change of slope follows the foot of the scarp where the terrain is gentler. Additionally, a convex change of slope exists in the central part of the headwall slope.

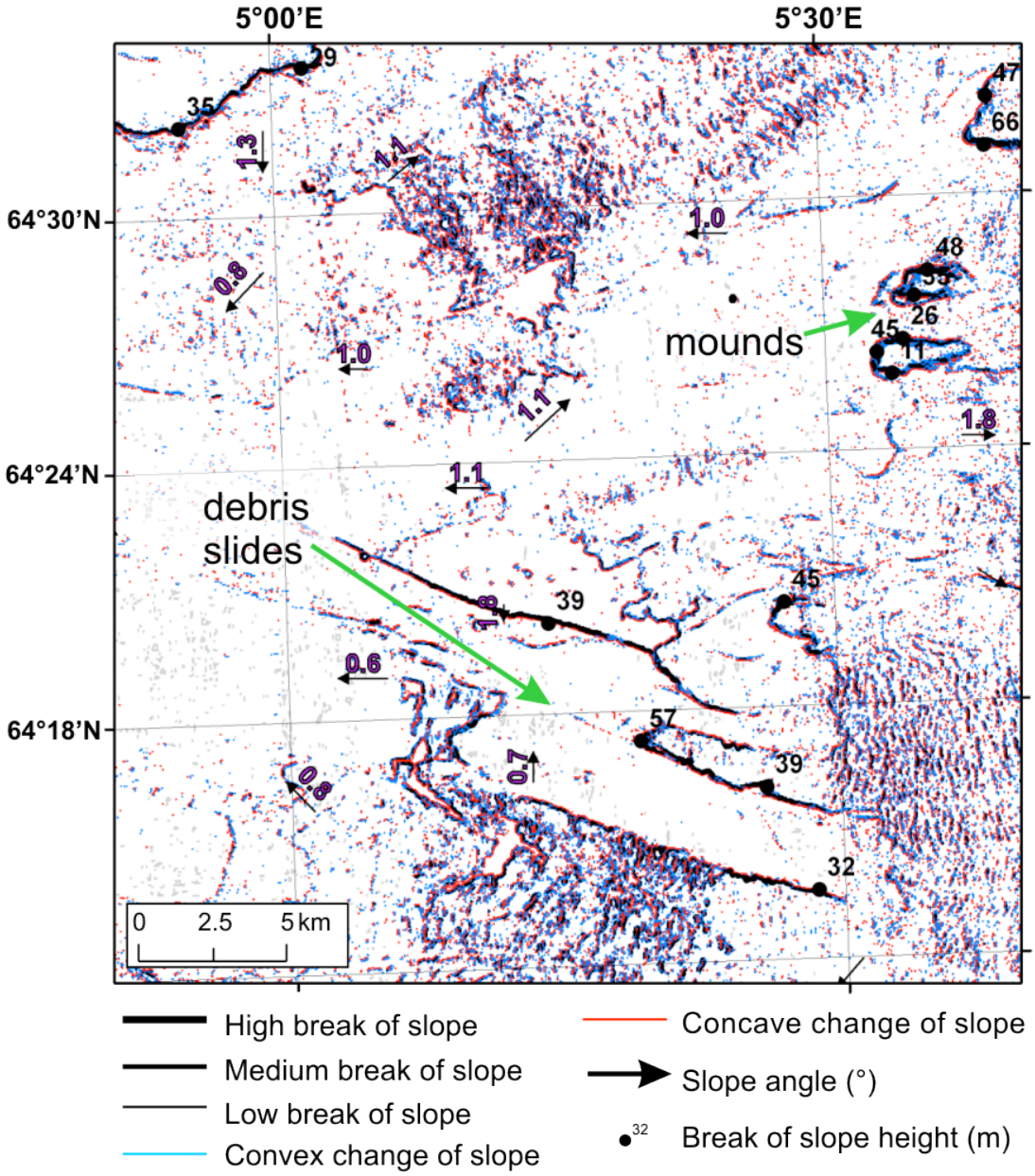

Figure 5.4: Part of the geomorphometric map south of the northern sidewall, with breaks of slope, changes of slope, sloping surfaces and breaks of slope heights. A break of slope is a change in slope gradient between adjacent cells that is higher than 10º (Low (10° - 20°), medium (20° - 30°) and high (>30°). A change of slope is a change in slope gradient that is > 5º and < 10º.

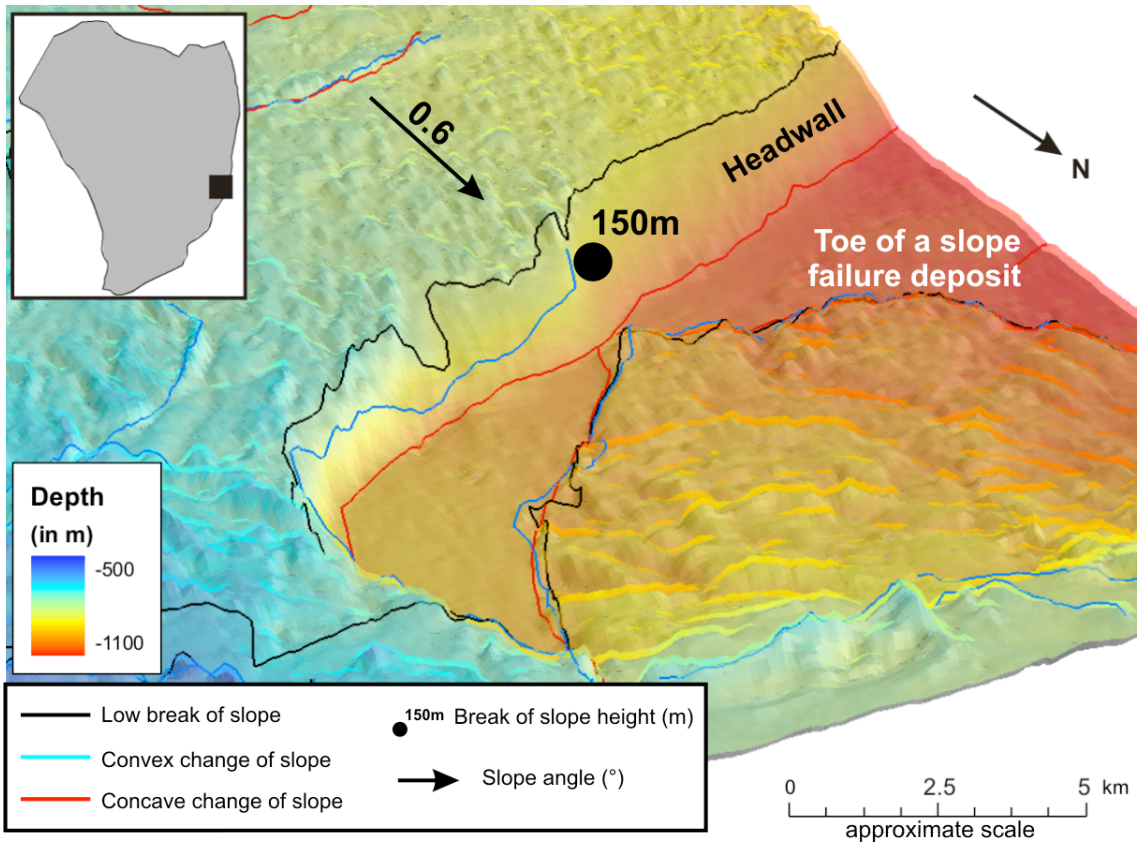

Figure 5.5: A geomorphometric map of a part of the Storegga Slide draped over a 3D visualisation of the landscape, showing that the numerical methods are able to extract geomorphometric elements reliably. Note the convex change of slope within the slide headwall, which could have been easily overlooked in a manual interpretation.

II RIDGE CHARACTERISATION

The Storegga Slide scar is characterised by terrain that is quite different to what is generally observed in subaerial landscapes. Apart from the headwalls and scars, the various sediment mobilisation and deposition processes within Storegga have resulted in a surface that consists of an extensive pattern of ridges, troughs and blocks. This pattern yields additional geomorphological information to that garnered from the breaks and changes of slope, and it was fundamental to *Haflidason et al.* [2004]'s identification of individual slide lobes in the Storegga Slide. The pattern in the study area ranges from the linear and repetitive to blocky and chaotic. For simplicity, we refer to these patterns as a ridge pattern from this point forward. Although the ridge pattern is occasionally picked out by the geomorphmetric mapping technique explained earlier,

here we propose a new method for the systematic extraction of the ridge pattern and associated morphological characteristics.

Ridges in the Storegga Slide were characterised using a suite of GIS tools. The ridge extraction approach involves implementing a runoff simulation technique to the Storegga Slide by considering the DEM as a dry impervious subaerial landscape. If a hypothetical precipitation event was to take place, water runoff would be expected to flow down the ridges' sides, accumulating in the troughs and leaving the crests dry. Thus, a standard GIS hydrology tool known as flow direction routine can be applied to the elevation data set to generate a raster file representing the theoretical flow direction of water in each raster cell. This file was then used in another GIS tool, known as flow accumulation routine, which created a raster file of accumulated flow to each cell by summing the weight of all cells that flow into each cell downslope. Since ridge crests would constitute the driest part of the landscape, they have zero flow accumulation. Thus, we extracted these cells. In this way, all the ridges in the study area were automatically vectorised and could be used for further ridge analysis. The resulting pattern is very detailed, counting 1.2 million lines, and is best observed on large maps. A part of the extracted ridge pattern is displayed in Figures 5.6a-d. A transect across a part of this ridge pattern displays the location of the extracted ridges as black dots above the corresponding bathymetric profile (Figure 5.6e). The ridge map was also draped over a 3D visualisation of the bathymetry to validate that the extracted ridge pattern corresponds to the ridge crests.

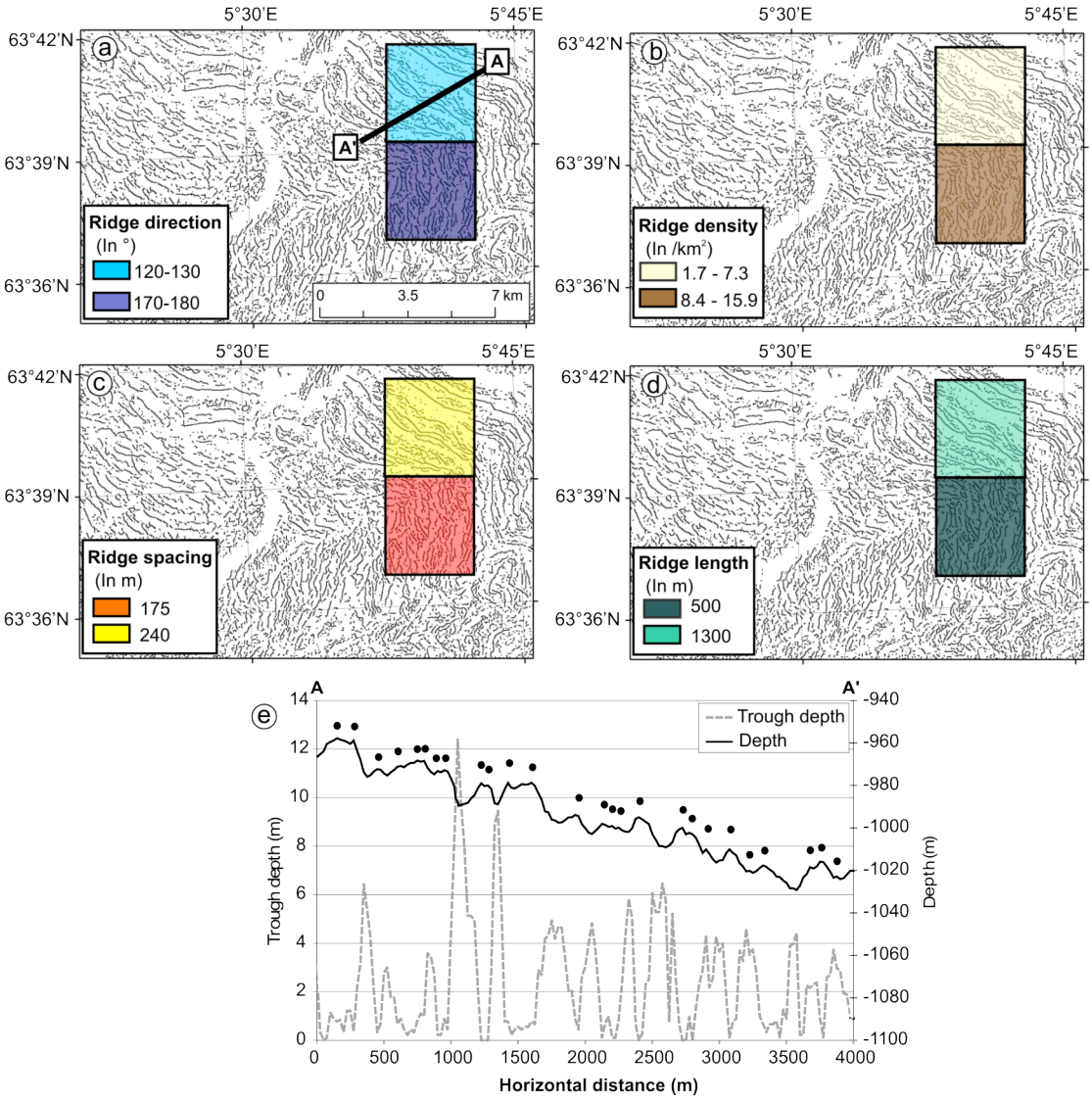

Figure 5.6: Ridge pattern maps for the northern Ormen Lange region, with two cells from: (a) the ridge direction map; (b) the ridge density map; (c) ridge spacing map; and (d) ridge length map. The cells show the mean of the ridge characteristic values over an area of 2.5 km × 2.5 km. (e) Comparison of the bathymetric profile for a 4 km transect, shown in Figure a, with the trough depth curve. The location of the transect is shown in Figure a. The black dots indicate the position of the identified ridges in the ridge pattern map.

Using the digital ridge map it was possible to extract five ridge characteristics: direction, trough depth, density, spacing and length. To obtain ridge direction, we divided the ridge pattern vector file into a grid, and a linear directional mean tool was applied to each grid cell. This tool calculates the mean orientation of lines inside each cell. This resulted in cells representing the orientation of lines in degrees. Figure 5.6a indicates how the direction of the ridge pattern in two adjacent cells can be different,

with the ridges in the southern cell having a more northerly direction than the ridges in the northern cell. The map differentiates the two patterns by attributing different values for the mean ridge direction.

Trough depth can be extracted using the flow accumulation raster image generated earlier. The elevations for the cells with zero flow accumulation values were extracted, converted into a point vector file, and interpolated to generate a raster surface that links the tops of all the crests. The interpolated surface was then subtracted from the original elevation raster image to produce a map of trough depths, which corresponds to the inverse of ridge heights. A comparison between the bathymetric profile and the trough depth curve for a 4 km transect clearly shows that the trough depth peaks coincide with the troughs in between ridges, so that the deeper the troughs, the higher the peaks of the trough depth curve (Figure 5.6e).

Ridge density, i.e. the total number of ridge lines per unit area, was calculated by applying the line density function to the grid cells layered on the ridge pattern map (Figure 5.6b). Ridges in the southern cell on Figure 5.6c are more frequent than those in the northern cell. The ridge density map portrays this by assigning values of 8.4 - 15.9 km^{-2} to the southern cell, compared to values 1.7 - 7.3 km^{-2} for the northern cell.

Ridge spacing was determined by converting the ridge pattern to a raster file. The distance of each cell from the closest ridge cell was measured using the Euclidean distance tool in GIS. The peak values of the generated distance raster file, which correspond to the highest distance of single cells from two adjacent ridges, were extracted in the same way as the ridge pattern was extracted from the elevation data set earlier. Once the peak values were available, they were multiplied by 2 to represent the spacing between two ridges. Figure 5.6c shows how the technique differentiates between the widely spaced ridges in the northern cell and the closely spaced ridges in the southern cell.

Finally, the length of each ridge was measured using the x- and y- co-ordinates of the ridge line vertices, and a mean value was taken for a grid cell. In Figure 5.6d, the

shorter ridges in the southern cell are assigned a mean ridge length of 500 m, whereas the calculated mean length for ridges in the northern cell is 1300 m.

5.2.4 AUTOMATED TOPOGRAPHIC CLASSIFICATION

So far we have concentrated on the identification of geomorphometric elements and boundaries as linear features. Also important for a thorough morphological assessment of a landscape is its segmentation into homogenous relief units enclosing regions with uniform landform distribution. The assumption for using this technique is that similar geological and geomorphological processes operate within regions sharing similar topographies [*Etzelmüller and Sulebak*, 2000]. We classify the Storegga Slide surface using two approaches.

I MOMENT STATISTICS

The first type of classification is based on the concept of surface roughness. Surface roughness has been defined in different ways in the past [*Evans*, 1990] and it lacks a definite measurement scale. In this paper we define surface roughness as the deviation of the terrain surface from a perfectly smooth terrain due to the presence of positive/negative relief features. The greater the height between the apex of the feature and the surrounding terrain, and the more frequent the features are, the higher the surface roughness. Therefore, the presence of features such as ridges, headwalls and blocky deposits increases the surface roughness of the terrain. *Evans* [1990] suggested that the following moment statistics of morphometric attributes can be used in measuring components of surface roughness: mean and standard deviation of slope gradient, and standard deviation of elevation, profile and plan curvature. Here we calculated these five moment statistics for grid cells 500 m × 500 m in area.

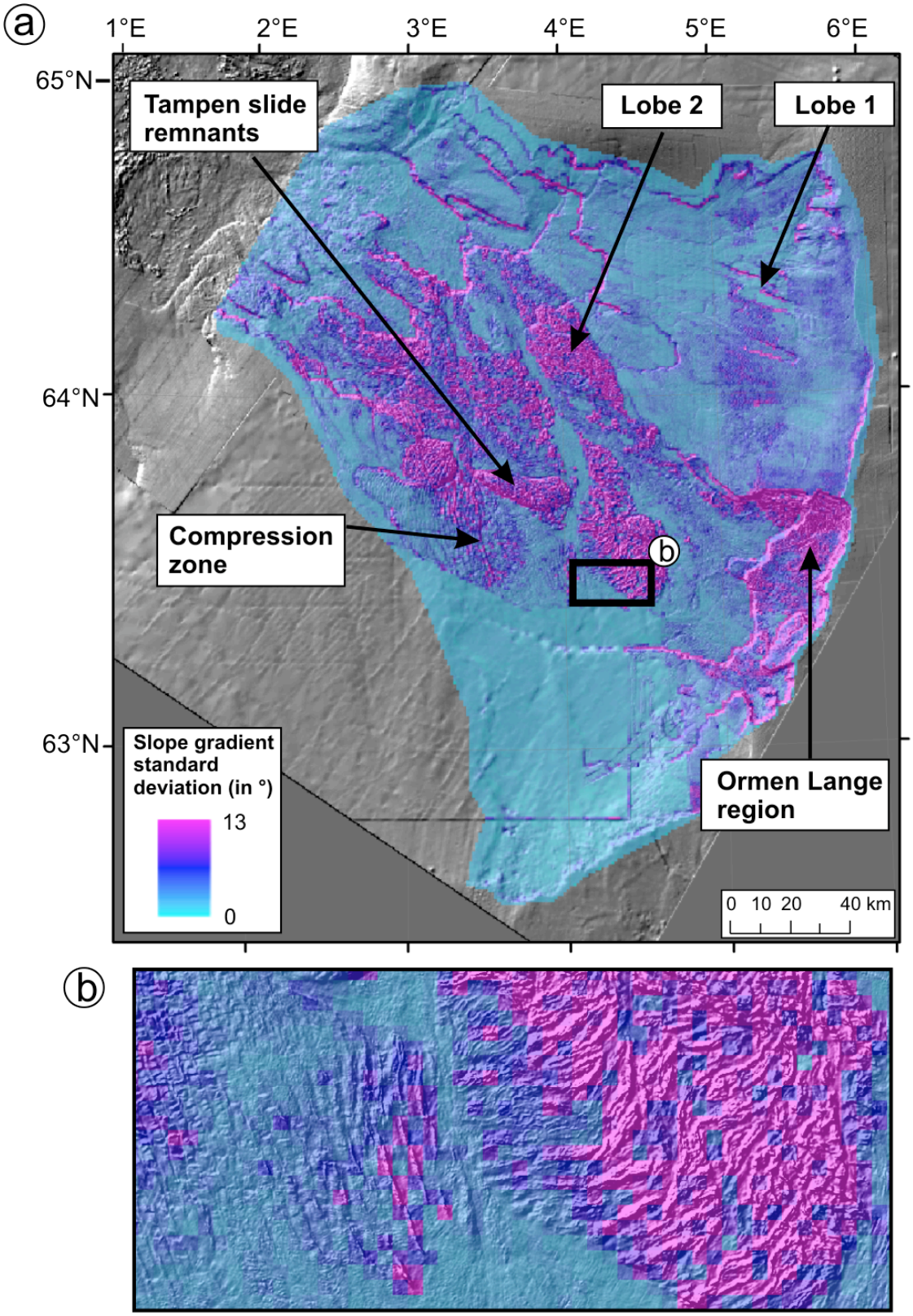

Figure 5.7: (a) Slope gradient standard deviation map of the Storegga Slide and the main topographic features. (b) Enlargement of the area enclosed by the black box, showing a progressive increase in surface roughness eastwards.

All the moment statistics are highly correlated (Table 5.2). Thus, only the standard deviation of slope gradient is considered in detail. Figure 5.7a shows the spatial variation of the standard deviation of slope gradient. The highest values for the slope gradient standard deviation are found in the headwalls, scarps, blocky deposits, Tampen slide remnants, Ormen Lange region and lobe 2 deposits. For example, the headwalls and spreads in the northern part of the Ormen Lange region are characterised by high values of slope gradient standard deviation, whereas lower values are recorded in the failure plane of lobe 1 located just north of this region. A more detailed inspection of the slope gradient standard deviation map draped on the shaded relief map (Figure 5.7b) confirms that a progressive reduction in slope gradient standard deviation westwards is equivalent to a lower surface roughness, which is distinguished by fewer and shallower ridges.

Table 5.2: Correlation of the five moment statistics used to represent surface roughness.

	Mean of slope gradient	**Standard deviation of slope gradient**	**Standard deviation of elevation**	**Standard deviation of profile curvature**	**Standard deviation of plan curvature**
Mean of slope gradient	-	0.90	0.82	0.89	0.81
Standard deviation of slope gradient	0.90	-	0.82	0.90	0.91
Standard deviation of elevation	0.82	0.82	-	0.79	0.83
Standard deviation of profile curvature	0.89	0.90	0.79	-	0.85
Standard deviation of plan curvature	0.81	0.91	0.83	0.85	-

II ISODATA

The second method involves the description of multivariate data in terms of clusters of data points that possess strong internal similarities [*Duda and Hart*, 1973]. One of the most widely used unsupervised clustering algorithms is Iterative Self-Organising Data Analysis Technique (ISODATA). This technique defines natural groupings of multivariate data in attribute space [*Adediran et al.*, 2004] and is a commonly used algorithm in satellite image classification and civil engineering [*Hall and Khanna*, 1977]. The ISODATA method uses the Euclidean distance between each pair of data points in a *k*-dimensional attribute space to form clusters. The technique is based upon estimating some reasonable assignment of cells to candidate clusters, and then moving them from one cluster to another so that the sum of the squared errors of the preceding session is reduced. The output of the classification is a digital thematic map where each cluster is represented by a different class. More detail on the technique can be found in *Richards* [1986]. There are several examples of ISODATA being applied to subaerial settings by using morphometric attributes as the input layers. In general, the technique has proved successful at improving the classification of landscapes and extracting morpho-units. *Adediran et al.* [2004] use slope gradient and slope aspect in the classification of a study area in north-central Crete whereas *Sulebak et al.* [1997] apply the technique in Norway using slope gradient and curvature. *Irvin et al.* [1997] use elevation, slope gradient, profile and tangent curvature, topographic wetness index and incident solar radiation as layers for the classification of a valley in Wisconsin, USA, whereas *Medler and Yool* [1998] test the technique using elevation, slope gradient and slope aspect.

This method of classification was applied using two sets of layers. In the first instance, ISODATA was applied to the Storegga Slide in the conventional way using the slope gradient, profile curvature and plan curvature morphometric attribute maps as layers for the classification. In the second instance we replaced these input layers by the standard deviation of slope gradient (section 5.2.4 – I) and the five ridge characteristics maps (section 5.2.3 – II). For both sets the data were aggregated into 500 m × 500 m cells. In both cases, the number of classes was limited to five, because tests carried out using a higher number of classes did not generate significantly different results.

The thematic maps generated by using ISODATA are shown in Figures 5.8b and c. These were evaluated by comparing them with a shaded relief map (Figure 5.8a) and a 3D visualisation. The thematic map produced by the first set of layers (Figure 5.8b) is dominated by scattered cells rather than a continuous coverage by cells from the same class, although a pattern can be distinguished. Class 1 covers the smoother part of the seabed whereas class 2 is representative of the repetitive pattern of shallow and short ridges located upslope of the headwall. Class 4 partly covers the deeper ridges in the south-eastern part of the image. Otherwise, the pattern is chaotic, even if a majority filter is applied to it. Figure 5.8c is the thematic map produced by the second set of layers. It is immediately apparent that the coverage by each class is more continuous. The deep and widely spaced ridges of class 3 are differentiated from the more closely spaced parallel pattern of class 2. Class 5 corresponds to the more disorganised pattern of deeper ridges, whereas the smooth terrain is represented by class 4. On the whole, the classification of the terrain is much improved compared to that in Figure 5.8b.

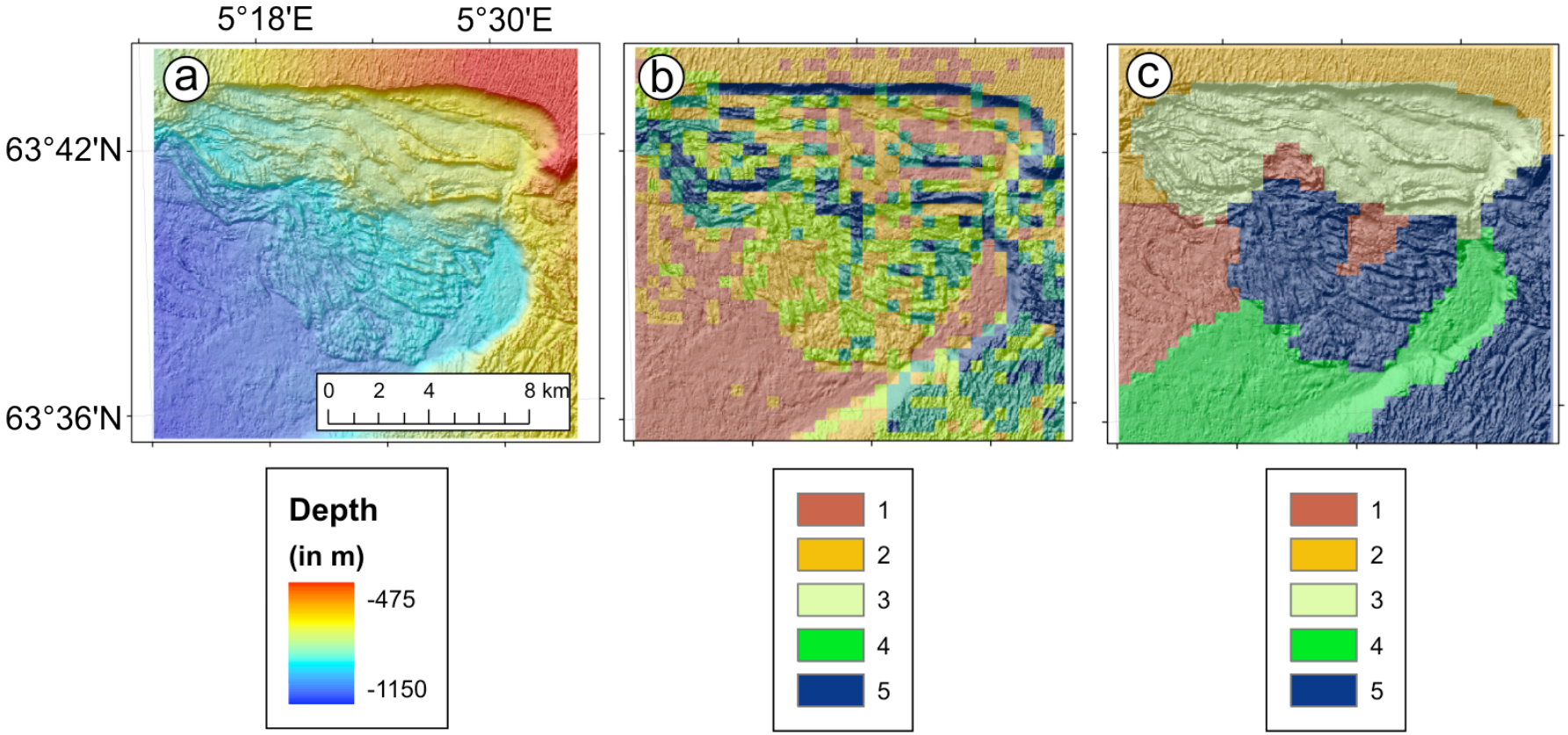

Figure 5.8: (a) Bathymetry of a landslide located north of the Ormen Lange region. (b) ISODATA thematic map produced with slope gradient, profile and plan curvature as input layers. (c) ISODATA thematic map produced with the five ridge characteristics and slope gradient standard deviation as the input layers. In all figures the image has been draped over a shaded relief map of the area.

5.3 DISCUSSION

5.3.1 MORPHOMETRIC ATTRIBUTES AND STATISTICS

Frequency distributions of morphometric attributes and their moment statistics provide morphological information and reveal patterns in a complex landscape. Bivariate analysis, in particular, can be used to examine the relationship between different morphometric attributes of single points in a DEM. This provides morphological information about particular features of the landscape, such as headwalls (Figure 5.2c), and makes them simpler to extract. The information is derived in quantitative form, allowing comparison between different landscapes. The technique also proves useful in providing values for thresholds to be used in geomorphometric mapping. However, it seems that only a limited amount of information may be obtained by applying these geomorphometric techniques to submarine landscapes. The slope gradient frequency distribution is very positively skewed and the majority of the data points are concentrated within a small range. This occurs because changes in elevations in submarine landscapes occur on a much larger scale compared to subaerial landscapes [*Shepard*, 1963]. In addition, the frequency distribution of slope aspect data points is characterised by an overrepresentation of the 45º intervals. This occurs because aspect algorithms do not work well in low relief regions [*Guth*, 2003]. These characteristics reduce the potential of using slope gradient, slope aspect and their derivatives to discriminate between different submarine landscapes. Overall, the frequency distributions and moment statistics of morphometric attributes should only be used for generating summary information about the morphology of a landscape.

5.3.2 GEOMORPHOMETRIC MAPPING

The geomorphometric map displays a complex landscape decomposed into its most elementary morphological units (Figure 5.4). The units are extracted automatically as lineaments that are complemented by topographic information, such as changes in slope gradient and break of slope heights. Draping the geomorphometric map on a shaded relief map and 3D visualisation of the terrain shows that the extracted elements coincide

precisely with the features they are supposed to represent (Figure 5.5). Using this technique on an example site, we were able to identify a convex change of slope in the middle of a steep headwall. This would have been difficult to distinguish if we only based our study on a qualitative interpretation of the site. Geomorphometric mapping is based entirely on the identification and portrayal of changes of form of the slide surface in two-dimensions. This excludes the subjective interpretation of the data set and enhances the accuracy of the morphological investigation. The spatial detail of the digitally generated geomorphometric maps only depends on the resolution of the bathymetric data set rather than the scale at which an observer is investigating the landscape. This ensures that the maximum amount of information available from the DEM is obtained. The only subjective component of this technique is that the user has to define thresholds for the identification of the different features. Because different values for the thresholds can be chosen, this offers versatility in the choice of what morphological units to extract from the bathymetry data set.

The two main drawbacks associated with this technique are that, as in seismic interpretation, correlations between complex landforms may be more easily picked by a human interpreter than by a computer, and that the resolution of the bathymetry data set does have a significant effect on the extraction process. This is evident in the southern part of the Storegga Slide, where data resolution is lowest and where hardly any features were identified. On the whole, computerised geomorphometric mapping is an efficient and versatile technique that produces a simplified representation of landscape in a quick and objective manner.

5.3.3 RIDGE CHARACTERISATION

The ridge pattern identified by the ridge extraction technique is observed to correspond to the bathymetric ridge crests (Figure 5.6), confirming the ability of the technique to identify ridge features in the bathymetric data set. The very detailed ridge pattern is in vector format, which permits the application of lineament analysis [e.g. *Casas et al.*, 2000]. The ridge characteristic maps distinguish between the different patterns of ridge directions, heights, densities, spacing and lengths (Figure 5.6). In this way these maps assist interpretation by extracting additional topographic information and organising it

into manageable grid sizes, as specified by the user. In contrast to the use of moment statistics, the user can control the aspects of ridge morphology on which to base his/her topographic classification.

The digitally extracted ridge characteristics can also be used for further morphometric analysis - one can plot frequency distributions, calculate their moment statistics and analyse their spatial pattern. For example, the trough depth map may be used as an accurate representation of surface roughness, as defined in this paper. The mean trough depth would thus correspond to roughness whereas the standard deviation would represent the variation of roughness within an area. Ridge direction, on the other hand, could be used to measure orderliness – the higher the standard deviation of the ridge direction, the more randomly orientated the features are.

5.3.4 AUTOMATED CLASSIFICATION

A qualitative inspection of the map in Figure 5.7 establishes that the highest values of the moment statistics of morphometric attributes coincide with the most evident irregularities in the terrain such as blocky debris flow deposits, spreading in the Ormen Lange region, compression zones and headwalls. This shows that moment statistics are good proxies for surface roughness and that the method does not depend strongly on the choice of attribute. On the other hand, the fact that the five moment statistic maps are very similar to each other indicates that, unlike in subaerial landscapes, terrain variability can be described by a few descriptors (Table 5.2). This may be practical for classification purposes, but it means that numerous properties of the surface morphology are not being accounted for.

We try to circumvent these problems by combining two types of topographic classification and using as much morphometric information as possible. By introducing moment statistics and ridge characteristics in the ISODATA classification, rather than using the conventional elevation and morphometric attributes, a more accurate and continuous coverage of ridge morphologies is achieved. The surface morphology is well differentiated by the classes, as shown by the different classes representing different ridge lengths, spacings and trough depths in Figure 5.8c. The main advantage

of ISODATA is that it generates summary information about a landscape that is easy to interpret and provides a simplified overview of a complex landscape. The technique is also quick, which allows different combinations of morphometric attributes to be tested. The main disadvantage of ISODATA is that of any unsupervised classification - prior knowledge of the landforms is essential for the results of the classification to be interpreted to their full potential.

There is an extension of the automated topographic classification, which is not discussed further in this paper. The ISODATA technique also generates a signature file that lists the value limits of the input layers used for each class. These limits can be utilised in a supervised classification of the same input layers over a larger area. If classes can be flagged to particular geomorphological features, it would be possible to extract landforms automatically using this technique.

5.4 APPLICATION OF THE TECHNIQUE FOR THE IDENTIFICATION OF DEBRIS FLOW LOBES

A part of the Storegga Slide, the Ormen Lange region, was chosen to test the performance of the proposed geomorphometric techniques in the identification of debris flow lobes (Figure 5.9a). This region is ideal for this study because the original morphology of the debris flow deposits has not been overprinted by subsequently deposited slide material, and the data resolution is highest in this part of the Storegga Slide.

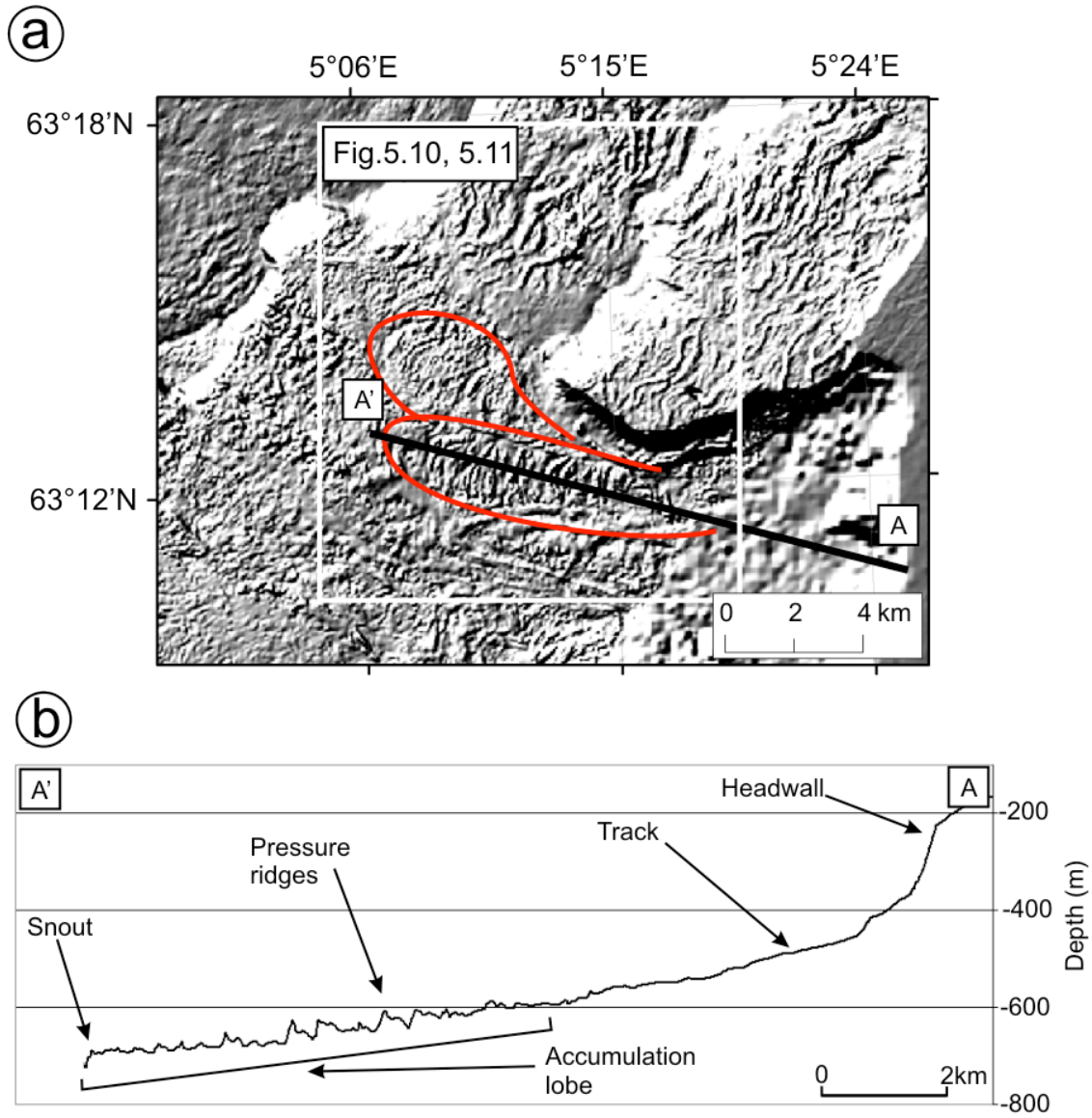

Figure 5.9: (a) Shaded relief map of the two debris flow lobes identified in the southern part of the Ormen Lange region (the red lines indicate the boundaries of the lobes); (b) profile of the transect shown in Figure a.

The dominant mass movement types in the southern part of Ormen Lange are debris flows. A debris flow is a rapid, non-Newtonian flow of dense sediment that covers long distances. The main sediment support system within a debris flow is the strength of the matrix [*Mulder and Cochonat*, 1996]. Three distinct morphological units characterise a typical debris flow [*Corominas et al.*, 1996]: a source, a track and an accumulation zone. The source region is generally characterised by a headwall. The track is the section where material is transmitted from the source to the accumulation zone and lacks the surface roughness that distinguishes the accumulation zone. The accumulation

zone comprises single or overlapping debris flows deposited at the foot of the track in the form of an expanded lobe with steep margins [*Johnson*, 1984]. The longitudinal profile of the accumulation zone consists of elevated terrain with a convex terminal snout. These are represented as a convex change of slope bordered by a concave change of slope. The surface of the accumulation zone may be characterised by rough terrain due to the presence of transverse pressure ridges [*Prior et al.*, 1982] and lateral levée deposits [*Nygård et al.*, 2002]. These features are distinguished by convex crests enclosed by parallel concave changes in slope.

We identified the accumulation zones of two debris flow lobes to test how geomorphometric techniques performed in identifying this type of feature (Figure 5.9a). When investigated in a 3D visualisation of bathymetry, these two features are seen to exhibit all the characteristics of debris flows: elevated accumulation zone with a rougher texture and a lobate form, and linear levées on the flanks. An east-west transect across the southern lobe shows a typical profile of a debris flow lobe (Figure 5.9b). From this plot it is observed that the main headwall of the Storegga Slide constitutes the source of the sediment for the debris flow, which has moved across a relatively steep and smooth track, at the end of which it deposited the sediment in accumulation lobes with pressure ridges and a convex snout.

Having identified the debris flow lobes, we tested how the geomorphometric techniques represent this type of mass movement (Figure 5.10). The geomorphometric map shows continuous, curved convex changes of slope bordered by concave changes of slope indicating the boundaries of a zone of elevated terrain (Figure 5.10a). These changes of slope delimit the snout and the flanks of the lobe and identify different textures on the lobe surfaces, such as the crests of pressure ridges. These have different patterns on the two lobes and can be easily discerned from the smoother surrounding areas (Figure 5.10a). The trough depth map (Figure 5.10b) shows how ridges characterise the accumulation zone of the lobes. These have a height of between 6.5 m and 13 m. The southern lobe (Figure 5.10b) is characterised by particularly high pressure ridges, as denoted by the blue arrow. Zones of low trough depths located outside the lobes, which demarcate the relatively smooth surrounding zones, are also important in distinguishing lobe boundaries. Slope gradient standard deviation (Figure 5.10c) marks the different

surface textures of the lobes. The surface texture of the southern lobe is distinguished by a higher slope standard deviation compared to the northern lobe. This means that the surface of the southern lobe is rougher due to the presence of higher and more ridges (Figure 5.10c). The ISODATA thematic map shows the five classes of ridge morphologies (Figure 5.10d). The southern debris flow lobe is represented by class 4, whereas the northern debris flow lobe is identified in class 2. The smoother surrounding terrain is represented by class 3.

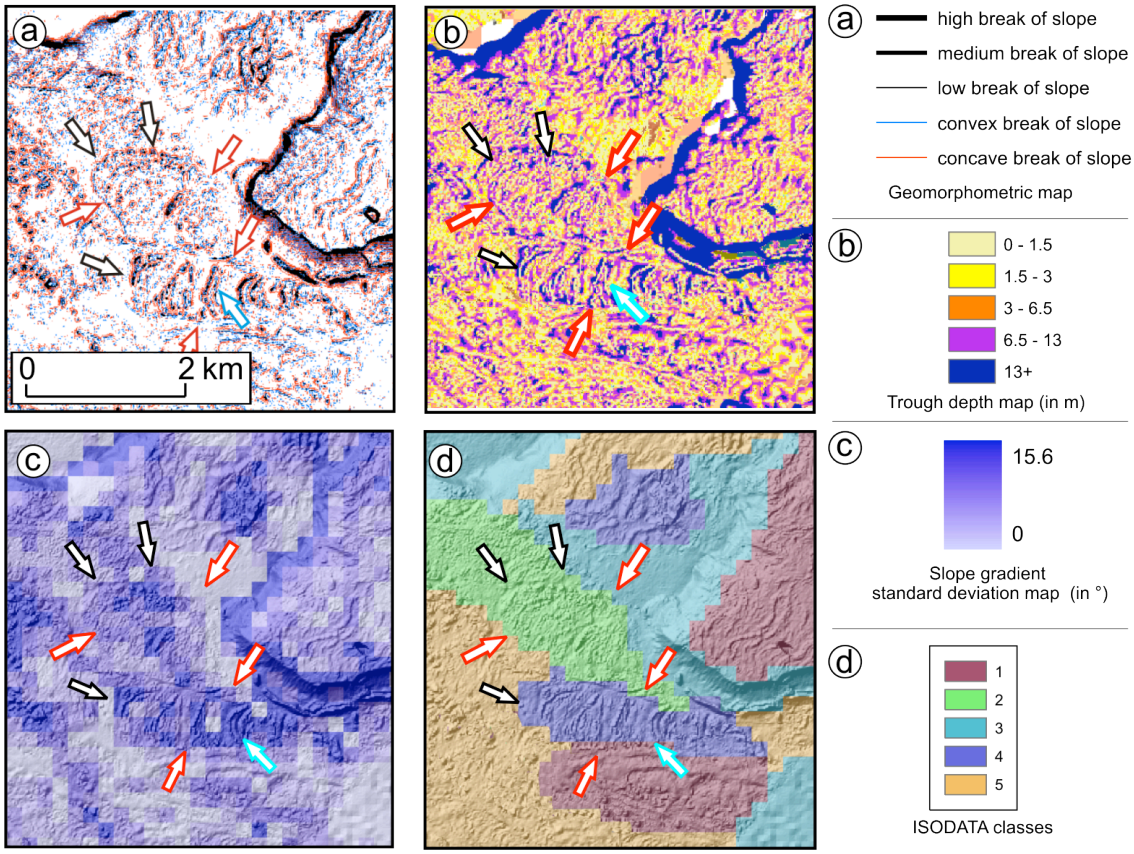

Figure 5.10: Results obtained when applying geomorphometric techniques on the area covering the two debris flow lobes: (a) geomorphometric map; (b) trough depth map; (c) slope gradient standard deviation map; (d) ISODATA thematic map using ridge characteristics and slope gradient standard deviation as input layers. The black reference arrows denote the snout of the identified debris flow lobes, whereas the red and blue arrows indicate the flanks and pressure ridges, respectively.

The results demonstrate how geomorphometric techniques can be used to characterise the morphology of submarine debris flows. The resulting maps delimit the boundaries of morphological features and differentiate between different surfaces. When combined, they allow an accurate geomorphological interpretation of the site to be carried out. To demonstrate this, a comparison is made between two interpretative maps. The first map is re-drawn from the interpretation of *Haflidason et al.* [2004] (Figure 5.11a). The second one (Figure 5.11c) is based on a morphological map produced combining the geomorphometric map with the ISODATA thematic map (Figure 5.11b). Using Figure 5.11b we were able to produce our interpretative map of the mass movements that have occurred within this area of Storegga. Figures 5.11a and 5.11c show the same interpretation in the northern part of the area. However, the two maps vary in the representation of the debris flow lobes in the southern part of the area. The northern debris flow lobe, labelled 'N1' in Figure 5.11c, has not been identified by *Haflidason et al.* [2004]. Furthermore, the boundaries of lobes E7 and E8 are interpreted as shorter and narrower, respectively (Figure 5.11c). Two new overlapping lobes, labelled 'N2' and 'N3', have been identified to the west and south of lobes E7 and E8.

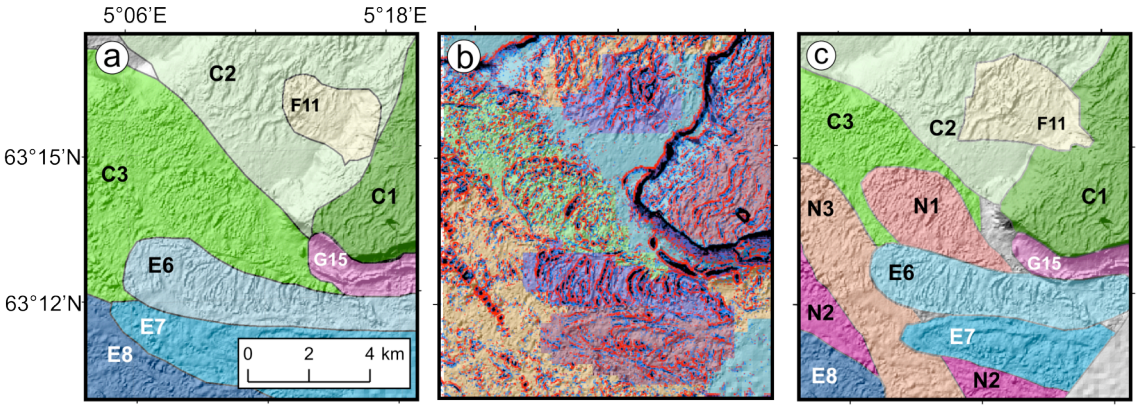

Figure 5.11: (a) An interpretative map of Figure 5.10 re-drawn from Figure 12H in *Haflidason et al.* [2004]. (b) A map combining the geomorphometric map in Figure 5.10a with the thematic map in Figure 5.10d. (c) An interpretative map of the same area produced from the interpretation of Figure b. The lowermost eastern corner of Figure c is noise.

Chapter 6:

RESULTS: SUBMARINE SPREADING

The morphology and mechanics of submarine spreading: A case-study from the Storegga Slide.

Aaron Micallef, Douglas G. Masson, Christian Berndt and Dorrik A.V. Stow

This chapter is a research article that has been published in the Journal of Geophysical Research – Earth Surface, Volume 112, Page F03023, doi: 10.1029/2006JF000739. The manuscript was submitted on the 20th December 2006, accepted on the 17th May 2007 and published on the 1st of September 2007.

An abridged version of this paper has been published in pages 119 – 128 of the book 'Advances in Natural and Technological Hazards Research' edited by Lykousis, V. Sakellariou, D. and Locat, J. and published by Kluwer Academic Publishers in 2007.

6.1 INTRODUCTION

Spreading is a type of mass movement during which a sediment unit is extended over a deforming mass of softer underlying material [*Dikau et al.*, 1996; *Varnes*, 1978]. Where this occurs, the overlying unit breaks into blocks that move on a gently sloping slip surface. The resulting topography is characterised by a 'ridge and trough' morphology, and the horizontal displacement is in the range of a few metres [e.g. *Kanibir et al.*, 2006]. Other terms, such as gravitational spreading, ridge spreading and lateral spreading, have been used to describe this type of mass movement. Spreading has mainly received coverage in the literature on subaerial geomorphology and geotechnical studies [e.g. *Youd et al.*, 2002], where it has been recognised as the most pervasive type of liquefaction-induced ground failure [*Bartlett and Youd*, 1995]. The occurrence of spreading in submarine environments has hardly been documented, as confirmed by its exclusion from submarine mass movement classification schemes [e.g. *Mulder and Cochonat*, 1996]. Only recently has spreading been reported in the Ormen Lange area of the Storegga Slide, a huge Holocene slide scar located offshore Norway. *Kvalstad et al.* [2005a] and *Gauer et al.* [2005] have commented on its occurrence in the Ormen Lange region and have represented the failure process using energy models and numerical simulations, respectively. Nevertheless, information about the characteristic morphology and distribution of submarine spreading, and understanding of the geological processes responsible for its occurrence, remain scant.

A deeper insight into the spreading process is important for at least two reasons. First, infrastructural work related to natural gas exploitation is currently taking place within the Storegga Slide scar, in the vicinity of areas thought to have been affected by spreading. Thus, a better understanding of this process will aid the risk assessment of this potential geohazard. Secondly, the characteristic spreading morphology, in the form of a recurring pattern of ridges and troughs, can be observed in numerous slides around the world, as demonstrated by bathymetric and sidescan sonar data from the Trænadjupet and Nyk Slides in the Norwegian Margin, and the BIG'95 and Eivissa channel Slides in the Mediterranean Basin (Figure 6.1). A similar morphology has also been identified in the recently discovered Hinlopen Slide offshore Norway [*Vanneste et al.*, 2006], the Grand Banks slope failures offshore Canada [*Piper et al.*, 1999] and in

mass movements offshore Mauritania [*Krastel et al.*, 2006]. This shows that spreading is a widespread type of mass movement, and its abundance suggests that it has played an important role in the development of the aforementioned slides. Understanding spreading is therefore a necessary step towards developing more comprehensive models of submarine slope failure.

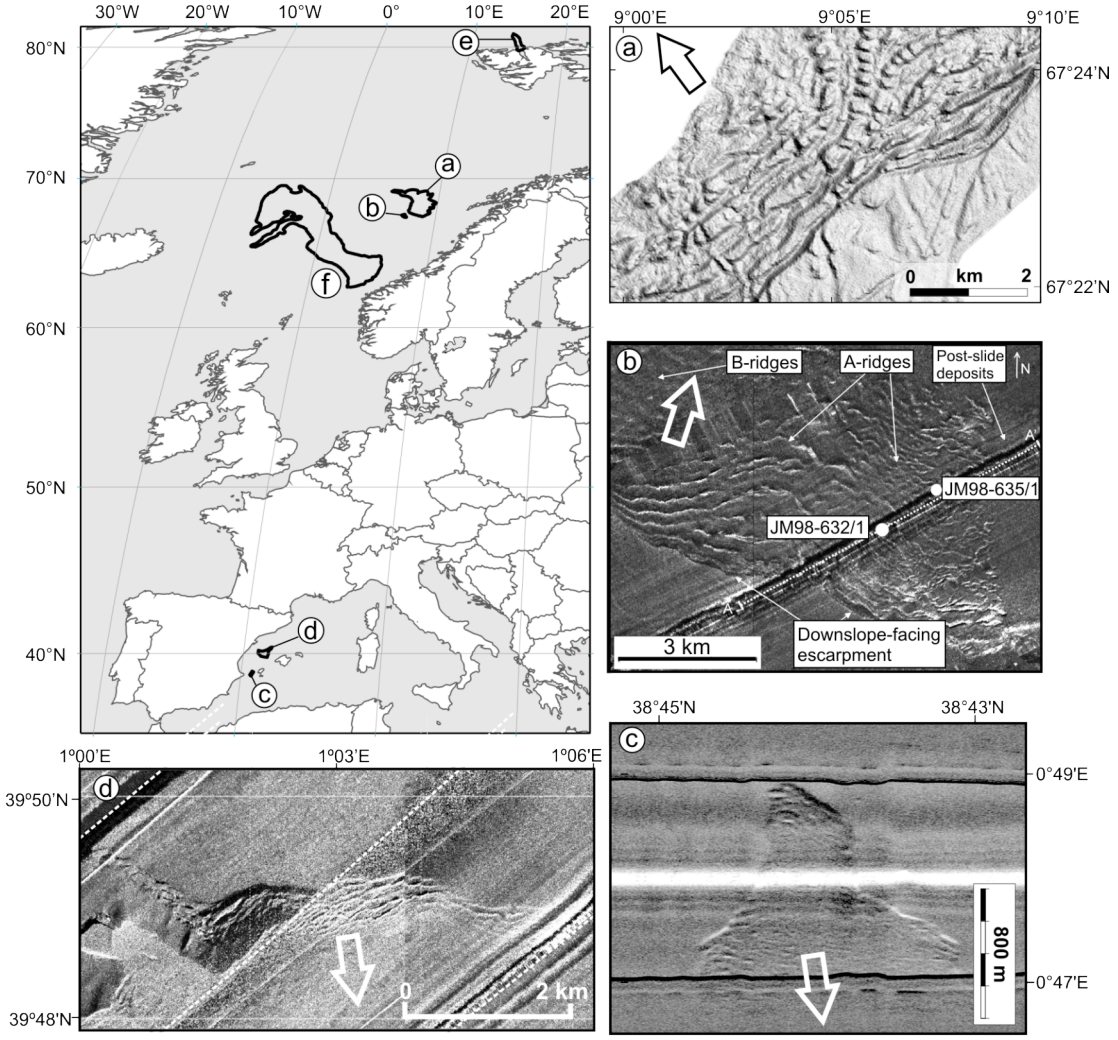

Figure 6.1: Examples of acoustic imagery of submarine slides that exhibit a ridge and trough morphology: (a) Shaded relief bathymetric map of the Trænadjupet Slide headwall, modified from *Laberg et al.* [2002]; (b) TOBI sidescan sonographs of the Nyk Slide headwall, modified from *Lindberg et al.* [2004]; (c) MAK-1M sonograph across the Nuna slide headwall scar, modified from *Lastras et al.* [2006]; (d) TOBI sidescan sonographs of the headwall of the BIG'95, modified from *Lastras et al.* [2003]. Also shown are the locations of (e) the Hinlopen Slide [*Vanneste et al.*, 2006] and (f) the Storegga Slide. The arrows indicate the direction of sediment movement.

This paper presents results from a detailed investigation of spreading within the Storegga Slide. The objectives of the study are: (i) to characterise the morphological signature of spreading; (ii) to understand the mode of failure and controlling factors of spreading, and identify the potential triggers; and (iii) to explain the physical boundary conditions that control the development of a spread and the associated style of sediment displacement.

6.2 REGIONAL SETTING

The Storegga Slide is located on the mid-Norwegian margin, with the main headwall about 120 km from the Norwegian coastline (Figure 6.2). The Storegga region has been the site of a number of large-scale mass failures [*Solheim et al.*, 2005], the latest of which was the Storegga Slide, dated at 8100±250 cal. yrs BP [*Haflidason et al.*, 2005]. The repeated sliding activity is due to the influence of climate on sedimentary processes, in particular the alternating deposition of glacial diamictons and ice-proximal sediments during glacial maxima, and of fine-grained glacimarine, hemipelagic and contouritic sediments during interglacials [*Berg et al.*, 2005]. The differences in the geotechnical properties of these sediments, coupled with seismicity, rapid sediment deposition and associated high pore pressures, and the regional topographic and structural setting, are responsible for more than twenty slope failures during the past 2.6 Ma [*Evans et al.*, 2005; *Solheim et al.*, 2005].

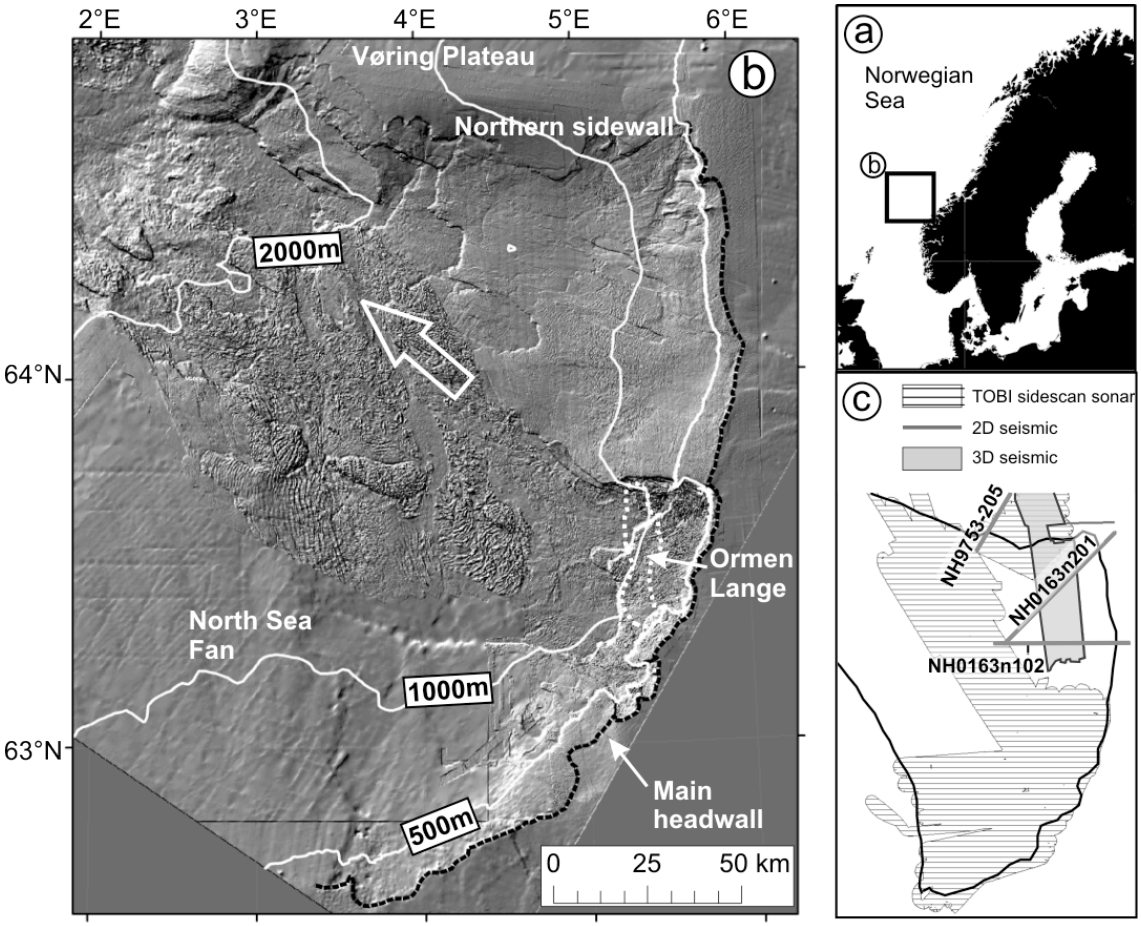

Figure 6.2: (a) Location of the study area. (b) Shaded relief map of the Storegga Slide scar with bathymetric contours (illumination from NW, 3× exaggeration). The arrow indicates the direction of sediment movement. (c) Spatial coverage of TOBI sidescan sonar and 2D/3D seismic data sets.

The headwall of the Storegga Slide is coincident with the present-day shelf break. The slide is bound by the Vøring Plateau to the north and the North Sea Fan to the south (Figure 6.2). With an estimated area of 95 000 km^2 and a volume of 2400-3200 km^3 [*Canals et al.*, 2004], it is one of the largest known submarine slides. The slide scar forms an amphitheatre-like depression with a 320 km long main headwall, narrowing downslope to 60 km at a depth of 2000 m. The slide has a depth range of 2700 m and a run-out distance of up to 810 km. 90% of the slide scar has a slope gradient of 4º or less, although headwalls reach gradients of 45º and heights of 160 m. According to the interpretation by *Haflidason et al.* [2004], the Storegga Slide has been classified as a complex retrogressive slope failure, consisting of 5 major and 58 smaller events, which have transferred most of the material to the Norwegian Basin.

6.3 DATA AND METHODS

This study is based on three acoustic data sets (Figure 6.2c). The first consists of a high-quality multibeam bathymetry data set covering the Storegga Slide from the slide headwall down to a water depth of ca. 2700 m (Figure 6.2b). The majority of the slide area is covered by data with a horizontal resolution of 25 m or better. The vertical precision varies from ± 10 cm to 2 m at depths of up to 800 m, to ±10 m at 2000 m depths or more. The second data set consists of Towed-Ocean-Bottom-Instrument (TOBI) sidescan sonar imagery covering ~60% of the slide scar. The TOBI images have a nominal horizontal resolution of 6 m. The third data set comprises 2D and 3D seismic reflection data. High-resolution 2D lines, located across the main headwall and northern sidewall, have a horizontal sampling density of 6.25 m and a vertical resolution of ~2 m. The industry-type 3D seismic data cover a 2000 km^2 area across the northern sidewall, have a 25 m bin spacing, and ~5 m vertical resolution near the surface.

Previous geomorphological studies of the Storegga Slide have been based on visual interpretation of shaded relief bathymetric maps [e.g. *Haflidason et al.*, 2004; 2005]. Recent studies show that geological interpretation is greatly improved if quantitative techniques are employed. *Micallef et al.* [2007] applied a suite of geomorphometric techniques to the Storegga bathymetry data set to extract quantitative morphological information, which enabled an improved interpretation of shaded relief maps. One of these techniques is called ridge characterisation. It involves the automatic extraction of ridge patterns and associated morphological characteristics. These techniques were applied to the Storegga Slide bathymetry data set, and the following ridge and trough characteristic maps were derived (Figure 6.3): (i) spreading direction; (ii) trough depth; (iii) ridge length; (iv) ridge density; (v) ridge spacing. The grid resolution over which all characteristics were measured was 1 km^2. A geomorphometric map [*Micallef et al.*, 2007] was also generated for the entire Storegga Slide.

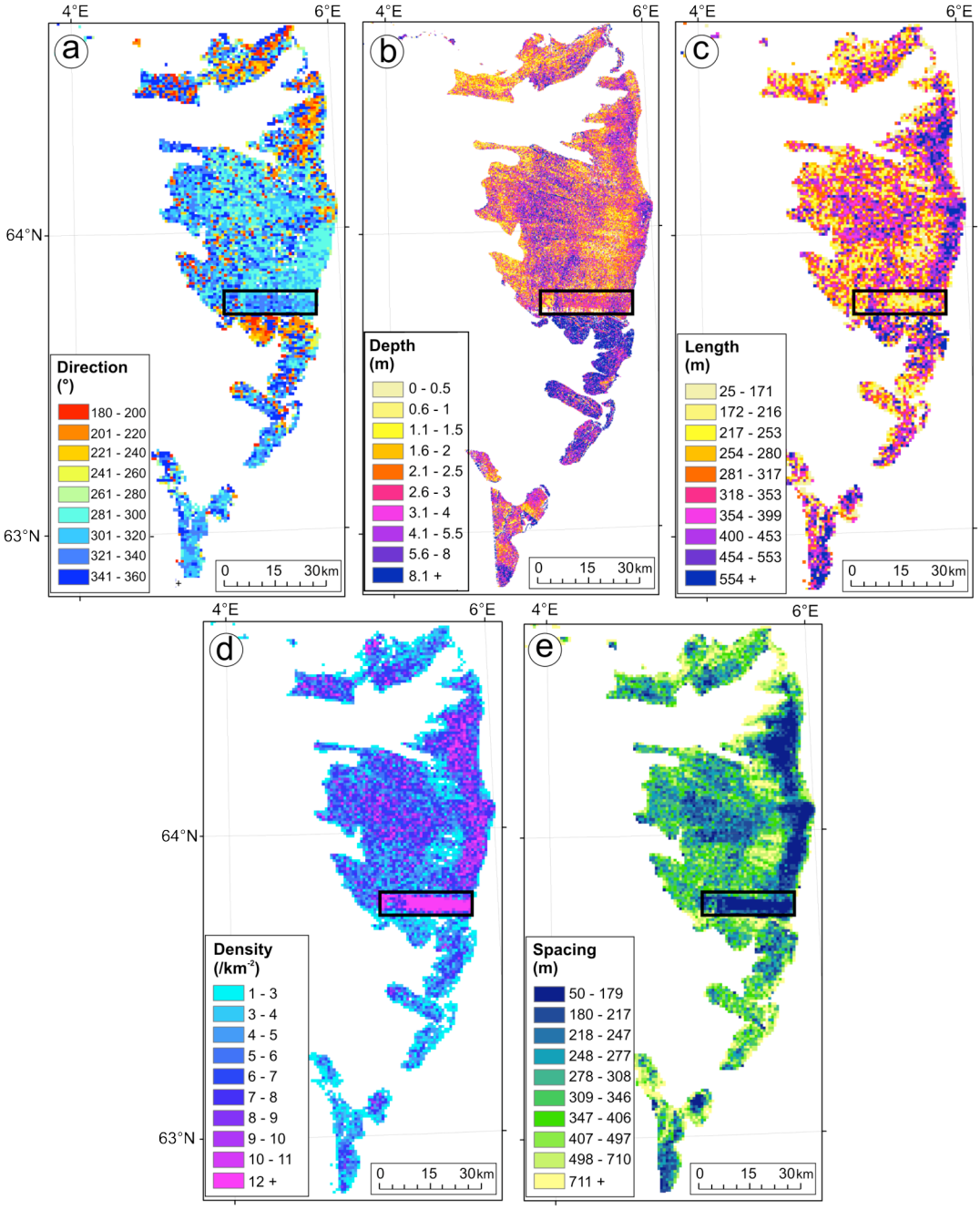

Figure 6.3: Ridge and trough characteristics maps: (a) spreading direction (downslope direction perpendicular to the mean orientation of ridges in a grid cell ; (b) trough depth (vertical distance between the base of a trough and the crests of the two adjacent ridges); (c) ridge length (mean length of individual ridge crests in a grid cell) ; (d) ridge density (mean number of individual ridge crests per unit area in a grid cell); (e) ridge spacing (mean distance between ridge crests in a grid cell). A grid cell has dimensions 1 km × 1 km. The area covered by the ridge and trough characteristic maps is shown in Figure 6.7. Note that the resolution of the bathymetry data from the southern part of the Storegga Slide scar is too low to allow calculation of meaningful ridge and trough characteristics. Noise from data merging is indicated by black rectangle.

6.4 RESULTS

6.4.1 RIDGE AND TROUGH MORPHOLOGY

Ridges and troughs at a variety of scales comprise one of the most common morphologies observed within the Storegga Slide (Figure 6.4). The ridges and troughs occur in a repetitive parallel to sub-parallel pattern and are generally aligned parallel to a headwall or escarpment. Most of the ridges and troughs are concentrated in a zone that extends up to 70 km downslope from the main headwall. Close to the main headwall of the Storegga Slide, the ridge crests are marked and continuous, with individual ridges having a concave-downslope or linear shape in plan (Figure 6.4a). Further downslope, the ridge and trough morphology becomes less distinct, with ridges being more discontinuous. On a few occasions, however, the ridges are unusually high, developing into a convex-downslope pattern in plan (Figure 6.4a). Areas characterised by ridge and trough morphology are generally wider along-slope than downslope. Ridges and troughs can be observed in water depths down to 1500 m. A bathymetric profile across the ridge and trough morphology within the Ormen Lange region shows groups of small and frequent ridges that are located between higher and more infrequent ridges (Figures 6.2; 6.4b).

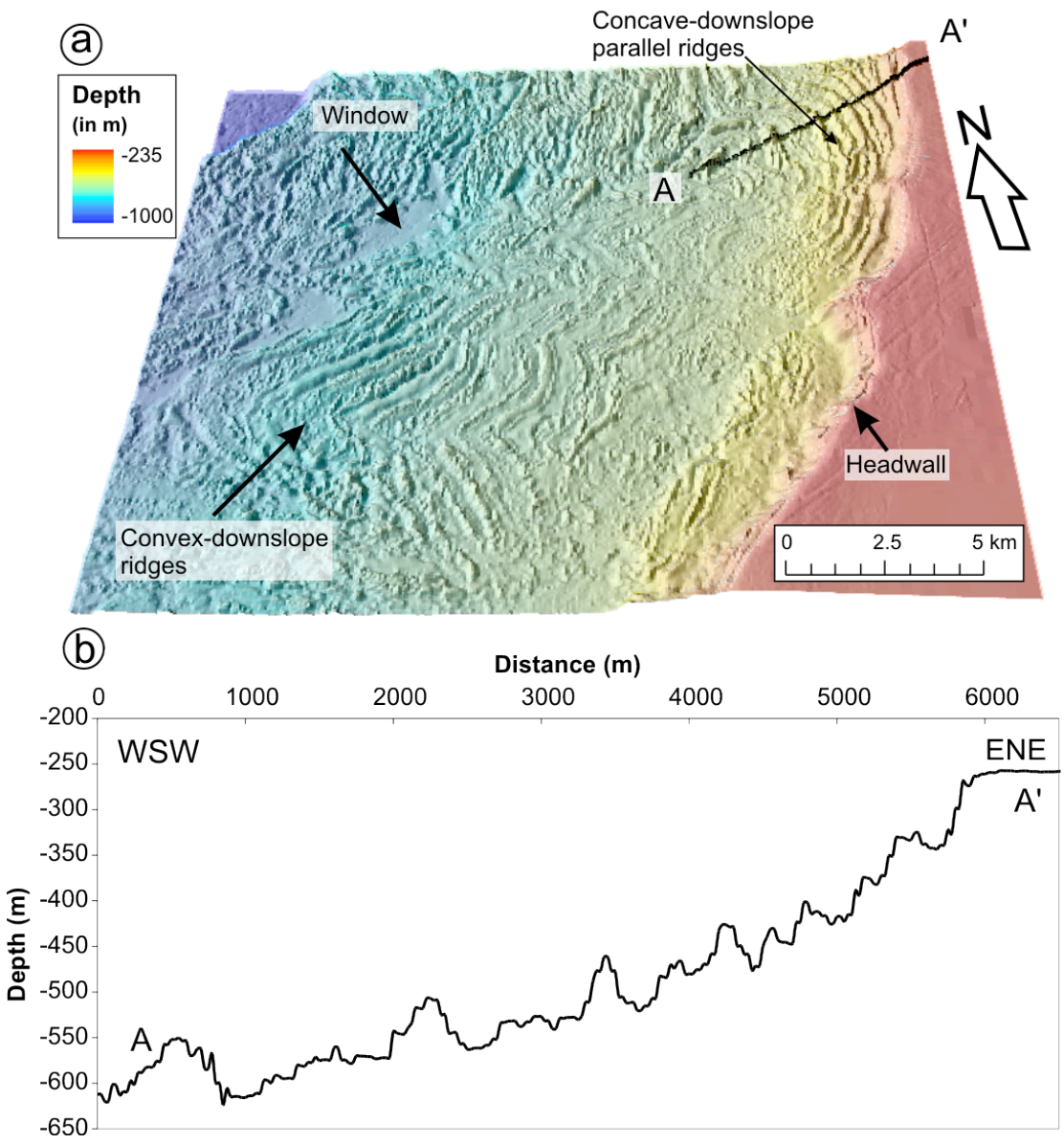

Figure 6.4: (a) Bathymetric map draped on a 3D shaded relief image of ridge and trough morphology within the Ormen Lange region of the Storegga Slide. Location is shown in Figure 6.7. Distinct ridge and trough morphology and windows are annotated on the image. A window is defined as a part of the seabed where the slip surface, above which sediment was mobilised during a mass movement, is exposed. (b) Bathymetric profile across ridge and trough morphology close to the main headwall (A-A'). Note that groups of small and frequent ridges are located between higher and more infrequent ridges.

The patterns extracted by the geomorphometric techniques show that ridge and trough characteristics vary spatially across the Storegga Slide (Figure 6.3). In the majority of cases, zones with the longest ridges coincide with the least widely spaced ridges, the lowest ridge densities and, in most parts, with the shallowest troughs. These patterns are best observed in the northern half of Figures 6.3b-d. The ridge direction map (Figure 6.3a) indicates that the majority of the ridges face a west-northwest direction, with the ridges in the northeast and Ormen Lange area facing a south-southwest direction.

6.4.2 INTERNAL ARCHITECTURE

A seismic dip profile that is perpendicular to the main headwall shows the seismic expression of the ridge and trough morphology (Figures 6.5; 6.6). The seabed reflection is predominantly characterised by downslope dipping segments of consistently high amplitude (Figure 6.6). Below them, a sequence formed by groups of short downslope-dipping high-amplitude reflections, parallel to the surface reflections, are observed, each of them having the same number and pattern of seismic reflections. The downward prolongations observed at the peak of some of these short reflectors are considered to be mainly due to diffraction of the seismic energy. The groups of short reflectors are separated at regular intervals by upslope dipping segments that extend to the peaks of the downslope-dipping surface reflections. A series of four planar, continuous, consistently high amplitude reflections are observed immediately below this sequence (Figures 6.6).

The ridge crests from a bathymetric profile correspond to the peak of the downslope dipping seabed reflections (Figure 6.5b). These downslope dipping reflections are thus interpreted as the downslope faces of the ridges. The groups of sub-seabed reflections are interpreted as blocks that are separated by upslope-dipping interfaces. Using a seismic P-wave velocity of 1700 m s^{-1} for the depth conversion, the dip of the upslope-dipping interfaces ranges between 24º and 29º, with an average of 25º. Generally the blocks have the shape of a rhomb or trapezium, with top and bottom ~130 m in length. The thickness of the blocks varies between 25 m and 80 m, with a mean of 50 m. Along the entire profile, the base of the blocks corresponds to the topmost continuous high-amplitude reflector of the series of planar reflections. The dip of this reflector, which

changes from 1.2º upslope to 0.9º downslope, is lower than the dip of the seabed reflectors. The groups of downslope dipping sub-seabed and surface reflectors generally become progressively steeper with distance downslope. The block pattern is best distinguished near the headwall, but becomes less evident downslope. A seismic section downslope of Figure 6.5b shows that the groups of downslope dipping reflectors, located above the series of planar reflections, are more widely spaced and tilted in comparison to Figure 6.5b (Figure 6.5c). The seismic reflections are less coherent and the dip of the seabed reflections is more irregular.

The downslope dipping seismic reflectors are interpreted as layers in a stacked sediment package. The blocks of sub-seabed reflections in the shallower part of the seismic section are interpreted as coherent sediment blocks. The planar continuous reflectors in the deeper part of the seismic section are thought to represent the undeformed sediment unit acting as a slip layer. Layering is preserved in both the upper deformed part and the deeper undeformed part. The sediment blocks are separated by upslope dipping reflectors. These reflectors are interpreted as shear planes and are thought to have formed due to extension because they dip at the angle expected for Mohr-Coulomb failure of these types of sediment [*Kvalstad et al.*, 2005b]. To accommodate this extension, the blocks have translated downslope along a planar slip surface. The surfaces of the blocks are generally steeper than the slip surface on which they are displaced, which indicates that the blocks have tilted downslope. During tilting, the upslope top part of each block is exposed, creating a step-like pattern that is responsible for the ridge and trough morphology observed at the surface. The blocks tilt further downslope with increasing distance from the headwall, which suggests increased extension in this direction. The upslope dipping faces of the ridges are generally steeper than the downslope faces. The seismic profile and the ridge and trough morphology are considered representative of spreading within the Storegga Slide. Spreading has occurred along the entire seismic profile (Figure 6.5a), but the block pattern is best preserved near the headwall (Figure 6.6a), with increased deformation downslope (Figure 6.5c).

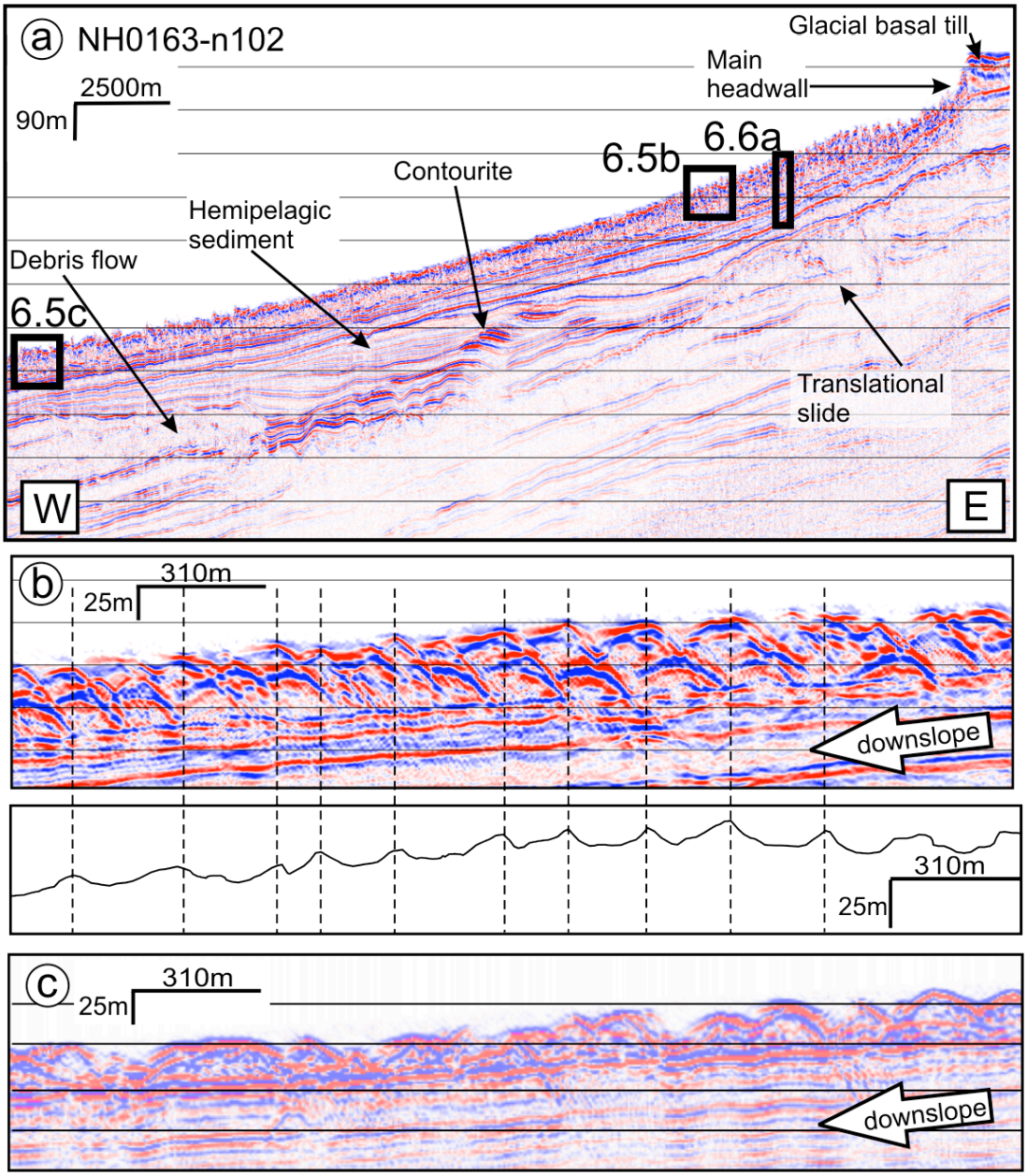

Figure 6.5: (a) Seismic time section from profile NH0163-n102, located on Figure 6.7. The seismic signature of the most prominent underlying geological features is indicated. (b) Comparison of a seismic section with the corresponding bathymetric profile extracted from the bathymetry data set. The peaks of the downslope dipping surface reflectors mainly correspond to the ridge crests in the bathymetric profile, although in some places this is masked by side reflections from adjacent ridges and by other reflection hyperbolae. (c) Enlarged section of part of the seismic section in Figure a, illustrating the seismic expression of the ridge and trough morphology downslope of Figure b. In comparison to Figure b, the spreading blocks are characterised by increased deformation and tilting, and longer spacing between the blocks. The sub-horizontal seismic reflections are still visible within the blocks. The scales in Figures a – c represent data at sediment velocity (1700 m s^{-1}).

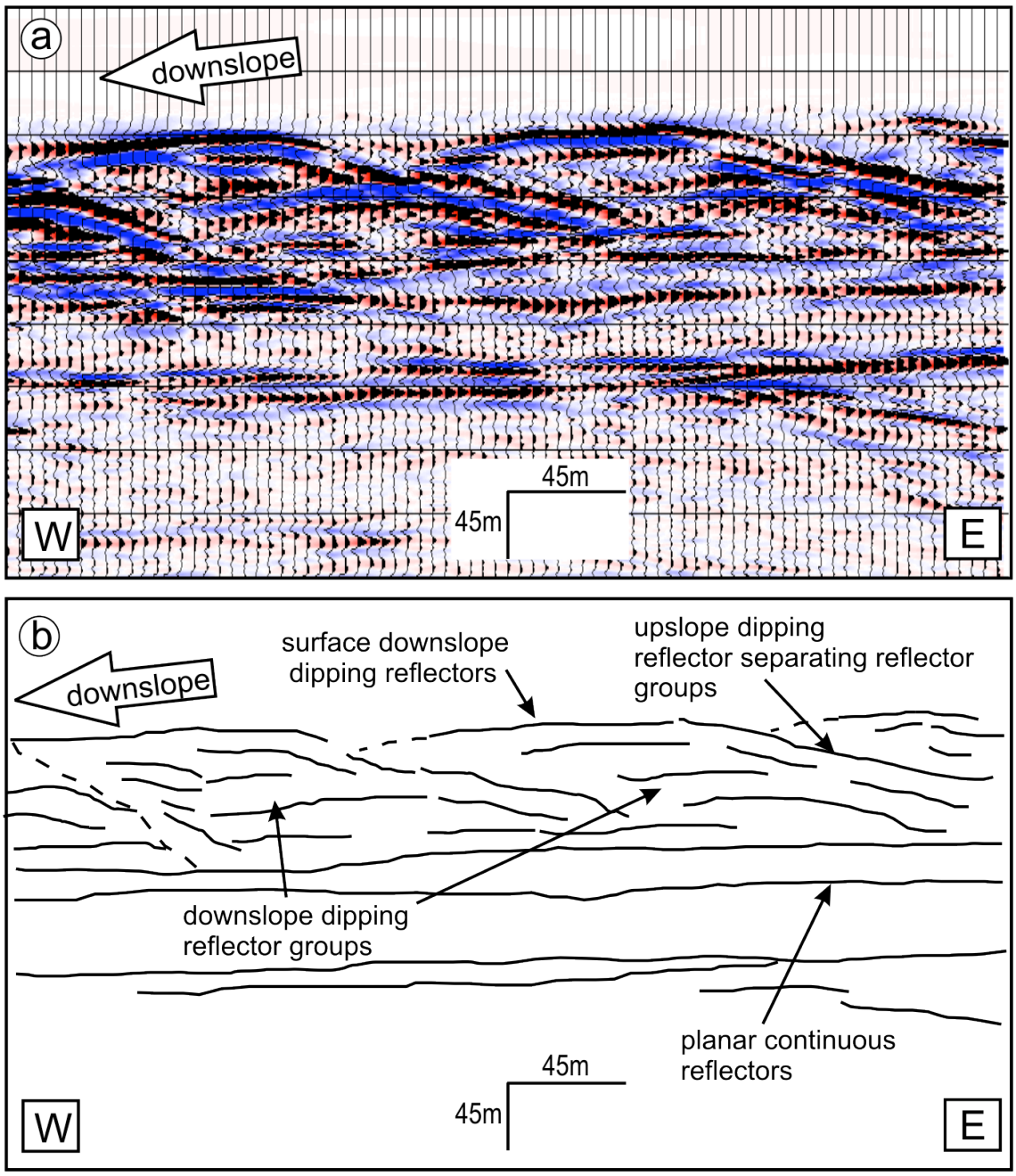

Figure 6.6: (a) Enlarged section of part of the seismic time section in Figure 6.5a, with amplitude peaks overlay, illustrating the seismic expression of the ridge and trough morphology at the limit of the data resolution. (b) Labelled interpretation of the seismic section in Figure a. The scales in Figures a – b represent data at sediment velocity (1700 m s^{-1}).

An alternative interpretation of the seismic section in Figure 6.6 would be that the blocks were initially formed by Mohr-Coulomb failure with shear planes dipping downslope, and the blocks were subsequently tilted anticlockwise by an angle of ~130º. Such a process has not been observed in nature so far and would involve significant

distortion of the sediment layers within the blocks. Judging from the seismic data (Figures 6.5; 6.6) the internal structure of the blocks is still largely intact and we discard this model as a possible mechanism of spreading.

Our observations are very different from the interpretation of a seismic line proposed for spreading in the Ormen Lange area [*Kvalstad et al.*, 2005a]. These authors interpret almost intact triangular wedges and intermediate distorted rhombs (Figure 5 in *Kvalstad et al.* [2005a]). In their model, shear planes dipping both upslope and downslope delineate the boundaries of the triangular wedges.

6.4.3 SPATIAL DISTRIBUTION OF SPREADING

Having interpreted the ridge and trough morphology as indicative of spreading, we investigated its distribution within the Storegga Slide. We combined information from the geomorphometric map with sidescan sonar imagery, seismic data and published geological information to map the spatial distribution of spreading and other mass movements within the Storegga Slide (Figure 6.7). The mass movements were interpreted on the basis of morphology and internal structure, in accordance with criteria established by *Buma and van Asch* [1996] for spreading and *Mulder and Cochonat* [1996] for submarine mass movements. Only spreads and translational slides are mapped in detail (Figure 6.7), although topples, rotational slides, debris flows and turbidity currents are known to have occurred [*Bryn et al.*, 2005a; *Haflidason et al.*, 2004]. The current coverage of spreading and complex spreading is 6670 km^2 and 300 km^2, respectively, which add up to ~25% of the total slide scar area (Figure 6.7). Sediment mobilisations of these types are concentrated along the main headwall. Spreading occurs in the north-eastern and southern part of the slide scar, whereas complex spreading is mainly found in the central Ormen Lange region. The area affected by translational sliding (426 km^2) is considerably smaller, and is made up of isolated events located at the distal, western limit of spreading in the north-eastern part of the slide scar and in the Ormen Lange region. Upslope of these translational slides are numerous windows that expose the underlying slip surface (Figure 6.7).

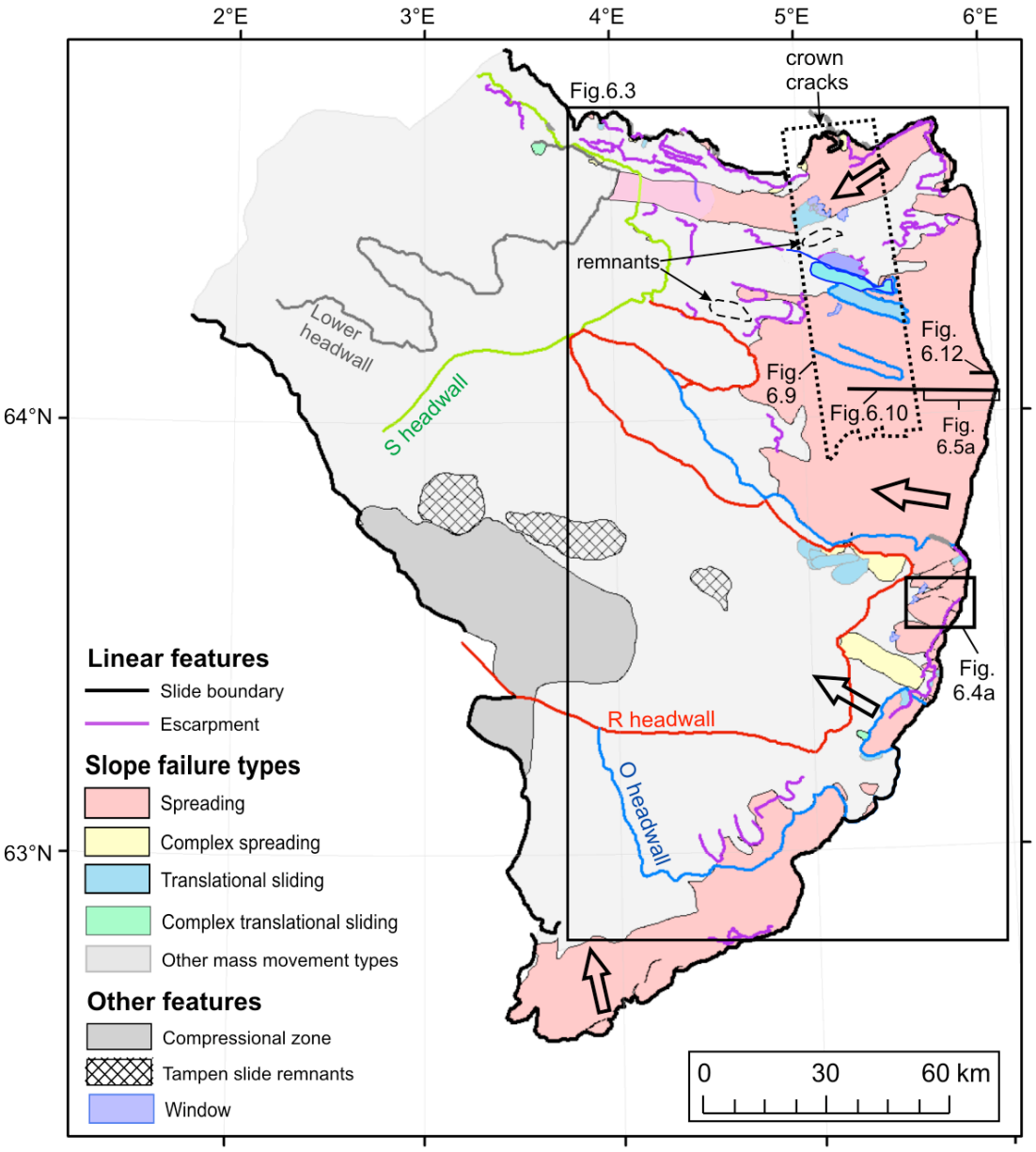

Figure 6.7: Map of the distribution of mass movement types, headwalls and other geological features within the Storegga Slide. A complex slope failure is one that was activated as one type of mass movement (as a spread in a complex spread, and as a slide in a complex translational slide), but then evolved into a different type of mass movement with distance downslope. Crown cracks indicate zones of incipient failure. The compressional zone in the western part of the slide is due to the impact from large debris flows originating in the Ormen Lange region, and is not associated with spreading. Block arrows represent the general direction of mass movement. The names of the headwalls are derived from the sediment units in which failure took place [*Bryn et al.*, 2005a]. Boxes and lines indicate the location of Figures 6.3, 6.4a, 6.5, 6.9, 6.10 and 6.12.

6.4.4 SCALES OF SPREADING

We grouped the spreading areas into three zones by combining the five ridge and trough characteristics maps (Figure 6.3) with TOBI sidescan sonar imagery (Figure 6.8). The morphological characteristics of these zones are listed in Table 6.1.

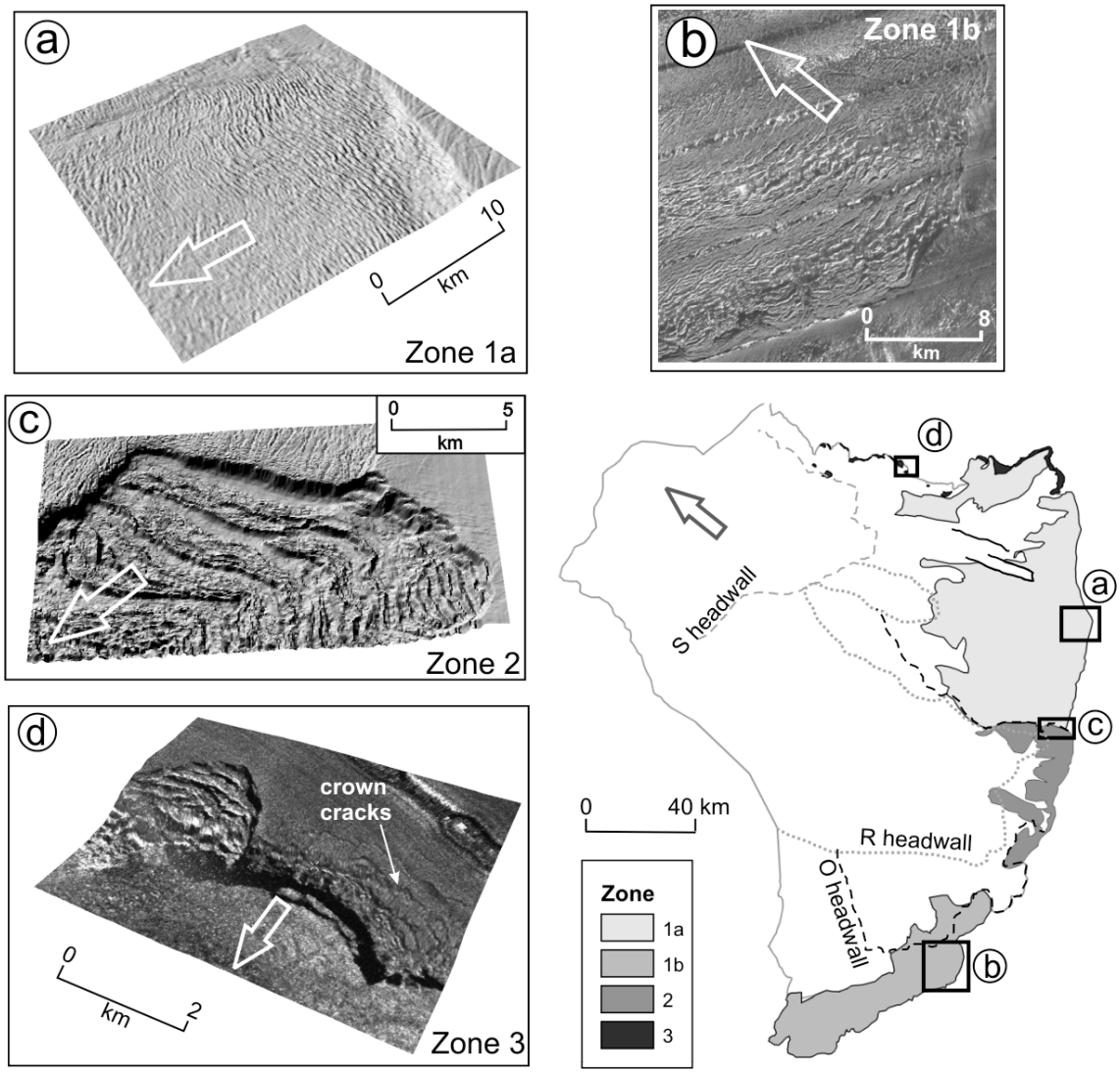

Figure 6.8: Zonation of spreading within the Storegga Slide: (a) 3D shaded relief of bathymetry from zone 1a; (b) TOBI sidescan sonar image for zone 1b; (c) 3D shaded relief image of bathymetry from zone 2; (d) Fusion of TOBI sidescan sonar image with bathymetry in 3D for zone 3. The arrows indicate the direction of sediment movement.

Table 6.1: Ridge, trough and headwall morphological characteristics for Zones 1-3. The standard error for the listed means is also shown.

	Zone 1a: Northern main headwall	**Zone 1b: Southern main headwall**	**Zone 2: Ormen Lange**	**Zone 3: Northern sidewall**
Area (km^2)	4255	1770	750	150
RIDGE AND TROUGH CHARACTERISTICS				
Mean ridge length (m)	334 (±9.3)	345 (±10.1)	397 (±8.1)	292 (±6.1)
Mean trough depth (m)	3.1 (±0.5)	3.9 (±0.6)	10.5 (±4.3)	4.9 (±0.8)
Mean ridge spacing (m)	287 (±27.4)	261 (±26.2)	361 (±20.2)	213 (±12.8)
Mean spreading direction (º)	293 (±13.1)	316 (±9.5)	272 (±8.6)	235 (±14.1)
Mean ridge density (km^{-2})	6.0 (±0.9)	6.8 (±1.0)	3.8 (±1.7)	8.1 (±0.8)
HEADWALL CHARACTERISTICS				
Mean headwall height (m)	50 (±4.3)	45 (±2.6)	99 (±18.1)	21 (±2.2)
Range headwall height (m)	13 - 95	21 - 54	74 -135	10 - 45
Mean slope gradient (º)	4.83 (±0.8)	6.48 (±1.4)	14.5 (±7.1)	4.05 (±0.5)
Maximum slope gradient (º)	23	23	32.5	21

I ZONE 1: NORTHERN AND SOUTHERN MAIN HEADWALL

Zone 1 is by the far the most extensive spreading area. It consists of two disconnected areas, named zones 1a and 1b. Zone 1a has a surface area of 4255 km^2. It is located in the northeastern part of the Storegga Slide and reaches a width of up to 100 km, extending downslope over 50 km. Currently this spread zone extends from the main headwall, which has a mean height of 50 m, down to the S headwall (Figure 6.7). In this case most of the downslope section was removed by subsequent mass movements, although some remnants can still be observed in the form of a subtle ridge and trough morphology [*Micallef et al.*, submitted] (Figure 6.7). The spreading pattern has also been disrupted by debris flows and turbidite pathways in the northeast of zone 1a. Upslope of the R headwall, the ridge and trough pattern is predominantly curved concave downslope or linear. The morphological characteristics of these ridges and troughs are given in Table 6.1. Three groups of anomalously high, convex-downslope ridges and troughs are located in the middle of the slope and may indicate retardation, halting and possibly compression of the displaced sediment. Although spreading is predominantly an extensional process, some of the ridges and troughs may thus have been formed by localised events of compression. Windows are located downslope of

some of these compressional ridges and troughs (Figure 6.7). In general, the ridges of zone 1a have a gentle downslope face and a steeper upslope face.

Zone 1b comprises an area of 1770 km^2 and ridges are located both upslope and downslope of the O headwall (Figure 6.7; 6.8). High-resolution bathymetry has not been acquired for this region, and interpretations have been based entirely on TOBI sidescan sonar imagery. The ridge and trough morphology and headwall characteristics are very similar to those in the southern half of zone 1a (Table 6.1). Both linear and curved ridges can be observed (Figure 6.8b), which are slightly longer than those in zone 1a (Table 6.1). The ridges are slightly more closely spaced than in zone 1a and the spreading direction is mainly north-west.

Spreading within zone 1 mainly occurs in the shallow O3 sediment sub-unit (130-30 ka), which consists of thin stratified deposits of fine-grained normal hemipelagic and glacimarine clays [*Bryn et al.*, 2005a]. In some areas of zone 1, spreading occurs in O1-O2 sediment sub-units (30-15 ka), which are made up of basal and deformation till, with sub-unit O3 acting as the slip surface [*Haflidason et al.*, 2004]. The increase in clay content observed in the lower part of sub-unit O3 [*Berg et al.*, 2005] may explain the location of the slip surface within this sub-unit.

II ZONE 2: ORMEN LANGE REGION

Zone 2 comprises an area of 750 km^2 in the Ormen Lange region between zone 1a and zone 1b, extending from the main slide headwall to the R headwall. Compared to the other zones, the ridges in zone 2 are generally the longest, the widest and the most widely spaced (Figure 6.8c; Table 6.1). The troughs are on average almost three times as deep as those in zone 1, whereas the headwall reaches heights of up to 135 m, with a mean slope gradient of 14.5º. The mean direction of spreading is westwards, although the ridges have many orientations. Where the spreads collapse over an escarpment, the ridge and trough morphology is generally preserved. The headwall is higher in the southern part of zone 2 and the adjacent ridges are linear, whereas concave-downslope spreading ridges merge with a lower headwall in the northern part. Shear zones in the ridge and trough pattern, caused by different events or rates of spreading, can be

observed in this zone. Remnants of zone 1a spreading ridges can be distinguished on top of ridges from zone 2, indicating that spreading in zone 2 post-dates events in zone 1a (Figure 6.8c). In contrast to zone 1, the downslope face of the ridges in zone 2 is generally steeper than the upslope face. Numerous windows have been identified in this zone (Figures 6.4a and 6.7). Pronounced, long convex-downslope ridges and troughs are located upslope of these features. Spreading in zone 2 mainly occurs in the deep and thick O4-O7 sediment sub-units (200-130 ka), consisting of glacial till and debris flow deposits [*Berg et al.*, 2005]. The glacial to normal hemipelagic clays of sub-unit R2 (330-200 ka) comprise the slip surface [*Kvalstad et al.*, 2005a].

III ZONE 3: NORTHERN SIDEWALL

Zone 3 has an area of 150 km^2. It consists of a concentration of small spreads on the top of the northern sidewall and just above the main headwall. The spreading areas are elongated, narrow and found on top of escarpments created by larger failures. Where the spread zone extends farther upslope, it is arcuate in plan, with sub-parallel ridges and troughs that are concave downslope. Numerous zones of incipient failure exhibiting systems of crown cracks occur adjacent to or upslope of the spreads (Figure 6.8d). The spacing of the crown cracks is about 100 m. The fact that the shape of these open fractures is similar to that of the ridges and troughs to the west implies that the latter have formed by extension. Additionally, within zone 3, iceberg ploughmarks can be seen running from the ridges and troughs to the undisrupted slope, indicating limited extensional displacement of the ridges since the Last Glacial Maximum (LGM). Zone 3 is characterised by the lowest headwall, shortest ridges, shortest ridge spacing and highest ridge density. The mean trough depth is 4.88 m, slightly deeper than for zones 1a and 1b. The ridges of zone 3 have a steep downslope face and a gentler upslope face. Spreading in zone 3 takes place in the uppermost sediment sub-units (O1-O2).

6.4.5 THICKNESS OF FAILED SEDIMENT AND SLIP SURFACE CHARACTERISTICS

I SEDIMENT THICKNESS AND ASSOCIATED RIDGE AND TROUGH MORHPOLOGY

The 3D seismic data were used to interpret the slip surface of the spreading within zone 1a and to generate an isopach map for the sediment above this slip surface (Figure 6.9a). Time-to-depth conversion of the seismic data was carried out using a seismic P-wave velocity of 1700 m s^{-1} for the sediment. For zone 1a, the range of thicknesses is 22 - 44 m. In general, the thickness of the sediment affected by spreading in zone 1a decreases downslope from east to west. Given the amount of vertical strain that appears to have occurred with distance of movement downslope, we infer that the deformation of the spreading sediment is not entirely brittle, but a significant part of the sediment has undergone quasi-plastic deformation. When compared to the ridge and trough characteristics maps in this area of the Storegga Slide (Figure 6.3), the thinnest parts of the section affected by spreading coincide with the deepest troughs, shortest ridge spacing, highest ridge density and decreasing ridge length.

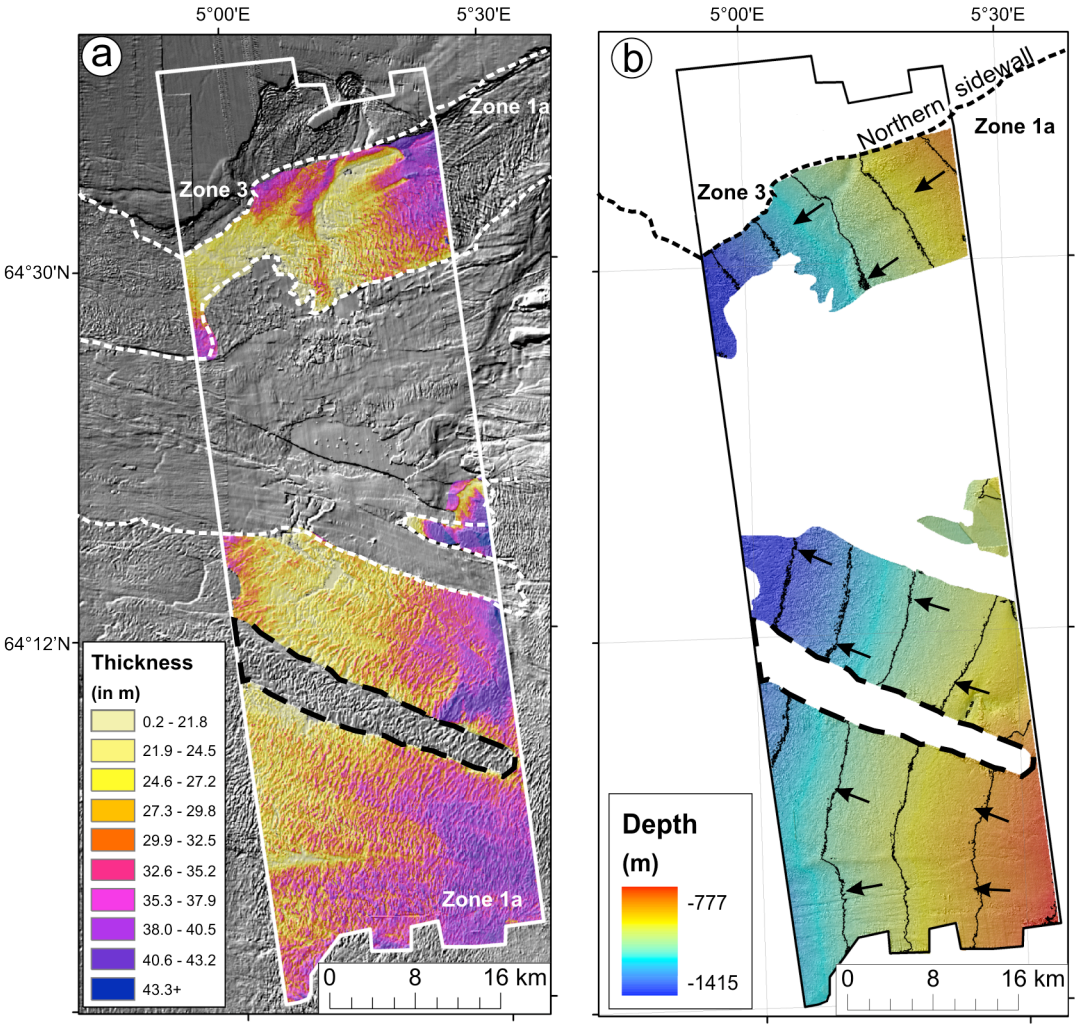

Figure 6.9: (a) Isopach map of zone 1a spread. The solid white line indicates the limits of the 3D seismic data, whereas the dotted white line shows the boundary of the spreading zone 1a. (b) Shaded relief map and contours (at 100 m intervals) of the interpreted slip surface. The arrows indicate the general spreading direction of the overlying ridges. The maps are derived from the 3D seismic data set, the location of which is shown in Figure 6.7. Since the error associated to the detection threshold of the 3D seismic data is quite high in relation to the spread thickness, the values in Figures a and b are not absolute. However, these values do allow us to understand the relative integral variation of thickness and elevation. The gaps in the data observed in the southern central parts of Figures a and b (outlined by a dashed black line) are due to the fact that the slip surface, above which spreading has occurred, is deeper in this region.

The interpreted seabed and slip surface of a spread in zone 1a along a high-resolution 2D seismic line shows that the calculated thickness of the sediment gradually decreases with distance downslope (Figure 6.10a). The corresponding ridge and trough characteristics at the surface of the spread also change systematically downslope (Figure 6.10b), and match the relations observed in the 3D seismic data. Trough depth shows a general increase from 1.5 m near the headwall to 5.5 m towards the toe. The ridge length peaks at the centre of the slope with 410 m, and decreases both upslope towards the headwall and downslope towards the distal limit. Ridge density increases away from the headwall, whereas the ridge spacing decreases downslope. These trends in ridge and trough morphological characteristics indicate that the spreading blocks are undergoing progressive fragmentation, deformation and tilting with distance downslope. Similar patterns of variation in ridge and trough morphology with distance downslope can be observed in spreads from zone 2, although the values of the morphological characteristics are considerably larger than those of zone 1a. The lack of bathymetric data from zone 1b and the limited amount of downslope block displacement in zone 3 do not allow the identification of similar changes in ridge and trough morphology.

In both the 2D and 3D seismic data sets, the thickness of the spread layer is thinner than what could be assumed for the pre-slide thickness, which at the headwall is ~80 m (Figures 6.9a; 6.10a). Both data sets show a clear reduction of sediment thickness with distance downslope and there are no trends of increasing sediment thickness, and possibly compression. These indicate that the spreading process is mainly extensional, although part of the reduction of sediment thickness with distance downslope may be attributed to inherent stratigraphical variation [*Berg et al.*, 2005].

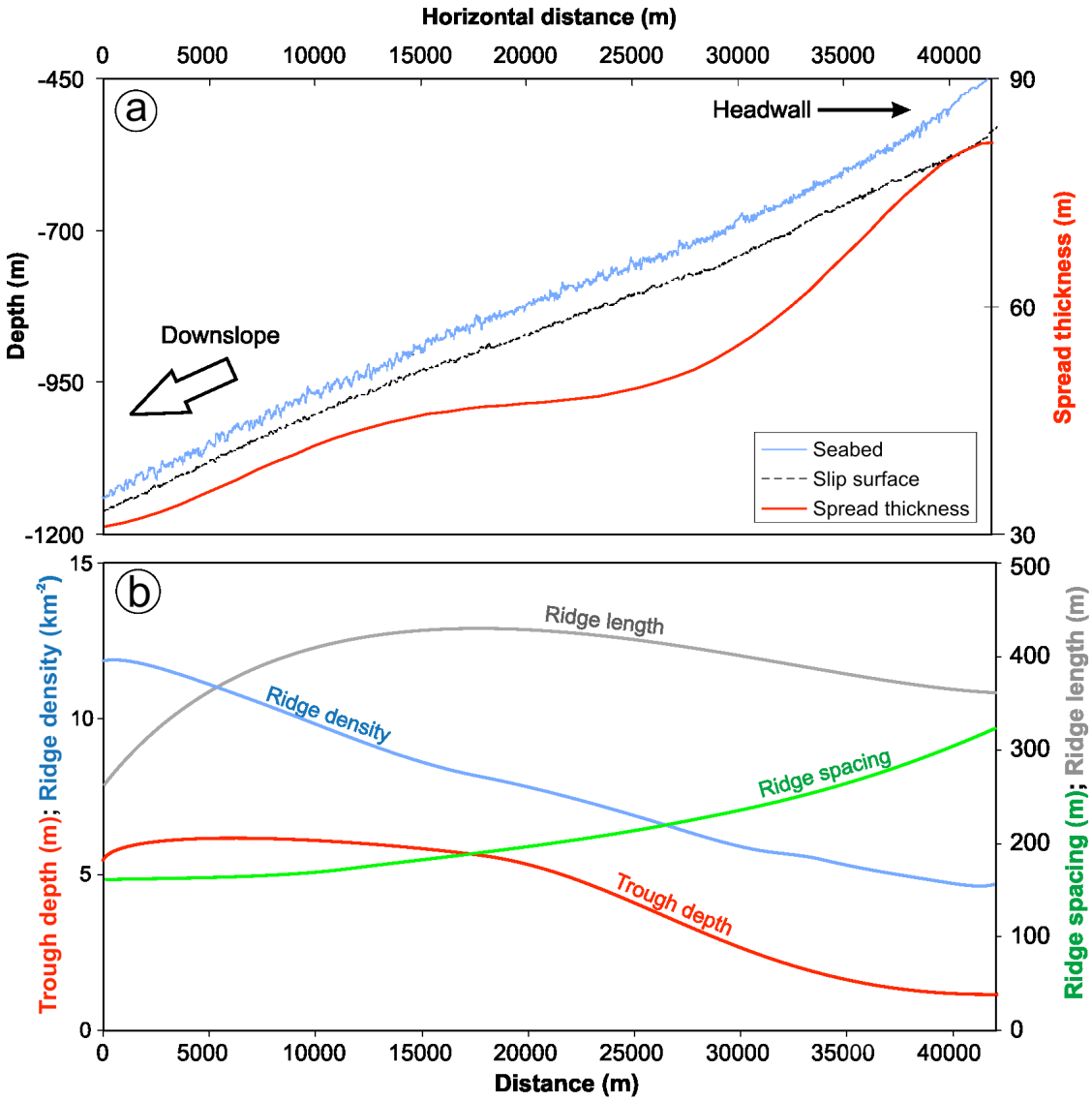

Figure 6.10: (a) Cross-sectional profile across a spread from zone 1a in seismic line NH0163-n102, showing the interpreted seabed and slip surface. The calculated thickness of the spread, which is also shown, varies from 80 m near the headwall to 32 m further downslope. (b) Polynomial trend lines fitted to the corresponding variation of ridge and trough characteristics across the surface of the spread in Figure a. The location of line NH0163-n102 is shown in Figure 6.7.

II SLIP SURFACE MORPHOLOGY

The shaded relief image of the interpreted slip surface exhibits the same general morphology as the seabed, but with a lower mean slope gradient of 0.5º (Figure 6.9b). The arrows in Figure 6.9b represent the spreading direction of the ridges, which is generally perpendicular to the depth contours of the interpreted slip surface. This

indicates that the spreading direction is determined by the aspect of the slip surface. This is also confirmed by the high correlation ($R^2 = 0.91$) between spreading direction of the ridges and the slope aspect of the slip surface for the entire 3D block using 1 km^2 grids.

6.4.6 DISPLACEMENT ASSOCIATED WITH SPREADING

Interblock displacement is the increase in the distance between identical reference points on two successive blocks when spreading occurs. Figure 6.11a shows a cross-section of two blocks before spreading occurs, with *o* being the distance between the top upslope corners of the two blocks, here considered as the two reference points. Figure 6.11b shows the displaced and tilted blocks after spreading has occurred, with *n* representing the new distance between the two reference points. *h* is the sum of the vertical distances that the downslope corner of the upslope block and the upslope corner of the downslope block have moved, and α represents the angle of tilting. The interblock displacement can therefore be calculated as:

$$\text{Interblock displacement} = n - o = n - (h / \text{Sin}\ \alpha) \quad (1)$$

- *o* distance between two reference points (here regarded as the top upslope corners of the two blocks) prior to failure, in m
- *n* new distance between the two reference points after failure, in m
- *h* sum of the vertical distances that the downslope corner of the upslope block and the upslope corner of the downslope block in the model have moved during failure, in m
- α angle of anticlockwise tilting of a block, in °

Since *n* and *h* can be measured from the bathymetry, and α from the seismic profile, the interblock displacement can be calculated.

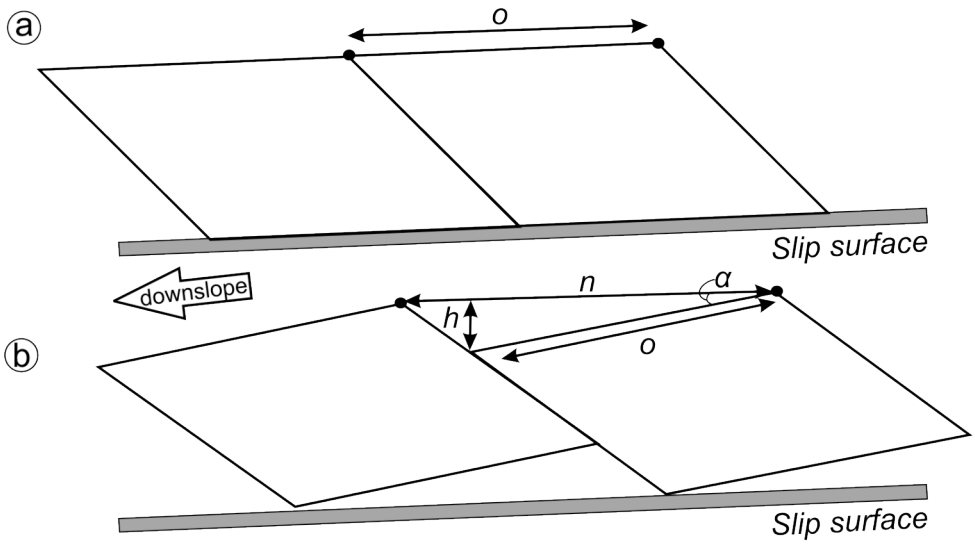

Figure 6.11: Schematic representation of two blocks within a spread before failure (Figure a) and after failure (Figure b). *o* is the initial distance between two reference points, *n* is the final distance between the two reference points, *h* is the sum of the vertical distances moves by the two reference points, and α is the angle of tilting of the block. Reference points are marked by a black circle. This representation does not take into account the deformation that occurs at the base of the spread.

Being able to estimate the interblock displacement for successive pairs of blocks allows us to calculate the cumulative displacement of each block from its original position. This is achieved by adding up the values of the interblock displacement upslope of a block, as well as taking into consideration the length of any windows located between this block and the headwall. The approach was tested on a 5 km length of spread located downslope of the main Storegga headwall, where the widths of the blocks are almost identical and where windows are absent. The resulting graph for the displacement of successive blocks along the profile shows a gentle exponential decay of displacement with distance upslope (Figure 6.12). This decay is an indication that the tilting of the blocks increases progressively downslope. The exponential decay in displacement is composed of successive clusters of blocks that also exhibit an exponential decay in displacement with distance upslope. The extension factor calculated for the section of the slope under consideration is 1.10. This value indicates that a sediment unit undergoing spreading is extended by ~10% of its original length. This should be considered as a minimum estimate because sub-seismic scale deformation is not being taken into consideration and can accommodate considerable extension [*Marrett and Allmendinger*, 1992].

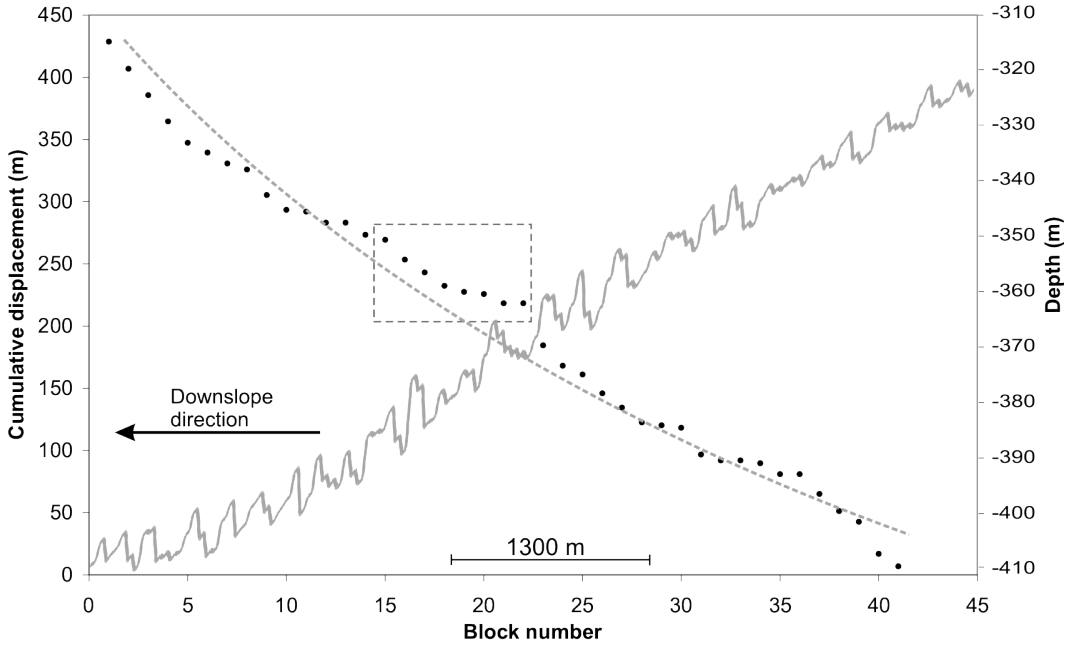

Figure 6.12: Plots of the bathymetric profile showing the ridge and trough morphology (solid grey line; location is shown in Figure 6.7), and the estimated cumulative displacement of the associated blocks vs. block number (black solid circles). Block number refers to the order in which the blocks are mobilised. The dotted grey curve is the line of best-fit and is indicative of a gentle exponential decay of displacement with distance upslope. A sub-group of blocks showing exponential decay of displacement is enclosed in a dotted grey square.

6.5 DISCUSSION

6.5.1 MODE OF FAILURE

Two modes of failure may be proposed for spreading within the Storegga Slide (Figure 6.13): (i) Model 1: Spreading develops retrogressively along the slip surface by the repeated failure of the headwall. The failure propagates upslope via the fracturing of the sediment into a number of coherent blocks. The blocks progressively undergo translation and disintegration; (ii) Model 2: The material above the slip layer behaves as a thin coherent slab that is extended downslope by gravity, and having drag forces resisting the movement at the base. The resultant downslope stress to which the slab is subjected is higher downslope than upslope, generating the necessary tension to break the slab up.

Model 1 is essentially the model suggested by *Kvalstad et al.* [2005a] for mass movements within the Ormen Lange region (our zone 2) (Figure 6.13a). Unloading of the headwall at the base of the slope results in the formation of shear planes that define a triangular failing sediment block accelerating downslope. This is pushed forward along the slip surface by an inverted triangular wedge that undergoes internal distortion. The process is assisted by pore pressure development in the toe area due to shear-induced contraction of the marine clay [*Kvalstad et al.*, 2005a]. For this model to be applicable the fracturing between the blocks should obey the Mohr-Coulomb failure criterion and the shear planes should be downslope dipping. The first condition is observed in our seismic data from zone 1, whereas the second is not (Figure 6.6). Furthermore, the downslope faces of the ridges formed by model 1 should be steeper than the upslope faces (as in Figure 7 in *Kvalstad et al.* [2005a]). This is seen within zones 2 and 3 of spreading, but not in zone 1. This means that model 1 can only be applied to spreading in zones 2 and 3, but that the mode of failure in zone 1 must be different.

In model 2, gravitational forces act on a thin and long slab of semi-consolidated material possibly underlain by a failure surface or a liquefied weak layer (Figure 6.13b). Material under tension in this way can be expected to rupture in a closely-spaced series of coherent blocks, resulting in ridges and troughs at the surface (similar to 'boudinage' occurring on the flanks of folds). This model is put forward as the mechanism responsible for spreading in zone 1, where the failed sediment was thin relative to the distance across which failure can be observed (Figures 6.5; 6.6). The upslope dip of the internal extension faults within the slab is interpreted as an indication that the extensional forces acting on the slab decreased upslope and the frictional drag on the base of the slab increased upslope. The latter may have been due to a decrease in excess pore pressure in the failing layer upslope (away from the source of the overall retrogressive Storegga Slide, as suggested by *Strout and Tjelta* [2005]). Alternatively, the physical character or thickness of the failing layer (believed to be contouritic glaciomarine sediments [*Berg et al.*, 2005]) may have varied with water depth, as is seen in the present day distribution of post-Storegga Slide sediments [*Bryn et al.*, 2005b]. In model 2, failure can potentially start from anywhere along the slope. In this model, the formation of shear planes is expected to obey the Mohr-Coulomb failure

criterion and the upslope faces of the ridges should be steeper than the downslope faces. Both conditions are observed in spreading within zone 1 (Figure 6.6).

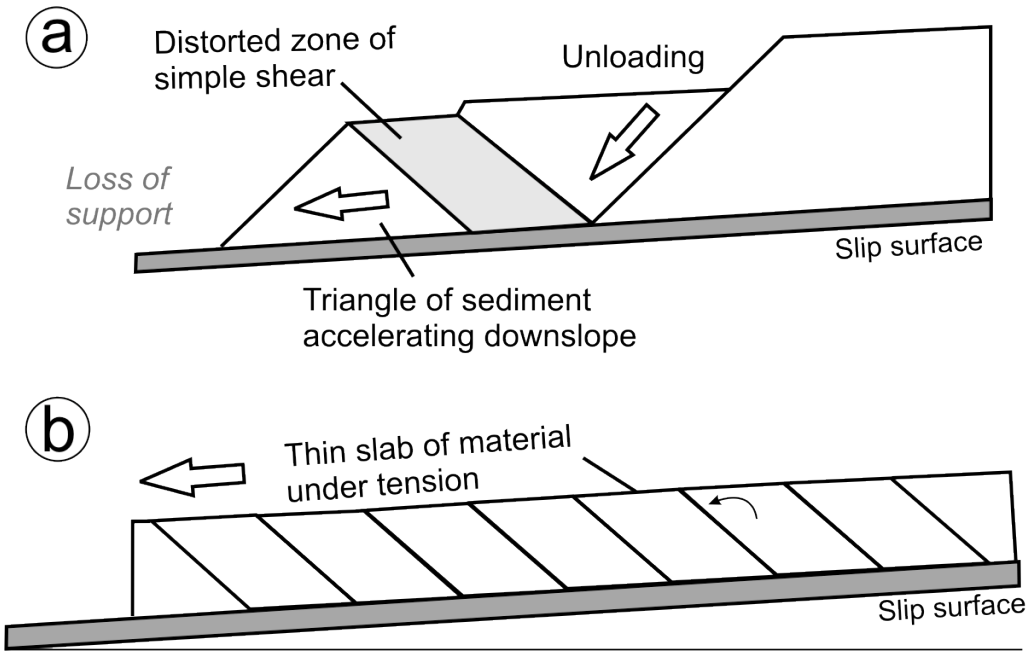

Figure 6.13: Schematic illustration of the two models of failure: (a) model 1 (repeated failure of the headwall, adapted from *Kvalstad et al*. [2005]); (b) model 2 (slab extension and rupturing).

6.5.2 MODELLING SPREADING

Models of spreading have previously been used to determine horizontal ground displacements. In subaerial settings, modelling has been carried out in three main ways: (i) empirical methods [e.g. *Youd et al.*, 2002]; (ii) simplified analytical models [e.g. *Dobry and Baziar*, 1992]; and (iii) finite element methods [e.g. *Kanibir et al.*, 2006]. Modelling of submarine spreading is limited to a numerical model based on the energy approach [*Kvalstad et al.*, 2005a] and the combination of computational fluid dynamics with strain-softening material models [*Gauer et al.*, 2005]. We model submarine spreading using limit-equilibrium and mechanical models that are applicable to the two modes of failure discussed in section 6.5.1. In this way we can identify the potential triggers of a spread, model the pattern of block displacement, and understand which factors control the spreading process.

I THE LIMIT-EQUILIBRIUM MODEL

We consider a thin slab of sediment resting on a planar slip surface, which is initially supported by another slab of sediment downslope. The static forces acting on the upslope slab are illustrated in Figure 6.14. To simplify calculations, the slab consists of a number of adjacent and equidimensional blocks. The static forces acting on each block can be divided into driving forces:

$$Sin\theta\ [W_T] \tag{2}$$

and resisting forces [*Terzaghi and Peck*, 1967]:

$$Tan\ \phi\ [W_T(Cos\ \theta) - u] + c + P \tag{3}$$

θ slope gradient of slip surface, in °
W_T total weight of sediment upslope of a block = γSl, in N
γ submerged unit weight (in 2D), in N m^{-2}
S sediment unit thickness prior to failure, in m
l distance from a fixed point upslope, in m
ϕ angle of internal friction, in °
u pore water pressure (in 2D), in N m^{-2}
c cohesion, in N m^{-2}
P supporting force from slab downslope, in N

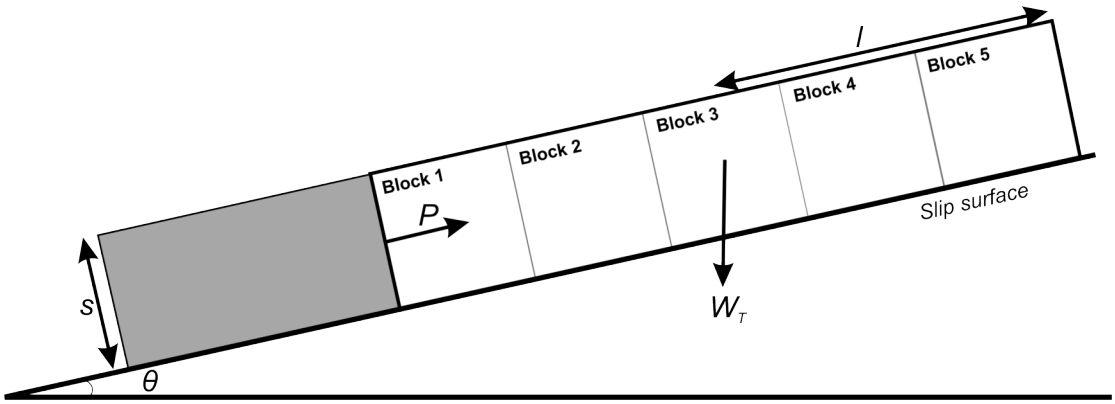

Figure 6.14: Illustration of the mechanical model, showing some of the static forces that act on a sediment slab prior to failure, as well as the dimensional attributes. The dark grey block at the downslope part represents the part of the slope that will fail first, activating spreading in the sediment slab enclosed by the bold black border.

At equilibrium, the driving forces are equal to the resisting forces. An increase in the driving forces or a decrease in the resisting forces will put the system out of equilibrium. This will result in a resultant force downslope and the consequent extension of the upslope slab (as for model 2) or the repeated failure of the headwall (as for model 1). Using equations (2) and (3) we are able to calculate the resultant force at different positions within the slab.

II INITIATION OF DISPLACEMENT

According to static stability analyses carried out using our model, the factor of safety of the slope decreases if there is: (a) a decrease in P; (b) an increase in u; (c) an increase in W_T; (d) an increase in γ; (e) an increase in S; (f) an increase in l; (g) an increase in θ; (h) a decrease in ϕ; and/or (i) a decrease in c. These results provide an insight into the potential triggers of a spread. Failure can be triggered by a temporal, rather than a spatial, change in one or many of the above variables. The variables that are more likely to undergo a temporal change are P, W_T and u. A spread can thus be initiated in a number of ways. A first trigger involves the loss of support at the foot of the slope, such as a slope failure occurring downslope of the spread and the consequent creation of a headwall. As noted in section 6.4.4, a steep escarpment or a slope failure scar is located at the distal part of most spreads within the Storegga Slide. A second trigger consists of an increase in W_T, which can be caused by loading of sediment from a slope failure occurring upslope of a spread. There are no indications that this process was responsible for triggering spreading within the Storegga Slide. However, we think that sediment redistribution and loading are potentially active during compression, and that these processes may reactivate sliding of blocks and the subsequent formation of windows within spreads. A third trigger of spreading can be an increase in pore pressure. This can be a result of contraction due to gas hydrate dissociation or seismic loading. Gas hydrate dissociation is dismissed as a potential trigger because there are no signs of gas hydrates in geoborings from spreading areas [*Kvalstad et al.*, 2005a]. *Kvalstad et al.* [2005a] argue that seismic loading is an unlikely cause of spreading because it has to be of high magnitude and take place over very large areas simultaneously. The Møre Basin, where the Storegga Slide is located, is a deep sedimentary basin that is surrounded by large structures with harder rocks, such as the volcanic marginal high in the southwest,

the Caledonian basement and pre-rift sediments in the east, and the Oligocene/Miocene sediments of the Helland-Hansen Arch in the north. In such a structural setting, the seismic energy is likely to become trapped and the influence of the earthquake prolonged, thus affecting large areas instantaneously [*Lindholm et al.*, 2005]. The source of such a seismic event could have been the glacial isostatic rebound of the Fennoscandian shield and eustatic sea level rise following the LGM [*Atakan and Ojeda*, 2005]. Therefore, we propose that an increase in pore pressure could have been induced by seismic loading. Seismic activity is itself a potential fourth trigger because it may have initiated spreading in two other ways. Seismic loading induces downslope shear stresses that can lead to short-term failure in the sediment. Glacial isostatic rebound, to which the seismic activity is associated, may result in both the sediment and the slip surface becoming steeper, which would also promote instability. Additionally, the combined effect of pore pressure build-up and seismic shear stresses may lead to plastification or liquefaction of the slip layer. Sediment samples taken from the weak layer can actually liquefy under sufficient dynamic loading [*Sultan et al.*, 2004a] and seismic data from the northern sidewall show subsurface sediment disturbance that could be the result of liquefaction [*Berndt et al.*, 2003; 2004]. It is therefore possible that liquefaction controlled the properties of the slip layer for the spreading, particularly as this process is considered to be the main cause of spreading in subaerial environments [*Bartlett and Youd*, 1995]. If liquefaction is only possible for some sedimentary layers and not for most others, this would explain why the spreads occur consistently on the same slip surfaces. Seismic activity has also been identified as the most probable trigger of the entire Holocene Storegga Slide [*Bryn et al.*, 2005a]. On the basis of all the above considerations we conclude that loss of support and seismic loading are the most likely triggers of spreading within the Storegga Slide.

III THE MECHANICAL MODEL

Our model can also be used to constrain the behaviour of the sediment blocks after slope failure has occurred. Assuming that shear planes are formed between the individual blocks in Figure 6.14, equations of motion were applied to each block separately. If we consider the failure as instantaneous, the resultant force, acceleration, velocity and distance travelled by each block can be calculated for different distances

downslope from a fixed point upslope. Fluid resistance and friction at the base of the block are included in the mechanical model. They are assumed to be responsible for decelerating the blocks and are considered constant along the entire length of the slab. Initially, we also assume that the mass of a failed block does not change as it moves downslope. Although we study the movement of each block separately, in reality the blocks move as a group.

This model was applied using values for the different geological and dimensional parameters from a 35 km long section of the seismic line NH0163-n102 (Figure 6.5a). The values of the parameters were either estimated from the seismic line or from published geological data. The width of each block used is 130 m (resulting in a total of 269 blocks over a length of 35 km) whereas the slope gradient of the slip surface (θ) changes from 1º at the headwall to 0.96º in the distal part (a decrease of 1.15º per 1000 km) (Figure 6.5a). Along the entire slab, the sediment thickness (S) prior to failure is considered constant at 80 m (this corresponds to the thickest part of the failed sediment in Figure 6.10). The sediments in this region are thought to become more consolidated upslope towards the shelf edge due to compaction by glacial advance during glacial maxima [*Gauer et al.*, 2005]. Therefore we use values of 9 kN m^{-2} for the unit weight (γ) and 25º for the angle of internal friction (ϕ) at the downslope limit of the slab, which increase linearly to 10 kN m^{-2} for γ and 27.5º for ϕ at the upslope limit (which is the slope gradient of the headwall at this point) [*Gauer et al.*, 2005; *Kvalstad et al.*, 2005a]. An overconsolidated sediment layer that developed during the LGM is known to occur close to the main headwall [*Bryn et al.*, 2005a]. Thus, at 1.5 km from the upslope limit we increase γ linearly from 10 kN m^{-2} to 10.5 kN m^{-2} at the headwall [*Kvalstad et al.*, 2005a]. Unloading of the sediment after the LGM has reduced pore pressures in sediments close to the headwall, whilst measured pore pressures are higher near the North Sea Fan [*Bryn et al.*, 2003; *Strout and Tjelta*, 2005]. Pore pressure (u) is thus decreased from 1000 kN m^{-2} at the downslope limit to 600 kN m^{-2} at the upslope limit of the slab [*Strout and Tjelta*, 2005]. The cohesion (c) in this part of the Storegga Slide is spatially constant at 7 kN m^{-2} [*Sultan et al.*, 2004b]. The supporting force (P) prior to failure is determined for each block by balancing the driving and resisting forces.

Since loss of support is the most likely trigger of spreading within the Storegga Slide, the spread in the mechanical model is triggered by the removal of the sediment at the

distal part of the slope and reduction of P to 0 for block 1. The graph in Figure 6.15(a) shows the velocity attained and distance covered by blocks in the middle section of the slab. The first block to be released has the highest values of W_T, l and u, and the lowest values of γ, ϕ and θ. These conditions generate the highest possible resultant force, and therefore the highest velocity and longest distance covered. For successive blocks upslope, W_T, l, u, γ, ϕ and θ change, resulting in a lower resultant force, and thus lower velocities and shorter distances travelled (Figure 6.15a). The variation of the displacement for each block is also shown. The curve illustrates that the displacement of the blocks increases exponentially with distance downslope. This pattern is similar to the empirically estimated ridge displacement pattern (Figure 6.12).

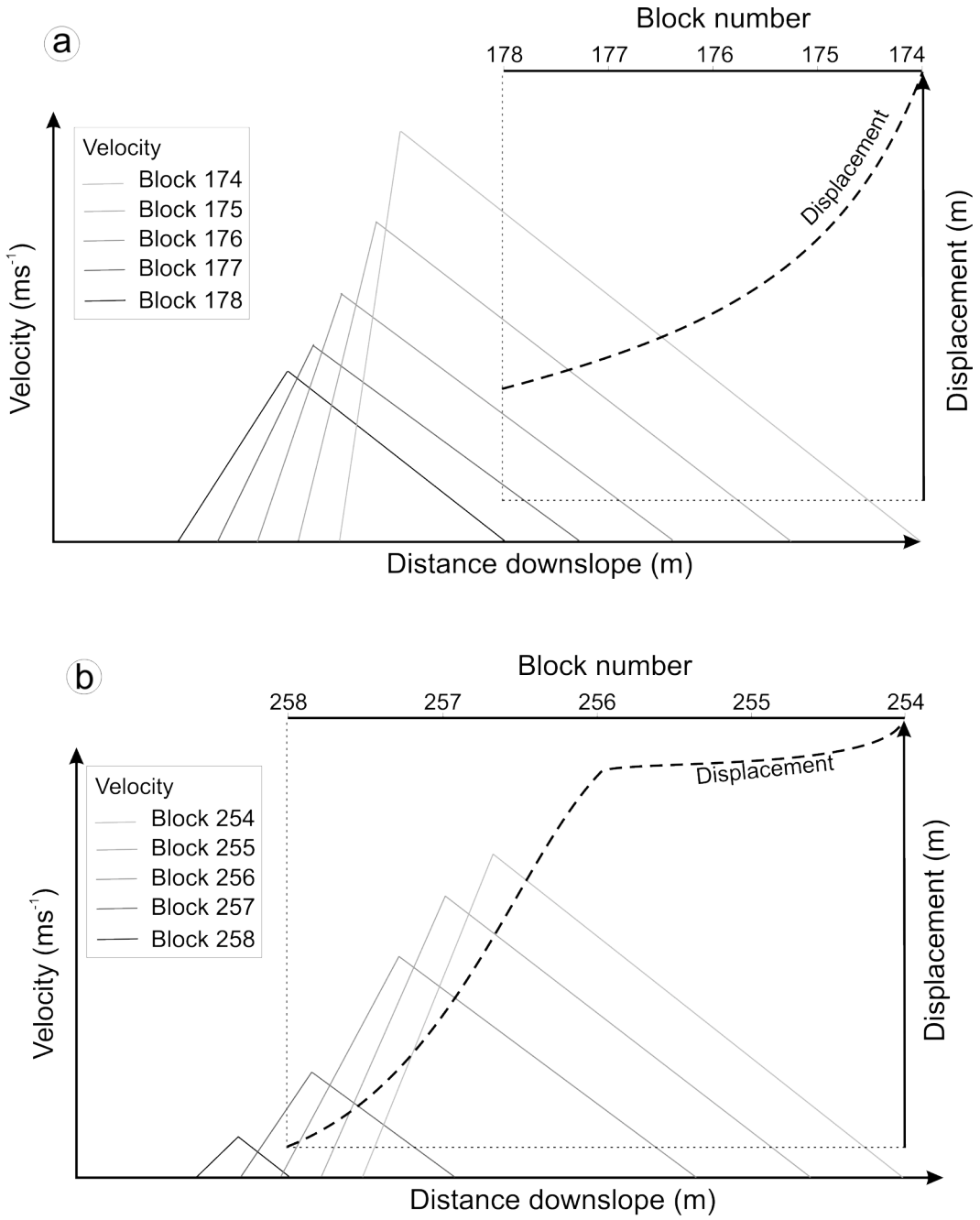

Figure 6.15: Plots of velocity vs. distance downslope for a group of blocks in a theoretical spreading event modelled using values from the Storegga Slide in the mechanical model. The block numbers refer to the order in which a group of blocks in an upslope section of the slope is displaced. Also shown is the variation of block displacement with block number. (a) Block movement pattern observed in the middle of the slab. The resulting pattern is an exponential increase of displacement of blocks with distance downslope. (b) Block movement pattern for the upslope 1.5 km of the slab where an increase in angle of internal friction occurs due to an overconsolidated layer developed during the LGM. The resulting pattern shows a steep decrease in displacement, which should coincide with the formation of a steep headwall.

The graph in Figure 6.15(b) shows the velocity attained and distance covered by blocks in the upslope 1.5 km of the slope, where a further increase in γ occurs. The abrupt decline in displacement of blocks 257 and 258 explains the spreading pattern observed near some sections of the main Storegga headwall, where the displacement of the extended ridges decreases rapidly upslope and a steep, stable headwall is formed (Figure 6.8c). Without the increase in γ upslope, we would expect the displacement of the blocks to decrease gradually upslope until a low and gentle headwall is formed (Figure 6.8d).

In the above mechanical model we assumed that the failure was instantaneous. It is important to appreciate that the block displacement pattern illustrated in Figure 6.15 could also be the result of an increase in the duration of movement of successive blocks with distance downslope. The geophysical data does not provide any information to understand whether the increase in displacement with distance downslope is due to an increase in velocity alone, or due to an increase in both velocity and time (Figures 6.5; 6.6).

In our mechanical model we do not consider tilting, distortion, plastic deformation or loss of excess pore pressure due to block fragmentation. If these factors were to be taken into account, their combined effect would be to slow down the movement of the downslope blocks most, expending the kinetic energy and resulting in a subdued exponential decay (as observed in Figure 6.12). In the model we also assume that the failure is triggered by loss of support in the distal part of the slab. An alternative scenario, as explained in section 6.5.1, is that failure in a spread is initiated somewhere along the slab by a change in the sediment properties and/or boundary conditions (Figure 6.13b). When spreading initiates along the slab, the displacement pattern of the sediment blocks upslope of the point of failure is expected to be similar to that shown in Figure 6.15a and involve propagation by retrogression. Downslope of the failure point, compression and/or failure of the sediment slab due to loading are expected to occur, potentially resulting in a window.

The distance travelled by the blocks in the distal part of the slope would theoretically increase continuously with the length of the slope. This is, of course, not the case, as we do observe that the distal parts of spreads stopped either on the slope or after

crossing an escarpment. Apart from fluid friction and kinetic friction with the underlying sediments, other factors are involved in slowing down a spread. With increasing translation downslope, the distal part of the spread undergoes increasing fragmentation and remoulding due to either friction or collapse over a headwall. This disintegration may allow escape of excess pore pressure from the base of the spread, reducing the resultant force acting on the spread and bringing it to a halt. Additionally, as the spread extends and breaks up, it is likely to become thinner. Such thinning can be observed in the seismic data (Figures 6.9a; 6.10a). The decrease in *S,* combined with the decrease in θ with distance downslope, will also reduce the resultant force acting on the spreading unit, retarding the block displacement further.

6.5.3 DEVELOPMENT OF SPREADING WITHIN THE STOREGGA SLIDE

We use the results from the previous calculations and models to describe how spreads develop within the Storegga Slide (Figure 6.16). The most probable trigger for spreads is either loss of support, due to mass movements occurring downslope of a potential spreading unit, or seismic loading, which results in pore pressure development and downslope shear stresses. A spread may thus initiate somewhere along its length, with the failure propagating upslope from this point, or it may initiate instantaneously over large portions of its area. Once a spread is triggered, the sediment unit breaks up into a number of blocks. The formation of the shear planes between the blocks obeys the Mohr-Coulomb failure criterion. A pattern of parallel to sub-parallel ridges and troughs forms at the surface. The ridges are orientated perpendicular to the direction of movement. The blocks at the leading edge of the spread are displaced the most. The distal end generally collapses over the pre-existing downslope headwall created by the mass movement that triggered the spread, and the sediment either evolves into a debris flow or translates on a different slip surface, preserving the ridge and trough morphology. The seafloor located downslope of the headwalls in the distal part of zone 1 is characterised by a blocky morphology, whereas subtle ridge and trough morphology can still be observed in spreading material that has crossed the distal headwall in zone 2. This means that what happens to the material at the distal end of a spread depends on its sediment properties, in particular its consolidation and thickness.

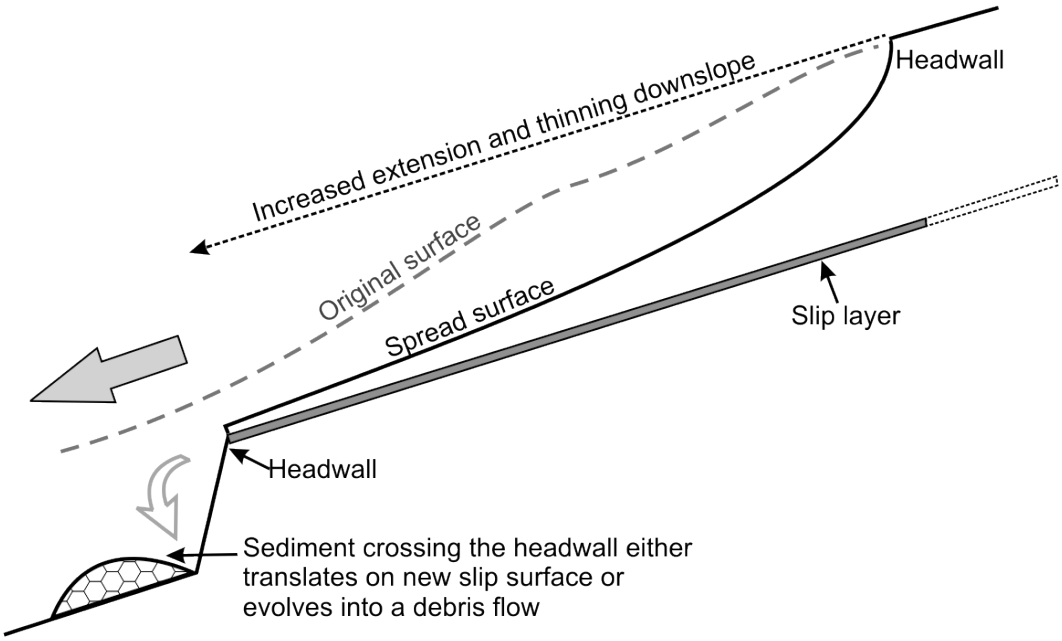

Figure 6.16: Schematic cross-section through a typical spread within the Storegga Slide.

Spreading primarily involves extensional deformation. In some places, however, the spread may have undergone compression, as suggested by the presence of groups of high convex-downslope ridges and troughs (Figure 6.4a), and as previously described in other mass movements [e.g. *Lastras et al.*, 2006]. This compression is attributed to the slowing down of the leading edge due to, for example, increased fragmentation and the associated reduction in pore pressure, or a decrease in the gradient of the slip surface. Consequently, the ensuing blocks may collide with the immobilised blocks, resulting in overthrusting and compression. The morphological signature of compression is a series of ridges and troughs that tend to be longer and more pronounced than those formed by extension. During compression, the spreading layer may heave and become thicker. Where this occurs, the increased thickness in the sediment may reactivate mobilisation in the form of translational mass movements.

Extension, friction and water resistance, acting on the major part of the spread, fragment and remould the blocks as they move downslope. These result in the escape of excess pore pressure from the sediment and thinning of the failing unit, which slow and finally halt the mobilised sediment. Fragmentation of the blocks decreases upslope. The displacement of blocks decreases exponentially upslope until the driving and resisting forces reach equilibrium at the headwall. In reality, the block extension pattern may be

more complex and involve different scales of fracturing. Figures 6.4(b) and 6.12 indicate that the sediment unit may initially break up into a number of relatively large blocks. Subsequently, each of these blocks fragments into a number of smaller blocks. The groups of small blocks exhibit an exponential decay of displacement upslope, in accordance with the general pattern displayed by all the blocks (Figure 6.12). A gradual decrease in the thickness of the spreading unit also accompanies the increasing displacement downslope (Figures 6.9a; 6.10). The overall extension of a sediment unit during spreading results in the lowering of the seabed. According to the observed pattern of block displacement, we would expect the spread to gradually transform into a stable slope as it extends upslope, forming a shallow and gentle headwall. This only occurs in zone 3, however, because the presence of overconsolidated sediment due to glacial compaction in zones 1 and 2 retards block displacement further and results in a higher and steeper headwall.

As shown in section 6.5.2 - III, the factors that vary the most across a sediment sub-unit are the angle of internal friction, pore pressure and the gravitationally-induced stress, the latter being determined by the thickness of the sediment, the length of slope upslope and the unit weight. These three factors are thus considered the major controls of the extent of spreading and responsible for the exponential increase of block displacement with distance downslope (see Appendix for an estimation of the relative control of each factor on the extent of spreading). The decrease in the thickness of the O3 sediment sub-unit upslope [*Berg et al.*, 2005] may also play a role in determining the position of the main headwall in zone 1 and in giving rise to downslope-increasing extension. As shown in Figure 6.9b, the gradient of the slip surface mainly controls the direction in which a sediment unit spreads. This has also been observed in terrestrial spreading in Japan [*Youd and Kiehl*, 1996].

There are two modes of spreading within the Storegga Slide. Within zone 1a the failing sediment behaves as a slab that is extended and breaks up into a number of blocks (model 2). The similarity in ridge and trough morphology indicates that zone 1b fails in the same way. Spreading within zones 2 and 3 occurs via the retrogressive unloading of the headwall, as explained by *Kvalstad et al.* [2005] (model 1). The different behaviour of zones 1 and 2 presumably reflects differences in sediment type. In zone 1, failure occurs in thin, stratified sediment with a high clay content (up to 65%), which enables

it to behave as a thin slab undergoing extension along its entire length [*Berg et al.*, 2005]. The thicker sediment in zone 2 has lower clay content (up to 40%), and failure occurs along a distinct stratigraphic boundary. Zone 3, on the other hand, might represent a variation on zone 2 where the O3 sediment sub-unit, acting as the slip layer, is on the point of pinching out. Because of this, the extent of spreading upslope of the scarp is restricted. The failure of these sediments as a spread, rather than other types of mass movement, is attributed to the deep burial of the sub-units O3 and O4-O7. These sediments are more compacted and thus favour brittle deformation, although the sediment in the distal part of the spread undergoes plastic deformation. The plastic deformation may be attributed to the higher deformation and the increasing pore pressure in the sediment with distance downslope [*Strout and Tjelta*, 2005]. Failure generally occurs in stratigraphically inhomogeneous sediments, which promote mass movement through basal deformation [*Laberg and Vorren*, 2000]. Spreading occurs along surfaces within the fine-grained contouritic sediments (O3 and R2 sub-units), which are characterised by higher water content, pore overpressure (due to low permeability), clay content and plasticity, and lower unit weight with respect to the glacial sediments [*Kvalstad et al.*, 2005b]. The fine-grained sediments are thus more geotechnically sensitive than the poorly sorted and coarser-grained glacial sediments [*Bryn et al.*, 2005b].

The properties of the sediment unit in which spreading occurs also have a direct control on ridge and trough morphology. The ridges in zone 2 are the longest, the most widely spaced and they have the deepest troughs. The larger spacing can be explained by the greater burial depth and higher consolidation of the sediments, which results in a higher angle of internal friction and unit weight [*Berg et al.*, 2005]. The sediment failing in zone 2 is also the thickest. Overall these conditions generate a high gravitationally-induced stress. This results in a higher acceleration of the blocks, as well as a steeper exponential decay in block displacement with distance downslope, which is reflected in higher ridge spacing. The latter also causes the troughs between the blocks to be deeper. The blocks are more consolidated and they do not break down as easily as blocks in the shallower sediments, resulting in longer ridges. As spreading occurs in progressively shallower, thinner and less consolidated units (zones 1a, 1b and 3), the ridges are observed to be shorter, more closely spaced and separated by shallower troughs (Table 6.1). The sediment also undergoes more plastic deformation.

Chapter 7:

RESULTS: FRACTAL STATISTICS AND MORPHOLOGY

Scale invariant characteristics of the Storegga Slide and implications for large-scale submarine mass movements.

Aaron Micallef, Christian Berndt, Douglas G. Masson and Dorrik A.V. Stow

This chapter is a research article that has been submitted for publication to Marine Geology on the 10th April 2007. It has been accepted for publication on the 1st September 2007 and is currently in press.

An abridged version of this paper has been published in pages 3 – 10 of the book 'Advances in Natural and Technological Hazards Research' edited by Lykousis, V. Sakellariou, D. and Locat, J. and published by Kluwer Academic Publishers in 2007.

7.1 INTRODUCTION

Submarine landslides are a common phenomenon on continental margins. In particular on lower and middle latitude active margins, large landslides are a dominant geomorphic agent that transfers sediment across the continental slope [*Masson et al.*, 2006], and they play a major role in the evolution of submarine landscapes. The Storegga Slide, located 120 km offshore Norway, is one of the largest known submarine landslides (Figure 7.1). Dated at 8100±250 cal. yr BP [*Haflidason et al.*, 2005], the Storegga Slide is the last in a series of slope failures that have characterised the mid-Norwegian Margin during the past 2.6 Ma [*Solheim et al.*, 2005a]. It generated one of the largest tsunamis ever documented in the North Atlantic Ocean, with a run-up of up to 20 m [*Bondevik et al.*, 2005]. The Storegga Slide consisted of sixty-three quasi-simultaneous mass movements, which span an area of 95 000 km^2 and have evacuated 2400-3200 km^3 of sediment [*Haflidason et al.*, 2004]. These mass movements formed an amphitheatrical depression that contains numerous headwalls and scarps, the largest of which being the 320 km long main headwall located at the shelf break. The scar also encloses morphological features recognised as spreads, debris flows, turbidity current pathways and compressional ridges, which occur across a depth range of ~2700 m. The sedimentological framework of the Storegga Slide area is characterised by the alternation of glacial diamictons and ice-proximal sediments deposited during glacial maxima, and fine-grained glacimarine, hemipelagic and contouritic sediments deposited during interglacials [*Berg et al.*, 2005]. Because of its complexity and size, we consider the Storegga Slide as a macro-scale geomorphological system [*Summerfield*, 1991].

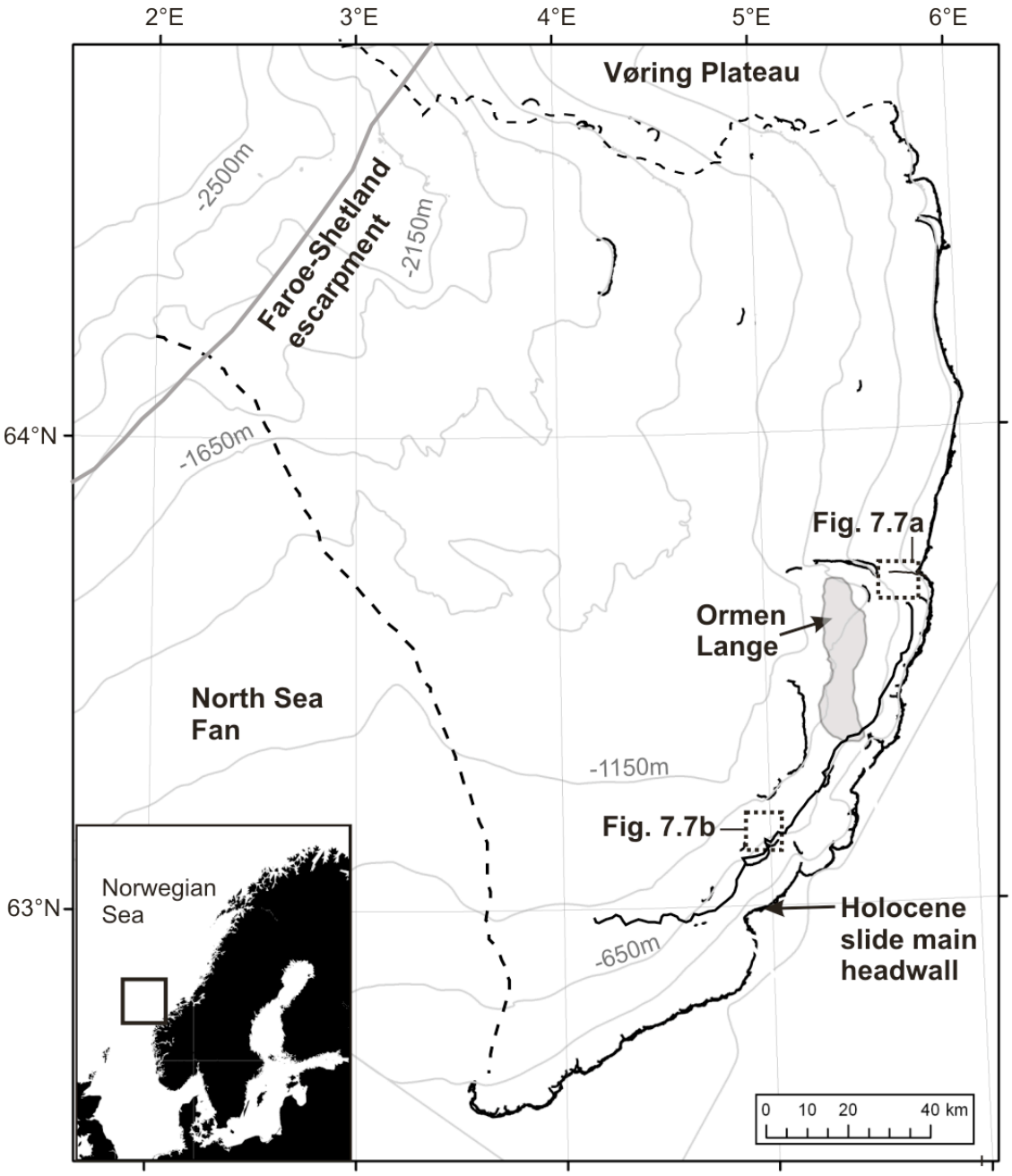

Figure 7.1: Bathymetric map of the Storegga Slide. Bathymetric contours at 250m intervals are shown as grey lines, whereas the extracted headwalls are represented by solid black lines. The dashed black line indicates the boundaries of the Storegga Slide. The location of the slide is shown in the inset.

Concepts associated with non-linear dynamic systems, such as fractals, chaos and self-organisation, have gained considerable attention in many aspects of the geosciences. The fractal model, for instance, captures aspects of topography that other morphometric

measures do not [*Klinkenberg*, 1992], and it provides a powerful approach to the representation of geoscientific data. The growing use of digital elevation models and the increasing resolution of topographic data sets have enabled geomorphologists to identify fractal structures and scale invariance in numerous subaerial environments [e.g. *Pelletier*, 1999; *Southgate and Möller*, 2000]. The statistical characteristics of large populations of landslides, for example, have become a recent focus of study in geology and geomorphology [e.g. *Guzzetti et al.*, 2002; *Hergarten*, 2003; *Turcotte et al.*, 2006]. Submarine mass movements, however, are still generally studied as isolated slope failure events using an engineering approach [e.g. *Kvalstad et al.*, 2005a; *Sultan et al.*, 2004a]. As the exploration and exploitation of the ocean floor moves into the deeper continental slope, there is an increasing demand for the quantification of risk associated with submarine slope failures. Probabilistic hazard assessments, for example, depend on the extrapolation of mass movement inventories. In order to perform such assessments, the frequency-magnitude relations of mass movements and their scaling behaviour must be identified and understood [*Wolman and Miller*, 1960].

The available statistics of submarine mass movement data are generally poorly characterised when compared to those of subaerial mass movements. The Storegga Slide scar, on the other hand, has been thoroughly surveyed using state-of-the-art acoustic imaging techniques. This provides us with the opportunity to investigate this geomorphological system at a large scale and carry out a statistical and fractal analysis of the constituent mass movements. The purpose of the study is to: (a) Assess whether the Storegga Slide exhibits scale invariance in terms of the statistics and morphology of its constituent mass movements; (b) Identify the origin of the scale invariance in terms of system dynamics and geological processes.

7.2 CONCEPTUAL FRAMEWORK

7.2.1 GEOMETRIC SIMILARITY

In mathematics, geometric similarity is used to describe two objects that are congruent under uniform scaling. A similarity transformation consists of a function from a Euclidean space into itself by multiplying all Euclidean distances by the same positive

scalar *r*. Homothety, or central similarity, is a special type of similarity transformation, whereby orientation and angles are preserved. In a homothetic transformation, distances are dilated by a factor *r* with respect to a fixed point *O*, called the origin. A homothetic transformation maps a point *X* in Euclidean space to *X'*, as:

$$O - X' = r(O - X) \tag{1}$$

7.2.2 FRACTALS

Geometric similarity at different scales is the basis of the concepts of scale-invariance and fractals. A fractal is a term coined to define a set/function for which the Hausdorff-Besicovitch dimension exceeds the topological dimension [*Mandelbrot*, 1977]. Fractal geometry includes shapes characterised by irregularities that conform to non-Euclidean structures. The best way to describe a fractal is through its attributes. The most important characteristic of a fractal geometric object is self-similarity at a variety of scales, whereby the object contains scaled copies of itself. Another attribute of a fractal object is infinite length and complexity. Known as the Steinhaus paradox [*Steinhaus*, 1960], the degree of detail of a fractal object increases infinitely as the scale decreases. A fundamental property of fractals is their fractal or similarity dimension (*D*). This is a single, non-integer value representing the scaling relationship between the apparent length and measuring scale. The fractal dimension also gives a useful measure of the complexity or roughness of a spatial pattern. Unlike mathematical fractals, natural objects are not strictly self-similar, but rather statistically self-similar. In a statistically self-similar object, measurable statistical parameters are repeated at all scales. The object does not comprise exact copies of itself at all scales, but the object will contain no geometric indication of its scale [*Goodchild and Mark*, 1987].

The fractal model and the concepts of self-similarity have been successfully applied to different types of geoscientific data: e.g. fluvial systems [*Pelletier*, 1999; *Rigon et al.*, 1996]; slope instabilities [*Guzzetti et al.*, 2002; *Hergarten*, 2003]; and coastal profiles [*Southgate and Möller*, 2000]. The statistical self-similarity of linear and areal phenomena are generally evaluated by demonstrating a single power law exponent based on iterative measurements across at least one order of magnitude [*Mandelbrot*,

1983]. The self-similar properties of data inventories are investigated using frequency-magnitude relationships. A power law distribution implies that when we compare the number of events of size A or greater, with the number of events of size ηA or greater (where η is an arbitrary factor), the number always differs by the same factor of $\eta^{-\beta}$, regardless of the absolute size of the events. It has also been shown that the power law distribution can be replaced with other measures of the size of the event [*Hergarten*, 2003]. This means that a power law distribution is free of a characteristic scale and is thus fractal [*Mandelbrot*, 1983].

7.3 MATERIALS AND METHODS

7.3.1 DATA SETS

Our investigation of the Storegga Slide is mainly based on a high-resolution multibeam bathymetry data set that covers the slide scar from the main headwall down to a water depth of ca. 2700 m (Figure 7.1). Most of the data have a horizontal resolution of 25 m or better. Two other acoustic data sets complement our analyses. The first comprises Towed-Ocean-Bottom-Instrument (TOBI) sidescan sonar imagery that covers 20 000 km^2 of the slide scar area with a nominal horizontal resolution of 6 m. The second consists of high resolution 2D seismic lines, located across the main headwall and northern sidewall, and 2000 km^2 of industry-type 3D seismic data located across the northern sidewall.

7.3.2 EXTRACTION OF HEADWALLS AND ESTIMATION OF THE AREA OF MASS MOVEMENTS

A mass movement is defined as a single episode of slope failure where sediment moves downslope under the influence of gravity. The mass movement area is defined by a headwall at the upslope limit, which is a steep escarpment created by the evacuation of sediment during the mass movement, and a depositional section at the distal point of the mass movement. Mass movement area is a suitable proxy for the magnitude of mass movement events [*Guzzetti et al.*, 2005]. Area, volume and thickness of mass movements were shown to be strongly correlated with each other, and a distribution can

be converted between these variables [e.g. *Hergarten*, 2003; *Hovius et al.*, 1997; *Pelletier et al.*, 1997]. In addition, measurements of area tend to be more reliable than those of volume or energy [*Canals et al.*, 2004]. On the other hand, the delineation of the boundaries of individual mass movements in a complex retrogressive landslide like the Storegga Slide is difficult. This is because the distal parts of some mass movements have collapsed over a headwall and evolved into plastic flows [*Micallef et al.*, submitted]. The mass movements within the Storegga Slide occurred quasi-simultaneously [*Haflidason et al.*, 2005], and the deposits of some mass movements have intersected or overlapped other deposits. Furthermore, TOBI sidescan sonar imagery is not available for the entire slide scar, which makes the differentiation between seafloor textures and the boundaries of adjacent mass movements more problematic. In comparison to mass movement boundaries, headwalls constitute prominent morphological features that are both easily identifiable and large compared to noise in the data. The terminations of a headwall are defined by the zone where sediment movement has occurred perpendicularly to the headwall (in contrast to parallel, which defines the sidewall).

Previous studies, based on the visual interpretation of bathymetric and sidescan sonar data from the Storegga Slide, have identified sixty-three mass movements and determined their dimensions [*Haflidason et al.*, 2004]. We first used published data on fifty-eight of these landslides to investigate the relationship between headwall length and mass movement area within the Storegga Slide (Figure 7.2). We excluded data on the five larger lobes (lobes 1 – 5) because their boundaries have not been determined accurately. $R^2 = 0.91$ implies a strong statistical dependency between area and length in the form of a power law:

$$A = 0.8705\, l^{1.9828} \qquad (2)$$

- A area of mass movement, in m^2
- l length of headwall, in m

We assume that this relationship applies to all mass movements within the Storegga Slide, and that we are able to estimate the area of a mass movement if we know the length of the associated headwall.

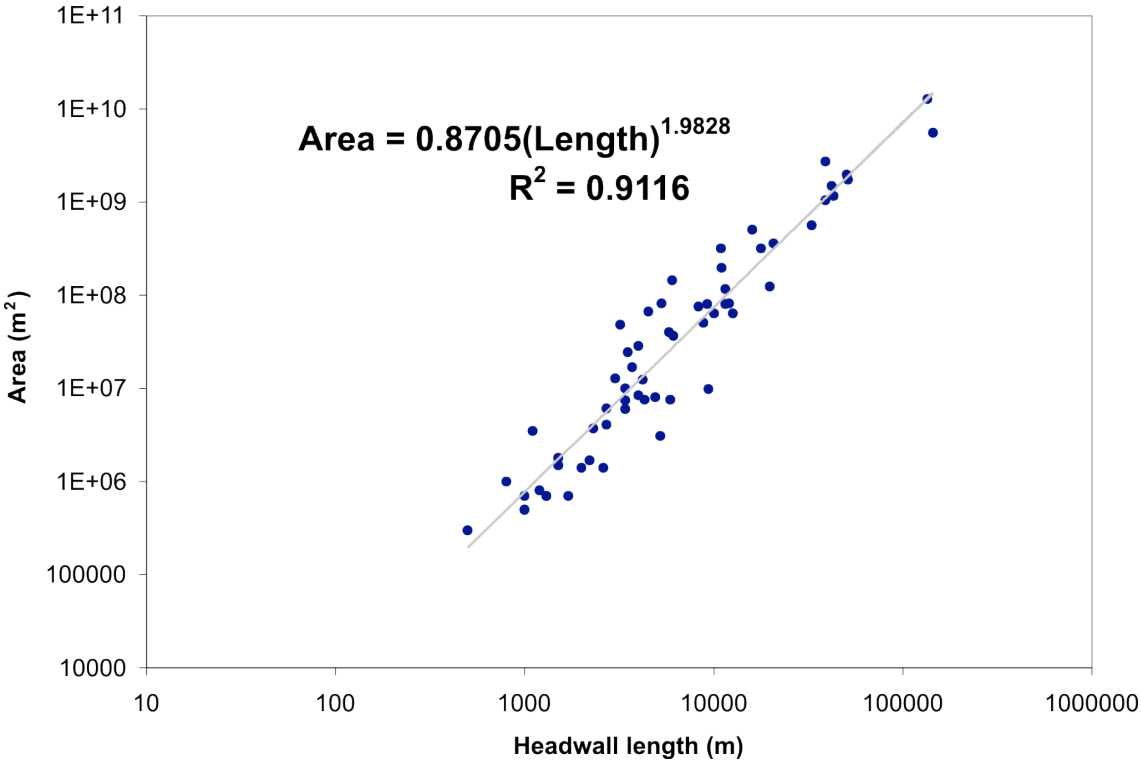

Figure 7.2: Plot of mass movement area vs. headwall length of fifty-eight mass movements (excluding the five largest lobes) identified in *Haflidason et al.* [2004].

Building on this simple analysis, the headwalls of the mass movements were extracted automatically from the bathymetric data set. A geomorphometric map, which is a parametric representation of a landscape decomposed into its elementary morphological units, was generated for the study area. The morphological units, which include breaks and changes of slope, are extracted automatically as lineaments that are complemented by topographic information. The method of producing a geomorphometric map is described in *Micallef et al*. [2007a]. Headwalls, identified as continuous lineaments of breaks of slope, were assigned to a mass movement by using the sidescan sonar imagery, seismic data and geological information available in the literature. The terminations of the headwalls were determined manually by identifying the sections of the breaks of slope where sediment has been mobilised in a direction perpendicular to the lineaments. The lineaments that comprise a headwall were then grouped together and reduced into a single lineament having a thickness of one cell. In comparison to manual digitisation, the automatic extraction of headwalls from bathymetric data has the advantage of delineating headwalls at the highest resolution of the bathymetric data rather than at the

scale at which the investigator is observing the data set. The technique is thus more rapid and accurate than manual digitisation [*Micallef et al.*, 2007a].
Using geomorphometric mapping we were able to identify one hundred and fifteen headwalls, which comprised headwalls created by single (termed individual headwalls) or multiple (termed composite headwalls) mass movement events (Figure 7.1). We restricted our choice to headwalls that are clearly discernible from the bathymetric data set, and ignored headwalls with unconstrained terminations. The types of mass movement associated with each headwall were interpreted on the basis of morphology, internal structure and the inferred process of material mobilisation. The interpretation was carried out in accordance with the criteria established for identification of mass movements [*Mulder and Cochonat*, 1996] and for spreading [*Micallef et al.*, 2007b]. The x- and y- co-ordinates (in Universal Transverse Mercator co-ordinate system) of each vertex point in the headwall lineament were extracted and the length of each headwall was calculated using a Geographic Information System. The area of the mass movement associated with each headwall was estimated using equation (2). A cumulative frequency-area graph was plotted for the individual mass movements, from which a non-cumulative distribution was derived.

7.3.3 ESTIMATING THE FRACTAL DIMENSION *D* OF HEADWALLS

Numerous methods have been proposed to determine the fractal dimension of topography [*Goodchild*, 1982; *Klinkenberg and Goodchild*, 1992; *Mandelbrot*, 1983]. Only a few of these are suitable for calculating the fractal dimension of 2D features [*Klinkenberg*, 1994]. We used a standard technique known as the divider method. The basis for this vector-based technique is that the statistical variation between samples is a function of the distance between them. A divider is "walked" along the headwall lineament using a set width step (τ) and the number of steps required to cover the entire line is recorded. This number is then used to calculate the length of the lineament (L). τ is then increased by a fixed increment and the stepping process is repeated. The relation between length of the steps and calculated length of the lineament is:

$$L \propto \tau^{1-D} \tag{3}$$

The fractal dimension D can thus be determined by plotting log L against log τ and estimating the slope using a least squares linear regression.

$$D = 1 - \lim_{\tau \to 0} \delta \log L / - \delta \log \tau \quad (4)$$

This method was carried out using a FORTRAN code.

As suggested by *Klinkenberg* [1994], the following procedures were implemented to improve the reliability of this technique: (i) the remainder, produced because the number of steps required to cover a lineament most often is a non-integer number, was added to the number of steps as a fraction; (ii) the last intersected point along a lineament was used as the next "walking point" rather than the first; (iii) ten starting points were selected and the calculated values were averaged; (iv) the smallest step size was twice the shortest distance between any two points and one-half the average distance between adjacent points. Examples of the use of this technique in geosciences include *Goodchild and Mark* [1987] and *Aviles et al.* [1987]. Compared to other methods, the divider method is less computationally expensive, easier to use and gives equally good results [*Angeles et al.*, 2004].

7.3.4 DETERMINING THE GEOMETRIC SIMILARITY OF HEADWALLS

We based the determination of geometric similarity on the homothetic transformation concept. For each of the one hundred and fifteen headwalls, the following method was used. The extracted headwall was rotated so that its initial and final vertices were aligned horizontally from west to east (Figure 7.3a). The curved part of the headwall was always on the top. The mid-point between the initial and final vertex of each headwall was determined, and the mid-points for all headwalls were moved to a common position, *O*.

For each pair of headwalls, it was first ensured that both headwalls had the same number of co-ordinates. This involved using simple linear interpolation for the shorter headwalls to estimate the position of intermediate points between the extracted co-

ordinates. Then, for each headwall, the distance of each co-ordinate of the headwall from *O* was calculated (in m) (Figure 7.3a). The same was repeated for the second headwall. At this point we had two sequences of data. We used regression analysis to understand how similar these sequences were. The distance of each point from the first headwall was plotted against the distance of the corresponding point from the second headwall. A linear trend line starting from the origin was fitted to the plot using least squares linear regression, and the R^2 value was determined. This value represents how similar the sequences of data, and therefore the two headwalls, are (with 1 indicating perfect similarity, and 0 showing no similarity). This value is termed the similarity co-efficient. This procedure was carried out for all pairs of headwalls in Storegga (a total of >13 000 pairs).

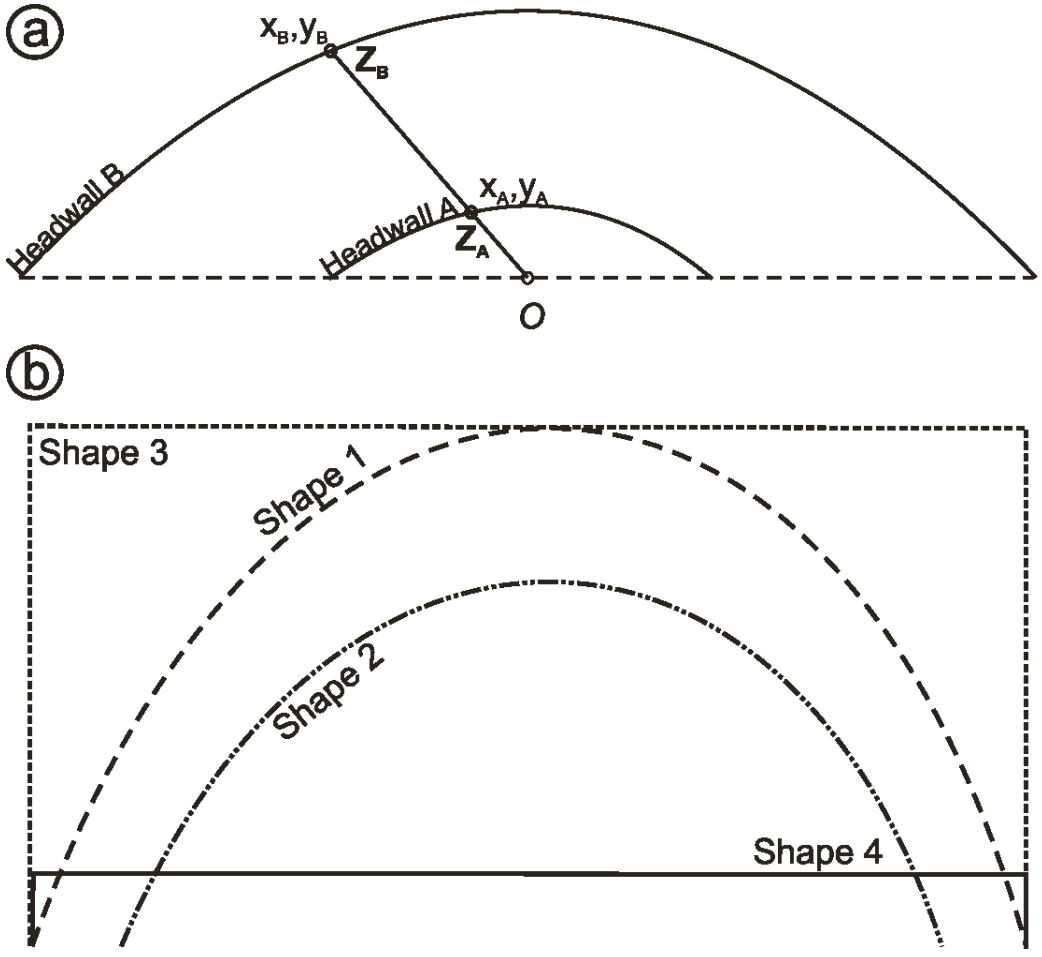

Figure 7.3: (a) Illustration of the method used to determine geometric similarity. The distance of point Z_A on headwall A was calculated from *O* using the x- and y- co-ordinates. The same was repeated for the corresponding point on headwall B. This was

carried out for all the points on the headwalls. The two sequences of data were then compared using linear regression. (b) Shapes used for the sensitivity analysis of the method for the calculation of the similarity coefficient.

I SENSITIVITY ANALYSIS

The above technique was tested using the basic shapes shown in Figure 7.3b. The calculated similarity coefficients for pairs of shapes are shown in Table 7.1. The highest similarity is observed between shapes 1 and 2, and the lowest between shapes 2 and 4. A visual comparison of the shapes supports the results (Figure 7.3b).

Table 7.1: Geometric similarities for pairs of shapes considered in the sensitivity analysis.

	Shape 1	**Shape 2**	**Shape 3**	**Shape 4**
Shape 1	**1**	0.8895	0.5272	0.0196
Shape 2	0.8895	**1**	0.4418	0.0110
Shape 3	0.5272	0.4418	**1**	0.0563
Shape 4	0.0196	0.0110	0.0563	**1**

7.4 RESULTS

7.4.1 FREQUENCY-MAGNITUDE RELATIONSHIPS

The estimated areas of the mass movements identified within the Storegga Slide range between 0.27 km^2 and 1174 km^2, with a mean of 42.92 km^2 and a median of 7.19 km^2. To enable comparison with previous studies and model results, the distribution is presented as a non-cumulative distribution (Figure 7.4). A non-cumulative distribution is defined in terms of the negative of the derivative of the cumulative distribution with respect to A [*Guzzetti et al.*, 2002]. It is calculated by approximation of the slope of the best-fit line to five adjacent cumulative data points. The result is then normalised to total area. The majority of the data in the non-cumulative distribution can be best correlated with a negative power function:

$$dN/dA = 4000.2\ A^{-1.6320} \quad (5)$$

N cumulative number of mass movements with an area > A

This distribution implies that the low magnitude (small area) mass movements are more frequent than the higher magnitude (large area) mass movements, and that the change in frequency is to the power of 1.63. The range of area over which this relationship is valid is 1 – 100 km^2. The data set varies from power law scaling for A < 1 km^2 and A > 100 km^2.

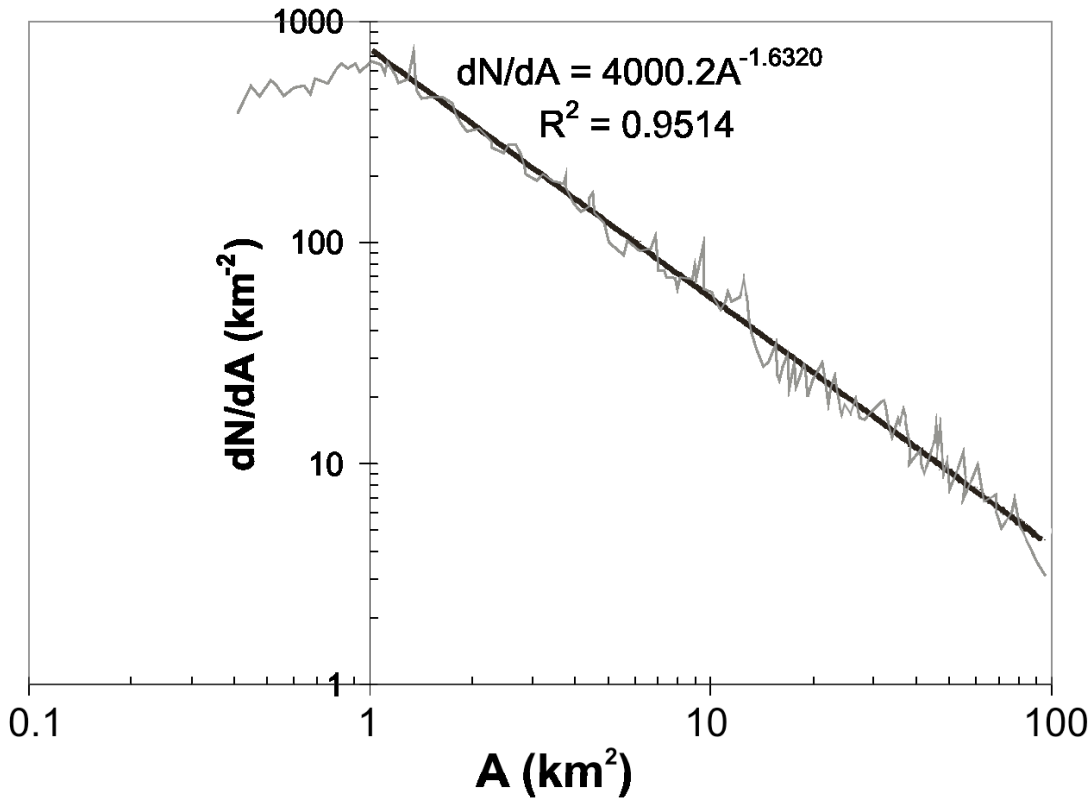

Figure 7.4: Non-cumulative frequency-area distribution for the mass movements associated with the one hundred and five individual headwalls extracted in this study. The roll-over of data away from power law scaling occurs at an area of 1 km^2.

7.4.2 FRACTAL ANALYSIS

The $\log_{10}$ of L and τ (both in m) were plotted for each headwall on a Richardson plot (Figure 7.5). For most headwalls, the right hand side of the Richardson plot is

characterised by a null slope because the highest magnitudes of τ cannot discriminate the large-scale roughness elements. This is an edge effect in the measurement that tends to reduce the apparent fractal dimension of the headwalls, and thus it was removed from the data before calculating the fractal dimension D. Additionally, on the left hand side of the Richardson plot, as τ decreases and approaches the limit of data resolution, L is also asymptotic (Figure 7.5). The values affected by this were also excluded from the calculations. A least-squares line was fitted to the remaining data (Figure 7.5). The R^2 value obtained for each headwall was generally higher than 0.95. To test how well the assumption of linear regression for the data points is satisfied, and to assess whether the headwalls exhibit systematic deviation from strict self-similarity, we analysed the residual structure of the least squares linear regression for each headwall [*Andrle*, 1992; *Klinkenberg and Goodchild*, 1992]. The standardised residuals were plotted from the best fitting line and the data distribution was analysed. In all the cases, the distribution of the residuals shows no obvious pattern, the data points are evenly distributed and they lie between ±2 standard deviations. This shows that the linear regression model is appropriate for our data set. Therefore the gradient of each line of fit was determined from the Richardson plot and the fractal dimension calculated accordingly.

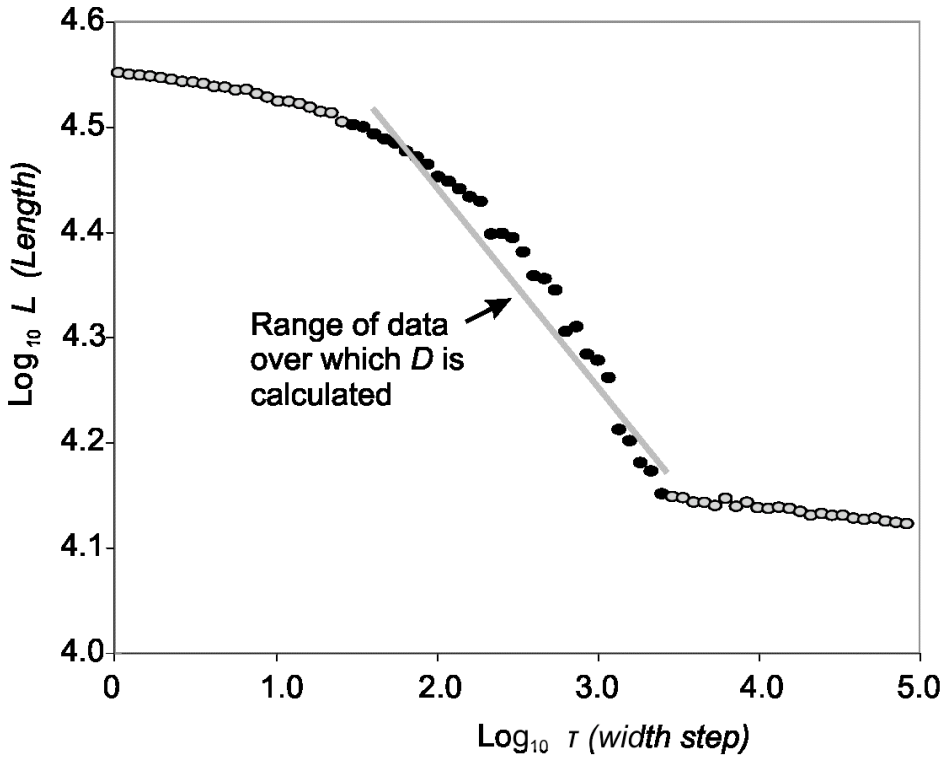

Figure 7.5: Richardson plot for a composite headwall. The data points shaded in grey indicate the section of the plot where edge effects reduce the fractal dimension *D* of the headwall. The range over which linear regression can be applied, and *D* estimated, is indicated by the black data points.

The fractal dimensions *D* of the individual and composite headwalls are shown in Figure 7.6. All the values of *D* for individual headwalls are statistically significantly higher than 1, which means that all headwalls have a detectable fractal behaviour. The values of *D* for the composite headwalls range between 1.15 and 1.25, whereas the values of *D* for the individual headwalls are close to the Euclidean value of 1. This means that composite headwalls are more irregular features than the individual headwalls. Since composite headwalls are comprised of individual headwalls, the scale over which scale invariance is observed in the composite headwalls is not infinite, but it occurs above the lengths of individual headwalls. The values of *D* for both individual and composite headwalls do not correlate with size, mass movement type, sediment thickness or depth, which indicates that *D* is generally homogeneous.

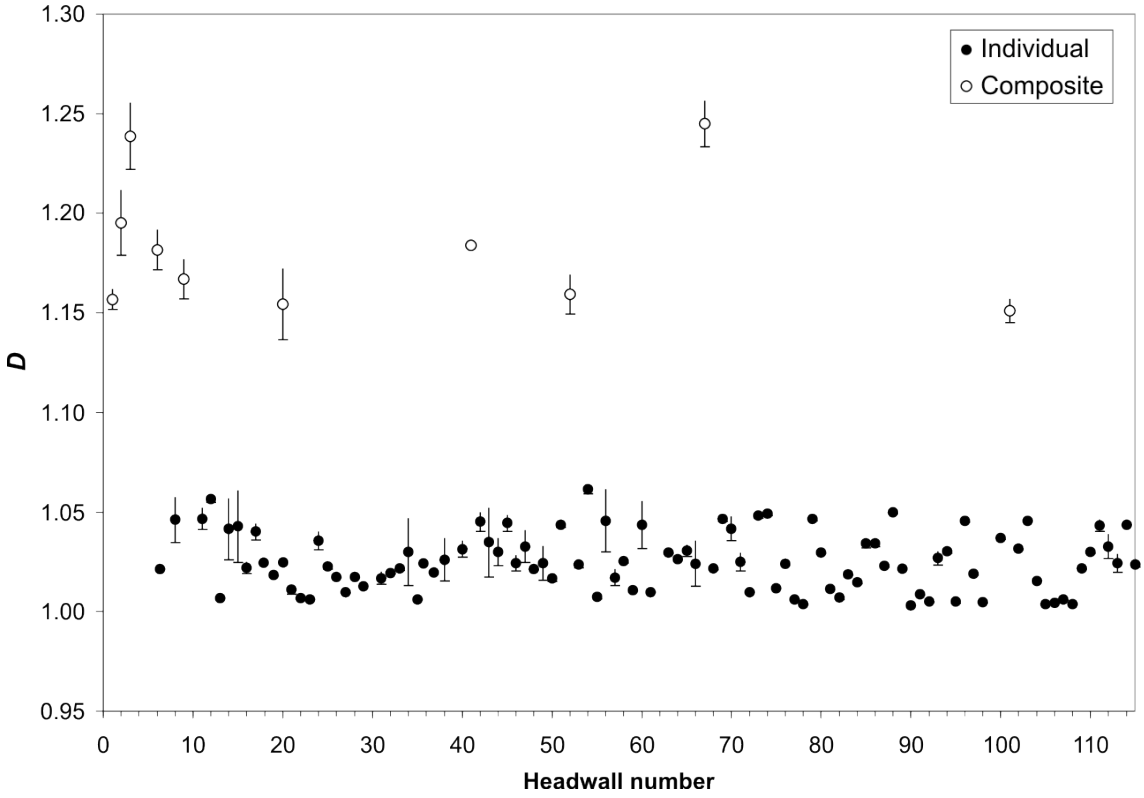

Figure 7.6: Plot of the calculated fractal dimension *D* for all extracted headwalls. The standard deviation for each headwall is also shown.

7.4.3 GEOMETRIC SIMILARITY

The hundred and five individual headwalls were grouped into two classes according to the type of mass movement that formed the headwall: (i) Class 1: headwalls formed by spreads; (ii) Class 2: headwalls formed by debris flows. The mean similarity coefficients within and between classes are shown in Table 7.2. The mean similarity coefficients within classes are higher than 0.7. The differences in similarity coefficients between classes are higher than the standard deviation. This means that the differences are statistically significant and that the headwall morphology is determined by the formative mass movement. A visual examination of the headwalls reveals that, in general, headwalls formed by debris flows are more curved than those formed by spreads (Figure 7.7). The mean length-width ratio for headwalls in class 1 is 5.64, compared to 3.63 for headwalls in class 2. The length-width ratio (L-W ratio) refers to the quotient of the length of a straight line joining the headwall extremities, to the maximum perpendicular distance of the headwall from this line. The headwall lengths in both classes span over almost the entire range of lengths, indicating that spreads and debris flows occur at all scales.

Table 7.2: Mean similarity coefficients (and associated standard deviations) for the two identified classes of individual headwalls.

	Class 1	**Class 2**
Class 1	**0.7666 (±0.0221)**	0.6112 (±0.0895)
Class 2	0.6112 (±0.0895)	**0.7399 (±0.0210)**

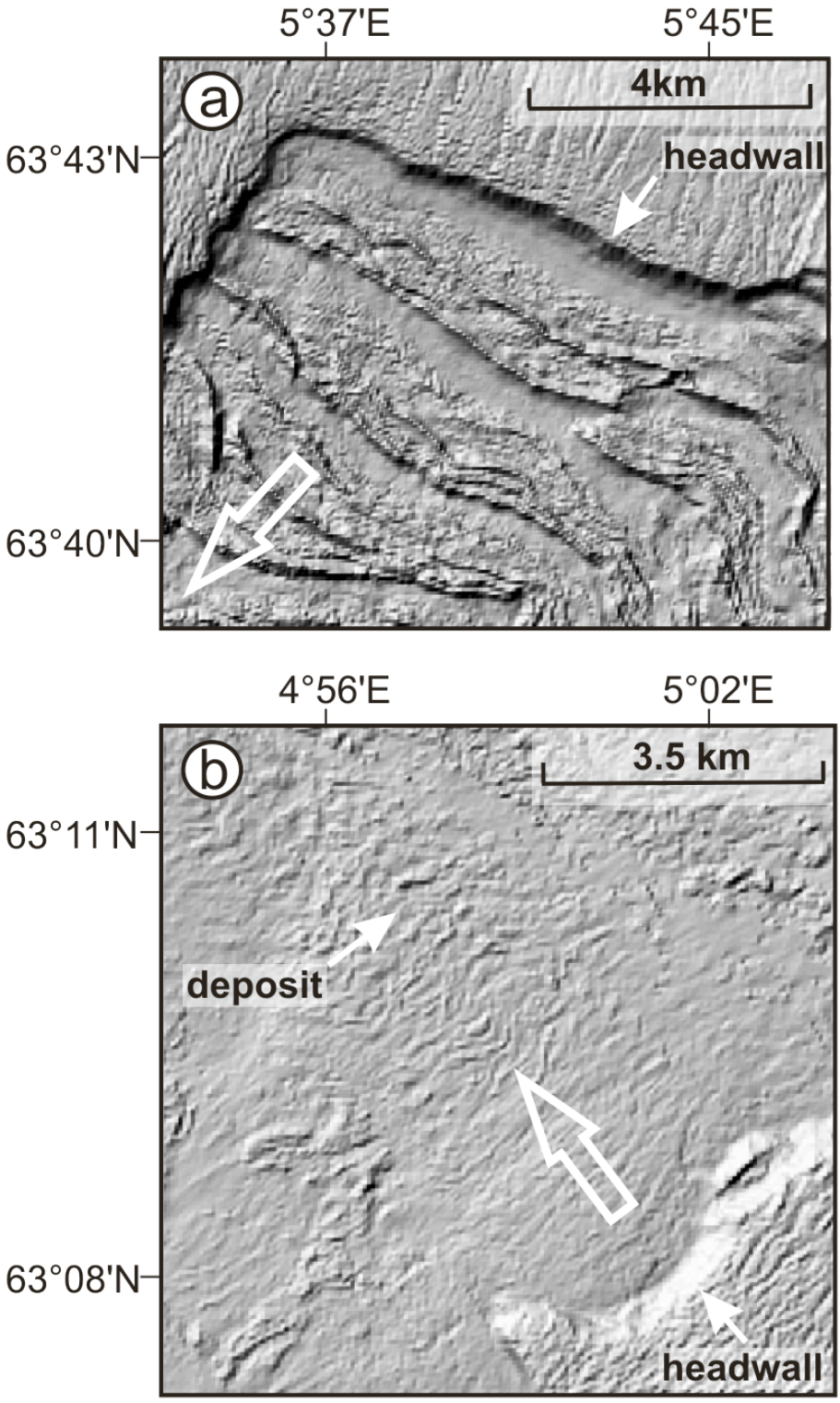

Figure 7.7: Shaded relief map of (a) a spread and (b) a debris flow. The headwall formed by the debris flow is more curved compared to that formed by the spread. The

large white arrow indicates the direction of mass movement. The locations of the maps are shown in Figure 7.1.

Composite headwalls consist of individual headwalls of varying lengths formed by debris flows or spreads. The ten composite headwalls were arranged into two groups, classes A and B, until the highest intra-group mean similarity coefficients were achieved (Table 7.3). Within each class, the mean similarity coefficient is very high (>0.8). The difference between the two classes based on geometric similarity is also statistically significant. Figures 7.8a-b display an example of a composite headwall from each class. The headwalls in class B, particularly the main slide headwall, can be described as cauliflower-shaped [*Canals et al.*, 2004]. The headwalls of numerous submarine landslides around the world can be described in this way, e.g. Gebra Slide [*Imbo et al.*, 2003], Hinlopen Slide [*Vanneste et al.*, 2006], Arecibo Slide [*ten Brink et al.*, 2006b]. A comparison of the headwall shapes in Figure 7.8 confirms that the shape and length-width ratio of the headwalls of the Gebra, Hinlopen and Arecibo slides are similar to the composite headwall in class B. The ratio of the total length of composite headwalls formed by debris flows to that formed by spreads is plotted in Figure 7.9. This shows that the majority of the headwall components in class A are formed by debris flows, whereas the majority of the headwalls in class B are comprised of spreads. Thus, the shape of the composite headwalls is dependent on the mass movement processes.

Table 7.3: Mean similarity coefficients (and associated standard deviations) for the two identified classes of composite headwalls.

	Class A	**Class B**
Class A	**0.8090 (±0.0103)**	0.6667(±0.0187)
Class B	0.6667 (±0.0187)	**0.8237 (±0.0109)**

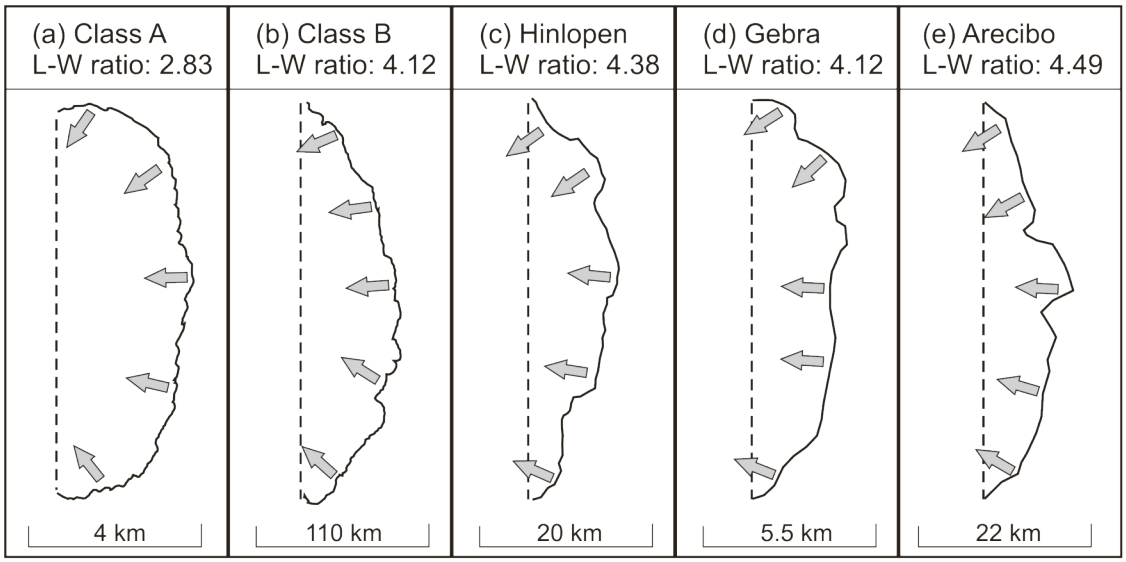

Figure 7.8: Comparison of examples of composite headwalls from classes A and B, with the main headwalls of the Hinlopen, Gebra and Arecibo slides. The headwall in Figure b is the Storegga main headwall. The (c) Hinlopen, (d) Gebra and (e) Arecibo slide headwalls were traced from *Vanneste et al.* [2006], *Imbo et al.* [2003] and *ten-Brink et al.* [2006b], respectively. The length-width ratio (L-W ratio) refers to the quotient of the length of a straight line joining the headwall extremities, to the maximum perpendicular distance of the headwall from this line. The shape and L-W ratio of the Hinlopen, Gebra and Arecibo slides are more similar to the class B headwall.

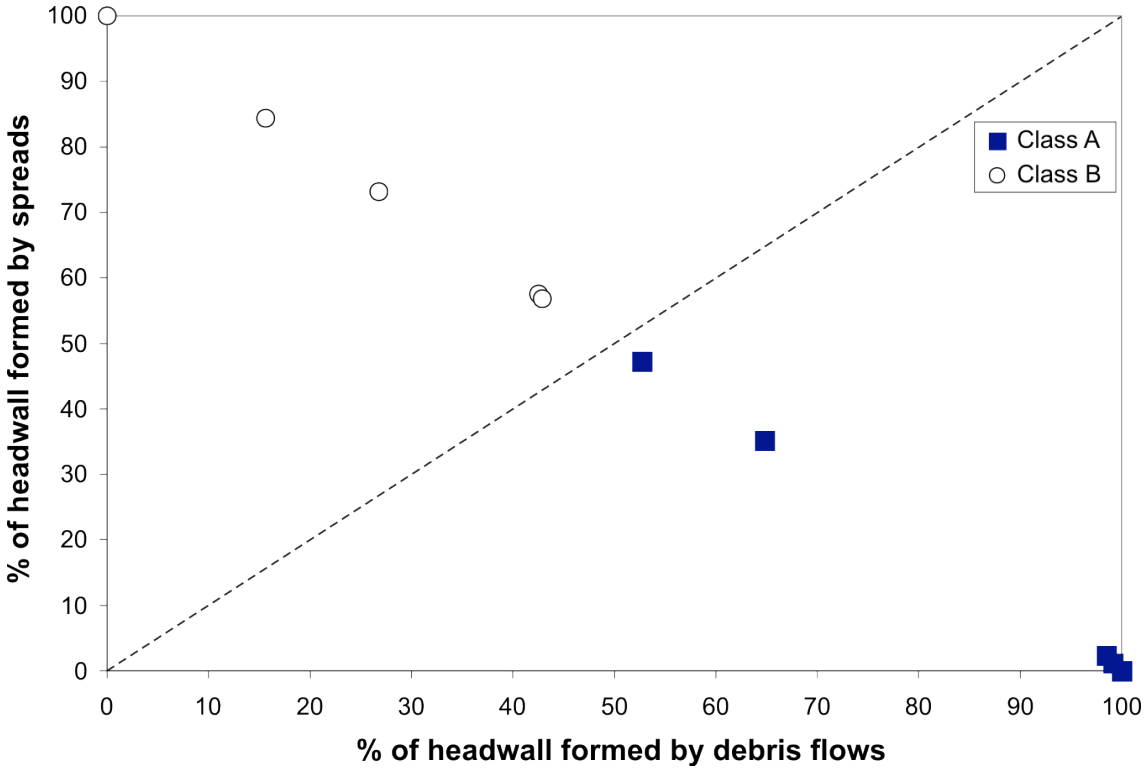

Figure 7.9: Plot of the percentage length formed by either spreads or debris flows within each of the ten composite headwalls. The composite headwalls have been divided into classes A and B according to the estimated geometric similarity between them. The plot shows that the majority of the length of the composite headwalls in class A is formed by debris flows, whereas the majority of the length of the composite headwalls in class B is formed by spreads.

The mean similarities between the two classes of composite headwalls and the two classes of individual headwalls are shown in Table 7.4. Class A headwalls are more similar to class 2 headwalls (formed by debris flows), whereas class B headwalls are more similar to class 1 headwalls (formed by spreads). This indicates that a composite headwall has a similar shape to the majority of the individual headwalls that form it, which implies self-similarity.

Table 7.4: Mean similarity coefficients (and associated standard deviations) between the classes of composite headwalls (A-B) and classes of individual headwalls (1-2).

	Class 1	**Class 2**
Class A	0.6099 ±0.0139)	0.7847 (±0.0107)
Class B	0.8518 ±0.0023)	0.6018 (±0.0072)

7.5 DISCUSSION

7.5.1 SCALE-INVARIANT CHARACTERISTICS OF SUBMARINE MASS MOVEMENTS: ORIGIN AND SIGNIFICANCE

The results in section 7.4 are evidence of spatial scale invariance within the Storegga Slide. The first type of spatial scale invariance is observed in the distribution of mass movement areas. The frequency of occurrence of submarine mass movements within the Storegga Slide is a function of the mass movement area (or magnitude) according to an inverse power law, and can thus be described as fractal. Similar power law distributions have been identified in numerous inventories of subaerial mass movements of different types and sizes, occurring in a range of environmental settings and triggered by a variety of mechanisms [e.g. *Dai and Lee*, 2002; *Dussauge et al.*, 2003; *Guzzetti et al.*, 2002; *Hovius et al.*, 1997; *Ohmori and Hirano*, 1988]. A difference between these studies of subaerial landslide populations and our study is that the former have taken into consideration individual landslides that are independent of each other, whereas we investigated a single, large landslide complex. The distributions of other natural phenomena, such as earthquakes, are also known to exhibit power law scaling [*Turcotte et al.*, 2006]. In this study, the power law scaling of mass movement area with frequency is observed over 2 orders of magnitude of the area (Figure 7.4) (compared to ~3 for data from subaerial mass movements [*Hergarten and Neugebauer*, 1998]), and can thus be applied to the majority of the mass movements under consideration.

Explaining the origin of this first type of spatial scale invariance in geological terms is difficult. One explanation is that the fractal distribution is a manifestation of self-organised criticality (SOC) [*Bak et al.*, 1987, 1988], a concept which has found wide application in physics, biology and economics [*Bak*, 1996]. Self-organised criticality is a property of a complex system related to principles of energy dissipation and the occurrence of spatio-temporal chaos [*Phillips*, 1995]. It is typically observed in slowly-driven non-equilibrium systems. Self-organised criticality may explain the phenomenon whereby, despite complexity and heterogeneity at the level of individual elements (e.g. grains of sediment), the aggregate behaviour of the system at the larger scale exhibits order in the form of a fractal distribution. In this complex system, the

"input" is nearly constant and the "output" is characterised by a series of events, the frequency-size distribution of which follows a power law in space and time. Emergence of this order occurs through autogenic dynamics and internal feedback mechanisms of the system [*Phillips*, 1995]. There are a number of necessary conditions for identifying self-organised criticality in a system [*Bak et al.*, 1987]: (a) the distribution of event sizes is scale invariant, (b) the system is in a quasi-stationary (critical) state and (c) the temporal behaviour of the system is a $1/f$ (red) noise [*Bak et al.*, 1987]. Within the Storegga Slide, the distribution of mass movements has been shown to be spatially scale invariant, but we cannot characterise the temporal behaviour due to a low temporal resolution of submarine mass movement data. Landsliding is a dissipative phenomenon because material is moved downslope or removed from the slide scar. A continuous, long term driving force is thus required to keep the landslide in a quasi-stationary state. In Storegga, this force is represented by the continuous and variable deposition of glacially-derived material (during glacial maxima) and hemipelagic sedimentation (during interglacials) that has been taking place along the mid-Norwegian Margin during at least the last 3 million years [*Rise et al.*, 2005]. These processes have resulted in a progressive increase in sediment pore water pressure, gravitationally-induced stress and surface slope gradient, all of which promote slope instability. Another driving force may comprise seismic activity, because glacially-induced tectonic movements enable the Storegga Slide system to exceed thresholds and trigger slope instabilities [*Evans et al.*, 2005]. Such conditions are all typical of a system in a critical state. In consideration of the above, we conclude that the Storegga Slide is a geomorphological system that may exhibit self-organised criticality.

One of the most widespread models of self-organised criticality is the Bak-Tang-Wiesenfeld (BTW) model [*Bak et al.*, 1988], also known as the 'sandpile' model. This simple cellular automata model consists of a lattice where particles are dropped into a randomly selected grid at time steps. When the total number of particles in a grid exceeds a specific threshold, the site collapses and the particles are redistributed into the adjacent grids. The redistribution of particles can lead to an 'avalanche'. Numerical studies have shown that, in a 'sandpile' model, the non-cumulative number of 'avalanches' with the 'avalanche' area satisfies a power law distribution, and that the value of the exponent of the power law is ~1 [*Kadanoff et al.*, 1989]. The exponent associated with the spatial power law scaling of subaerial mass movements is

significantly higher than 1. The values range between 2.2 and 3.3 for mass movements occurring in a variety of environmental settings [*Dai and Lee*, 2002; *Guzzetti et al.*, 2002; *Hovius et al.*, 1997; *Malamud et al.*, 2004; *Van Den Eeckhaut et al.*, 2007]. The value of the exponent obtained for submarine mass movements within the Storegga Slide is 1.63. This value is still higher than the 'sandpile' model value of 1. This difference can be attributed to the simplicity of the 2D 'sandpile' model, which contrasts with the multitude of forces and controls operating on a variety of spatio-temporal scales in 3D in mass movements. For example, a higher exponent of landslide frequency-size distribution has been obtained when incorporating factors such as geological heterogeneity [*Sugai et al.*, 1994], soil moisture content [*Pelletier et al.*, 1997] and slope stability considerations [*Hergarten and Neugebauer*, 1998] into landslide models. On the other hand, the value of the exponent for submarine mass movements is considerably lower than for subaerial mass movements, and closer to the 'sandpile' model value. This could imply that, in comparison to subaerial mass movements, submarine mass movement systems are less complex and that their dynamics are qualitatively more analogous to those of the 'sandpile' model. The elements in the 'sandpile' model can be related to the components of the Storegga Slide system. The dropping particles represent sediment deposition, the avalanches are the individual mass movements, and the thresholds are associated with changes in slope gradient, pore pressure and gravitationally-induced stress. In subaerial systems, driving forces such as tectonic uplift and fluvial incision tend to interact with weathering forces, variable degrees of saturation, high geological heterogeneity and topographic roughness, yielding a higher exponent for the power law distribution of mass movements. Since the sediments failing within the Storegga Slide are mainly clays, cohesion may also play an important role. Slope failures in cohesive sediments generally tend to exhibit lower exponents than slope failures occurring in less cohesive material [*Dussauge et al.*, 2003]. Since the exponent for the Storegga mass movements' distribution is <2 and lower than the values obtained for subaerial mass movements, we can also infer that the larger mass movements are more dominant in submarine environments and that the change in frequency of mass movements is slower.

The applicability of the 'sandpile' model to submarine mass movements is not without problems, however. First, aspects of inertia, cohesion and stratigraphic control of failure depth are overlooked in the 'sandpile' model. These three factors are particularly

important in landsliding within the Storegga Slide. Secondly, self-organised criticality is not a property unique to cellular automata models. *Hergarten and Neugebauer* [1998], for example, developed a model of landsliding that exhibits self-organised criticality using partial differential equations only. For our study area, another explanation of the fractal distribution of the mass movements is the fact that the Storegga Slide was a retrogressive slope failure [*Haflidason et al.*, 2005; *Kvalstad et al.*, 2005a]. Instability did not occur across the entire slip surface simultaneously, but started as one or a few large mass movements located close to the Faroe-Shetland Escarpment [*Haflidason et al.*, 2004]. Failure in this region destabilised the neighbouring areas and the instability propagated upslope via the progressive collapse of the headwall. The areas of mass movements within Storegga become smaller with distance upslope [*Haflidason et al.*, 2004; *Issler et al.*, 2005], whilst the number of mass movements increases (Figure 7.10). Therefore, as the slope failure propagated upslope, each mass movement triggered an increasing number of smaller mass movements, in the style of a cascade. The continental slope is characterised by extensive areas of uniform gentle topography [*Shepard*, 1963]. In such a setting the boundary conditions are largely homogeneous and a retrogressive cascade would be allowed to develop unobstructed. The Storegga retrogressive cascade continued until the boundary conditions changed at the limits of the present Storegga Slide scar. These changes include the decrease in the slope gradient of the seabed where the continental slope meets the continental shelf, and the gradation into pronounced morphological barriers (the North Sea Fan in the south and the Vøring Plateau in the north). Another factor responsible for halting the retrogressive cascade must have been the increase in the consolidation of the sediments in the region of the main headwall of the Storegga Slide, due to glacial compaction during the Last Glacial Maximum [*Gauer et al.*, 2005]. The Storegga retrogressive cascade is qualitatively similar to the activation of avalanches in the 'sandpile' model and may explain the power law of the frequency-area distribution of the submarine mass movements. Other cascade models, such as the inverse cascade model, have been shown to reproduce the self-organised critical behaviour of another cellular automata model, the forest-fire model [*Turcotte et al.*, 1999].

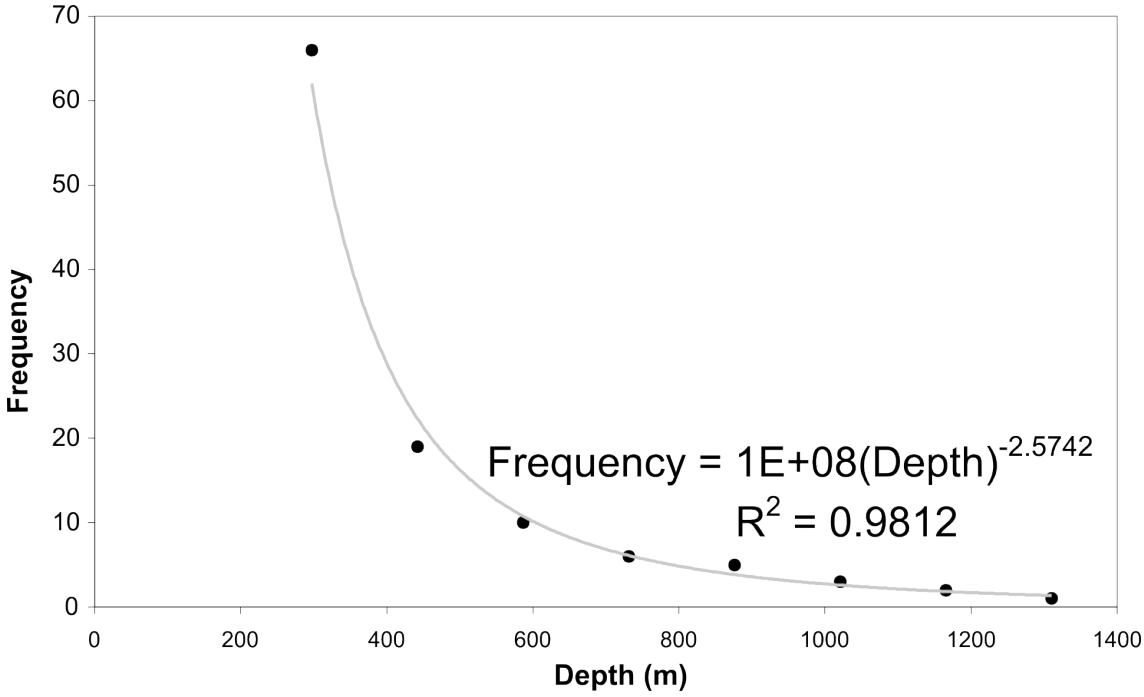

Figure 7.10: Frequency-depth distribution of the one hundred and five individual headwalls.

Self-organised criticality is, however, not the only explanation of the observed spatial power law scaling in submarine mass movements. Pre-defined geological structures and natural variability may also result in a spatial power law distribution in mass movements, without the need of self-organised criticality [*Hergarten*, 2003; *Pelletier et al.*, 1997]. Detailed information about the spatial variability of geotechnical properties and geological structures within the Storegga Slide is not available. Thus we are unable to confirm a potential relationship between the power law distribution of mass movements and geological structures.

In the non-cumulative frequency-area distribution of the Storegga mass movements, power law scaling terminates at a landslide area of 1 km^2, where a roll-over effect is observed (Figure 7.4). The roll-over is typical of frequency-magnitude distributions [*Guthrie and Evans*, 2004], and it has generally been interpreted as an artefact of survey resolution due to under-mapping of the smaller-scale landslides [*Katz and Aharonov*, 2006; *Stark and Hovius*, 2001]. Other studies, in contrast, have suggested that the origin of the roll-over is geological [*Guzzetti et al.*, 2002; *Pelletier et al.*, 1997]. In most cases, the roll-over has been attributed to the transition from the control of resistance to the downslope-oriented driving forces by friction for the larger landslides,

to resistance controlled by cohesion for the smaller landslides [*Pelletier et al.*, 1997; *Van Den Eeckhaut et al.*, 2007]. In the case of our data, we favour the interpretation of the roll-over as not an artefact of survey resolution because the bin-size is considerably larger than the data resolution (Figure 7.4).

A second type of spatial scale invariance within the Storegga Slide is identified in mass movement morphology. The plot of headwall length vs. mass movement area in Figure 7.2 shows strong power law scaling. The geometric similarity of headwalls at different scales (Table 7.2) and the self-similar properties of the composite headwalls (Table 7.4; Figure 7.6) are also indicative of morphological scale invariance. These results complement the observations made by *Issler et al.* [2005] for mass movements within the Storegga Slide, where the area of a longitudinal section across the mass movements was found to scale with the released volume. The geometric scaling behaviour of landslides implies that the form and the geological processes associated with submarine mass movements are the same at the investigated scales. In the absence of other factors, such as heterogeneities in the failing material, this observation indicates that *Issler et al.* [2005] 's inclusion of hydroplaning and shear wetting in physical models of slope failures can be extended to the different scales investigated in this study.

7.5.2 HEADWALLS AS MORPHOLOGICAL PROXIES

The two classes of composite headwalls are geometrically similar to the majority of their constituent headwalls. This observation, combined with the high values of the fractal dimension D observed in composite headwalls, indicates that the composite headwalls formed by submarine mass movements are self-similar at scales higher than those of the constituent individual headwalls. This means that when headwalls from separate mass movements coalesce, the resulting headwall has a shape similar to its constituent headwalls, or to that which occupies the largest portion of the headwall (if formed by different types of mass movement). The shape of individual headwalls was shown to be indicative of its principal formative geological processes. This also applies to composite headwalls. Headwalls formed by spreads have a length-width ratio higher than ~4 and their shape ranges between cauliflower-shaped and linear. Headwalls formed by debris flows are more curvilinear and have a length-width ratio lower than ~4.

This observation provides a basis for a morphological classification of submarine landslides and allows the identification of mass movement type even when the resolution of the bathymetric data is low and only the shape of the headwall is discernible. We explain the difference in headwall shape by the fact that plastic deformation is required to evacuate a curvilinear headwall, in comparison to a quasi-linear headwall, where deformation entails brittle deformation of the sediment into coherent blocks. The dissimilarity between the two classes of headwalls is not very strong due to the fact that mass movements entail a continuum of processes and features that cannot be placed into a systematic arrangement of groups (Table 7.2). The control of mass movement process on headwall morphology can be observed in other submarine landslides. In the Hinlopen Slide, for example, a headwall formed by a debris flow (Figure 7.11a) is more curvilinear compared to a headwall formed by a spread (Figure 7.11b). Such differences in headwall morphologies are perhaps more discernible within the Storegga and Hinlopen Slides because debris flows and spreads have occurred in a similar type of sediment within each slide. The value of 4 for the length-width ratio, differentiating between headwalls formed by debris flows and spreads, only applies to the Storegga Slide, however, and has not been validated in other submarine landslides. The reasons for why some slope failures form spreads, whereas other transform into debris flows, may be various. Subtle differences in the physical properties of the sediment could influence the type of deformation. Boundary effects, presence of gas hydrates, variation in sediment facies (e.g. presence of contouritic drift deposits), and evolution of the landslide, may also be important. The fractal dimension of headwalls, on the other hand, can be used to reveal whether a headwall is formed by one or more mass movements. Thus, headwalls can be used as morphological proxies for the identification of submarine mass movements. The links between the fractal dimension and the geological processes which produce it have, however, not been identified yet.

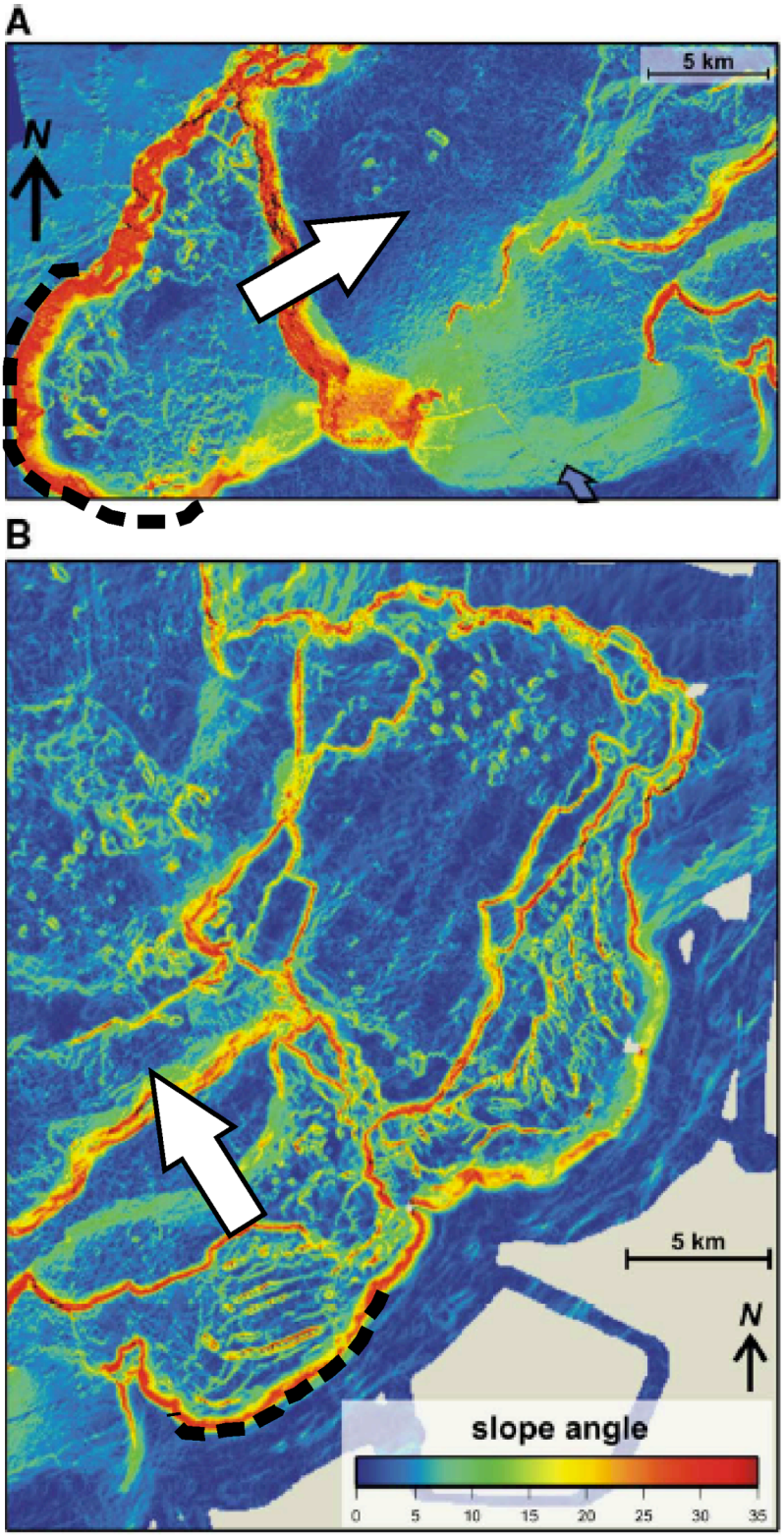

Figure 7.11: Slope gradient map from (a) the western part of the Hinlopen Slide scar formed by a debris flow and (b) the eastern part of the Hinlopen Slide scar formed by a number of spreads. The dotted black lines represent an individual headwall. White block arrows indicate the direction of sediment movement.
Source: *Vanneste et al.* [2006].

Chapter 8:

DISCUSSION: DEVELOPMENT OF THE NORTH-EASTERN STOREGGA SLIDE

Development and mass movement processes of the north-eastern Storegga Slide.

Aaron Micallef, Douglas G. Masson, Christian Berndt and Dorrik A.V. Stow

This chapter is a research article that has been submitted for publication to Marine Geology. The manuscript was submitted on the 31st July 2007 and is currently in review.

8.1 INTRODUCTION

First described by *Bugge* [1983], the Storegga Slide is a giant submarine landslide situated in the Møre Basin, on the mid-Norwegian margin, about 120 km off the western coast of Norway (Figure 8.1). The Storegga region has a long history of slope instability related to the cyclic nature of sedimentation during glacial to interglacial climatic oscillations [*Solheim et al.*, 2005a]. Glacigenic debris flow deposits, proximal glacial marine sediments and till, deposited during glacial periods, are interlayered with contouritic, hemipelagic and glacial marine sediments, deposited during interglacial periods [*Berg et al.*, 2005]. This stratigraphic framework, combined with the development of high pore water pressures due to rapid deposition of the glacial sediments, have preconditioned the Storegga region to fail during each interglacial period in the last 0.5 Ma [*Berg et al.*, 2005; *Bryn et al.*, 2003]. Isostatic adjustments following glacial retreat provided an elevated postglacial earthquake activity and a likely trigger [*Bungum et al.*, 2005].

The discovery of the Ormen Lange gas field close to the main headwall of the Storegga Slide has renewed the interest of industry and academia in this submarine landslide during the past decade. Today a very large database of acoustic and geotechnical data is available for the Storegga Slide. These data sets have been used to analyse various aspects of this submarine landslide. The development of the Storegga Slide, in particular, has been investigated in detail in three papers [*Bryn et al.*, 2005a; *Haflidason et al.*, 2004; *Haflidason et al.*, 2005]. These studies have been based on a thorough visual interpretation of the bathymetric data from the slide scar, complemented by the analyses of sidescan sonar imagery and seismic data.

Geomorphometry, a field of research that was developed within the broader discipline of geomorphology, involves the quantitative characterisation of terrain surfaces. In geomorphometry, mathematical and statistical processing techniques are employed to quantify aspects of the land surface and facilitate the mapping, modelling and understanding of the formative geological processes. Geomorphometric techniques

have been shown to be rapid, accurate, reproducible and avoid problems of subjectivity [*Drăgut and Blaschke*, 2006; *Evans*, 1990]. Recent studies show that the geological interpretation of bathymetric data is also improved if geomorphometric techniques are used [e.g. *Micallef et al.*, 2007a; *Mitchell and Clarke*, 1994]. For example, *Micallef et al.* [2007a] applied a suite of geomorphometric techniques in the study of a small part of the Ormen Lange bathymetric data set to derive high-resolution information on the geological processes.

In this paper we employ a number of geomorphometric techniques to characterise the morphology of the Storegga Slide and improve the development model put forward by *Haflidason et al*. [2004]. This will provide a more profound understanding of the formative submarine mass movements, the associated geological processes and controls, and the way in which submarine mass movements are interrelated. Comprehension of the causes and development of submarine mass movements within the Storegga Slide also provides an insight into the geological processes responsible for other submarine landslides located along the Norwegian margin, as the geological setting in which they occur is very similar [*Rise et al.*, 2005]. Submarine mass movements are a potential geohazard to hydrocarbon extraction and transport structures located on the Storegga Slide seabed. Improved modelling of submarine landslides is thus essential for assessing the risk associated with these geohazards. The highest resolution and density of acoustic data are found in the Ormen Lange region, and most of the studies on the Storegga Slide have been based on data from this part of the slide scar [e.g. *De Blasio et al.*, 2004; *Gauer et al.*, 2005; *Kvalstad et al.*, 2005a]. Much less attention has been given to mass movements in the north-eastern Storegga Slide, which will be the focus of multiple proposed IODP drill sites in the near future [*Brown et al.*, 2006]. We therefore focus our geomorphometric analyses on data from the north-eastern Storegga Slide.

The objectives of this paper are: (a) to map the submarine mass movements that have shaped the north-eastern Storegga Slide; (b) to identify the geological factors and processes responsible for these mass movements; and (c) to propose a revised development model for the north-eastern Storegga Slide.

The nomenclature that will be used in the rest of this paper is as follows:

- Zone: An area of seabed with specific and uniform morphological characteristics.
- Lobe: Individual or a group of mass movements as identified by *Haflidason et al.* [2004] in the presently-accepted development model of the Storegga Slide.
- Event: Individual or group of mass movements as identified by us in the proposed and revised development model of the Storegga Slide.

8.2 REGIONAL SETTING

8.2.1 THE STOREGGA SLIDE: MORPHOLOGY AND SLIDE DEVELOPMENT

The Storegga Slide, dated to ca. 8100±250 cal. yr BP [*Haflidason et al.*, 2005], influenced a total area of 95 000 km^2. During this event, a maximum estimated sediment volume of 3200 km^3 was mobilised over a distance of ~800 km. Almost 30% of the Storegga Slide area is comprised of the slide scar, which is characterised by an amphitheatre-shaped bathymetric depression located downslope of the shelf break (Figure 8.1). The main headwall of the slide is 320 km long; it is up to 160 m high and has slope gradients of up to 45°. The slide scar surface has a mean slope gradient of 0.7°.

A detailed study of the morphology and internal architecture of the slide scar by *Haflidason et al.* [2004] has revealed that the Storegga Slide was a quasi-simultaneous multi-phase retrogressive event. This event mobilised five main partially superimposed slide lobes (lobes 1 – 5, in chronological order), which represent more than 99% of the total volume of sediment involved in the Storegga Slide (Figure 8.1). Lobe 1 covered the northern half of the Storegga Slide scar; during its development, sediment was removed in the form of debris flows and turbidity currents, and transported into the

Norwegian Sea Basin. Lobe 1 extends upslope, on average, to within 20 km of the main Storegga Slide headwall. In lobe 2, detachment followed a deeper failure plane compared to lobe 1. Lobe 2 consisted of debris flows that have mobilised large blocks of consolidated sediment. During the development of lobe 2, the mobilisation of sediment from the Ormen Lange region is thought to have been responsible for the generation of a tsunami and the compression zones in the western part of the slide scar (Figure 8.1) [*Bryn et al.*, 2005a]. Lobe 3 occurred along the same failure surface as the first lobe. It failed in the same way as lobe 1, although it affected a somewhat smaller area and extended further upslope to the main headwall. Lobe 4 was released after lobe 2 and is characterised by sub-parallel partly disintegrated blocky structures located in the southern part of the slide scar. Lobe 5 was the last major debris flow and it influenced sediments inside and downslope of the Ormen Lange region. In addition to these five lobes there are more than sixty smaller individual slide events identified within lobes 2, 4 and 5. The dimensions of the lobes range from an area of 38 740 km^2 and a run-out distance of 450 km for first major phase, to an area of 0.3 km^2 for the minor slides located close to the main headwall [*De Blasio et al.*, 2003; *Haflidason et al.*, 2004].

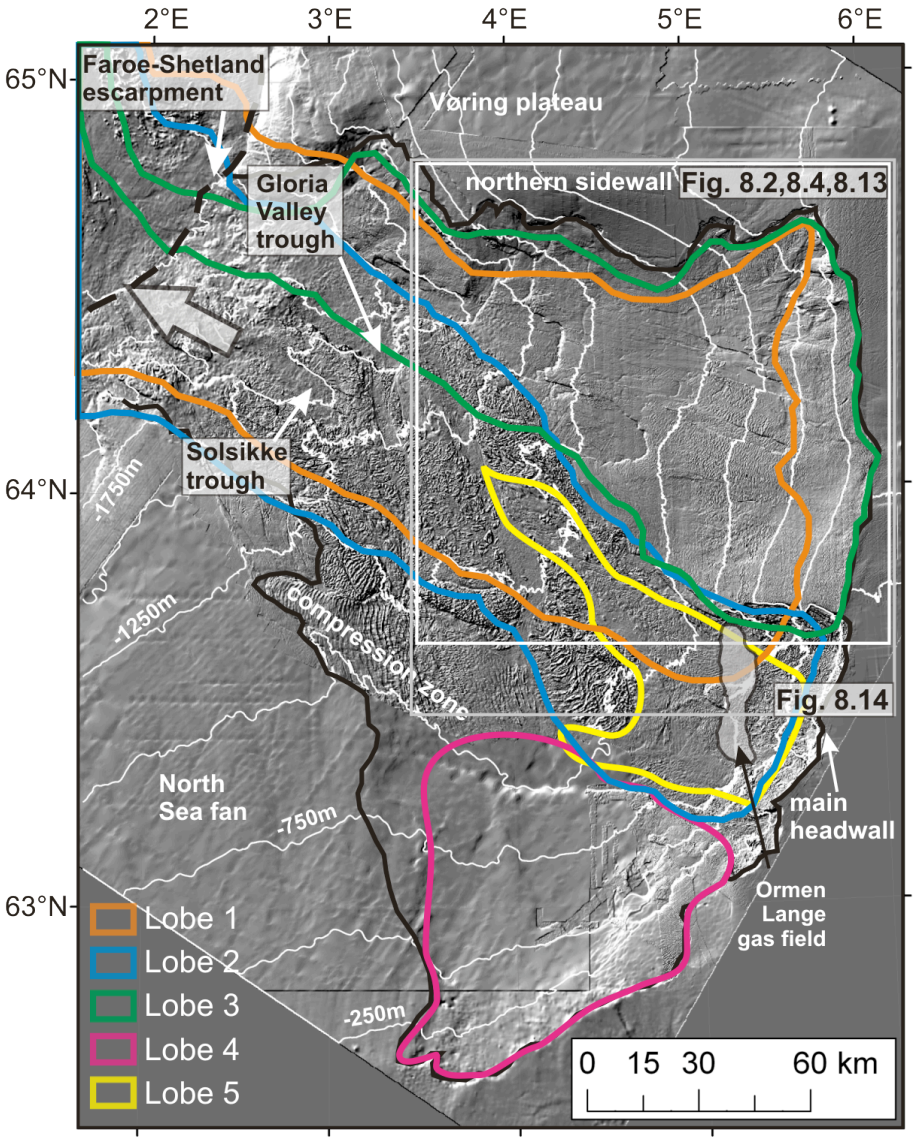

Figure 8.1: Shaded relief image of the Storegga Slide (illumination from north-east, 5× exaggeration). The solid black line indicates the boundary of the slide scar. Bathymetric contours are at 250 m intervals. The five major slide lobes, identified by *Haflidason et al.* [2004], are superimposed on the shaded relief image. The block arrow denotes the direction of sediment movement. The boundary of Figure 8.2 defines the study area.

8.2.2 STUDY AREA: PHYSIOGRAPHY AND STRATIGRAPHY

The study area is the north-eastern Storegga Slide scar, north of the Ormen Lange gas field (Figures 8.1; 8.2a). It is bound by the northern sidewall and Vøring Plateau to the north, the main Storegga headwall to the east, the S and R headwalls to the west, and the O headwall to the south. The area of seafloor under consideration is ~6850 km^2.

The average slope gradient is 2.14°; the upslope part of the study area is steeper, becoming gentler with increasing depth (Figures 8.2b; 8.3b). The depth of the seabed increases gently from ~250 m at the main headwall, to 1550 m at the S headwall (Figure 8.2b). Overall, the study area has the shape of a basin, because the depth of the seafloor decreases northwards in the direction of the northern sidewall, and southwards in the direction of the Ormen Lange gas field (Figures 8.2b; 8.3a).

Failure in the study area mainly occurs in the O unit (200 – 8 ka), the youngest unit of the Naust formation. The Naust formation encompasses a thick, low-angle wedge of clastic sediments and sheet-like units of Plio-Pleistocene age that overlies the older Kai and Brygge formations [*Bryn et al.*, 2005a]. The Naust sedimentary sequence is characterised by pronounced changes in lithology because its development was controlled by the Fennoscandian ice sheet growth and retreat patterns [*Laberg et al.*, 2002b]. The deepest sub-units within the O unit are the O4-O7 sediment sub-units (200-130 ka). These units are glacial tills or debris flow deposits that consist of diamicton with shell fragments and a variable content of gravel and large clasts [*Berg et al.*, 2005]. The O3 sediment sub-unit (130-30 ka), emplaced by glacimarine and contouritic deposition, is comprised of silty clay with sand, scattered gravel and shell fragments. The O1-O2 sediment sub-units (30-15 ka) are made up of unsorted silty, sandy and gravely clay deposited as basal and deformation till. The O3 sediment sub-unit has higher clay and water content, and lower unit weight, sand and gravel content than the other sediment sub-units.

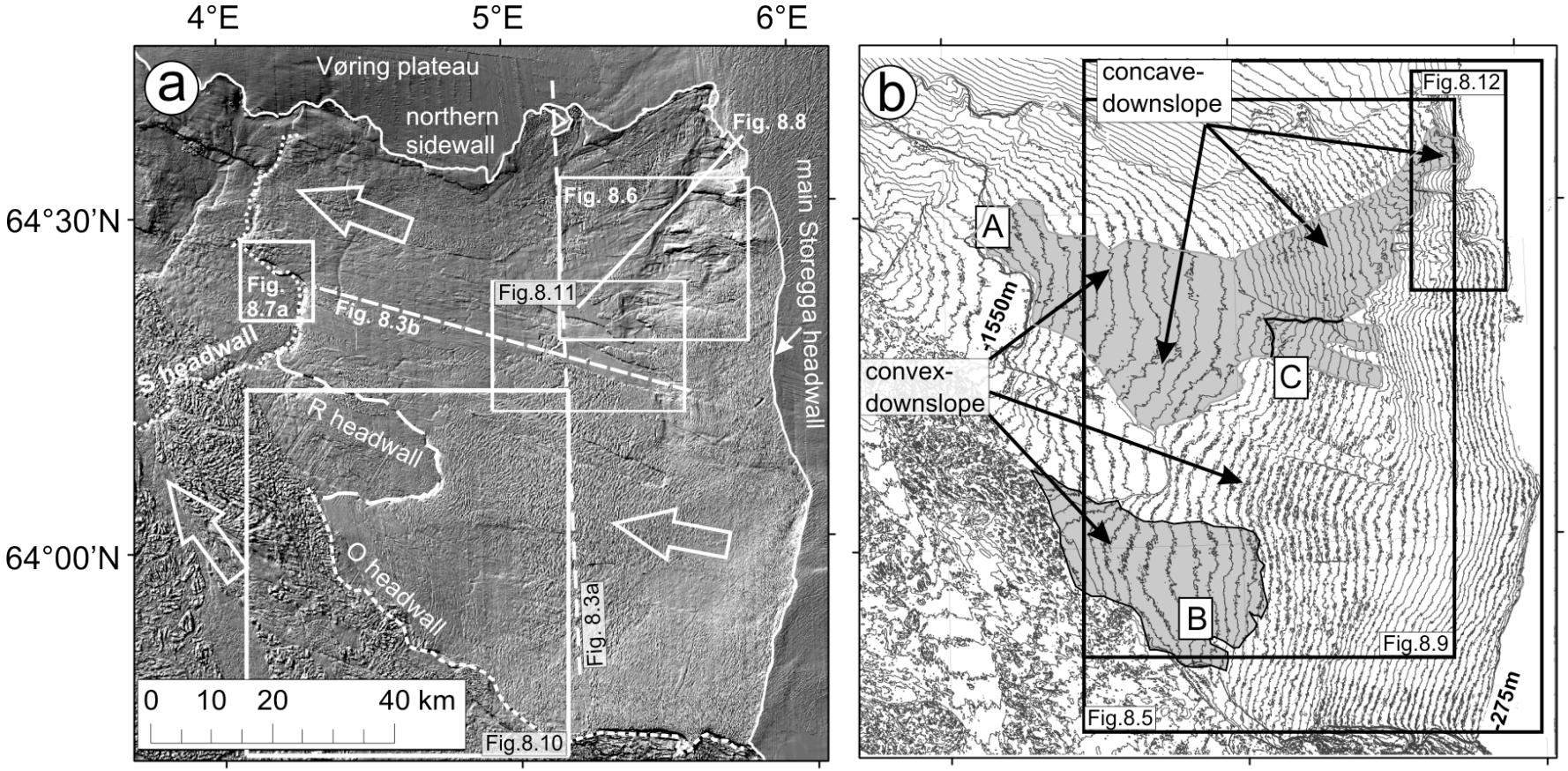

Figure 8.2: (a) Shaded relief image of the study area in the north-eastern Storegga Slide scar (illumination from north-east, 5× exaggeration). The block arrows denote the direction of sediment movement. The O and R headwalls are glide plane jumps to different stratigraphic levels within the Naust formation during the retrogressive development of the Storegga Slide. The S headwall is an older feature. (b) Bathymetric contour map of the study area at 25 m intervals. The zone of smooth terrain A and B, and the debris flow and debris slide (C), are shaded in grey. The distribution of convex and concave downslope contour deflections indicates first order erosional and depositional provinces, respectively.

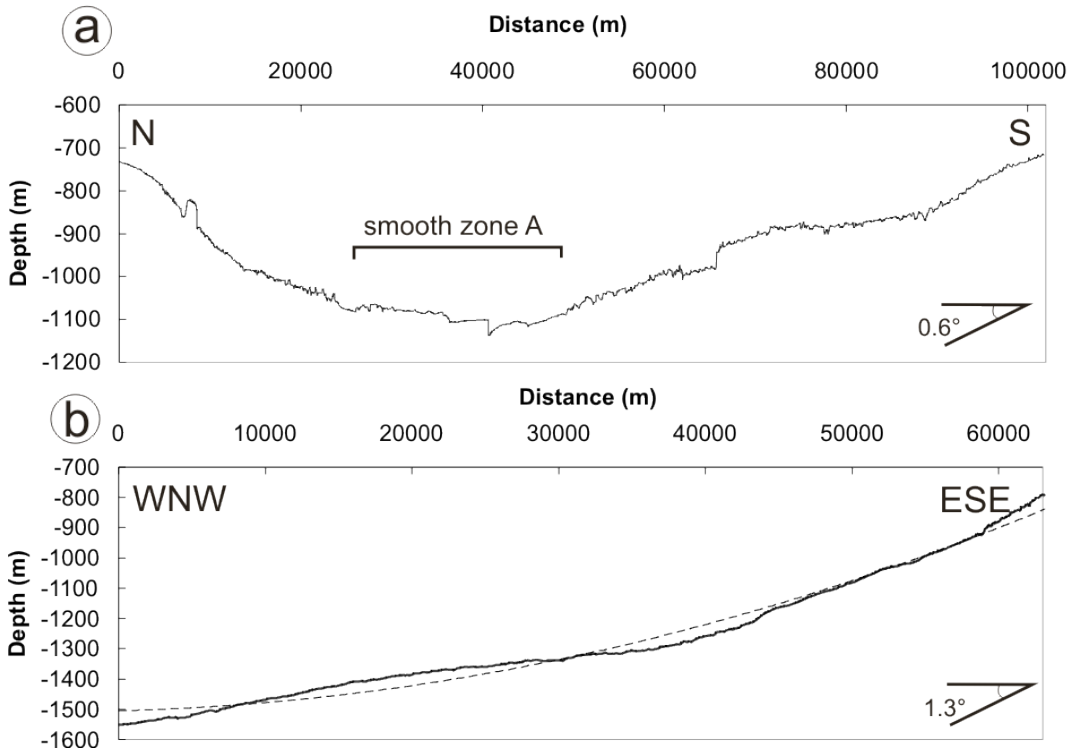

Figure 8.3: Bathymetric profiles across the study area, oriented (a) north-south and (b) west-north-west to east-south-east. In figure b, the dotted line is the polynomial trend line fitted to the elevation data.

8.3 DATA AND METHODS

Three high-resolution acoustic data sets are available for the study area. The bathymetric data set comprises the Storegga Slide seafloor from the main slide headwall at the continental shelf edge (~200 m depth) down to a water depth of ~2700 m. These data have a horizontal resolution of 25 m. The bathymetric data is a compilation derived from multibeam echosounder data and seafloor picks of 3D seismic data. The second data set consists of Towed-Ocean-Bottom-Instrument (TOBI) sidescan sonar imagery that covers ~50% of the study area with a nominal horizontal resolution of 6 m. The third data set comprises a series of 2D seismic lines and a 3D seismic polygon. The 2D seismic lines, with a horizontal sampling density of 6.25 m and a vertical resolution of ~2 m, are located across the main headwall. The industry-type 3D seismic data have a 25 m bin spacing and ~5 m vertical resolution near the surface. The 3D seismic data cover a 2000 km^2 polygon across the northern sidewall.

A suite of geomorphometric techniques for the quantitative characterisation of bathymetric data has been put forward by *Micallef et al*. [2007a]. A number of these techniques have been applied to our bathymetric data set. First, a shaded relief map and slope gradient map were produced for the study area. The first technique involves the generation of a standard deviation of slope gradient map, which can be used to measure components of surface roughness. This map was produced for grid cells of 1 km^2 in area.

The second technique is the production of a geomorphometric map, where a landscape is decomposed into the most elementary morphological units. These units, which include breaks and changes of slope, are automatically extracted as lineaments.

The third technique is ridge characterisation. A ridge pattern is automatically extracted from the bathymetry data by implementing a runoff simulation technique. Three morphological characteristics are then determined from the ridge pattern: (a) trough depth, which is the difference in elevation between a trough and the two adjacent ridge crests; (b) ridge length, which is the mean length of individual ridge crests; and (c) ridge spacing, the mean perpendicular distance between ridge crests. The calculations of the mean ridge length and spacing were carried out for grid cells 1 km^2 in area.

The fourth technique is ISODATA (Iterative Self-Organising Data Analysis Technique), which is an unsupervised clustering algorithm that defines natural groupings of multivariate data in attribute space. The data layers input into this classification algorithm are trough depth, ridge length, ridge spacing and the standard deviation of slope gradient map. A thematic map with five classes of seabed morphology is generated by ISODATA. As some parts of the map were dominated by scattered cells, a low-pass filter is applied to produce a continuous coverage.

All these geomorphometric techniques were implemented in ArcGIS Version 9.1.

8.4 RESULTS

8.4.1 RIDGE AND TROUGH MORPHOLOGY

Spreading is a type of mass movement whereby a sediment unit is extended and broken up into coherent blocks that are displaced and tilted along a planar slip surface [*Micallef et al.*, 2007b]. The morphological signature of spreading is a repetitive pattern of parallel to sub-parallel ridges and troughs that are oriented perpendicular to the direction of sediment movement. Loss of support and seismic loading have been identified as the most likely triggers of submarine spreading [*Micallef et al.*, 2007b]. Ridge and trough morphology can be observed across ~25% of the Storegga Slide scar [*Micallef et al.*, 2007b], and it is the most common morphology observed within the study area. Ridges and troughs cover >4000 km^2 of the study area as a continuous pattern that extends from the main headwall down to the S headwall (Figure 8.4). The ridges and troughs are mainly concave-downslope or linear in plan. Spreading across the study area occurs within the O3 sediment sub-unit [*Micallef et al.*, 2007b].

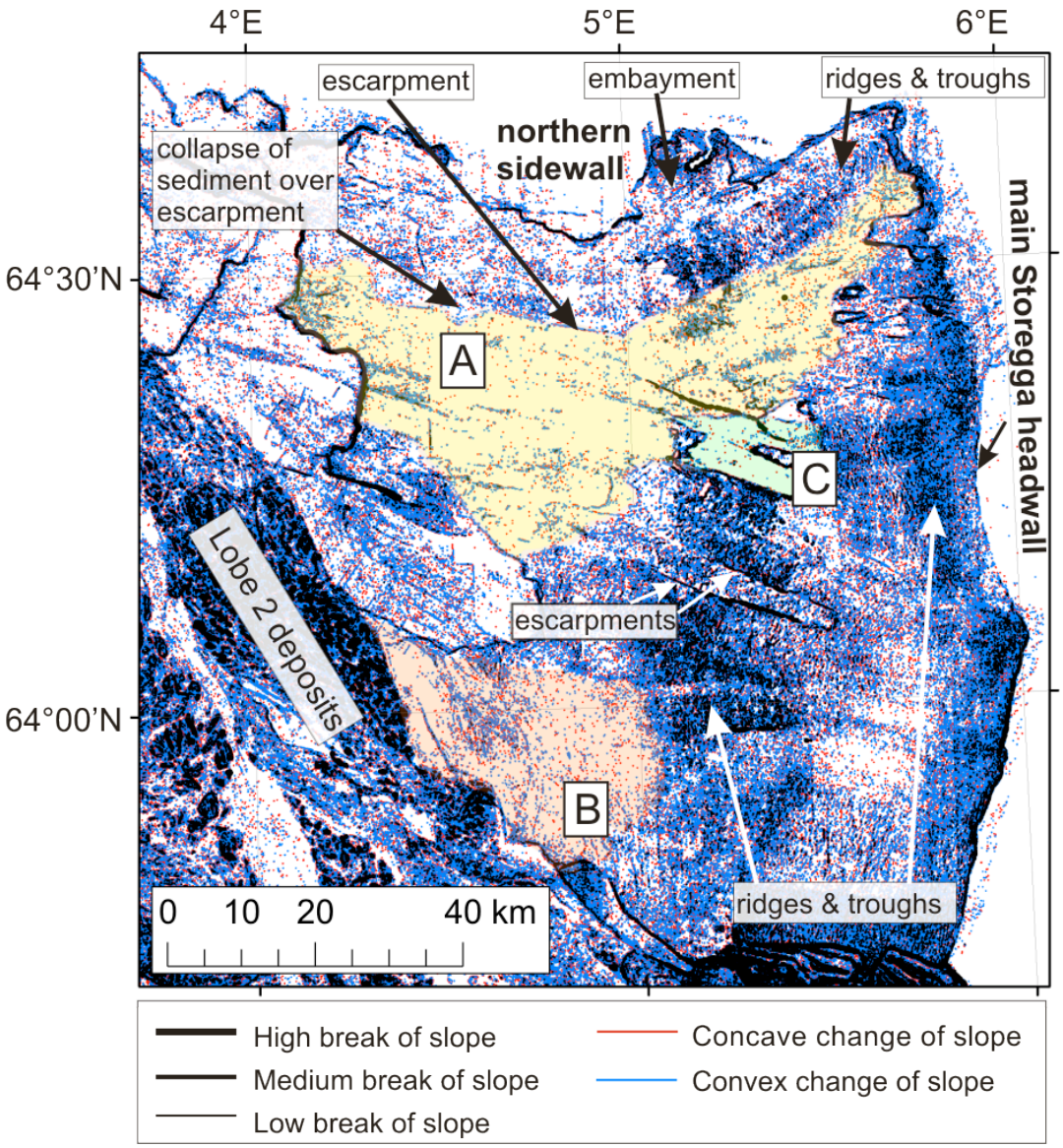

Figure 8.4: Geomorphometric map of the study area. The zones of smooth terrain A, B and the debris slides (C) are shaded in yellow, pink and green, respectively. Important morphological features are also labelled. The escarpment defining the northern boundary of the downslope section of zone A consists of a change of slope.

8.4.2 SPATIAL VARIATION IN RIDGE AND TROUGH MORPHOLOGY

Micallef et al. [2007b] proposed a development model for submarine spreading based on mechanical modelling and ridge and trough morphological characteristics. In this model, the displacement of spreading blocks increases exponentially with distance downslope. Ridge spacing therefore increases with distance from the headwall. The longer the distance a spreading block is displaced, the more fragmented it becomes. As

a result, the ridges become progressively shorter with increasing distance from the headwall. Higher displacement also means that the sediment blocks are tilted further downslope, which results in troughs becoming deeper with distance downslope. These variations in ridge and trough morphology are valid under the assumptions that the initial size of the spreading blocks is uniform and that the fluid and frictional forces resisting block movement are constant. Spatial variations can be observed in the maps of trough depth, ridge length and ridge spacing for spreading in the study area (Figure 8.5a-c). The thematic classification map generated by using these three ridge and trough characteristics maps, together with a standard deviation of slope gradient map, in an ISODATA classification is shown in Figure 8.5d. The ridge and trough morphology across the entire study area can be divided into five main classes. The ridge and trough morphological characteristics for each class are listed in Table 8.1. According to the model for submarine spreading, the map in Figure 8.5d should comprise a progressive change from class 1 to class 2 to class 3 with increasing distance from the main headwall. In this direction, ridges should become shorter, ridge spacing should increase and troughs should become deeper. This is not the case, however. In the southern half of the spreading zone, this pattern is disrupted by class 5. Class 5 is located between classes 1 and 2 and consists of the shallowest troughs, shortest ridges and largest spacing (Figure 8.5d). The ridge and trough morphology along the northern sidewall is also different to what the spreading model predicts. Classes 4 and 5 dominate this region, where ridges are shorter and more spaced when compared to the ridges at the same distance from the main headwall in the southern half of the spreading area (Figure 8.5d). The south-western part of the study area, covered by class 3, has shorter ridges, higher ridge spacing and deeper troughs than the adjacent terrain to the north (class 2) (Figure 8.5d).

Table 8.1: Mean (and standard deviation) of the ridge and trough morphological characteristics for the five different classes identified by the ISODATA classification technique.

	Trough depth (m)	**Ridge length (m)**	**Ridge spacing (m)**
Class 1	3.8 (±1.0)	434 (±147)	192 (±52)
Class 2	5.4 (±1.2)	336 (±115)	286 (±92)
Class 3	5.5 (±1.0)	303 (±112)	332 (±104)
Class 4	3.5 (±0.9)	320 (±136)	396 (±222)
Class 5	1.2 (±0.9)	292 (±114)	517 (±320)

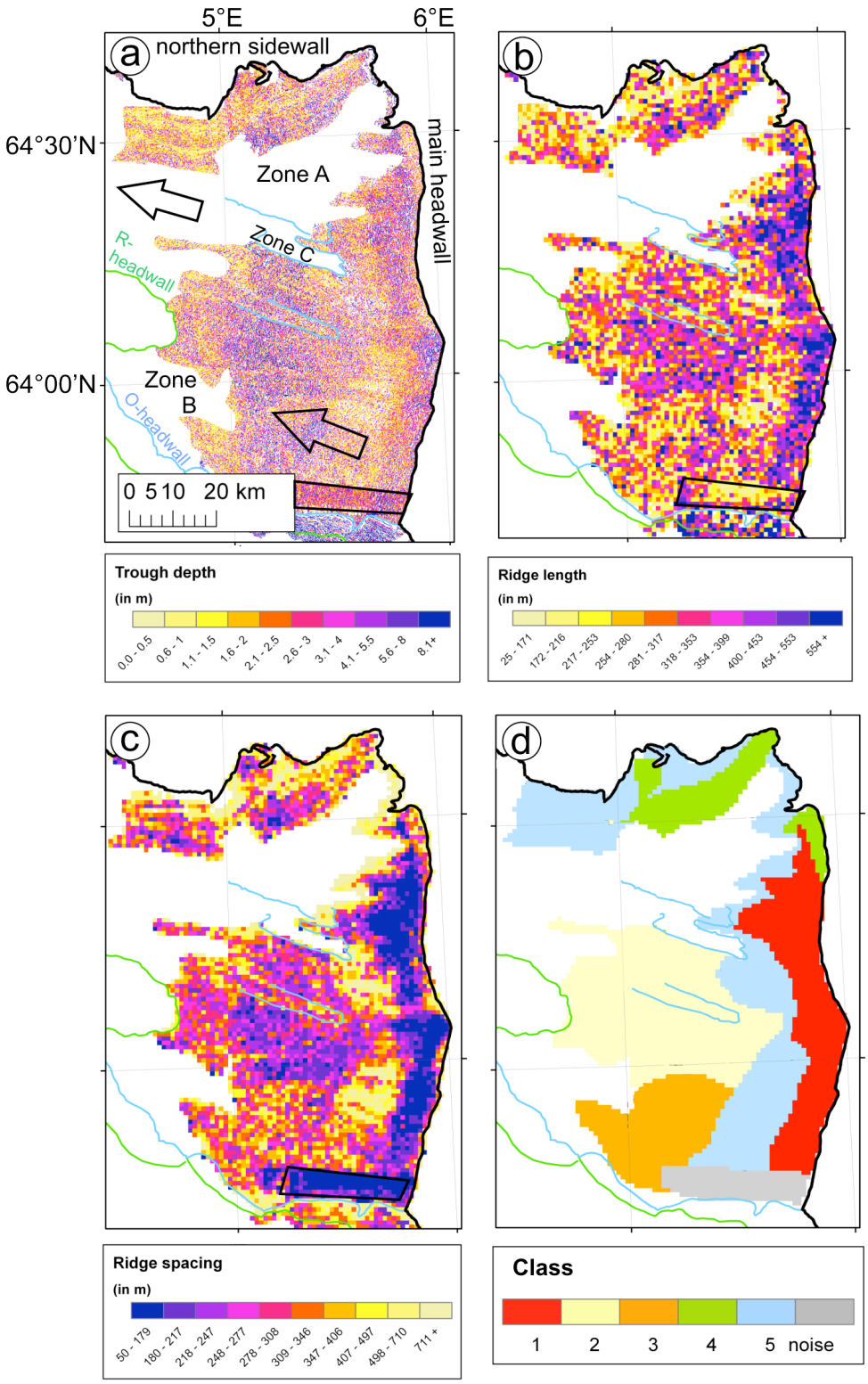

Figure 8.5: (a) Trough depth; (b) Ridge length and (c) Ridge spacing maps extracted from the areas where spreading is proposed to occur in the study area. Noise due to merging of data of different resolution is enclosed by a black rectangle. (d) ISODATA classification thematic map, which divides the study area into five classes. Some parts

of the thematic map were dominated by scattered cells, so a low-pass filter was applied to produce a continuous coverage.

8.4.3 DISCONTINUITY IN RIDGE AND TROUGH MORPHOLOGY

The ridge and trough morphology is not spatially continuous across the entire study area, but it is disrupted by:

I. A zone of smooth seabed in the north-eastern to central northern part of the study area (zone A)
II. A zone of smooth seabed in the south-west of the study area (zone B)
III. Two debris slides in the central part of the study area (zone C)
IV. Windows

I. ZONE OF SMOOTH SEABED IN THE NORTH-EASTERN TO CENTRAL NORTHERN PART OF THE STUDY AREA (ZONE A)

MORPHOLOGY

Zone A is an extensive region of smooth terrain in the north-eastern to the central northern part of the study area that contrasts with the adjacent ridges and troughs, and the blocky morphology elsewhere in the slide scar (Figures 8.2b; 8.4; 8.5b). Zone A has a total area of 2380 km^2 and covers a depth range from 530 – 1550 m, over which the mean slope gradient is 1.08°. The border of the smooth zone is characterised by either a very gentle or no change in slope. In the downslope half, however, zone A is slightly deeper than the surrounding spreading area, and at the northern border of zone A there is a 35 km long escarpment (Figure 8.4). The height of this escarpment is never larger than 15 m. In some areas, the spreading sediment from the north collapses over this escarpment into zone A (Figure 8.4). The northern border of zone A is mostly oriented parallel to the northern sidewall, as is the general direction of movement of the spreading ridges and troughs in this part of the Storegga Slide. In general, the bathymetric contours in zone A are concave downslope, suggesting sediment evacuation (Figure 8.2b). This contour pattern changes in the downslope half of zone A, where the contours are convex downslope in the northern part, implying sediment deposition

(Figure 8.2b). A bathymetric profile trending downslope across zone A has a gross form that is concave upwards with a generally steeper upslope section, and a more gently sloping lower section (Figure 8.3b). The distal part of the profile, which is convex in shape, shows relatively elevated terrain (Figure 8.3b). This corresponds to the convex downslope contours in this area and denotes deposition (Figure 8.2).

There are a number of prominent morphological features within zone A:

(a) Escarpments: A number of shallow escarpments are located in the upslope and midslope sections of zone A. Most of these escarpments are linear and trending perpendicular to the contours, although some of them are arcuate, contour-parallel and concave-downslope in plan (Figure 8.6). A few linear and saw-tooth escarpments can also be identified. The escarpments are up to 30 km long and have a maximum height of 35 m. Some of the escarpments have a deep and smooth scar located downslope. Two long escarpments extend south-east into the southern half of the spreading area (Figure 8.4). Between these escarpments, spreading has occurred along a deeper slip surface.

(b) Elongated areas of subtle ridge and trough morphology: Small areas of ridge and trough morphology can be observed within zone A, where the troughs are shallower in comparison to the surrounding spreads (Figure 8.6). These areas have positive relief, are elongated in shape and trend across slope. The areas of subtle ridge and trough morphology are up to 7 km wide and 15 km long.

(c) Elongated blocky terrain: Zone A is also characterised by a number of thin, long, downslope-oriented areas of positive relief blocky fabric (Figure 8.7a). These areas are up to 7.5 km wide and 45 km long. They are concentrated in the downslope section of zone A and extend across the S headwall, where convergence of elongated areas of the blocky terrain occurs (Figure 8.7a). These features are located directly downslope from some escarpments. The trend of the blocky terrain is perpendicular to the contours.

(d) Lineations: Numerous lineations oriented perpendicular to the bathymetric contours are observed across most of zone A (Figures 8.6; 8.7a). The lineations are generally parallel, although some convergence occurs in the upslope part of zone A. The lineations are up to 45 km long and 300 m wide, and they trend in

the same direction as the elongated areas of subtle ridges and troughs and the blocky terrain. The lineations have a modest topographic expression as narrow furrows with a maximum depth of 3 m (Figure 8.7b). Most lineations can be traced back upslope to an escarpment or the main headwall. Some lineations can be observed in the spreading areas as well. A number of lineations terminate within spreading class 5.

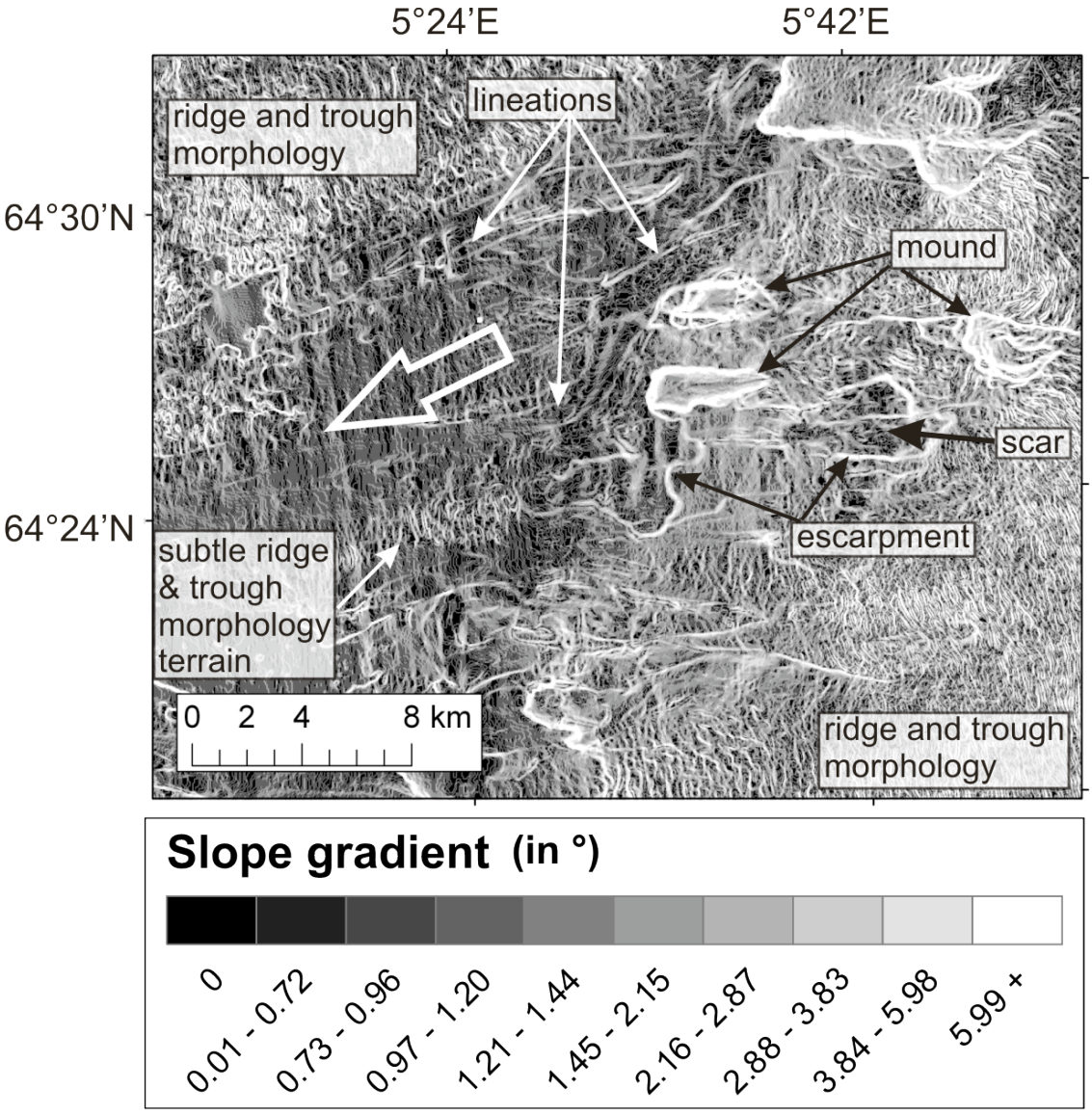

Figure 8.6: Slope gradient map of the north-eastern zone A. The location of lineations, escarpments, elongated subtle ridge and trough morphology is indicated. The ridges and troughs are located outside of zone A. The block arrow denotes the direction of sediment movement.

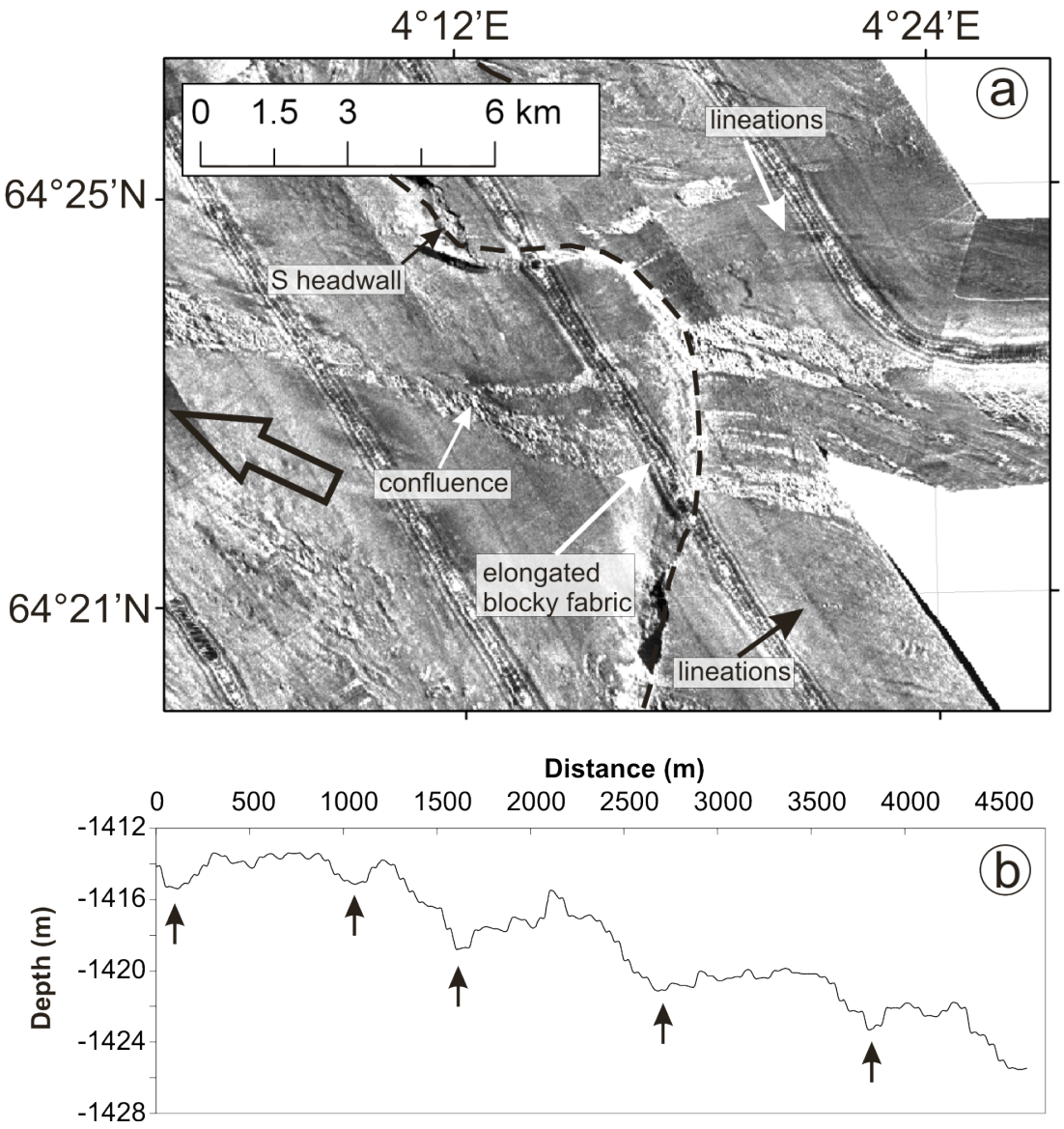

Figure 8.7: (a) TOBI sidescan sonar image from the downslope section of the study area showing lineations and elongated blocky terrain across the S headwall. (b) A bathymetric profile across lineations in Figure 8.11b. The small black arrows indicate the narrow and shallow furrows.

INTERNAL ARCHITECTURE

The seismic character of the seabed in zone A is illustrated in Figure 8.8. The sequence in Figure 8.8 belongs to the top units of the Plio-Pleistocene Naust formation. The seabed is characterised by a gently sloping, high amplitude reflector that is interrupted by a step at the main headwall. Upslope of the headwall, the seabed is shallower and partly consists of a number of upslope and downslope dipping segments, which

correspond to a spreading event. The seismic facies underneath the seabed reflector is thick, generally transparent and is underlain by a strong high amplitude reflector that extends across the entire seismic profile. It has already been established that the Naust formation upslope of the main headwall has not been eroded by the Storegga Slide [*Berg et al.*, 2005]. The seismic facies between the seabed reflector and the strong high amplitude reflectors upslope of the headwall scarp is therefore interpreted as representative of the O1-O7 sediment sub-units. The strong, high amplitude reflector is interpreted as the INO7 horizon, which is the base of the O7 sediment sub-unit [*Berg et al.*, 2005]. The O1-O7 sediment sub-unit is dissected by a thin, high amplitude reflector, which is interpreted as the INO3 horizon at the top of the O4 sediment sub-unit. The O3 sediment sub-unit, which is known to pinch out at the main headwall, is not visible [*Berg et al.*, 2005]. The sediments above the INO3 horizon are therefore interpreted as the O1-O2 sediment sub-units, whereas those underneath are the O4-O7 sediment sub-units.

The sediment within the slide scar consists of a chaotic seismic facies with some weak internal reflections (Figure 8.8). This facies extends from the main headwall down to the south-west of the seismic profile. The facies becomes thinner in this direction and we interpret it as a debris flow consisting of O unit sediments. In the south-western half of the seismic profile, this facies is underlain by a series of parallel, high-amplitude reflectors (Figure 8.8). These are interpreted as the contourite drift deposits of the R1-R2 sediment sub-units, and are thought to have comprised the failure surface above which the debris flow has failed. This debris flow has eroded into this contourite drift deposit in the central part of the seismic profile. The underlying failure surface is exposed as a window in the south-western part of the seismic profile (Figure 8.8).

An alternative interpretation of the seismic profile is that the identified debris flow consists entirely of O4-O7 sediment sub-units and is an older feature than the Storegga Slide. This interpretation is backed by the fact that the seismic character of the O4-O7 sediment sub-units upslope of the headwall and within the slide scar is chaotic. On the other hand, no sharp sediment thickness variations or onlaps could be observed in the surface sediments in the 3D seismic data (Figure 8.9). In fact, these surface sediments

drape Storegga-related mass movements further south. Also, there is no clear boundary between debris flows of potentially different ages in Figure 8.8.

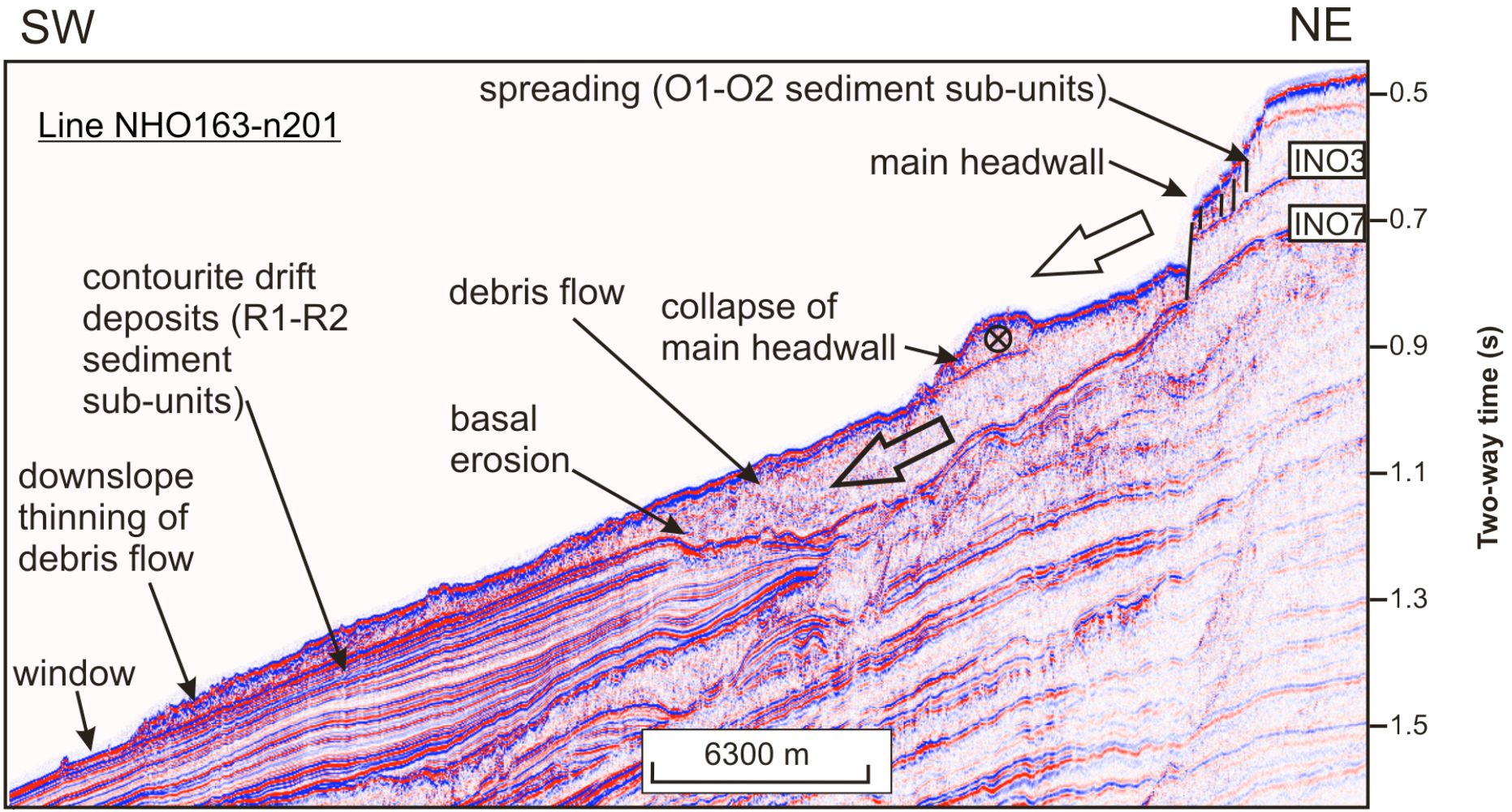

Figure 8.8: Seismic dip profile across the slide scar in zone A and the main headwall. Location of profile is shown in Figure 8.2.

ISOPACH MAP

An isopach map was generated by interpreting a horizon that is located underneath the slip surface of the spreading areas and that extends over the entire study area. The thickness of the sediment from this horizon to the surface was then calculated (Figure 8.9). A seismic velocity of 1700 m s^{-1} was used to calculate sediment thickness. For zone A and the spreading classes 4 and 5 south of the northern sidewall, the thickness varies between 0.5 m and >30m. The sediment thickness decreases downslope and then increases again. The sediment in zone A and the spreading classes 4 and 5 south of the northern sidewall is, on average, thinner compared to the surrounding spreading areas in the south (Figure 8.9).

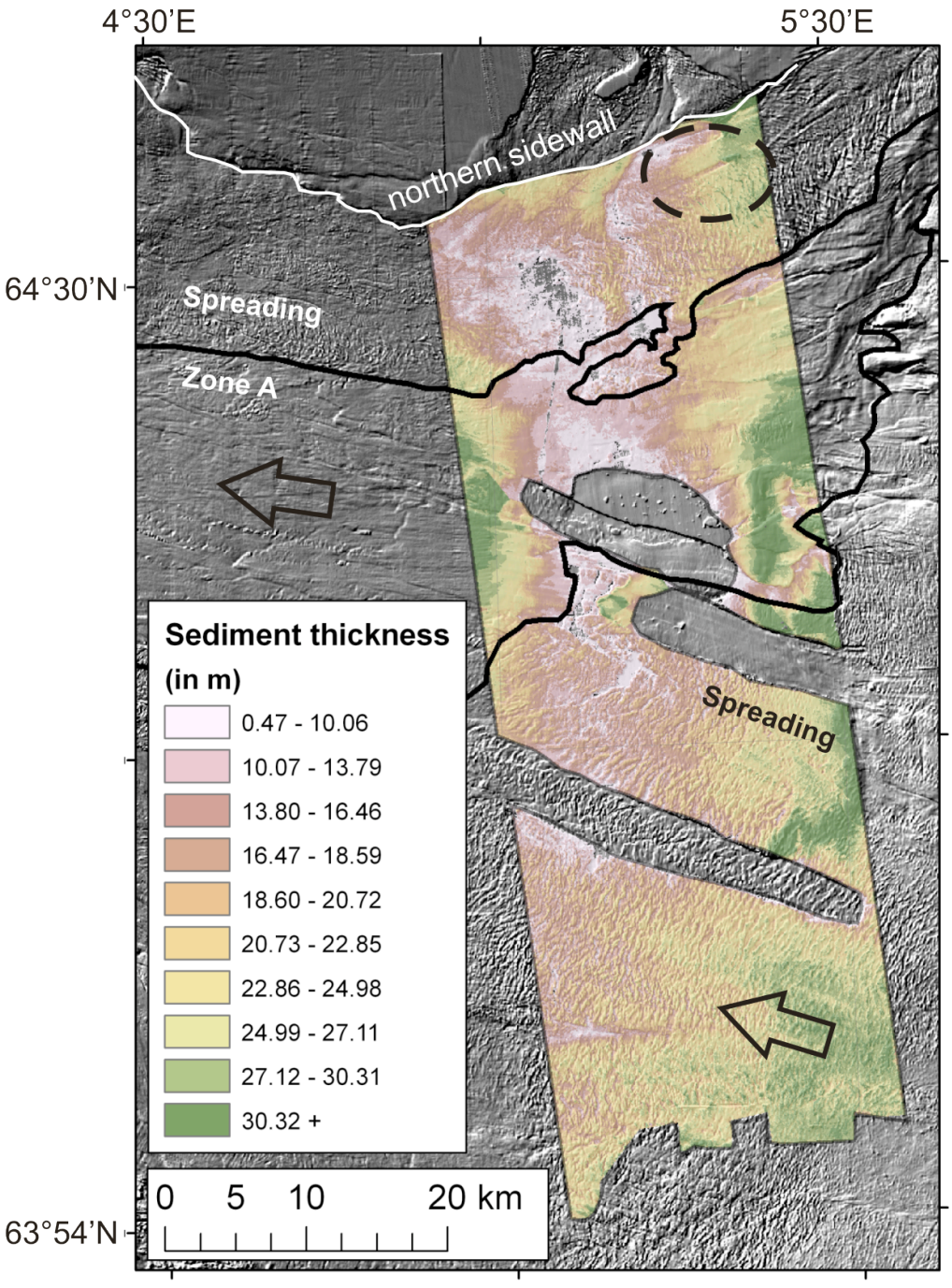

Figure 8.9: Isopach map derived from 3D seismic data set. The figure shows the thickness of the sediment above a common horizon. The solid black line denotes the boundary of zone A. The dotted black ellipse indicates a linear depression formed by spreading (class 5 in Figure 8.5d) being obstructed by positive relief features. The calculated displacement of the material at this point is 7.5 km. At a similar distance from the main headwall as the positive relief feature, the estimated displacement of sediment in spreading class 1 is estimated at a maximum of 1.7 km (10% extension) [*Micallef et al.*, 2007b].

II. ZONE OF SMOOTH SEABED IN THE SOUTH-WESTERN PART OF THE STUDY AREA (ZONE B)

A second zone of smooth terrain is located in the south-west of the study area, at the limit of the ridge and trough morphology (Figures 8.2b; 8.4; 8.10). This zone has an area of 450 km^2, it is characterised by convex downslope contours (Figure 8.2b) and the seafloor is slightly deeper in comparison to the adjacent ridges and troughs. The smooth terrain is disrupted by a number of long and deep troughs oriented north-south, as well as a number of downslope-oriented lineations and contour-parallel escarpments (Figure 8.10). A small area of distinct positive relief compared to the surrounding terrain is located to the south of zone B, between the O and R headwalls (Figure 8.10a). The surface of this area is characterised by a well-defined pattern of long convex downslope ridges and troughs. The seismic dip profile in Figure 8.10b demonstrates that the seismic character of the seabed in zone B is characterised by a continuous high amplitude reflector. Underneath this reflector is a chaotic seismic facies that is ~67 ms (TWT) thick. This contrasts with the segments of upslope and downslope dipping reflectors in the spreading area to the east. A number of blocks of parallel, high amplitude reflectors can be identified within the chaotic seismic facies (Figure 8.10b).

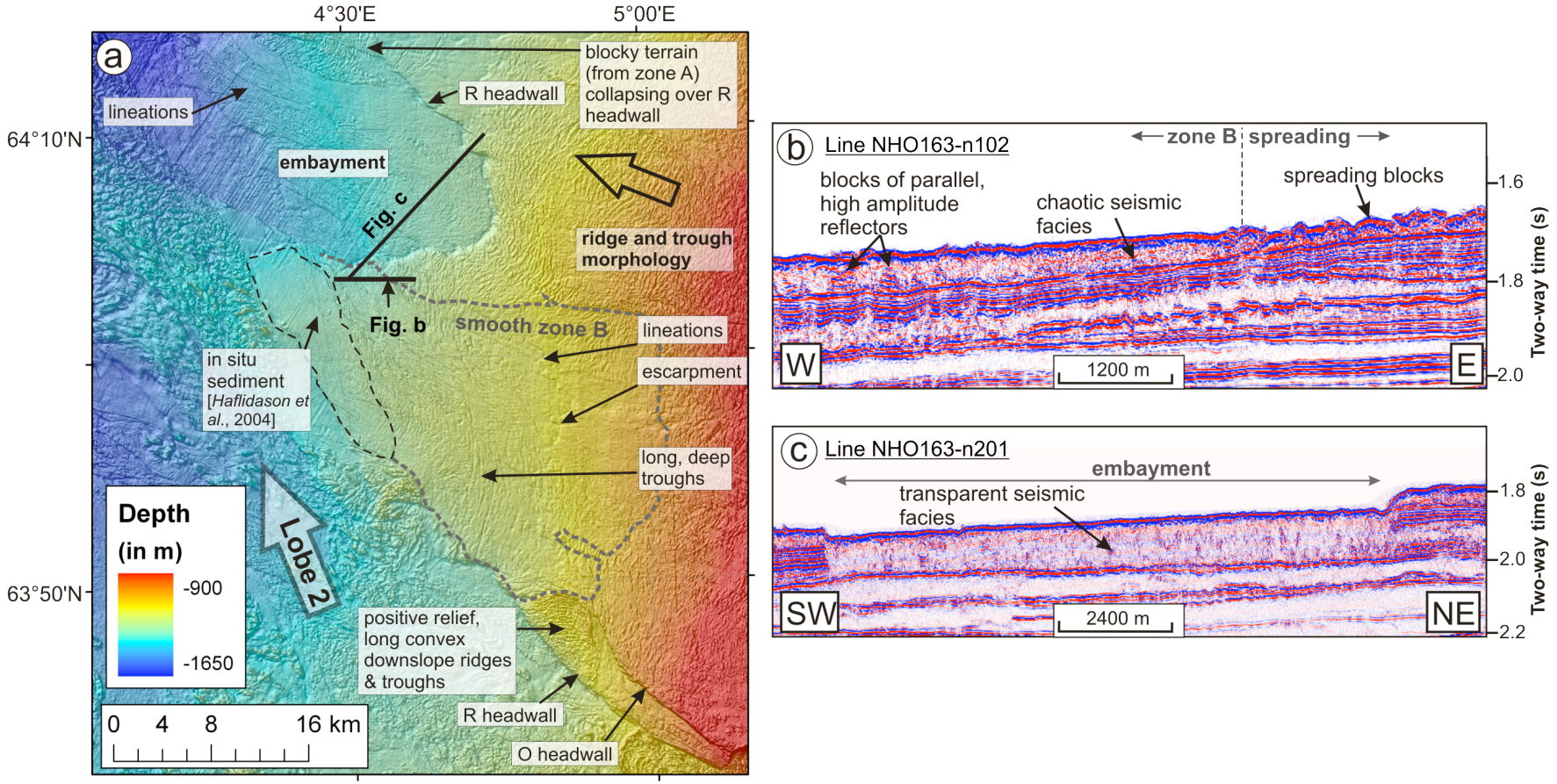

Figure 8.10: (a) Bathymetry draped on a shaded relief map of zone B and the elongated embayment (illumination from north-east, 5× exaggeration). Zone B is enclosed by a grey dotted line. The main morphological features are labelled. (b) Labelled seismic dip profile across the northern part of zone B and the adjacent spreading terrain. (c) Labelled seismic dip profile across the elongated embayment.

III. TWO DEBRIS SLIDES IN THE CENTRAL PART OF THE STUDY AREA (ZONE C)

Two parallel features, interpreted as discrete mass movement features (labelled 1 and 2 in Figure 8.11a), are located at the southern border of zone A (Figure 8.4). These are characterised by parallel, steep flanks and a shallow headwall. The scars are up to 3.8 km wide and the flanks have a maximum depth of 35 m. The mass movements extend into the ridge and trough morphology upslope. Lineations can be observed both inside and downslope of the mass movement scars (Figure 8.11b). The 3D seismic data reveal that the mass movements have slip surfaces that are parallel to the slope stratigraphy and that are deeper than the slip surface of the adjacent spreading sediment. In the case of mass movement 2, a tensional depression is located between the headwall and the distal limit. The latter is characterised by a convex snout, underneath of which the sediment layering is preserved. Mass movement 2 is therefore interpreted as a debris slide. In the case of mass movement 1 (Figure 8.11a), the accumulation zone is not clearly identifiable in the seismic data. The northern sidewall of mass movement 1 is covered by a subtle uneven morphology to the west, whereas to the east sediment has collapsed over the escarpment in a lobate form (Figure 8.11a). Since mass movement 1 has similar scar morphology to that of mass movement 2 and shares the same slip surface, it is tentatively interpreted as a debris slide.

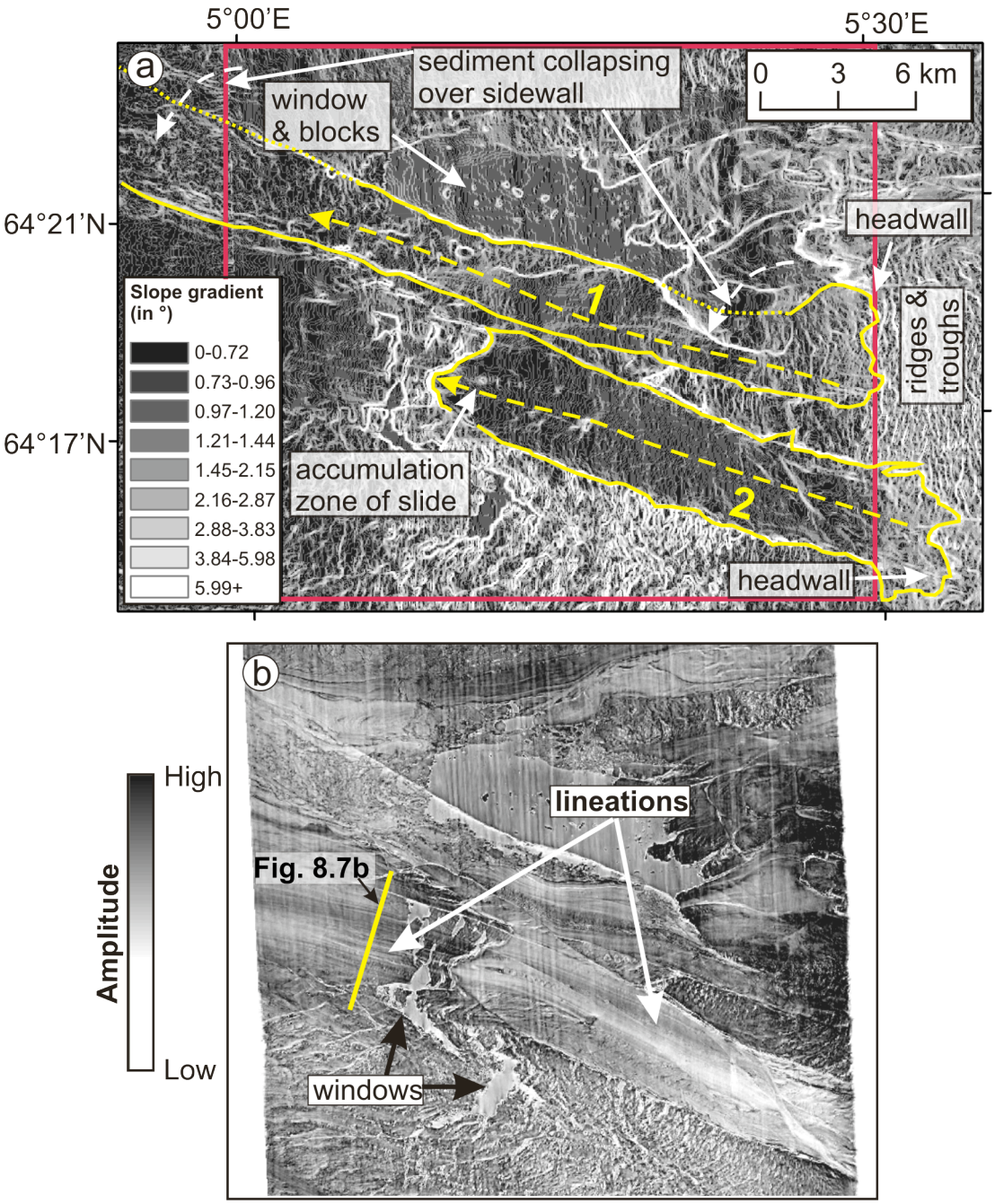

Figure 8.11: (a) Slope gradient map of mass movements 1 and 2 (outlined in a solid yellow line) in the central part of the study area (zone C). The dotted arrows indicate the direction of sediment movement. (b) Seismic amplitude map of the seabed enclosed by a solid red square in Figure a. The lineations and windows are clearly visible.

IV. WINDOWS

A window is a part of the slide scar where the underlying slip surface is exposed. A number of windows are located downslope of pronounced ridges and troughs in the western downslope limit of the spreading areas (Figure 8.11b).

8.4.4 ELONGATED EMBAYMENT

North of zone B, the R headwall is characterised by an elongated embayment trending north-west to south-east (Figure 8.10a). The embayment is 33 km long and 15 km across. The walls of the embayment are steep and ~60 m deep. The seabed between these walls is characterised by downslope-trending lineations and a subtle blocky morphology. The ridges and troughs located upslope of the embayment are concave-downslope in plan and parallel to the embayment wall (Figure 8.10a). Some of the blocky terrain identified within zone A extends into the embayment across the northern wall (Figure 8.10a). The downslope part of the southern wall is covered by large blocks of debris. The seismic dip profile within the embayment shows a continuous, smooth, high amplitude reflector (Figure 8.10c). This is underlain by a 136 ms (TWT) thick transparent and homogeneous seismic facies. The walls at the flanks of the embayment consist of a series of parallel, high amplitude reflectors. The morphology and the seismic character of the embayment are very similar to those of the Solsikke and Gloria Valley troughs in the distal part of the Storegga Slide scar [*Riis et al.*, 2005] (Figure 8.1).

8.4.5 HEADWALL MORPHOLOGY

In the study area, the main Storegga headwall can be divided into two sections. The northern section, which is 26.5 km in length, is characterised by an abrupt concave break of slope, upslope of which is located a gentler convex break of slope, with spreading ridges and troughs found in between (Figure 8.12). The headwall has a mean height of 72 m and features a number of narrow embayments. This section of the main headwall is located upslope of zone A and spreading class 4 south of the northern sidewall (Figure 8.5d). In the southern section, the main headwall is located upslope of

spreading ridges and troughs in class 1 (Figures 8.5d; 8.12). It consists of a very gentle convex break of slope, where ridges and troughs grade into a gentle undisturbed slope (Figure 8.12). The mean headwall height for the southern section is 24 m, although heights of 50 m are recorded in the southern half of this section.

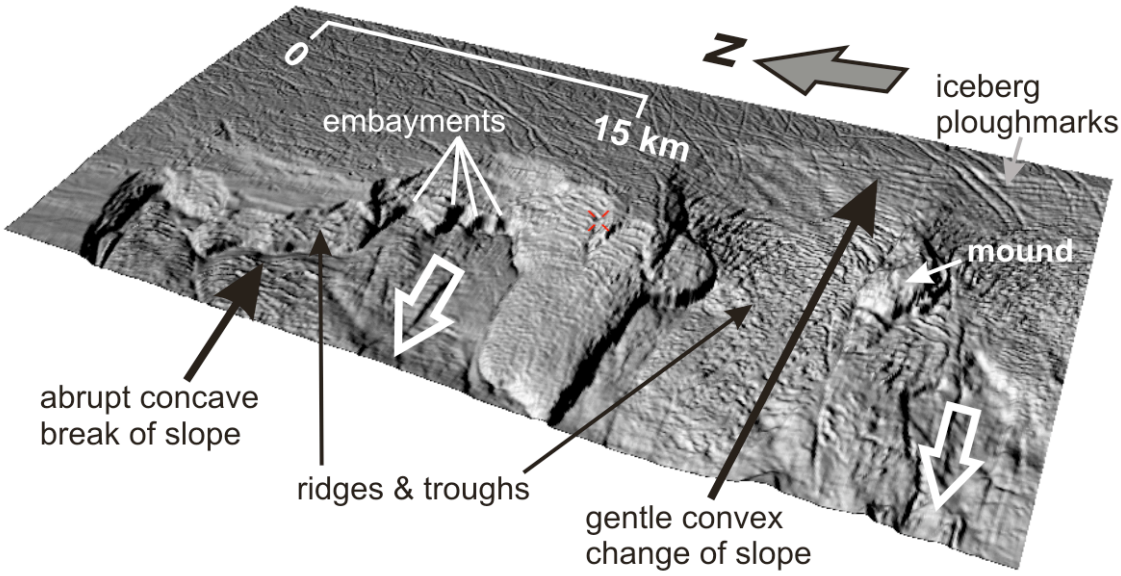

Figure 8.12: 3D shaded relief bathymetry (illumination from north-east, 5× exaggeration) showing the two different morphologies of the main headwall upslope of zone A.

The northern sidewall generally consists of an abrupt break of slope that is up to 50 m high (Figures 8.2; 8.4). The upslope half of the northern sidewall is disrupted by a deep embayment that is ~15 km wide and that extends 9 km upslope into the northern sidewall (Figure 8.4). The terrain in this embayment consists of ridges and troughs spreading in a south-west direction. The morphology of these ridges and troughs is similar to those in the spreading classes 4 and 5 (Figures 8.4; 8.5d). The ridge and trough morphology in the embayment is broken up by a number of downslope-oriented lineations. The areas upslope of the northern sidewall in this embayment are also affected by spreading, although they are characterised by a more closely-spaced pattern of shallow ridges and troughs. Small spreading events and debris flows are located along the downslope section of the northern sidewall.

8.4.6 POCKMARKS

Pockmarks are seafloor depressions resulting from the expulsion of fluids *[Bouriak et al*., 2000; *Judd and Hovland*, 1992]. They are very common on the undisturbed seafloor outside of the slide scar area; they are concentrated in a narrow band striking west-north-west to east-south-east, which extends from the northern sidewall to an area upslope of the northern section of the main headwall [*Bouriak et al.*, 2000; *Bünz et al.*, 2003] (Figure 8.13).

8.5 DISCUSSION

We will first interpret the geomorphological features described in section 8.4 in terms of the formative mass movement processes. This interpretation will then be used to propose a revised development model for the north-eastern Storegga Slide. Finally, an attempt is made at identifying the geological causes and controls of spatial variation in mass movement types within the north-eastern Storegga Slide.

8.5.1 INTERPRETATION

I. SPATIAL VARIATION IN RIDGE AND TROUGH MORPHOLOGY

Spreading classes 3 and 5 in the southern half of the study area, and classes 4 and 5 south of the northern sidewall, do not fit into the morphology expected for a typical submarine spread (Figure 8.5). These classes have shorter ridges, higher ridge spacing and shallower troughs than would be expected based on observations elsewhere in the slide area. Classes 3, 4 and 5 are hypothesised to be indicative of higher displacement and remoulding of the spreading blocks along the northern sidewall and in the southern half of the spreading areas, in comparison to the spreading areas elsewhere (Figure 8.13). The linear depression identified in zone 4 in Figure 8.9 is another indication of higher block displacement.

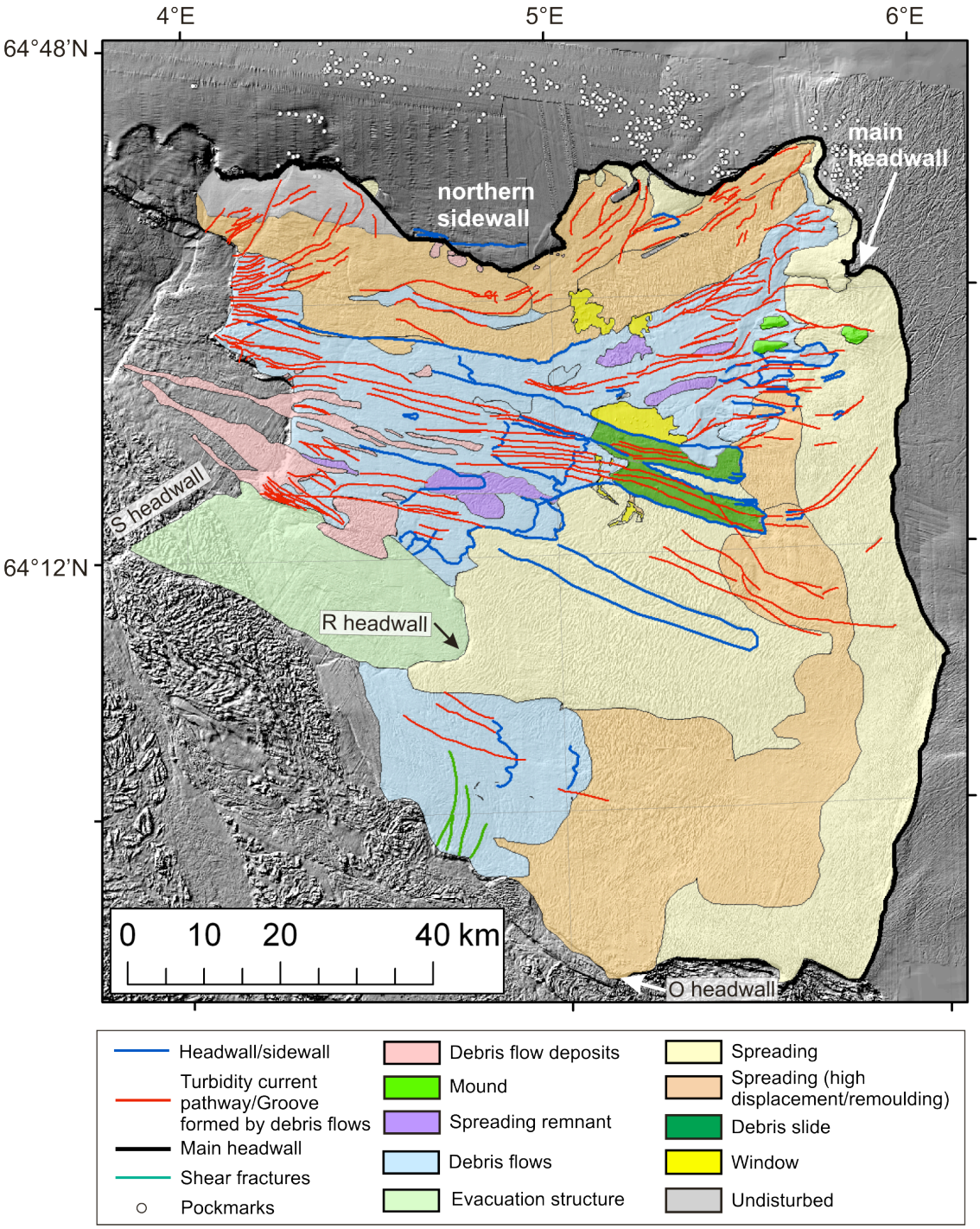

Figure 8.13: Interpretative map of the mass movements and geological processes that have shaped the north-eastern Storegga Slide scar.

II. ZONES OF SMOOTH TERRAIN

ZONE A

The smooth terrain and the numerous escarpments, lineations and elongated zones of blocky terrain and ridges and troughs within zone A contrast with the surrounding widespread ridges and troughs. We interpret the different morphology within zone A as having been formed by debris flows and later overprinted by turbidity currents. In our interpretation the escarpments are the sidewalls and headwalls of debris flows (Figure 8.13). The lineations, which bathymetry indicates are narrow furrows and many of which can be traced back to these headwalls, are interpreted as having a dual origin: they are either the pathways eroded by the high energy head of turbidity currents into the underlying failure surface, or grooves formed at the base of individual debris flows (Figure 8.7a; 8.13). The lineations that originate from spreading classes 4 and 5 (Figure 8.5d) and the embayment within the northern sidewall, are interpreted as turbidity current pathways. It is possible that some of the spreading in the areas of higher displacement and remoulding evolved into turbidity currents, but the turbidity current pathways can also be later features. The elongated blocky terrain in zone A is interpreted as residual debris flow deposits (Figure 8.13). The deposits are located downslope of the headwalls and they are concentrated in the distal part of zone A. The grading from a furrowed seafloor to a field of longitudinal deposits indicates that the flow regime decreases gradually downslope (Figure 8.13). Changes in the contour shape within zone A from concave downslope to convex downslope in plan confirm this change of flow regime (Figure 8.2b). The zones of subtle ridges and troughs within zone A are interpreted as remnant spreading morphology that was shaped into an elongated form by debris flows and turbidity currents at the sides (Figure 8.13). The presence of these remnants suggests that spreading initially extended over parts of zone A. It has already been established that lobe 1 has eroded the O1-O2 sediment sub-units and that spreading occurred in the O3 sediment sub-unit [*Haflidason et al.*, 2004; *Micallef et al.*, 2007b]. The absence of the latter from within the slide scar and the presence of the remnant spreading morphology may indicate that the debris flows and turbidity currents have deformed or removed the spreading blocks formed in the O3 sediment sub-unit. Erosion by debris flows and turbidity currents would explain the

generally smoother, deeper terrain and the thinner sediment in zone A, in comparison to the surrounding spreading areas (Figures 8.2a; 8.9). The debris flows and turbidity currents may also be responsible for the irregular morphology of the main headwall upslope of zone A (Figure 8.12). The fact that the seismic facies of the sediment inside the slide scar in Figure 8.8 is generally more chaotic than the O4-O7 sediment sub-units upslope of the headwall indicates that debris flows have also mobilised the O4-O7 sediment sub-units themselves. The deformation of the O4-O7 sediment sub-units is also confirmed by the localised plastic deformation of the sediment in the midslope section of zone A, as indicated by the collapse of smooth sediment lobes across the northern sidewall of mass movement 1 (Figures 8.11; 8.13).

ZONE B

The morphology of zone B is similar to that of zone A. The smooth terrain, lineations and escarpments within zone B may all be indicative of sediment mobilisation in the form of debris flows and turbidity currents. This is corroborated by the chaotic seismic character of the surface sediment in this area (Figure 8.10b). The long and deep troughs oriented north-south within zone B, and the small area of positive relief located outside of zone B, are indicative of compression and transpressive shearing due to the mobilisation of sediment in a north-north-west direction in lobe 2 (Figures 8.10a; 8.13).

III. ELONGATED EMBAYMENT

The elongated embayment in Figure 8.10a is interpreted as an evacuation structure, similar to those identified in the distal part of the Storegga Slide by *Riis et al.* [2005] (Figure 8.13). These authors define evacuation structures as crater-like features that are formed and enlarged by the removal of ooze material during a mass flow. The ooze material is mobilised because of its low density, which enables it to rise to the top and form mounds. The evacuation structure is simultaneously infilled by material from the mass flow. In the case of the evacuation structure in Figure 8.10a, the embayment was filled with sediment from the O1-O2 sediment sub-units mobilised by lobe 1, and the O3 sediment sub-unit spreading upslope of the embayment. The ooze mounds are no longer visible. We think that the evacuation structure predates spreading because the

ridges and troughs upslope of the evacuation structure are concave-downslope in plan and parallel to the escarpment. This indicates that the ridges and troughs were formed due to loss of support at the escarpment. The collapse of blocky sediment from zone A into the evacuation structure indicates that the latter also predates the debris flows and turbidity currents in zones A and B (Figure 8.10a).

8.5.2 DEVELOPMENT MODEL FOR THE NORTH-EASTERN STOREGGA SLIDE

Based on the identification of spreading, debris slides, debris flows, turbidity currents, compressional features and an evacuation structure in the study area, we propose a revision of the development model for the north-eastern Storegga Slide as suggested by *Haflidason et al.* [2004] (Figures 8.1; 8.13; 8.14; Table 8.2).

In our development model, the Storegga Slide was most likely triggered by an earthquake with an epicentre in the area close to the S headwall [*Atakan and Ojeda*, 2005; *Bryn et al.*, 2005a]. Failure developed at the foot of the slope in this region and propagated upslope in an eastern direction. The surface sediment sub-units O1-O2 were removed during the development of event 1a (lobe 1), with the top of the O3 sediment sub-unit acting as the failure surface (Figure 8.14). The sediments were deposited as turbidites and debrites in the Norwegian Sea Basin [*Haflidason et al.*, 2004]. No deposits from event 1a could be identified in the study area. The surface sediments comprising the O1-O2 sediment sub-units failed as debris flows and turbidity currents because the sediments were deposited during the last glacial-interglacial cycle and had not undergone significant consolidation. The parts of O1-O2 sediment sub-units that were consolidated by glacial compaction during the Last Glacial Maximum are located at the main headwall. Event 1a extends across most of the study area and the region downslope from the S headwall down to the Norwegian Sea Basin (Figure 8.14). The area of event 1a also potentially extends into the region south of the study area [*Haflidason et al.*, 2004]. The maximum upslope extent of event 1a (lobe 1) was estimated at ~20 km from the main headwall [*Haflidason et al.*, 2004]. There are, however, no clear morphological features that define the maximum upslope extent of event 1a. We therefore infer that event 1a extended up to the main headwall, adding up

to an area of 40 804 km^2. This would explain the 50 m headwall height observed in the southern part of the study area. Loading of the deeper sediment in the lower part of the study area by sediment mobilised during event 1a is thought to have led to the formation and infilling of the evacuation structure (event 1b) (Figure 8.14).

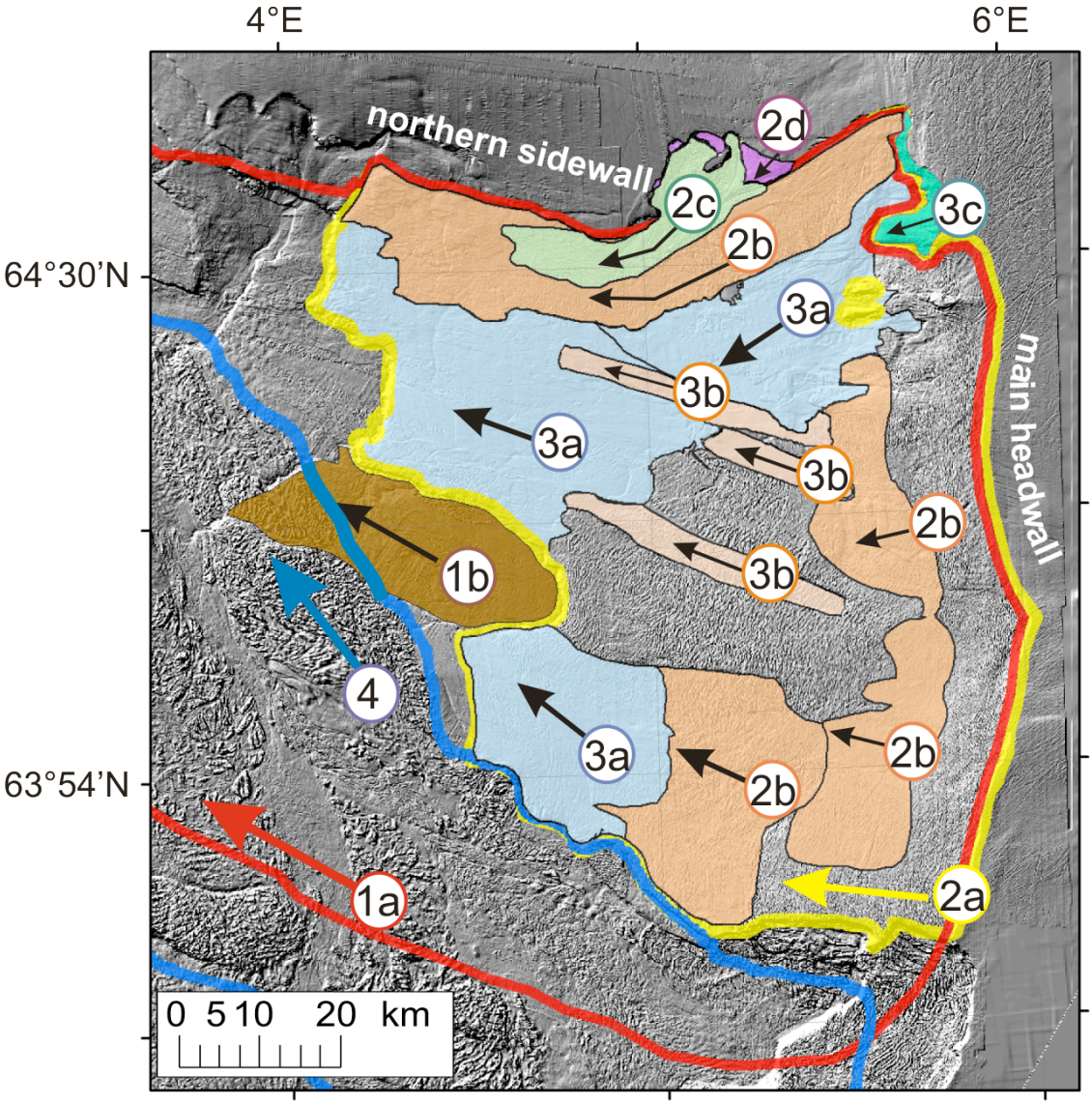

Figure 8.14: Slide development model for the north-eastern Storegga Slide. The development is described in terms of events, which are shaded and labelled.

Following the development of events 1a and 1b, we propose that spreading took place across the part of the study area previously affected by event 1a (event 2a). The failure surface was located somewhere within the O3 sediment sub-unit, and the spreading blocks were formed in the upper layers of the O3 sediment sub-unit [*Micallef et al.*, 2007b]. Spreading extended from the S headwall and the evacuation structure up to the

main headwall, affecting an area of 6870 km^2 and defining the shape of the majority of the main headwall in the study area as a shallow and gentle escarpment (Figures 8.12; 8.14). The development of this extensive mass movement was brought to a halt by the more consolidated sediment at the main headwall [*Kvalstad et al.*, 2005a; *Micallef et al.*, 2007b]. Spreading could have been triggered by either loss of support due to the reactivation of the S headwall, the formation of the evacuation structure and/or by seismic loading associated with the earthquake that initiated the Storegga Slide. The failure of the O3 sediment sub-unit as a spread rather than as a debris flow or turbidity current is attributed to its high consolidation and clay content [*Berg et al.*, 2005; *Micallef et al.*, 2007b]. Some spreading blocks have undergone a higher extent of displacement and remoulding compared to the ridges and troughs in event 2a (event 2b) (Figure 8.14). Event 2b encompasses the area south of the northern sidewall and a north-south trending area ~7 km downslope from the main headwall, totalling an area of ~2100 km^2. Minor slope failures in the form of spreads, debris flows and turbidity currents (events 2c and 2d), have occurred in O1-O2 sediments along the northern sidewall, presumably due to loss of support from sediment evacuated within the slide scar by events 1, 2a and 2b. Some of these failures are more recent events than the Storegga Slide, having been dated to be 2200 – 5700 cal. yr BP old [*Haflidason et al.*, 2005].

Event 3 covers the northern central and south-western part of the study area, extending from the S headwall to the main headwall and affecting a total area of ~2500 km^2. Event 3a consists of debris flows and turbidity currents that affected the seabed in zones A and C (Figure 8.4). These mass movements have deformed or removed most of the ridge and trough terrain formed by event 2 in the O3 sediment sub-unit, and mobilised the underlying O4-O7 sediment sub-units. The key observation that proves that the mass movements in event 3a either post-date or are coeval with spreading in event 2 is the presence of spreading remnants within zone A (Figure 8.13). Debris flows and turbidity currents developed upslope from the S headwall as the headwalls of these mass movements retrogressed in a south-east direction. These mass movements extended into the north-east of the study area where the direction of sediment movement changes from north-west to south-west (Figure 8.14). Loss of support resulting from these flows triggered two debris slides and a spreading event in the central part of the study area

(labelled collectively as event 3b in Figure 8.14, and partly corresponding to zone C in Figure 8.4). Loss of support due to removal of sediment by event 3a in the north-eastern part of the slide scar triggered spreading upslope of the main headwall (event 3c) (Figure 8.14).

Event 4 (lobe 2), consisting of a large blocky debris flow, is thought to have been initiated with lobe 1 [*Haflidason et al.*, 2004]. However, sediment in event 4 seems to have been mobilised later because it failed along a deeper slip surface [*Bryn et al.*, 2005a], which is expected to retrogress more slowly than a shallower failure. Event 4 eroded sediment as a large debris flow that extended into the Ormen Lange region, and retrogressed upslope as a series of spreads characterised by long ridges and deep troughs [*Micallef et al.*, 2007b]. The identification of short and shallow ridges and troughs on the top of larger spreading ridges in the Ormen Lange region is proof that failure in event 4 post-dates event 1 [*Kvalstad et al.*, 2005a; *Micallef et al.*, 2007b]. During event 4, sediment at the flanks of the debris flow was compressed against the south-western spreading areas in event 2a, creating localised compression and shear zones.

Table 8.2: Characteristics and timing of the different events in the revised development model of the Storegga Slide.

Event	Type of mass movement	Sediment sub-unit/s involved	Area (km^2)	Timing
1a	Debris flows and turbidity currents	O1-O2	40 804	1
1b	Formation and infilling of evacuation structure	Failed sediment: ooze material; infilling by O1-O3	480	2
2a	Spreads	O3	4770	3
2b	Spreads (higher displacement)	O3	2100	3
2c	Spreads, debris flows and turbidity currents	O1-O3	247	4
2d	Spreads	O1-O2	27	5
3a	Debris flows and turbidity currents	O3-O7	2200	6
3b	Debris slides and spreads	O3-O7	290	7
3c	Spreads	O1-O3	62	8

4	Debris flow	O1-O7	20 278	9

Although the slide development is explained in terms of temporally and spatially distinct events (Table 8.2), the Storegga Slide should be regarded as a quasi-simultaneous event [*Bryn et al.*, 2005a].

8.5.3 GEOLOGICAL CAUSES OF SPATIAL VARIATION IN SPREADING MORPHOLOGY AND THE OCCURRENCE OF DEBRIS FLOWS AND TURBIDITY CURRENTS (EVENTS 2B, 2C AND 3A)

The spreading ridge and trough morphology indicates that some areas (events 2b and 2c) have undergone higher displacement and remoulding, and some sediments have been removed or deformed by debris flows and turbidity currents (event 3a). Limit-equilibrium modelling shows that higher displacement of spreading blocks is achieved by high pore water overpressures, a steep slip surface, high unit weight and thickness, and low angle of friction and cohesion, of the failing sediment [*Micallef et al.*, 2007b]. Debris flows and turbidity currents, on the other hand, are the result of high pore water pressures, low cohesion and fine sediments, amongst others [*Mulder and Cochonat*, 1996]. We can thus put forward two potential geological causes for the lateral distribution of debris flows, turbidity currents, and higher displacement and remoulding of the spreading blocks in events 2b, 2c and 3a:

I. GAS-RELATED SLOPE INSTABILITY

Gas hydrates are an ice-like compound composed of a gas molecule, generally methane, surrounded by a rigid cage of water molecules [*Sloan*, 1998]. They occur under particular pressure/temperature conditions where pore water in marine sediments is saturated by methane. The BSR (bottom simulating reflector) marks the base of the hydrate zone and is thus used as an indicator for the presence of gas hydrates. The extent of the BSR within the Storegga Slide has been mapped by *Bünz et al.* [2003]. The BSR has a spatial extent of 4000 km^2 and it occurs beneath the seabed in water depths

of 550 – 1300 m. Gas hydrates occur continuously along the northern sidewall outside the Storegga Slide and into the north-eastern slide scar area (Figure 8.15a).

The role of gas hydrate dissociation in activating submarine slope instability has been actively discussed [*Paull et al.*, 2000]. At sufficient concentrations, gas hydrates may cement the sediment, modify its strength, fill the voids and prevent normal sediment compaction [*Sultan et al.*, 2004b]. The dissociation of the gas hydrates, due to changes in the pressure-temperature conditions, results in the release of free gases and water into the pore space. This decreases the shear strength of the sediment, creating weakened layers in the sub-seabed that are prone to failure [*McIver*, 1982; *Nixon and Grozic*, 2006]. As a result, gas hydrate dissociation may control the occurrence and location of submarine slope instabilities. Gas hydrate dissociation has been proposed as a trigger of slope instability within the Storegga Slide by numerous authors [*Bugge et al.*, 1987; *Bünz et al.*, 2005; *Mienert et al.*, 1998; *Mienert et al.*, 2005; *Sultan et al.*, 2004a; *Sultan et al.*, 2004b; *Vogt and Jung*, 2002]. The common conclusion of these studies is that gas hydrates dissociation may be a secondary process that weakened sediments and that partly explains the position of the main headwall of the Storegga Slide; it seems not, however, to be the primary cause of the Storegga Slide [*Mienert et al.*, 2005].

Within the study area we observe that the distribution of the BSR coincides with the location of a number of mass movements. The majority of areas affected by events 2b, 2c and 3a fall within the boundaries of BSR A, B and C (Figure 8.15a). The eastern limits of BSR A and C correspond to the upslope limits of events 2b and 3a. The location of the BSR in Figure 8.16 also correlates well with events 2b and 3a. Where the BSR intersects the main headwall, the morphology of the latter is steep and irregular (Figures 8.12; 8.15a). We therefore propose gas hydrate dissociation as one of the geological factors that determined the extent and style of failure in events 2b, 2c and 3a. Gas hydrate dissociation has likely occurred in the Storegga region due to warming after the last deglaciation, and by the time the Storegga Slide took place 8100±250 cal. yr BP, the thermal signal would have reached the base of the gas hydrate stability zone [*Vogt and Jung*, 2002]. In particular in the area between 400 and 800 m water depth, the gas hydrates would have dissociated, releasing free gas, increasing the pore pressure and destabilising the slope [*Mienert et al.*, 2005; *Nixon and Grozic*, 2006; *Sultan et al.*,

2004b]. The pockmarks located upslope of events 2b, 2c and 3a, which indicate periodic gas blow-outs due to the accumulation of gas and fluids beneath the gas hydrates, can be interpreted as evidence of this overpressure (Figure 8.13). Gas hydrate dissociation may also have taken place due to a decrease in lithostatic pressure after the removal of the O1-O2 sediment sub-units during event 1a, and the breaking up and mobilisation of the O3 sediment sub-unit during event 2a. The removal of overburden would decrease the confining pressures, leading to additional dissociation and overpressure. Although this was suggested by *Berndt et al.* [2004] for collapse structures at the northern sidewall of Storegga, it seems likely that this was only a secondary process.

An increase of pore pressure due to gas hydrate dissociation would have decreased the shear strength of the sediment, possibly leading to higher displacement and remoulding of the spreading blocks in events 2b and 2c, and the debris flows and turbidity currents of event 3a. These events would have mobilised and evacuated sediment downslope of the BSR outcrop. This scenario fits well into the development model proposed in section 8.5.2.

The proposed scenario is supported by two additional considerations. First, the BSR corresponds to the base of the hydrate stability zone, underneath which free gas has accumulated, but IODP drilling off Vancouver Island has shown that both gas hydrates and free gas are also present above the BSR and close to the seabed [*Riedel et al.*, 2006]. Secondly, one of the Tertiary dome structures that are known to be gas reservoirs is located underneath the BSR (Figure 8.16). The escape and ascent of gas from the dome structure to shallower levels is thought to be the source of gas ascending into the hydrate stability zone. The dome structure is also very similar to the one located in the Ormen Lange region, where the deepest slope failure within the Storegga Slide has occurred [*Bünz et al.*, 2005].

II. DEPOSITIONAL FRAMEWORK AND SEDIMENTOLOGY

The second geological cause being proposed is the spatial variation in the physical properties of the failing sediments and the setting in which they were deposited. The S and R Slides, dated at ~0.5 Ma and ~0.3 Ma respectively, evacuated sediment from the

north-eastern part of the Storegga Slide scar [*Solheim et al.*, 2005a]. Repeated failure in this area explains the basin-shaped seafloor in the north-eastern Storegga Slide (Figure 8.3b). The headwalls of the palaeoslides roughly coincide with the upslope limit of events 2b and 3a of the Storegga Slide (Figure 8.15b). Note that the north-eastern boundary of the R headwall coincides with that of the Storegga Slide, which confirms that the northern sidewall of the Storegga Slide scar was formed by an event older than the Holocene slide [*Brown et al.*, 2006]. This means that the direction of sediment mobilisation in the north-eastern Storegga Slide was controlled by a pre-existing structure. Events 2b, 2c and 3a fall within the extent of the S and R palaeoslides inside the study area (Figure 8.15b). We suggest that the scars formed by such palaeoslides have favoured the deposition of contourite drifts, transported northwards with the North Atlantic Current from the North Sea Fan area [*Bryn et al.*, 2005b]. The deposition of contourite drifts is rapid, resulting in the build up of thick sediment bodies and the development of excess pore pressure in response to loading [*Bryn et al.*, 2003]. The contourite deposits are also characterised by high water content, low permeability and low unit weight [*Berg et al.*, 2005]. Another important property of contourite drifts is their draping and smoothing of rough slide scars and glacial debris flow deposits, which facilitates the formation of extensive quasi-planar slip surfaces within the drift deposits. Because of all of these characteristics, the distribution of contourite drift deposits within the palaeoslide scars may have promoted instability and determined the extent of failure in events 2b, 2c and 3a.

Both the presence of gas and lithology changes may have controlled the nature and extent of failure in events 2b, 2c and 3a. Although we observe that all of the mass movements in events 2 and 3 occur within or above contourite drift deposits, only events 2b, 2c and 3a fail as highly displaced and remoulded spreading, debris flows and turbidity currents, whereas the remaining events predominantly involved spreading (Figure 8.16). Only these three events coincide with the presence of a gas hydrate BSR. This correlation would suggest that the presence of free gas, possibly as a result of gas hydrate dissociation, has played a role in the difference in failure style. However, our geophysical data base is not dense enough close to the headwall to rule out that lithology changes, such as the presence of debris flows, may have played a role in the

style of failure further upslope and overprinted the processes where we have full data coverage.

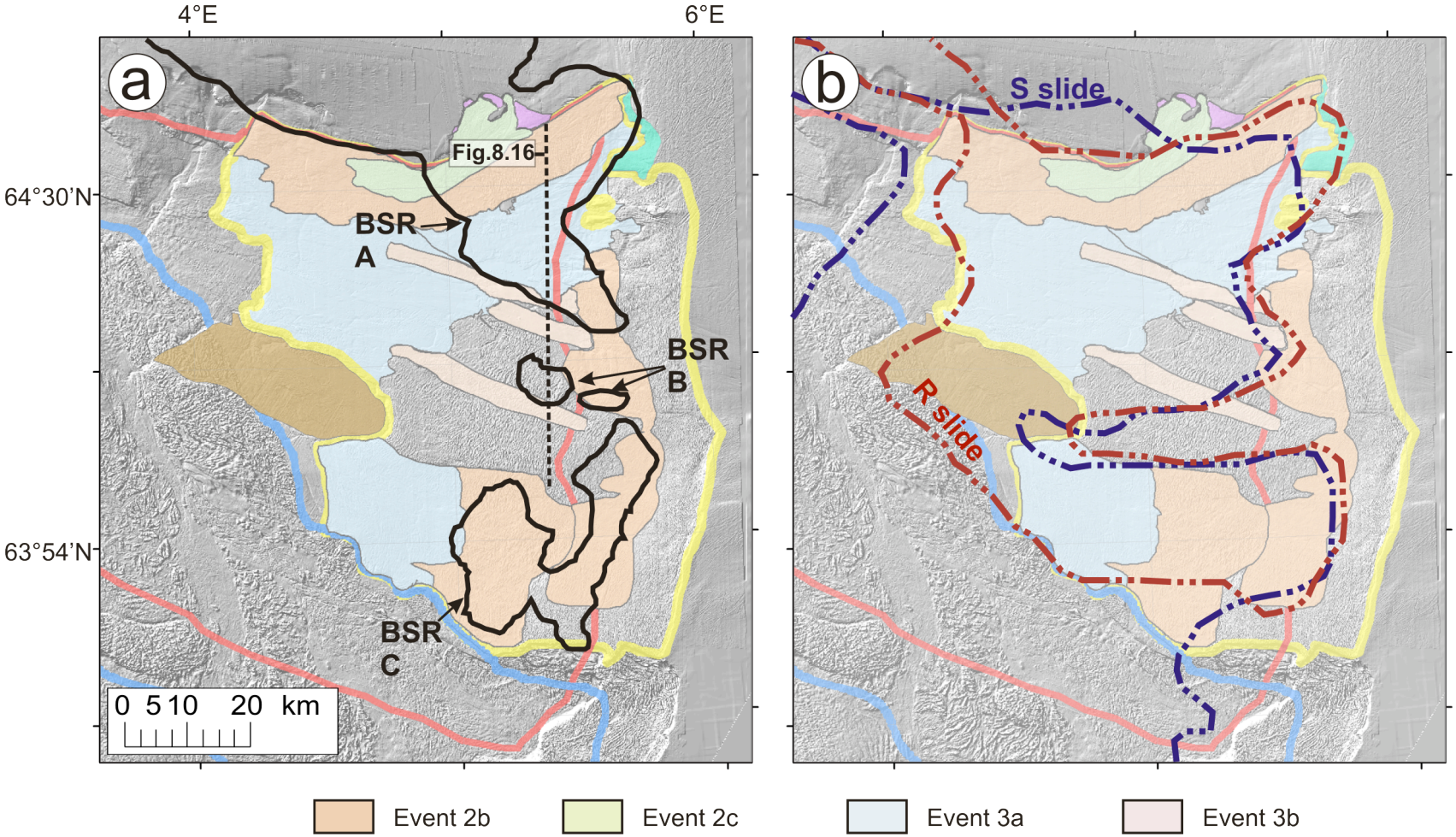

Figure 8.15: Overlay of (a) the gas hydrate BSR and (b) the R and S palaeoslides on the slide development map in Figure 8.14. (The BSR and palaeoslides' boundaries have been traced from *Bünz et al*. [2003] and *Solheim et al.* [2005a], respectively).

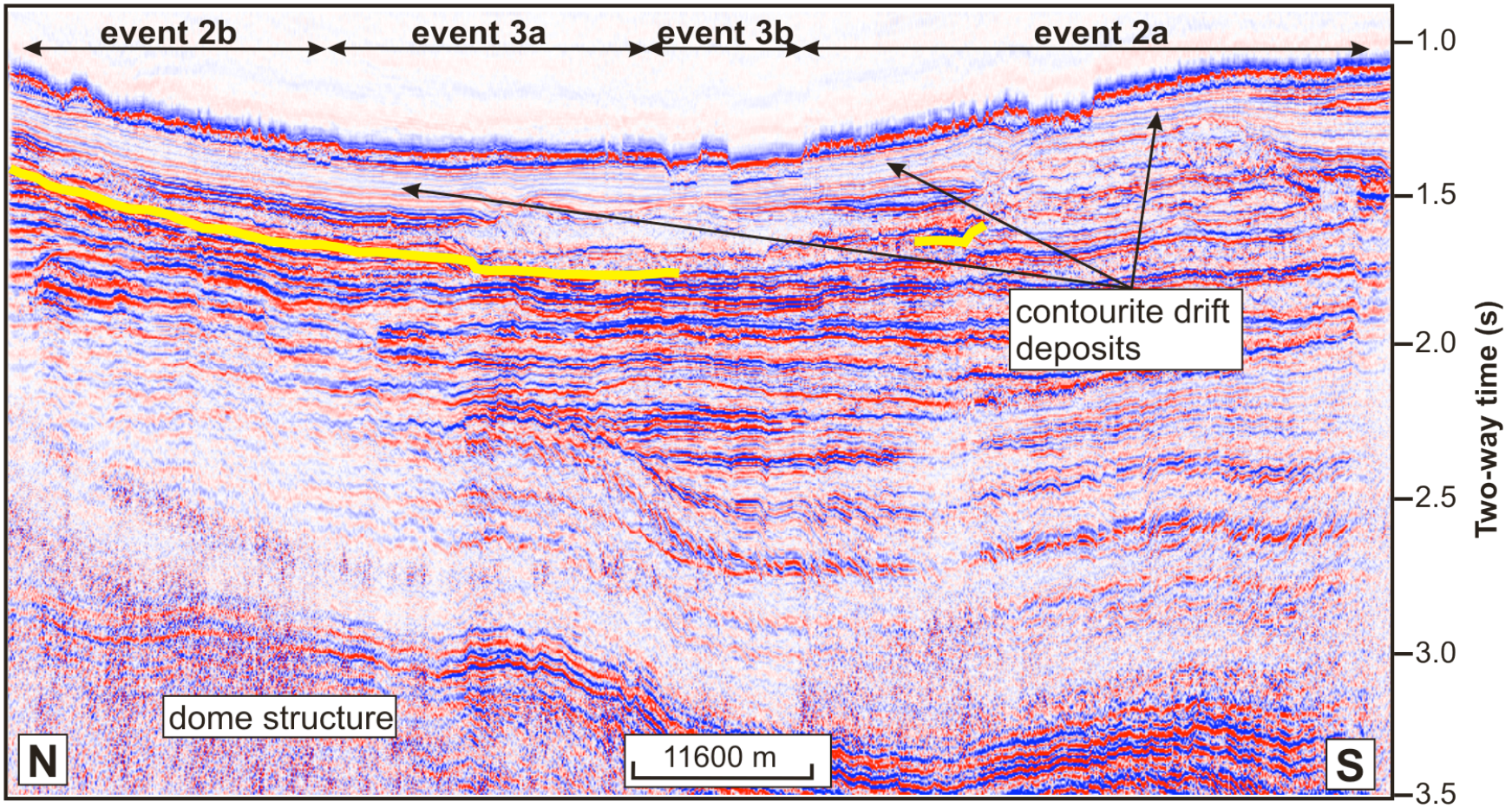

Figure 8.16: Seismic dip profile across the north-eastern Storegga Slide (location shown in Figure 8.15a). The thick yellow line indicates the gas hydrate BSR identified by *Bünz et al*. [2003] using seismic data of higher resolution than available for this study. Events 2a, 2b, 3a and 3b are all underlain by contourite drift deposits. However, only events 2b and 3a correlate well with the BSR underneath.

Chapter 9:

CONCLUSIONS

9.1 THE QUANTITATIVE GEOMORPHOLOGICAL APPROACH

Application of traditional geomorphometric techniques in the study of submarine landscapes is hindered by the spatial variability in bathymetric data resolution and the extensive scale over which changes in topography occur. A novel methodology has been proposed for the improved quantitative analysis of submarine elevation data by adapting numerical techniques, developed for subaerial analyses, to submarine environments. The method integrates three main morphometric techniques: (1) morphometric attributes and their statistical analyses, (2) feature-based quantitative representation, and (3) automated topographic classification. These techniques allow useful morphological information to be extracted from a digital elevation model. Morphometric attributes and their statistical analyses provide summary information about an area, which can be used to calibrate computer-generated geomorphometric maps. In these maps, the boundaries of geomorphological features are delineated, and they can thus be used as the basis for geomorphological interpretation. Ridge patterns and their morphological characteristics provide an accurate representation of specific aspects of terrain variability. Moment statistics are used as proxies of surface roughness to differentiate between surface types. ISODATA classification, carried out using ridge characteristics and moment statistics, reliably segments the surface into units of homogenous topography. A case study of debris flow lobes within the Storegga Slide shows that the techniques work robustly and that the new methodology integrating all the techniques can significantly enhance submarine geomorphological investigations based on visual interpretation.

The geomorphometric approach offers a number of benefits. The most important include: (1) a great spatial detail of analysis; (2) production of topographic information in quantitative format; (3) the generation of consistent and rapid results based on an established set of rules for landform delineation; (4) the possibility to use the techniques and results with other digital data sources, such as sidescan sonar imagery or 3D seismic data; (5) the potential to compare different landscapes. Furthermore, the techniques are simple to use and morphological information can be read directly from one map. All of these improve the morphological interpretation of bathymetric maps. In comparison, manual methods of interpretation are more time-consuming and subjective.

A few caveats do apply to the use of geomorphometric techniques in submarine environments. Knowledge of the study area is required to evaluate the reliability of the results and to choose terrain attributes. The techniques are also heavily dependent upon scale and data resolution. As topographic complexity and patterns partly change as a function of the scale of observation, the comparison of results obtained from different resolutions is problematic. Nevertheless, geomorphometric methods of feature extraction and landscape classification are promising techniques for submarine data evaluation. For the best results they should augment, rather than replace, manual methods of interpretation.

9.2 HOW DOES THE QUANTITATIVE GEOMORPHOLOGICAL APPROACH IMPROVE OUR UNDERSTANDING OF SUBMARINE MASS MOVEMENTS?

The geomorphometric technique was employed in the study of three aspects of submarine mass movements within the Storegga Slide: spreading, fractal statistics and morphology, and slide development. In this section I will explain how the technique was used and what the main results derived from each study were.

9.2.1 SPREADING

The study in Chapter 6 is the first thorough investigation of spreading in a submarine environment. Spreads are shown to cover at least 25% of the Storegga Slide scar area and they are concentrated close to the main headwall. The morphological signature of spreading is a repetitive pattern of parallel ridges and troughs that are oriented perpendicular to the direction of movement. This morphology occurs at a variety of scales: mean ridge length varies between 292 m and 397 m, mean trough depth ranges between 3.1 m and 10.5 m, and the mean ridge spacing varies between 213 m and 361 m. Two modes of failure can be identified within the Storegga Slide. The first involves retrogressive development via the unloading of the headwall and pore pressure development in the toe area due to strain softening. This mode of failure is observed in the Ormen Lange region and above the northern sidewall, where sediment is generally

thick, has low clay content and comprises a distinct stratigraphic boundary. In the second mode of failure, sediment behaves as a thin coherent slab of semi-consolidated material that is extended downslope by gravity and that has drag forces resisting the movement at the base. This type of spreading occurs in the remaining spreading zones along the main headwall, where sediment is thin, stratified and has high clay content. Both modes of failure involve the break up of the surface sediment units into coherent blocks. These blocks are displaced downslope along planar slip surfaces. Spreading is largely an extensional process; however, localised events of compression within the spread have resulted in pronounced ridges and troughs. Limit-equilibrium modelling indicates that loss of support and seismic loading are the main potential triggering mechanisms of spreading within the Storegga Slide. The extent of displacement of the spreading sediment is controlled by gravitationally-induced stress, angle of internal friction of the sediment, pore pressure escape and friction. The resulting block movement pattern in a spread entails an exponential increase of displacement, and thinning of the failing sediment, with distance downslope. The distal edge of the spread generally collapses over a headwall created by an earlier mass movement further downslope. At the upslope limit, the extension of the spread gradually declines to form a headwall. Ridge and trough morphological characteristics are representative of the extent of failure within a spread: with increasing distance from the headwall, trough depth increases, ridge length decreases, ridge spacing decreases and ridge density increases. The physical properties of the sediment also influence the ridge and trough morphology: as spreading occurs in progressively deeper, thicker and more consolidated sediment units, the ridges formed are longer, more widely spaced, and separated by deeper troughs. The extension associated with spreading is in the order of 10% of the original length of the sediment unit.

The ridge characterisation technique and geomorphometric mapping are the geomorphometric methods used in this study. They were employed to automatically map the distribution of ridge and trough morphology, to extract their morphological characteristics, to understand how these characteristics vary spatially and to estimate block displacement in a spread.

9.2.2 FRACTAL STATISTICS AND MORPHOLOGY

The study in Chapter 7 documents with field data the fractal characteristics of submarine mass movement statistics and morphology with the Storegga Slide. In this study, geomorphometric mapping is used to identify one hundred and fifteen mass movements from within the Storegga Slide scar and to extract morphological information about their headwalls. Analyses of this morphological information reveal the occurrence of spatial scale invariance within the Storegga Slide. Non-cumulative frequency-area distribution of mass movements within the Storegga Slide satisfies an inverse power law with an exponent of 1.63 for mass movements over 2 orders of magnitude. The headwalls exhibit geometric similarity at a wide range of scales and the lengths of headwalls scale with mass movement areas. Composite headwalls are self-similar for scales above the lengths of the constituent individual headwalls. One of the explanations of the observed spatial scale invariance in terms of mass movement areas is that the Storegga Slide is a geomorphological system that may exhibit self-organised criticality. In this system, the input of sediment is in the form of hemipelagic sedimentation and glacial deposition, and the output is represented by mass movements that are spatially scale invariant. In comparison to subaerial mass movements, the aggregate behaviour of the Storegga Slide mass movements is more comparable to that of the theoretical 'sandpile' model. The origin of spatial scale invariance may also be linked to the retrogressive nature of the Storegga Slide. The geometric similarity in headwall morphology suggests that the form and geological processes associated with submarine mass movements are similar at a wide range of scales. Headwall shape can be used as a proxy for the type of mass movement. This is important for the morphological classification of submarine mass movements, which can otherwise only be carried out with very high resolution acoustic data that are not commonly available. The fractal dimension of headwalls, on the other hand, indicates whether the headwall is formed by single or multiple mass movements.

9.2.3 SLIDE DEVELOPMENT

The north-eastern Storegga Slide has been shaped by a variety of submarine mass movements. These have been mapped in detail using morphometric attributes, geomorphometric mapping, ridge characterisation and ISODATA. We propose a development model of the north-eastern Storegga Slide consisting of four major events. The first event entailed the removal of the surface O1-O2 sediment sub-units by debris flows and turbidity currents when the Storegga Slide was triggered. Loading from this sediment resulted in the formation of an evacuation structure in the distal part of the study area. Loss of support from this structure, reactivation of the S headwall and seismic loading triggered extensive spreading in the O3 sediment sub-unit up to the main headwall. In some areas, spreading blocks have undergone higher displacement and remoulding. Parts of the spreading morphology and the underlying sediment sub-units elsewhere have been mobilised or removed by debris flows and turbidity currents. The higher displacement, remoulding and/or removal of the spreading morphology and the underlying sediments are attributed to two geological factors: (i) gas hydrate dissociation and pore pressure development, due to post-glacial ocean warming and a reduction in lithostatic pressure following the removal of the O1-O2 sediment sub-units in the first event, and (ii) the deposition of contourite drifts in palaoeslide scars.

9.3 IMPLICATIONS OF THE STUDY

9.3.1 GEOMORPHOMETRIC TECHNIQUE

There are two main implications associated with the methodology developed in this thesis. First, the increasing availability and accuracy of bathymetry data sets in digital format offers a unique opportunity to apply and improve the technique suggested in this thesis. Since geomorphometric techniques for submarine landscapes in general are not as well developed as those for subaerial environments, some of the problems associated with subaerial geomorphometry can be anticipated and circumvented. Secondly, although the geomorphometric technique has been developed for the study of submarine

landscapes, it is reasonable to assume that it performs equally well when applied to subaerial DEMs.

9.3.2 SPREADING

Submarine spreading has been largely overlooked because of the inability of acoustic data acquisition techniques to resolve its structure in sufficient detail. Recently acquired acoustic data sets demonstrate that the ridge and trough morphology, characteristic of spreading, can be observed in numerous slides around the world (Figure 6.1). The occurrence of spreading morphology in well-known submarine slides may lead to their re-examination and re-evaluation. This is particularly important in the case of the Storegga Slide, where spreading has not been mapped or considered when reconstructing the development stages of the Holocene slide [*Haflidason et al.*, 2004]. On the other hand, the occurrence of spreading does support the retrogressive development model that has been suggested for the Storegga Slide [*Bryn et al.*, 2005a]. Modern high-resolution data sets are expected to demonstrate that spreading is a significant and widespread style of mass movement in submarine landscapes, and that it has played an important role in the development of numerous submarine slide complexes. This is because the geological setting of the Storegga Slide, with distinct gently sloping failure planes that are parallel to the sedimentary bedding, is typical of many submarine landslides [*O'Leary*, 1991], particularly those located along the Norwegian margin [*Rise et al.*, 2005]. This factor, combined with the gentle slopes, and the uniformity of sediment properties and boundary conditions that are characteristic of continental slopes [*Shepard*, 1963], may result in spreading being more widespread in submarine landscapes than in subaerial settings. Submarine spreading should also be increasingly taken into consideration when interpreting seismic data, either to characterise palaeoslides or for petroleum exploration [e.g. *Solheim et al.*, 2005a].

Due to its distinct morphological signature and formative processes, spreading should be included as a type of mass movement in submarine mass movement classification schemes. In comparison to subaerial spreading, submarine spreading involves considerably larger displacements and the break up of the failing sediment unit into larger blocks. The morphology of submarine spreading is, however, similar to that of subaerial spreading, which means that the process dynamics may also be similar. The

modes of failure, controlling factors, and style of sediment displacement associated with submarine spreading and discussed in this thesis may thus be comparable to those of subaerial spreading.

Spreads tend to occur over relatively large regions and on gently sloping terrain that superficially would appear stable. With huge investments currently being made in deepwater oil and gas exploitation worldwide, the hazard posed by submarine spreading needs to be recognised and understood. Movement associated with spreading is not catastrophic as in debris flows; it is generally limited, in the range of hundreds of metres, which is sufficient to destroy seabed structures and disrupt pipelines. This is particularly important in regions such as Ormen Lange, where infrastructural work is taking place in terrain close to areas affected by spreading. The modelling and assessment of spreading as a geohazard is therefore very important.

9.3.3 FRACTAL STATISTICS AND MORPHOLOGY

There are several important implications that result from the study of the fractal statistics and morphology of the Storegga Slide.

The first relates to the design of systems to investigate and model submarine mass movements. Self-organised criticality is advocated as the most likely explanation of the observed power law in the frequency-area distribution of submarine mass movements within the Storegga Slide. The Storegga Slide may thus be modelled as a large-scale geomorphic system in a quasi-stationary state, and power law relations may be incorporated in the evolution modelling of this slide. Submarine mass movements are more comparable to the theoretical 'sandpile' model than their subaerial counterparts, and should therefore be simpler to model. Self-organised criticality is an emergent property that is not built into the physical equations a-priori [*Gupta*, 2004]. The ability of mass movement systems to create such ordered structures at large scales cannot be understood by a reductionist approach, which is at the basis of physical modelling. The aggregate behaviour of a large scale geomorphic system may be independent of the smaller-scale components, so that not all aspects of the submarine mass movement system can be reproduced by modelling the small-scale elements of the system, as

espoused by the engineering approach. This also means, however, that limitations in data acquisition techniques that do not have the adequate resolution can be circumvented when considering emergent features. The spatial scale invariant behaviour of mass movement morphology within the Storegga Slide contradicts the long-standing geographic tradition that geomorphic processes operate at specific spatial scales [*Schumm and Lichty*, 1965]. If mass movements are scale invariant, then the morphology and mechanisms of mass movements can be extrapolated from the small scale to the large scale (or vice versa). The occurrence of self-similarity and self-organised criticality in fluvial systems, for example, has been associated with the concept of minimum energy dissipation (minimum entropy production) [*Rigon et al.*, 1994; *Rinaldo et al.*, 1993]. Since energy is difficult to measure in a complex system such as the Storegga Slide, we can only hypothesise that fractal statistics, scale invariance and self-organised criticality are all emergent features of a geomorphological system that is minimising its energy. The retrogressive cascade, based on loss of support as the threshold exceeding mechanism in this open system, also explains the power law distribution of mass movements. It fits the self-organised critical behaviour well and emphasises the importance of considering the interconnectivity of individual slides. The evolution of a retrogressive cascade on a continental slope, where boundary conditions are generally homogeneous, would explain the large size of the Storegga Slide and similar submarine landslides elsewhere.

The second important implication is that our results also provide an explanation for the potential similarity in the shape of headwalls of submarine mass movements around the world. Spreading is a retrogressive mass movement [*Kvalstad et al.*, 2005a; *Masson et al.*, submitted]. Ridge and trough morphology, characteristic of spreading, can be observed in numerous submarine landslides around the world. In this study we observed that the cauliflower-shape of the Storegga Slide headwall is mainly associated with spreading, and that this shape is also common in submarine mass movements, particularly in formerly glaciated margins such as the Norwegian Margin. Analysis of landslides in the North Atlantic shows that mass movements mainly initiate in the mid-continental slope [*Hühnerbach and Masson*, 2004], and that they develop progressively upslope [*Kvalstad et al.*, 2005a]. If we combine these observations we can propose that the majority of submarine mass movements develop retrogressively, with spreading as the latest stage of the slide evolution that defines the main headwall. Since spreading

can be linked with the retrogressive cascade, self-organised critical behaviour could potentially be an emergent feature of numerous submarine mass movements throughout the world.

The third implication relates to mass movements as natural geohazards. Size-frequency plots of mass movements can be re-cast as probability distributions, providing a measure of the hazard risk posed by such slope failures [*Guzzetti et al.*, 2002]. By plotting the frequency-magnitude distribution of the mass movements we can estimate the event magnitude, along with the total number and area/volume of mass movements, and extrapolate incomplete inventories within the limits of power law behaviour (in the case of the Storegga Slide, for mass movements ranging between 1 – 100 km^2 in area). These considerations are particularly useful in tsunami hazard assessment, where knowledge of probabilities of the causative mass movement size is required [*ten Brink et al.*, 2006a]. Within the Storegga Slide, the larger mass movements are more dominant than in subaerial settings. This means that it is sufficient to obtain an accurate inventory of the larger mass movements in order to understand the frequency-magnitude characteristics of all the mass movements that comprise the Storegga Slide. In our acoustic data sets, as in those of other submarine landslides, the larger mass movements are generally well-resolved.

9.3.4 SLIDE DEVELOPMENT

Apart from attesting to the extensive spatial continuity of submarine mass movements and their potential to evolve between different types, the results in Chapter 8 demonstrate how the same sediment type can undergo failure in different ways. To determine the stability of a slope it is not enough to study its morphological, sedimentological and geotechnical characteristics, but it is also important to investigate its subsurface structures. This study also contributes evidence in support of gas hydrate dissociation as a preconditioning factor or trigger of submarine mass movements.

9.4 QUESTIONS FOR FURTHER STUDY

Potential research routes for the development of the geomorphometric technique and the study of submarine mass movements include the following:

9.4.1 GEOMORPHOMETRIC TECHNIQUE

- Continue improving and developing the geomorphometric technique, particularly for the extraction of specific landforms; test other methods that have not been addressed in this thesis.
- Apply the geomorphometric technique to high resolution data sets from other submarine landslides.
- Combine the geomorphometric technique with methods of side-scan sonar imagery classification.

9.4.2 SPREADING

- Collect detailed geotechnical data from spreading sites to improve the physical modelling of spreading, and potentially undertake empirical modelling to compare the results of the two types of models.
- Carry out detailed physical and finite modelling of the spreading process to consider factors such as tilting, distortion, plastic deformation and loss of excess pore pressure due to block fragmentation.
- Collect higher quality data from previously studied submarine landslides in order to look for spreading morphology.
- Investigate the role of seismic loading and liquefaction of the slip surface in the activation of spreading, because these triggers are very important in subaerial spreading.
- Identify which geological factors, amongst gravitationally-induced stress, angle of internal friction of the sediment, pore pressure escape and friction, controls the extent of spreading the most.

- Concentrate on the different scales of sediment break up within a spread (Figures 6.4b and 6.12) and the potential of fractal behaviour.
- Assess the potential of spreading to evolve into other mass movement types.

9.4.3 FRACTAL STATISTICS AND MORPHOLOGY

- Improve the data inventories of other submarine mass movements.
- Undertake an analysis of their frequency-size distribution and compare with results from the Storegga Slide.
- Constrain the temporal distribution of the Storegga submarine mass movements and test whether it exhibits power law behaviour; this could further corroborate the applicability of the self-organised criticality model to the Storegga Slide.
- Collect more information about the geology and structure of Storegga Slide to understand whether the power law distribution of mass movement areas is related to geological heterogeneity.
- Employ frequency-distribution analysis for hazard assessment within the Storegga Slide.
- Assess whether the planar and 3D shape of submarine mass movements also exhibit fractal characteristics.

9.4.4 SLIDE DEVELOPMENT

- Employ geomorphometric techniques to map and investigate the development of the rest of the Storegga Slide and the underlying palaeoslides.
- Investigate in more detail the role of gas hydrate dissociation as a preconditioning factor or trigger of submarine mass movements by: (i) modelling the potential of evacuation of the surface sediments (events 1a and 2a) to trigger gas hydrate dissociation, (ii) modelling the thermo-chemical dynamics of gas hydrate dissociation and (iii) constraining the boundary conditions that determine whether gas hydrate dissociation can trigger debris flows, turbidity currents or higher displacement/remoulding of spreading blocks.

APPENDIX

The control exerted by the parameters in the limit-equilibrium model on the extent of spreading.

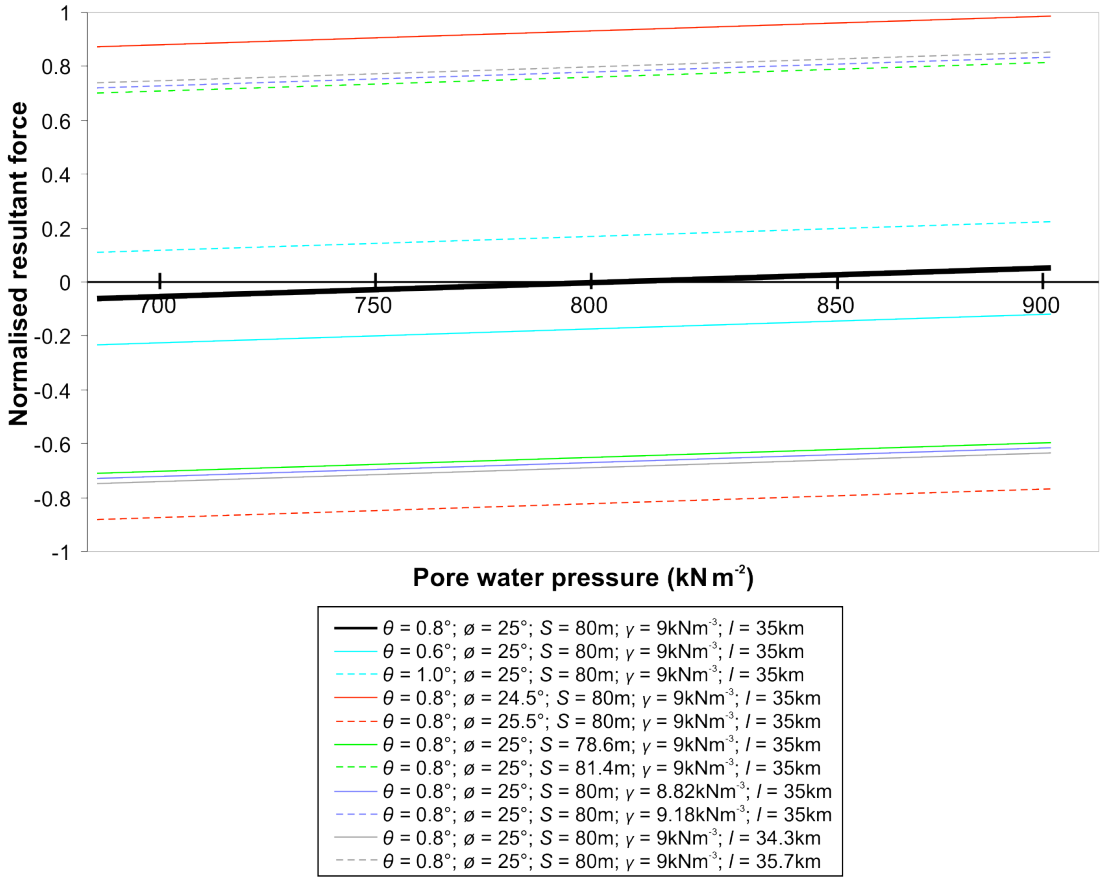

Figure a: Parameter space graph for the limit-equilibrium model in section 6.5.2.

θ slope gradient of slip surface, in °

W_T total weight of sediment upslope of a block = γSl, in N

γ submerged unit weight (in 2D), in N m^{-2}

S sediment unit thickness prior to failure, in m

l distance from a fixed point upslope, in m

$ø$ angle of internal friction, in °

u pore water pressure (in 2D), in N m^{-2}

P supporting force from slab downslope, in N

To understand which parameter exerts the major control on the extent of spreading (which depends on acceleration, and therefore on the resultant force acting on a block), a graph plotting the (normalised) resultant force with pore pressure was generated for different values of θ, $\varnothing$, S, γ and l (Figure a). In the graph, the value of each parameter is changed individually by ±2% of a constant value. The constant value selected for each parameter falls within the range of values used in the mechanical model in section 6.5.2 – III. W_T (γSl) and P in the limit-equilibrium model are intuitively considered the major controls of acceleration as the changes in these values along the slope are bound to be considerably larger than those of the other variables. This is also confirmed by the fact that changes in S, γ and l all result in large changes in the resultant force (Figure a) After W_T and P, S is the variable that results in the largest change in acceleration (Figure a). γ and $\varnothing$ come next, both having a similar degree of influence on the resultant force. Changes in θ have the least effect on the resultant force. A steeper slip surface is expected to impart greater static shear forces, which should result in greater block displacement. This correlation was verified in a model by *Yasuda et al.* [1992]. However, this model demonstrates the θ is not the principal determinant of the extent of block displacement. In fact, statistical studies of subaerial spreading in the field have shown a poor correlation between displacement magnitude and surface slope [*O'Rourke and Pease*, 1997]. Our result confirms that similarly, in submarine spreading, other factors than θ are more important in determining the extent of displacement.

REFERENCES

Adams, E. W., and W. Schlager (2000), Basic types of submarine slope curvature, *Journal of Sedimentary Research*, *70*, 814-828.

Adediran, A. O., I. Parcharidis, M. Poscolieri, and K. Pavlopoulos (2004), Computer-assisted discrimination of morphological units on north-central Crete (Greece) by applying multivariate statistics to local relief gradients, *Geomorphology*, *58*, 357-370.

Agterberg, F. P. (1984), Fractals, multifractals and change of support, in *Geostatistics for the Next Century*, edited by P. Dimitrakopoulos, Kluwer Academic Publishers, Dordrecht.

Aharonson, O., M. T. Zuber, and D. H. Rothman (2001), Statistics of Mars' topography from the Mars Orbiter Laser Altimeter: slopes, correlation and physical models, *Journal of Geophysical Research*, *106*, 23723-23735.

Andrle, R. (1992), Estimating fractal dimension with the divider method in geomorphology, *Geomorphology*, *5*, 131-141.

Angeles, G. R., G. M. E. Perillo, M. C. Piccolo, and J. O. Pierini (2004), Fractal analysis of tidal channels in the Bahía Blanca Estuary (Argentina), *Geomorphology*, *57*, 263-274.

Anhert, F. (1970), An approach towards a descriptive classification of slopes, *Zeitschrift für Geomorphologie N.F. Supplementband*, *9*, 70-84.

Assier-Rzadkiewicz, S., P. Heinrich, P. C. Sabatier, B. Savoye, and J. F. Bourillet (2000), Numerical modelling of a landslide-generated tsunami: The 1979 Nice event, *Pure and Applies Geophysics*, *157*, 1717-1727.

Atakan, K., and A. Ojeda (2005), Stress transfer in the Storegga area, offshore mid-Norway, *Marine and Petroleum Geology*, *22*, 161-170.

Atkinson, J., H. Jiskoot, R. Massari, and T. Murray (1998), Generalised linear modelling in geomorphology, *Earth Surface Processes and Landforms*, *23*, 1185-1195.

Atkinson, P. M., R. Webster, and P. J. Curran (1994), Cokriging with airborne mass imagery, *Remote Sensing of the Environment*, *50*, 335-345.

Aviles, C. A., C. H. Scholz, and J. Boatwright (1987), Fractal analysis applied to characteristic segments of the San Andrea Fault, *Journal of Geophysical Research*, *92*, 331-344.

Baas, A. C. W. (2002), Chaos, fractals and self-organization in coastal geomorphology: simulating dune landscapes in vegetated environments, *Geomorphology*, *48*, 309-328.

Bak, P., C. Tang, and K. Wiesenfield (1987), Self-organized criticality: An explanation of 1/*f* noise, *Physical Review Letters*, *59*, 381-384.

Bak, P., C. Tang, and K. Wiesenfield (1988), Self-organized criticality, *Physical Review A*, *38*, 364-374.

Bak, P. (1996), *How Nature Works: the Science of Self-Organized Criticality*, Copernicus, Springer, New York.

Band, L. E. (1986), Topographic partition of watersheds with digital elevation models, *Water Resources Research*, *22*, 15-24.

Bardet, J. P., N. Mace, and T. Tobita (1999), Liquefaction-induced ground deformation and failure.

Bartlett, S. F., and T. L. Youd (1992a), Empirical prediction of lateral spread displacement, 351-365 pp.

Bartlett, S. F., and T. L. Youd (1992b), Empirical analysis of horizontal ground displacement generated by liquefaction-induced lateral spreads, National Center for Earthquake Engineering Research, Buffalo, NY.

Bartlett, S. F., and T. L. Youd (1995), Empirical prediction of liquefaction-induced lateral spread, *Journal of Geotechnical Engineering*, *121*, 316-329.

Baxes, G. E. (1984), *Digital Image Processing: A Practical Primer*, Prentice-Hall, Englewood Cliffs.

Beauvais, A. A., and D. R. Montgomery (1997), Are channel networks statistically self-similar?, *Geology*, *25*, 1063-1066.

Benda, L., and T. Dunne (1997), Stochastic forcing of sediment supply to the channel network from landsliding and debris flow, *Water Resources Research*, *33*, 2849-2863.

Berg, K., A. Solheim, and P. Bryn (2005), The Pleistocene to recent geological development of the Ormen Lange area, *Marine and Petroleum Geology*, *22*, 45-56.

Berkson, J. M., and J. E. Matthews (1983), Statistical properties of seafloor roughness, in *Acoustics in the Sea-bed*, edited by N. G. Pace, pp. 215-223, Bath University Press, Bath.

Berndt, C., S. Planke, E. Alvestad, F. Tsikalas, and T. Rasmussen (2001), Seismic volcanostratigraphy of the Norwegian margin: Constraints on tectonomagmatic break-up processes, *Journal of the Geological Society*, *158*, 413-426.

Berndt, C., S. Bünz, and J. Mienert (2003), *Polygonal fault systems on the mid-Norwegian margin: A long term source for fluid flow*, 283-290 pp., Geological Society of London Special Publication.

Berndt, C., J. Mienert, M. Vanneste, and S. Bünz (2004), Gas hydrate dissociation and seafloor collapse in the wake of the Storegga Slide, Norway, in *Onshore-offshore relationships on the North Atlantic Margin, Norwegian Petroleum Society (NPF) Special Publication*, edited by B. T. G. Wandås, et al., pp. 285-292, Elsevier, Amsterdam.

Beven, K. J., and M. J. Kirkby (1979), A physically-based, contributing area model of basin hydrology, *Hydrological Sciences Bulletin*, *24*, 43-69.

Bezdek, J. C., R. Ehrlich, and W. Full (1984), FCM: The fuzzy *c*-means clustering algorithm, *Computers and Geosciences*, *10*, 191-203.

Bishop, M. P., J. F. Shroder Jr., B. L. Hickman, and L. Copland (1998), Scale-dependent analysis of satellite imagery for characterisation of glacier surfaces in the Karakoram Himalaya, *Geomorphology*, *21*, 217-232.

Blair, R. W. (1986), Regional landform analysis United States (NASA SP-486), in *Geomorphology from Space, a Global Overview of Regional Landforms*, edited by N. M. Short and R. W. Blair, pp. 1-22, Government Printing Office, Washington D.C.

Blondel, P., L. M. Parson, and V. Robigou (1998), TexAn: Textural analysis of sidescan sonar imagery and generic seafloor characterisation, paper presented at Oceans '98 IEEE/OES Conference Proceedings, Nice, France.

Bolongaro-Crevanna, A., V. T. Rodríguez, V. Sorani, D. Frame, and M. A. Ortiz (2004), Geomorphometric analysis for characterizing landforms in Morelos State, Mexico, *Geomorphology*, *67*, 407-422.

Bondevik, S., J. I. Svendsen, and J. Mangerud (1997), Tsunami sedimentary facies deposited by the Storegga tsunami in shallow marine basins and coastal lakes, western Norway, *Sedimentology*, *44*, 1115-1131.

Bondevik, S., F. Løvholt, C. Harbitz, J. Mangerud, A. G. Dawson, and J. I. Svendsen (2005), The Storegga Slide tsunami - comparing field observations with numerical simulations, *Marine and Petroleum Geology*, *22*, 195-208.

Booth, J. S., and D. W. O'Leary (1991), A statistical overview of mass movement characteristics on the North American Atlantic Outer Continental Margin, *Marine Geotechnology*, *10*, 1-18.

Boulanger, R. W., L. H. Mejia, and I. M. Idriss (1997), Liquefaction at Moss Landing during Loma Prieta Earthquake, *Journal of Geotechnical and Geoenvironmental Engineering*, *123*, 453-467.

Bouriak, S., M. Vanneste, and A. Saoutkine (2000), Inferred gas hydrates and clay diapirs near the Storegga Slide on the southern edge of the Vøring Plateau, offshore Norway, *Marine Geology*, *163*, 125-148.

Bouriak, S., A. Volkonskaia, and V. Galaktionov (2003), 'Split' strata-bounded gas hydrates BSR below deposits of the Storegga Slide and at the southern edge of the Vøring Plateau, *Marine Geology*, *195*, 301-318.

Brardinoni, F., and M. Church (2004), Representing the landslide magnitude-frequency relation: Capilano River Basin, British Columbia, *Earth Surface Processes and Landforms*, *29*, 115-124.

Brekke, H., and F. Riis (1987), Tectonics and basin evolution of the Norwegian shelf between 62 degrees N and 72 degrees N, *Norsk Geografisk Tidsskrift*, *67*.

Brekke, H. (2000), The tectonic evolution of the Norwegian Sea continental margin with emphasis on the Vøring and Møre basins, in *Dynamics of the Norwegian Margin*, edited by A. Nottvedt, pp. 327-378, Geological Society of London Special Publication.

Brown, H. E., W. S. Holbrook, M. J. Hornbach, and J. Nealon (2006), Slide structure and role of gas hydrate at the northern boundary of the Storegga slide, offshore Norway, *Marine Geology*, *229*, 179-186.

Bryn, P., A. Solheim, K. Berg, R. Lein, C. F. Forsberg, H. Haflidason, D. Ottesen, and L. Rise (2003), The Storegga Slide Complex: repeated large scale sliding in response to climatic cyclicity, in *Submarine Mass Movements and their Consequences*, edited by J. Locat and J. Mienert, pp. 215-222, Kluwer Academic Publishers, The Netherlands.

Bryn, P., K. Berg, C. F. Forberg, A. Solheim, and T. J. Kvalstad (2005a), Explaining the Storegga Slide, *Marine and Petroleum Geology*, *22*, 11-19.

Bryn, P., K. Berg, M. S. Stoker, H. Haflidason, and A. Solheim (2005b), Contourites and their relevance for mass wasting along the Mid-Norwegian Margin, *Marine and Petroleum Geology*, *22*, 85-96.

Bugge, T. (1983), Submarine slides on the Norwegian continental margin with special emphasis on the Storegga area, Technical University, Trondheim.

Bugge, T., S. Befring, R. H. Belderson, T. Eidvin, E. Jansen, N. H. Kenyon, H. Holtedahl, and H. P. Sejrup (1987), A giant three-stage submarine slide off Norway, *Geo-Marine Letters*, *7*, 191-198.

Bugge, T., R. H. Belderson, and N. H. Kenyon (1988), The Storegga Slide, *Philosophical Transaction of the Royal Society of London*, *325*, 357-388.

Buma, J., and T. van Asch (1996), Soil (debris) spreading, in *Landslide Recognition: Identification, Movement and Courses*, edited by R. Dikau, et al., pp. 137-148, John Wiley and Sons, Chichester.

Bungum, H., C. Lindholm, and J. I. Faleide (2005), Postglacial seismicity offshore mid-Norway with emphasis on spatio-temporal-magnitudal variations, *Marine and Petroleum Geology*, *22*, 137-148.

Bünz, S., J. Mienert, and C. Berndt (2003), Geological controls on the Storegga gas hydrate system of the mid-Norwegian continental margin, *Earth and Planetary Science Letters*, *209*, 291-307.

Bünz, S., and J. Mienert (2004), Acoustic imaging of gas hydrate and free gas at the Storegga Slide, *Journal of Geophysical Research*, *109*, B04102.

Bünz, S., J. Mienert, P. Bryn, and K. Berg (2005), Fluid flow impact on slope failure from 3D seismic data: A case study in the Storegga Slide, *Basin Research*, *17*, 109-122.

Burrough, P. A. (1981), Fractal dimensions of landscapes and other environmental data, *Nature*, *294*, 240-242.

Burrough, P. A., and R. A. McDonald (1998), *Principles of Geographical Information Systems*, Oxford University Press, Oxford.

Canals, M., G. Lastras, R. Urgeles, J. L. Casamor, J. Mienert, A. Cattaneo, M. De Batist, H. Haflidason, Y. Imbo, J. S. Laberg, J. Locat, D. Long, O. Longva, D. G. Masson, N. Sultan, F. Trincardi, and P. Bryn (2004), Slope failure dynamics and

impacts from seafloor and shallow sub-seafloor geophysical data: case studies from the COSTA project, *Marine Geology*, *213*, 9-72.

Carmichael, D. R., L. M. Linnett, S. J. Clarke, and B. R. Calder (1996), Seabed classification through multifractal analysis of sidescan sonar imagery, *IEE Proceedings - Radar and Sonar Navigation*, *143*, 140-148.

Carrara, A., E. Pugliese-Carratelli, and L. Merenda (1977), Computer based data banks and statistical analysis for slope instability phenomena, *Zeitschrift für Geomorphologie N.F.*, *21*, 187-222.

Casas, A. M., A. L. Cortés, A. Maestro, M. A. Soriano, A. Riaguas, and J. Bernal (2000), LINDENS: a program for lineament length and density analysis, *Computers and Geosciences*, *26*, 1011-1022.

Cayley, A. (1859), On contour and slope lines, *The London, Edinburgh, and Dublin Philosophical Magazine and Journal of Science*, *XVIII*, 264-268.

Cetin, K. O., T. L. Youd, R. B. Seed, J. D. Bray, J. P. Stewart, H. T. Durgunoglu, W. Lettis, and M. T. Yilmaz (2004), Liquefaction-induced lateral spreading at Izmit Bay during the Kocaeli (Izmit)-Turkey earthquake, *Journal of Geotechnical and Geoenvironmental Engineering*, *12*, 1300-1313.

Chakraborty, B., H. W. Schenke, V. Kodagali, and R. Hagen (2001), Analysis of multibeam-Hydrosweep echo peaks for seabed characterisation, *Geo-Marine Letters*, *20*, 174-181.

Chang, Y. C., G. S. Song, and S. K. Hsu (1998), Automatic extraction of ridge and valley axes using the profile recognition and polygon-breaking algorithm, *Computers and Geosciences*, *24*, 83-93.

Chappell, A. (1996), Modelling the spatial variation of processes in the redistribution of soil: Digital terrain models and ^{137}Cs in southwest Niger *Geomorphology*, *17*, 249-261.

Chappell, A., G. Heritage, I. C. Fuller, A. R. G. Large, and D. Milan (2003), Geostatistical analysis of ground-survey elevation data to elucidate spatial and temporal river channel change, *Earth Surface Processes and Landforms*, *28*, 349-370.

Chase, C. G. (1992), Fluvial landsculpting and the fractal dimension of topography, *Geomorphology*, *5*, 39-57.

Cheng, Q. (1999), Multifractality and spatial statistics, *Computers and Geosciences*, *25*, 949-961.

Cheng, Y. C., P. J. Lee, and T. Y. Lee (1999), Self-similarity dimensions of the Taiwan Island landscape, *Computers and Geosciences*, *25*, 1043-1050.

Chien-Yuan, C., Y. F. Chieh, L. Sheng-Chi, and C. Kei-Wai (2007), Discussion of landslide self-organized criticality and the initiation of debris flow, *Earth Surface Processes and Landforms*, *32*, 197-209.

Chorley, R. J., and H. A. Pogorzelsi (1957), A new standard for estimating drainage basin shape, *American Journal of Science*, *255*, 138-141.

Chorowicz, J., Y. J. Kim, S. Manoussis, J. P. Rudant, P. Foin, and Y. Veillet (1989), A new technique for recognition of geological and geomorphological patterns in Digital Terrain Models, *Remote Sensing of the Environment*, *29*, 229-239.

Chorowicz, J., C. Ichoko, S. Riazanoff, and Y. J. Kim (1992), A combined algorithm for automated drainage network extraction, *Water Resources Research*, *28*, 1293-1302.

Chu, B. L., S. C. Hsu, and Y. M. Chang (2003), Ground behavior and liquefaction analyses in central Taiwan-Wufeng, *Engineering Geology*, *71*, 113-139.

Clouard, V., and A. Bonneville (2001), A giant landslide on the southern flank of Tahiti Island, French Polynesia, *Geophysical Research Letters*, *29*, 2253-2256.

Collins, S. H. (1975), Terrain parameters directly from a digital terrain model, *Canadian Surveyor*, *29*, 507-518.

Conti, S., and G. Tosatti (1994), Caratteristiche geologico-strutturali della Pietra di Bismantova e fenomeni franosi connessi (Appennino reggiano), *Quaderni di Geologia Applicata*, *1*, 31-49.

Corominas, J., J. Remondo, P. Farias, M. Estevao, J. Zézere, d. T. Díaz, J., R. Dikau, L. Schrott, J. Moya, and A. Gonzáles (1996), Debris flows, in *Landslide Recognition: Identification, Movement and Causes*, edited by R. Dikau, et al., pp. 161-180, John Wiley and Sons, Chichester.

Cox, B. L., and J. S. Y. Wang (1993), Fractal surfaces: measurement and applications in the Earth Sciences, *Fractals*, *1*, 87-115.

Cross, A. M. (1999), Detection of circular geological features using the Hough transform, *International Journal of Remote Sensing*, *9*, 1519-1528.

Crosta, G. (1996), Landslide, spreading, deep-seated gravitation deformation: analysis, examples, problems and proposal, *Geografia Fisica e Dinamica Quaternaria*, *19*.

Cruden, D. M., and D. J. Varnes (1996), *Landslides types and processes*, 36-75 pp., Transport Research Board, National Academy of Sciences, Washington D.C.

Curtis, L. F., J. C. Doornkamp, and K. J. Gregory (1965), The description of relief in field studies of soils, *Journal of Soil Science*, *16*, 16-30.

Dahlgren, K. I. T., T. O. Vorren, and J. S. Laberg (2002), Late Quaternary glacial development of the mid-Norwegian margin - 65 to 68°N, *Marine and Petroleum Geology*, *19*, 1089-1113.

Dai, F. C., and C. F. Lee (2002), Landslide characteristics and slope instability modeling using GIS, Lantau Island, Hong Kong, *Geomorphology*, *42*, 213-228.

Dawson, A. G., D. Long, and D. E. Smith (1988), The Storegga Slides: evidence from Eastern Scotland for a possible Tsunami, *Marine Geology*, *82*, 271-276.

De Blasio, F. V., D. Issler, A. Elverhøi, C. B. Harbitz, T. Ilstad, P. Bryn, R. Lien, and F. Løholt (2003), Dynamics, velocity and run-out of the Giant Storegga Slide, *Geophysical Research Abstracts*, *5*, 223-230.

De Blasio, F. V., A. Elverhøi, D. Issler, C. B. Harbitz, P. Bryn, and R. Lien (2004), Flow models of natural debris flows originating from overconsolidated clay materials, *Marine Geology*, *213*, 439-455.

De Blasio, F. V., A. Elverhøi, D. Issler, C. B. Harbitz, P. Bryn, and R. Lien (2005), On the dynamics of subaqueous clay rich gravity mass flows - the giant Storegga slide, *Marine and Petroleum Geology*, *22*, 179-186.

De Moustier, C., and H. Matsumoto (1993), Seafloor acoustic remote sensing with multibeam echo-sounders and bathymetric sidescan sonar system, *Marine Geophysical Researches*, *15*, 27-42.

DeBoer, D. (1992), Hierarchies and scale in process geomorphology: A review, *Geomorphology*, *4*, 303-318.

Dehn, M., H. Gärtner, and R. Dikau (2001), Principles of semantic modelling of landform structures, *Computers and Geosciences*, *27*, 1005-1010.

Dikau, R. (1994), Computergestützte Geomorphographie und ihre Anwendung in der Regionalisierung des Reliefs, *Petermanns Georaphische Mitteilungen*, *138*, 99-114.

Dikau, R., D. Brunsden, L. Schrott, and M. L. Ibsen (Eds.) (1996), *Landslide Recognition: Identification, Movement and Causes*, John Wiley and Sons, Chichester.

Dimakis, P., A. Elverhøi, K. Høeg, A. Solheim, C. Harbitz, J. S. Laberg, T. Vorren, and J. Marr (2000), Submarine slope stability on high-latitude glaciated Svalbard-Barents Sea margin, *Marine Geology*, *162*, 303-316.

Dobry, R., and M. H. Baziar (1992), Modeling of lateral spreads in silty sands by sliding soil blocks, paper presented at A Speciality Conference on Stability and Performance of Slopes and Embankments, University of California, Berkeley.

Dodds, P. S., and D. H. Rothman (2000), Scaling, universality and geomorphology, *Annual Review of Earth and Planetary Sciences*, *28*, 571-610.

Doi, M., and M. Hamada (1992), A summary of case studies on liquefaction-induced ground displacements, 115-129 pp.

Dowdeswell, J. A., N. H. Kenyon, A. Elverhøi, J. S. Laberg, F. J. Hollender, J. Mienert, and M. J. Siegert (1996), Large-scale sedimentation on the glacier-influenced Polar North Atlantic margins: Long-range side-scan sonar images, *Geophysical Research Letters*, *23*, 3535-3538.

Drăgut, L., and T. Blaschke (2006), Automated classification of landform elements using object-based image analysis, *Geomorphology*, *81*, 330-344.

Duda, R. O., and P. E. Hart (1973), *Pattern Recognition and Scene Analysis*, John Wiley, New York.

Dussauge, C., J. R. Grasso, and A. Helmstetter (2003), Statistical analysis of rockfall volume distributions: Implications for rockfall dynamics, *Journal of Geophysical Research*, *108(B6)*, 2286.

Dymond, J. R., C. Derose, and G. R. Harmsworth (1995), Automated mapping of land components from digital elevation data, *Earth Surface Processes and Landforms*, *20*, 131-137.

Etzelmüller, B., and J. R. Sulebak (2000), Development in the use of digital elevation models in periglacial geomorphology and glaciology, *Physische Geographie*, *41*, 35-58.

Evans, D., E. L. King, N. H. Kenyon, C. Brett, and D. Wallis (1996), Evidence for long-term instability in the Storegga Slide region off western Norway, *Marine Geology*, *130*, 281-292.

Evans, D., S. McGiveron, Z. Harrison, P. Bryn, and K. Berg (2002), Along-slope variation in the late Neogene evolution of the mid-Norwegian margin in response to uplift and tectonism, in *Exhumation of the North Atlantic Margin: Timing, Mechanisms and Implications for Petroleum Exploration*, edited by A. G. Doré, et al., pp. 139-151, Geological Society Special Publications, London.

Evans, D., Z. Harrison, P. M. Shannon, J. S. Laberg, T. Nielsen, S. Ayers, R. Holmes, R. J. Hoult, B. Lindberg, H. Haflidason, D. Long, A. Kuijpers, E. S. Andersen, and P. Bryn (2005), Palaeoslides and other mass failures of Pliocene to Pleistocene age along the glaciated European margin, *Marine and Petroleum Geology*, *22*, 1131-1148.

Evans, I. S. (1972), General geomorphometry, derivatives of altitude and descriptive statistics, in *Spatial Analysis in Geomorphology*, edited by R. J. Chorley, pp. 17-90, Harper and Row, New York.

Evans, I. S. (1975), The effect of resolution on gradients calculated from an altitude matrix, 24 pp, Department of Geography, University of Durham, Durham.

Evans, I. S. (1977), The selection of class intervals, *Transactions of the Institute of British Geographers NS*, *2*, 98-124.

Evans, I. S. (1979), An integrated system of terrain analysis and slope mapping, University of Durham, Durham.

Evans, I. S. (1980), An integrated system of terrain analysis and slope mapping, *Zeitschrift für Geomorphologie N.F. Supplementband*, *36*, 274-295.

Evans, I. S. (1984), Correlation structures and factor analysis in the investigation of data dimensionality: statistical properties of the Wessex land surface, England, paper presented at Proceedings, International Symposium on Spatial Data Handling '84, Geogr. Inst. Universitat Zürich-Irchel, Zurich, Switzerland.

Evans, I. S. (1990), General geomorphometry, in *Geomorphological Techniques*, edited by A. S. Goudie, et al., pp. 44-56, Routeledge, London.

Evans, I. S. (1998), What do terrain statistics really mean?, in *Landform Monitoring, Modelling and Analysis*, edited by S. N. Lane, et al., pp. 119-138, John Wiley and Sons, Chichester.

Everts, C. J. G., and B. B. Mandelbrot (1992), Multifractal measures, Appendix B, in *Chaos and Fractals*, edited by H. O. Peitgen, et al., pp. 922-953, Springer Verlag, New York.

Fairfield, J., and P. Leymarie (1991), Drainage networks from grid digital elevation models, *Water Resources Research*, *27*, 709-717.

Fenneman, N. (1931), *Physiography of Western United States*, McGraw-Hill, New York.

Fiegel, G. L., and B. L. Kutter (1994), Liquefaction mechanism for layered soils, *Journal of Geotechnical Engineering*, *120*, 737-755.

Field, M. E., J. V. Gardner, A. E. Jennings, and B. D. Edwards (1982), Earthquake-induced sediment failures on a 0.25º slope, Klamath River delta, California, *Geology*, *10*, 542-546.

Field, M. E., and R. K. Hall (1982), Sonographs of submarine sediment failure caused by the 1980 earthquake off northern California, *Geo-Marine Letters*, *2*, 135-141.

Finn, W. D. L., R. H. Ledbetter, and G. Wu (1994), Liquefaction in silty soils: Design and analysis, in *Ground Failures Under Seismic Conditions, Géotechnique Special Publication No. 44*, edited by S. Prakash and P. Dakoulas, pp. 51-76.

Florinsky, I. (1996), Quantitative topographic method of fault morphology recognition, *Geomorphology*, *16*, 103-119.

Florinsky, I. V. (1998), Combined analysis of digital terrain models and remotely sensed data in landscape investigations, *Progress in Physical Geography*, *22*, 33-60.

Forsberg, C. F., and J. Locat (2005), Mineralogical and microstructural development of the sediments on the Mid-Norwegian margin, *Marine and Petroleum Geology*, *22*, 109-122.

Fox, C. G., and D. E. Hayes (1985), Quantitative methods for analyzing the roughness of the seafloor, *Reviews of Geophysics*, *23*, 1-48.

Fox, C. G. (1996), Objective classification of oceanic ridge-crest terrains using two-dimensional spectral models of bathymetry: Application to the Juan de Fuca Ridge, *Marine Geophysical Researches*, *18*, 707-728.

Fuyii, Y. (1969), Frequency distribution of the magnitude of landslides caused by heavy rainfall, *Journal of the Seismological Society of Japan*, *22*, 244-247.

Gao, J., and Z. G. Xia (1996), Fractals in physical geography, *Progress in Physical Geography*, *20*, 178-191.

Gardiner, V., and R. Dackombe (1983), *Geomorphological Field Manual*, Allen and Unwin, London.

Gardner, T. W., K. C. Sasowksy, and R. L. Day (1990), Automated extraction of geomorphometric properties from digital elevation data, *Zeitschrift für Geomorphologie N.F. Supplementband*, *80*, 57-68.

Gauer, P., T. J. Kvalstad, C. F. Forsberg, P. Bryn, and K. Berg (2005), The last phase of the Storegga Slide: Simulation of retrogressive slide dynamics and comparison with slide-scar morphology, *Marine and Petroleum Geology*, *22*, 171-178.

Gay, A., and C. Berndt (2007), Cessation/reactivation of polygonal faulting and effects on fluid flow in the Vøring Basin, Norwegian Margin, *Journal of the Geological Society, London*, *164*, 129-141.

Gee, M. J. R., A. B. Watts, D. G. Masson, and N. C. Mitchell (2001), Landslides and the evolution of El Hierro in the Canary Islands, *Marine Geology*, *177*, 271-293.

Gelabert, B., J. J. Fornós, J. E. Pardo, V. M. Rosselló, and F. Segura (2005), Structurally controlled drainage basin development in the south of Menorca (Western Mediterranean, Spain), *Geomorphology*, *65*, 139-155.

Gilbert, L. (1989), Are topographic data sets fractal, *Pure and Applies Geophysics*, *131*, 241-254.

Gilbert, L. E., and A. Malinverno (1988), A characterization of the spectral density of residual ocean floor topography, *Geophysical Research Letters*, *15*, 1401-1404.

Giles, P. T. (1998), Geomorphological signatures: classification of aggregated slope unit objects from digital elevation and remote sensing data, *Earth Surface Processes and Landforms*, *23*, 581-594.

Giles, P. T., and S. E. Franklin (1998), An automated approach to the classification of the slope units using digital data, *Geomorphology*, *21*, 251-264.

Goff, J. A., and T. H. Jordan (1988), Stochastic modelling of seafloor morphology: Inversion of Sea Beam data for second-order statistics, *Journal of Geophysical Research*, *93*, 13589-13608.

Goff, J. A., A. G. Jordan, M. H. Edwards, and D. J. Fornari (1991), Comparison of a stochastic seafloor model with SeaMARC II bathymetry and Sea Beam data near the East Pacific Rise 13° - 15° N, *Journal of Geophysical Research*, *96*, 3867-3885.

Goff, J. A., and B. E. Tucholke (1997), Multiscale spectral analysis of bathymetry on the flank of the Mid-Atlantic Ridge: Modification of the seafloor by mass wasting and sedimentation, *Journal of Geophysical Research*, *102*, 15447-15462.

Gonzáles, J., M. Schmitz, F. Audemard, R. Contreras, A. Mocquet, J. Delgado, and F. De Santis (2004), Site effects of the 1997 Cariaco, Venezuela earthquake, *Engineering Geology*, *72*, 143-177.

Goodchild, M. F. (1982), The fractional Brownian process as a terrain simulation model, *Modelling and Simulation*, *13*, 1133-1137.

Goodchild, M. F., and D. M. Mark (1987), The fractal nature of geographic phenomena, *Annals of the Association of American Geographers*, *77*, 265-278.

Gracia, E., J. J. Dañobeita, and PARSIFAL Team (2003), Mapping active faults offshore Portugal (36°N-38°N): Implications for seismic hazard assessment along the southwest Iberian margin, *Geology*, *31*, 83-86.

Graff, L. H., and E. L. Usery (1993), Automated classification of generic terrain features in digital elevation models, *Photogrammetric Engineering and Remote Sensing*, *59*, 1409-1417.

Greeley, R. (1994), *Planetary Landscapes*, 286 pp., Chapman and Hall, New York.

Gudmundsson, A. (1999), Postglacial crustal doming, stresses and fracture formation with application to Norway, *Tectonophysics*, *307*, 407-419.

Gupta, V. K. (2004), Emergence of statistical scaling in floods on channel networks from complex runoff dynamics, *Chaos, Solitons and Fractals*, *19*, 357-365.

Gutenberg, B., and C. F. Richter (1954), *Seismicity of the Earth and Associated Phenomena*, 2nd. ed., Princeton University Press, Princeton.

Guth, P. L. (2003), Eigenvector analysis of Digital Elevation Models in a GIS: Geomorphometry and Quality Control, in *Concepts and Modelling in Geomorphology: International Perspectives*, edited by I. S. Evans, et al., pp. 199-220, TERRAPUB, Tokyo.

Guthrie, R. H., and S. G. Evans (2004), Analysis of landslide frequencies and characteristics in a natural systems, coastal British Columbia, *Earth Surface Processes and Landforms*, *23*, 1321-1339.

Guthrie, R. H., and S. G. Evans (2007), Work, persistence, and formative events: The geomorphic impact of landslides, *Geomorphology*, *88*, 266-275.

Guzzetti, F., B. D. Malamud, D. L. Turcotte, and P. Reichenbach (2002), Power-law correlations of landslide areas in central Italy, *Earth and Planetary Science Letters*, *195*, 169-183.

Guzzetti, F., P. Reichenbach, M. Cardinali, M. Galli, and F. Ardizzone (2005), Probabilistic landslide hazard assessment at the basin scale, *Geomorphology*, *72*, 272-299.

Haflidason, H., A. Gravdal, and H. P. Sejrup (2003), The Northern Storegga Slide Escarpment - Morphology and Features, in *European Margin Sediment Dynamics: Side-scan Sonar and Seismic Images*, edited by J. Mienert and P. Weaver, pp. 45-53, Springer, London.

Haflidason, H., H. P. Sejrup, A. Nygård, P. Bryn, R. Lien, C. F. Forsberg, K. Berg, and D. G. Masson (2004), The Storegga Slide: Architecture, geometry and slide-development, *Marine Geology*, *231*, 201-234.

Haflidason, H., R. Lien, H. P. Sejrup, C. F. Forsberg, and P. Bryn (2005), The dating and morphometry of the Storegga Slide, *Marine and Petroleum Geology*, *22*, 123-136.

Hall, D. J., and D. Khanna (1977), *Statistical Methods for Digital Computers*, Wiley, New York.

Hamada, M., S. Yasuda, R. Isoyama, and K. Emoto (1986), Study on liquefaction induced permanent ground displacements, 87 pp.

Hamada, M., I. Towhata, S. Yasuda, and R. Isoyama (1987), Study on permanent ground displacement induced by seismic liquefaction, *Computers and Geotechnics*, *4*, 197-220.

Hamada, M. (1999), Similitude law for liquefied-ground flow, paper presented at 7th U.S.-Japan Workshop on Earthquake Resistant Design of Lifeline Facilities and Countermeasures Against Soil Liquefaction.

Hampton, M. A., H. J. Lee, and J. Locat (1996), Submarine landslides, *Reviews of Geophysics*, *34*, 33-59.

Haralick, R. M. (1983), Ridges and valleys on digital images, *Computer Vision Graphics Image Processing*, *22*, 28-38.

Harbitz, C. B. (1992), Model simulations of tsunamis generated by the Storegga Slides, *Marine Geology*, *105*, 1-21.

Hergarten, S., and H. J. Neugebauer (1998), Self-organized criticality in a landslide model, *Geophysical Research Letters*, *25*, 801-804.

Hergarten, S. (2003), Landslides, sandpiles and self-organised criticality, *Natural Hazards and Earth System Sciences*, *3*, 505-514.

Herzfeld, U. C. (1989), Geostatistical methods for evaluation of seabeam bathymetric surveys: Case studies of Wegener Canyon, Antarctica, *Marine Geology*, *88*, 83-95.

Herzfeld, U. C., I. I. Kim, and J. A. Orcutt (1995), Is the ocean floor a fractal?, *Mathematical Geology*, *27*, 421-462.

Herzfeld, U. C., and C. A. Higginson (1996), Automated geostatistical seafloor classification - principles, parameters, feature vectors and discrimination criteria, *Computers and Geosciences*, *22*, 35-52.

Herzfeld, U. C., and C. Overbeck (1999), Analysis and simulation of scale-dependent fractal surfaces with application to seafloor morphology, *Computers and Geosciences*, *25*, 979-1007.

Hjelstuen, B. O., H. P. Sejrup, H. Haflidason, A. Nygård, I. M. Berstad, and G. Knorr (2004), Late Quaternary seismic stratigraphy and geological development of the south Vøring margin, Norwegian Sea, *Quaternary Science Reviews*, *23*, 1847-1865.

Hjelstuen, B. O., H. P. Sejrup, H. Haflidason, A. Nygård, S. Ceramicola, and P. Bryn (2005), Late Cenozoic glacial history and evolution of the Storegga Slide area and adjacent slide flank regions, Norwegian continental margin, *Marine and Petroleum Geology*, *22*, 57-69.

Holzer, T. L., T. E. Noce, M. J. Bennett, C. Di Alessandro, J. Boatwright, J. C. Tinsley, R. W. Sell, and L. I. Rosenberg (2004), Liquefaction-Induced Lateral Spreading in Oceano, California, during the 2003 San Simeon Earthquake, 51 pp, U.S. Geological Survey.

Horton, R. E. (1945), Erosional development of streams and their drainage basins: Hydrophysical approach to quantitative morphology, *Bulletin of the Geological Society of America*, *56*, 275-370.

Hovius, N., C. P. Stark, and P. A. Allen (1997), Sediment flux from a mountain belt derived by landslide mapping, *Geology*, *25*, 231-234.

Hovius, N., C. P. Stark, C. Hao-Tsu, and L. Jiun-Chuan (2000), Supply and removal of sediment in a landslide-dominated mountain belt: Central Range, Taiwan, *The Journal of Geology*, *108*, 73-89.

Huang, C. P., L. F. Chaparro, and L. E. Vallejo (1997), Fractal dimension of profiles and surfaces using fuzzy morphological coverings, *Engineering Geology*, *48*, 245-253.

Huang, J., and D. L. Turcotte (1989), Fractal mapping of digitized images: Application to the topography of digitized images, *Journal of Geophysical Research*, *94*, 7491-7495.

Hühnerbach, V., and D. G. Masson (2004), Landslides in the North Atlantic and its adjacent seas: an analysis of their morphology, setting and behaviour, *Marine Geology*, *213*, 343-362.

Hungr, O., S. G. Evans, and J. Hazzard (1999), Magnitude and frequency of rock falls and rock slides along the main transportation corridors of southwestern British Columbia, *Canadian Geotechnical Journal*, *36*, 224-238.

Hutchinson, M. F., and J. C. Gallant (2000), Digital elevation models and representation of terrain shape, in *Terrain Analysis: Principles and Applications*, edited by J. P. Wilson and J. C. Gallant, pp. 29-49, Wiley, New York.

Hutchinson, N. J. (1988), General report: morphological and geotechnical parameters of landslides in relation to geology and hydrogeology, paper presented at 5th. International Symposium on Landslides.

Huvenne, V. A. I., P. Blondel, and J. P. Henriet (2002), Textural analyses of sidescan sonar imagery from two mound provinces in the Porcupine Seabight, *Marine Geology*, *189*, 323-341.

Imbo, Y., M. De Batist, M. Canals, M. J. Prieto, and J. Baraza (2003), The Gebra Slide: a submarine slide on the Trinity Peninsula Margin, Antarctica, *Marine Geology*, *193*, 235-252.

Irvin, B. J., S. J. Ventura, and B. K. Slater (1997), Fuzzy and isodata classification of landform elements from digital terrain data in Pleasant Valley, Wisconsin, *Geoderma*, *77*, 137-154.

Issler, D., F. V. De Blasio, A. Everhøi, T. Ilstad, H. Haflidason, P. Bryn, and R. Lien (2003), Issues in the assessment of gravity mass flow hazards in the Storegga area off the western Norwegian coast, in *Submarine Mass Movements and their Consequences*, edited by J. a. M. Locat, J., pp. 231-238, Kluwer Academic Publishers, The Netherlands.

Issler, D., F. V. De Blasio, A. Elverhøi, P. Bryn, and R. Lien (2005), Scaling behaviour of clay-rich submarine debris flows, *Marine and Petroleum Geology*, *22*, 187-194.

Iwahashi, J., S. Watanabe, and T. Furuya (2003), Mean slope-angle frequency distribution and size frequency distribution of landslide masses in Higashikubiki area, Japan, *Geomorphology*, *50*, 349-364.

Jamieson, S. S. R., H. D. Sinclair, L. A. Kirstein, and R. S. Purves (2004), Tectonic forcing of longitudinal valleys in the Himalaya: morphological analysis of the Ladakh Batholith, North India, *Geomorphology*, *58*, 49-65.

Jansen, E., and J. Sjøholm (1991), Reconstruction of glaciation over the past 6 Myr from ice-borne deposits in the Norwegian Sea, *Nature*, *349*, 600-603.

Jansen, E., Befring, S., Bugge, T., Eidvin, T., Holtedahl, H. and Sejrup, H.P. (1987), Large submarine slides on the Norwegian Continental Margin: sediments, transport and timing, *Marine Geology*, *78*, 77-107.

Jarvis, R. S., and N. J. Clifford (1990), Specific gemorphometry, in *Geomorphometric Techniques*, edited by A. S. Goudie, et al., pp. 63-70, Routledge, London.

Jenson, S. K., and J. O. Domingue (1988), Extracting topographic structure from digital elevation data for Geographic Information System Analysis, *Photogrammetric Engineering and Remote Sensing*, *54*, 1593-1600.

Jiang, M., W. Stewart, and M. Marra (1993), Segmentation of seafloor sidescan imagery using Markov random fields and neural networks, paper presented at Proceedings OCEANS, Victoria, Australia.

Johnson, A. M. (1984), Debris flows, in *Slope Instability*, edited by D. Brunsden and D. B. Prior, pp. 257-362, Wiley, Toronto.

Jordan, G. (2003), Morphometric analysis and tectonic interpretation of digital terrain data: a case study, *Earth Surface Processes and Landforms*, *28*, 807-822.

Jordan, G., B. M. L. Meijninger, D. J. J. van Hinsbergen, J. E. Meulenkamp, and P. M. van Dijk (2005), Extraction of morphotectonic features from DEMs: Development and applications for study areas in Hungary and NW Greece, *International Journal of Applied Earth Observation and Geoinformation*, *7*, 163-182.

Judd, A. G., and M. Hovland (1992), The evidence of shallow gas in marine sediments, *Continental Shelf Research*, *12*, 1081-1095.

Kadanoff, L. P., S. R. Nagel, L. Wu, and S. M. Zhou (1989), Scaling and universality in avalanches, *Physical Review A*, *39*, 6524-6533.

Kanibir, A., R. Ulusay, and O. Aydan (2006), Assessment of liquefaction and lateral spreading on the shore of Lake Sapanca during the Kocaeli (Turkey) earthquake, *Engineering Geology*, *83*, 307-331.

Katz, O., and E. Aharonov (2006), Landslides in vibrating sand box: What controls types of slope failure and frequency magnitude relations?, *Earth and Planetary Science Letters*, *247*, 280-294.

Kennett, J. P., K. G. Cannariato, I. L. Hendy, and R. J. Behl (2003), Methane Hydrates in Quaternary Climate Change: The Clathrate Gun Hypothesis, *American Geophysical Union Special Publication*, *54*, 216.

Kent, C., and J. Wong (1982), An index of littoral zone complexity and its measurement, *Canadian Journal of Fisheries and Aquatic Science*, *39*, 847-853.

Kenyon, N. H. (1987), Mass-wasting features on the continental slope of northwest Europe, *Marine Geology*, *74*, 57-77.

King, E. L., H. P. Sejrup, H. Haflidason, A. Elverhøi, and I. Aarseth (1996), Quaternary seismic stratigraphy of the North Sea Fan: glacially-fed gravity flow aprons, hemipelagic sediments and large submarine slides, *Marine Geology*, *130*, 293-315.

Klinkenberg, B. (1992), Fractals and morphometric measures: is there a relationship?, *Geomorphology*, *5*, 5-20.

Klinkenberg, B., and M. F. Goodchild (1992), The fractal properties of topography: A comparison of methods, *Earth Surface Processes and Landforms*, *17*, 217-234.

Klinkenberg, B. (1994), A review of methods used to delineate the fractal dimensions of linear features, *Mathematical Geology*, *26*, 23-46.

Koike, K., S. Nagano, and O. Michito (1995), Lineament analysis of satellite images using a segment tracing algorithm (STA), *Computers and Geosciences*, *21*, 1091-1104.

Koike, K., S. Nagano, and K. Kawaba (1998), Construction and analysis of interpreted fracture planes through combination of satellite-image derived lineaments and digital terrain elevation data, *Computers and Geosciences*, *24*, 573-584.

Krastel, S., R. B. Wynn, T. J. J. Hanebuth, R. Henrich, C. Holz, H. Meggers, H. Kulhmann, A. Georgiopoulou, and H. D. Schulz (2006), Mapping of seabed

morphology and shallow sediment structure of the Mauritania continental margin, North-west Africa: some implications for geohazard potential, *Norwegian Journal of Geology*, *86*, 163-176.

Krause, D. C., and H. W. Menard (1965), Depth distribution and bathymetric classification of some seafloor profiles, *Marine Geology*, *3*, 169-193.

Kutter, B. L., S. Gaian, K. K. Manda, and A. Balakrishnan (2004), Effects of layer thickness and density on settlement and lateral spreading, *Journal of Geotechnical and Geoenvironmental Engineering*, *130*, 603-614.

Kvalstad, T. J., L. Andersen, C. F. Forsberg, K. Berg, P. Bryn, and M. Wangen (2005a), The Storegga slide: evaluation of triggering sources and slide mechanisms, *Marine and Petroleum Geology*, *22*, 245-256.

Kvalstad, T. J., F. Nadim, A. M. Kaynia, K. H. Mokkelbost, and P. Bryn (2005b), Soil conditions and slope stability in the Ormen Lange area, *Marine and Petroleum Geology*, *22*, 299-310.

Laberg, J. S., and T. O. Vorren (2000), The Trænadjupet Slide, offshore Norway - morphology, evacuation and triggering mechanisms, *Marine Geology*, *171*, 95-114.

Laberg, J. S., T. O. Vorren, J. A. Dowdeswell, N. H. Kenyon, and J. Taylor (2000), The Andoya Slide and the Andoya Canyon, north-eastern Norwegian-Greenland Sea, *Marine Geology*, *162*, 259-275.

Laberg, J. S., T. O. Vorren, J. Mienert, P. Byrn, and R. Lien (2002a), The Trænadjupet Slide: a large slope failure affecting the continental margin of Norway 4000 years ago, *Geo-Marine Letters*, *22*, 19-24.

Laberg, J. S., T. O. Vorren, J. Mienert, D. Evans, B. Lindberg, D. Ottesen, N. H. Kenyon, and S. Henriksen (2002b), Late Quaternary palaeoenvironment and chronology in the Trænadjupet Slide area offshore Norway, *Marine Geology*, *188*, 35-60.

Lakhtakia, A., R. Messier, V. V. Varadan, and V. K. Varadan (1986), Self-similarity versus self-affinity: the Sierpinski gasket revisited, *Journal of Physics A: Mathematical and General*, *19*, L985-L989.

Lastras, G., M. Canals, and R. Urgeles (2003), Lessons from sea-floor and subsea-floor imagery of the BIG'95 debris flow scar and deposit, in *Submarine Mass*

Movements and Their Consequences, edited by J. Locat and J. Mienert, pp. 425-431, Kluwer Academic Publishers, Dordrecht.

Lastras, G., M. Canals, D. Amblas, M. Ivanov, B. Dennielou, L. Droz, A. Akhmetzhanov, and TTR-14 Leg 3 Shipboard Scientific Party (2006), Eivissa Slides, western Mediterranean sea: morphology and processes, *Geo-Marine Letters*, *26*, 225-233.

Lastras, G., Canals, M., Hughes-Clarke, J.E., Moreno, A., De Batist, M., Masson, D.G. and Cochonat, P. (2002), Seafloor imagery from the BIG'95 debris flow, western Mediterranean, *Geology*, *30*, 871-874.

Lathrop, R. G., and D. L. Peterson (1992), Identifying structural self-similarity in mountainous landscapes, *Landscape Ecology*, *6*, 233-238.

Lavallé, D., S. Lovejoy, P. Ladoy, and D. Schertzer (1993), Non-linear variability of landscape topography: Multifractal analysis and simulation, in *Fractals in Geography*, edited by N. S. N. Lam and L. De Cola, Prentice-Hall, New Jersey.

Le Bas, T. P., Mason, D.C. and Millard, N.C. (1995), TOBI image processing - the state of the art, *IEEE Journal of Oceanic Engineering*, *20*, 85-93.

Lindberg, B., J. S. Laberg, and T. O. Vorren (2004), The Nyk Slide - morphology, progression, and age of a partly buried submarine slide offshore northern Norway, *Marine Geology*, *213*, 277-289.

Lindholm, C., M. Roth, H. Bungum, and J. I. Faleide (2005), Probabilistic and deterministic seismic hazard results and influence of the sedimentary Møre Basin, NE Atlantic, *Marine and Petroleum Geology*, *22*, 149-160.

Lindsay, J. B. (2005), The Terrain Analysis System: a tool for hydro-geomorphic applications, *Hydrological Processes*, *19*, 1123-1130.

Locat, J. (2001), Instabilities along ocean margins: a geomorphological and geotechnical perspective, *Marine and Petroleum Geology*, *18*, 503-512.

Locat, J., and H. J. Lee (2002), Submarine landslides: advances and challenges, *Canadian Geotechnical Journal*, *39*, 191-212.

Locat, J., and J. Mienert (Eds.) (2003), *Submarine Mass Movements and Their Consequences*, 540 pp., Kluwer Academic Publishers, Dordrecth.

Lovejoy, S., and D. Schertzer (1995), How bright is the coast of Brittany?, 102-151 pp, Luxembourg Office for Official Publications of the European Communities.

Lu, S. Y., and Y. C. Cheng (1990), An iterative approach to seismic skeletonization, *Geophysics*, *55*, 1312-1320.

Luoto, M., and M. Seppälä (2002), Modelling the distribution of palsas in Finnish Lapland with logistic regression and GIS, *Permafrost and Periglacial Processes*, *13*, 17-28.

Lykousis, V., G. Roussakis, M. Alexandri, P. Pavlakis, and I. Papoulia (2002), Sliding and regional slope stability in active margins : North Aegean Trough (Mediterranean), *Marine Geology*, *18*, 281-298.

Malamud, B. D., G. Morein, and D. L. Turcotte (1998), Forest-fires: an example of self-organized critical behavior, *Science*, *281*, 1840-1842.

Malamud, B. D., D. L. Turcotte, F. Guzzetti, and P. Reichenbach (2004), Landslides inventories and their statistical properties, *Earth Surface Processes and Landforms*, *29*, 687-711.

Mandelbrot, B. (1967), How long is the coast of Britain? Statistical self-similarity and fractional dimension, *Science*, *156*, 636-638.

Mandelbrot, B. (1977), *Fractals: Form, Chance and Dimension*, WH Freeman, San Francisco.

Mandelbrot, B. B. (1983), *The Fractal Geometry of Nature*, W.H. Freeman, New York.

Mark, D. M. (1978), Concepts of data structure for Digital Elevation Models, paper presented at Proceedings of the American Society of Photogrammetry, Digital Terrain Models Symposium, St. Louis, Missouri, USA, May 9-11.

Mark, D. M., and P. B. Aronson (1984), Scale-dependent fractal dimensions of topographic surfaces: An empirical investigation, with applications in geomorphology and computer mapping, *Mathematical Geology*, *16*, 671-683.

Marrett, R., and R. W. Allmendinger (1992), Amount of extension on "small" faults: An example from the Viking graben, *Geology*, *20*, 47-50.

Masson, D. G., M. Canals, B. Alonso, R. Urgeles, and V. Huhnerbach (1998), The Canary Debris Flow: source area morphology and failure mechanisms, *Sedimentology*, *45*, 411-432.

Masson, D. G., C. B. Harbitz, R. B. Wynn, G. Pedersen, and F. Løvholt (2006), Submarine landslides: processes, triggers and hazard prediction, *Philosophical Transaction of the Royal Society*, *364*, 2009-2039.

Masson, D. G., R. B. Wynn, V. Hühnerbach, and A. Micallef (submitted), What controls where giant submarine landslides occur?, *Science*.

Massons, J., D. Domingo, and J. Grau (1996), Automatic classification of VIS-IR METEOSAT images, *Computers and Geosciences*, *22*, 1137-1146.

Matheron, G. (1963), Principles of geostatistics, *Economic Geology*, *58*, 1246-1266.

Matsuzaki, M., and H. Takayasu (1991), Fractal features of the earthquake phenomenon and a simple mechanical model, *Journal of Geophysical Research*, *96*, 19925-19931.

Maxwell, J. C. (1870), On contour lines and measurements of heights, *The London, Edinburgh, and Dublin Philosophical Magazine and Journal of Science*, *40*, 421-427.

McAdoo, B. G., L. F. Pratson, and D. L. Orange (2000), Submarine landslide geomorphology, US continental slope, *Marine Geology*, *169*, 103-136.

McBratney, A. B., and J. J. De Gruijter (1992), A continuum approach to soil classification by modified fuzzy *k*-means with extragrades, *Journal of Soil Science*, *43*, 159-175.

McIver, R. D. (1982), Role of naturally occurring gas hydrates in sediment transport, *American Association of Petroleum Geologists Bulletin*, *66*, 789-792.

Medler, M. J., and S. R. Yool (1998), Computer-assisted terrain stratification, *Physical Geography*, *19*, 433-443.

Micallef, A., C. Berndt, D. G. Masson, and D. A. V. Stow (2007a), A technique for the morphological characterization of submarine landscapes as exemplified by debris flows of the Storegga Slide, *Journal of Geophysical Research*, *112*, F02001.

Micallef, A., D. G. Masson, C. Berndt, and D. A. V. Stow (2007b), Morphology and mechanics of submarine spreading: A case study from the Storegga Slide, *Journal of Geophysical Research*, *112*, F03023.

Micallef, A., C. Berndt, D. G. Masson, and D. A. V. Stow (in press), Scale invariant characteristics of the Storegga Slide and implications for large-scale submarine mass movements, *Marine Geology*.

Micallef, A., D. G. Masson, C. Berndt, and D. A. V. Stow (submitted), Development and mass movement processes of the north-eastern Storegga Slide, *Marine Geology*.

Mienert, J., J. Posewang, and M. Baumann (1998), Gas hydrates along the northeastern Atlantic Margin; possible hydrate-bound margin instabilities and possible release of methane, in *Gas Hydrates: Relevance to World Margin Stability and Climate Change*, edited by J. P. Henriet and J. Mienert, pp. 275-291, Geological Society of London Special Publication.

Mienert, J., C. Berndt, J. S. Laberg, and T. O. Vorren (2002), Submarine landslides on continental margins, in *Ocean Margin Systems*, edited by G. Wefer, et al., pp. 179-193, Springer Verlag.

Mienert, J., and P. P. E. Weaver (Eds.) (2002), *European Margin Sediment Dynamics, Side-Scan Sonar and Seismic Images*, 309 pp., Springer-Verlag, Berlin.

Mienert, J., M. Vanneste, S. Bünz, K. Andreassen, H. Haflidason, and H. P. Sejrup (2005), Ocean warming and gas hydrate stability on the mid-Norwegian margin at the Storegga Slide, *Marine and Petroleum Geology*, *22*, 233-244.

Miliaresis, G. C., and D. P. Argialas (1999), Segmentation of physiographic features from the global digital elevation model/GTOPO30, *Computers and Geosciences*, *25*, 715-728.

Miliaresis, G. C. (2001), Extraction of bajadas from digital elevation models and satellite imagery, *Computers and Geosciences*, *27*, 1157-1167.

Mitchell, N. C., and M. L. Somers (1989), Quantitative backscatter measurements with a long-range side-scan, *IEEE Journal of Oceanic Engineering*, *14*, 368-374.

Mitchell, N. C., and J. E. H. Clarke (1994), Classification of seafloor geology using multibeam sonar data from the Scotian Shelf, *Marine Geology*, *121*, 143-160.

Mitchell, N. C., and R. C. Searle (1998), Fault scarp statistics at the Galapagos spreading centre from Deep Tow data, *Marine Geophysical Researches*, *20*, 183-193.

Mitchell, N. C., M. A. Tivey, and P. Gente (2000), Seafloor slopes at mid-ocean ridges from submersible observations and implications for interpreting geology from seafloor topography, *Earth and Planetary Science Letters*, *183*, 543-555.

Mitchell, N. C., D. G. Masson, A. B. Watts, M. J. R. Gee, and R. Urgeles (2002), The morphology of the submarine flanks of volcanic ocean islands: A comparative study of the Canary and Hawaiian hotspot islands, *Journal of Volcanology and Geothermal Research*, *115*, 83-107.

Mitchell, N. C. (2003), Susceptibility of mid-ocean ridge volcanic islands and seamounts to large-scale landsliding, *Journal of Geophysical Research*, *108*, 2397.

Mitchell, N. C., W. B. Dade, and D. G. Masson (2003), Erosion of the submarine flanks of the Canary Islands, *Journal of Geophysical Research*, *108*, 6002.

Mitchell, N. C. (2004), Form of submarine erosion from confluences in Atlantic USA continental slope canyons, *American Journal of Science*, *304*, 590-611.

Mitchell, N. C. (2005), Interpreting long-profiles of canyons in the USA Atlantic continental slope, *Marine Geology*, *214*, 75-99.

Mitchell, N. C. (2007), Comparing the smooth, parabolic shapes of interfluves in continental slopes to predictions of diffusion transport models, *Marine Geology*, *236*, 189-208.

Moore, I. D., and J. L. Neiber (1989), Landscape assessment of soil erosion and non-point source pollution, *Journal of Minnesota Academy of Science*, *55*, 18-24.

Moore, I. D., R. B. Grayson, and A. R. Ladson (1991), Digital terrain modelling: a review of hydrological, geomorphological and biological applications, *Hydrological Processes*, *5*, 3-30.

Moore, I. D., A. K. Turner, J. P. Wilson, S. K. Jenson, and L. E. Band (1993), GIS and land-surface-subsurface process modelling, in *Environmental Modeling with GIS*, edited by M. F. Goodchild, Parks, B.O. and Steyaert, L.T., pp. 196-230, Oxford University Press, New York.

Morse, D., J. Lowton, M. Dodson, and M. Williamson (1985), Fractal dimension of vegetation and the distribution of anthropod body lengths, *Nature*, *314*, 731-733.

Mulder, R., and P. Cochonat (1996), Classification of offshore mass movements, *Journal of Sedimentary Research*, *66*, 43-57.

Neidell, N. S. (1966), Spectral studies of marine geophysical profiles, *Geophysics*, *31*, 122-134.

Newmark, N. M. (1965), Effects of earthquakes on dams and embankments, *Géotechnique*, *15*, 139-159.

Nisbet, E. G., and D. J. W. Piper (1998), Giant submarine landslides, *Nature*, *392*, 329-330.

Nixon, M. F., and J. L. H. Grozic (2006), A simple model for submarine slope stability analysis with gas hydrates, *Norwegian Journal of Geology*, *86*, 309-316.

Noever, D. A. (1993), Himalayan sandpiles, *Physical Review E*, *47*, 724-725.

Nogami, M. (1995), Geomorphometric measures for digital elevation models, *Zeitschrift für Geomorphologie N.F. Supplementband*, *101*, 53-67.

Nouzé, H., I. Contrucci, J. P. Foucher, B. Marsset, Y. Thomas, E. Thereau, A. Normand, É. Le Drezen, S. Didailler, J. P. Regnault, S. Le Conte, S. Guidart, W. Lekens, S. Dean, and A. Throo (2004), Premiers resultants d'une etude géophysique sur le flanc nord des glissements de Storegga (Norvège), *Comptes Rendus Geoscience*, *336*, 1181-1189.

Nygård, A., H. P. Sejrup, H. Haflidason, and E. L. King (2002), Geometry and genesis of glacigenic debris flows on the North Sea Fan: TOBI imagery and deep-tow boomer evidence, *Marine Geology*, *188*, 15-33.

Nygård, A., H. Haflidason, and H. P. Sejrup (2003), Morphology of a non-glacigenic debris flow lobe in the Helland Hansen area investigated with 3D seismic data, in *European Margin Sediment Dynamics: Side-scan Sonar and Seismic Images*, edited by J. a. W. Mienert, P., pp. 63-65, Springer, London.

Nygård, A., H. P. Sejrup, H. Haflidason, and P. Bryn (2005), The glacial North Sea Fan, southern Norwegian Margin: architecture and evolution from the upper continental slope to the deep-sea basin, *Marine and Petroleum Geology*, *22*, 71-84.

O'Leary, D. W. (1991), Structure and morphology of submarine slab slides: clues to origin and behaviour, *Marine Geotechnology*, *10*, 53-69.

O'Rourke, T. D., and P. A. Lane (1989), Liquefaction hazards and their effects on buried pipelines, National Center for Earthquakes Engineering Research, Buffalo, NY.

O'Rourke, T. D., and J. W. Pease (1997), Mapping liquefiable layer thickness for seismic hazard assessment, *Journal of Geotechnical and Geoenvironmental Engineering*, *123*, 46-56.

Ohmori, H., and M. Hirano (1988), Magnitude, frequency and geomorphological significance of rocky mud flows, landcreep and the collapse of steep slopes, *Zeitschrift für Geomorphologie (Supplementband)*, *67*, 55-65.

Oliver, M. A. (1987), Geostatistics and its application to soil science, *Soil Use and Management*, *3*.

Onorati, G., and M. Poscolieri (1988), The Italian mean heights archive, a digital data set useful for thematic mapping and I units analysis, paper presented at Proceedings of the 8th Symposium EARSeL, Commission of the European Communities, Luxembourg, EURIISSIEN, Capri, Italy 17-20 May,.

Onorati, G., M. Poscolieri, R. Ventura, V. Chiarini, and U. Crucilla (1992), Analysis of the digital elevation model for Italy for quantitative geomorphology and structural geology, *Catena*, *19*, 147-178.

Ouchi, S., and M. Matsushita (1992), Measurement of self-affinity on surfaces as a trial application of fractal geometry to landform analysis, *Geomorphology*, *5*, 115-130.

Outcalt, S. I., K. M. Hinkel, and F. E. Nelson (1994), Fractal physiography?, *Geomorphology*, *11*, 91-106.

Owen, M., S. Day, and M. Maslin (2007), Late Pleistocene submarine mass movements: occurrence and causes, *Quaternary Science Reviews*, *26*, 958-978.

Parsons, A. J. (1988), *Hillslope Form*, Routeledge, London.

Pasuto, A., and M. Soldati (1996), Rock spreading, in *Landslide Recognition: Identification, Movement and Causes*, edited by R. Dikau, et al., pp. 122-136, John Wiley and Sons, Chichester.

Paull, C. K., W. Ussler, and W. P. Dillon (1991), Is the extent of glaciation limited by marine gas hydrates?, *geophysical Research Letters*, *18*, 432-434.

Paull, C. K., W. Ussler, and W. P. Dillon (2000), Potential role of gas hydrate decomposition in generating submarine slope failures, in *Natural Gas Hydrates in Oceanic and Permafrost Environments*, edited by M. D. Max, pp. 149-156, Kluwer Academic Publishers, Netherlands.

Paull, C. K., W. Ussler, and W. S. Holbrook (2007), Assessing methane release from the colossal Storegga submarine landslide, *Geophysical Research Letters*, *34*, L04601.

Pavlidis, T. (1977), *Structural pattern recognition*, 302 pp., Springer-Verlag, New York.

Pelletier, J. D., B. D. Malamud, T. Blodgett, and D. L. Turcotte (1997), Scale-invariance of soil moisture variability and its implications for the frequency-size distribution of landslides, *Engineering Geology*, *48*, 255-268.

Pelletier, J. D. (1999), Self-organization and scaling relationships of evolving river networks, *Journal of Geophysical Research*, *104*, 7359-7375.

Phillips, J. D. (1995), Self-organization and landscape evolution, *Progress in Physical Geography*, *19*, 309-321.

Pike, R. J., and W. J. Rozema (1975), Spectral analysis of landforms, *Annal of the Association of American Geographers*, *65*, 499-516.

Pike, R. J. (1988), The geometric signature: Quantifying landslide terrain types from digital elevation models, *Mathematical Geology*, *20*, 491-511.

Pike, R. J., and R. Dikau (1995), Advances in geomorphometry, *Zeitschrift für Geomorphologie*, *Supplementband 101*.

Pike, R. J. (2000), Geomorphometry - diversity in quantitative surface analysis, *Progress in Physical Geography*, *21*, 1-20.

Piper, D. J. W., P. Cochonat, and M. L. Morrison (1999), The sequence of events around the epicentre of the 1929 Grand Banks earthquake: initiation of debris flows and turbidity currents inferred from sidescan sonar, *Sedimentology*, *46*, 79-97.

Pratson, L. F., and W. B. F. Ryan (1996), Automated drainage extraction in mapping the Monterey submarine drainage system, California margin, *Marine Geophysical Researches*, *18*, 757-777.

Preston, J. M., A. C. Christney, S. F. Bloomer, and I. L. Beaudet (2001), Seabed classification of multibeam sonar images, paper presented at Proceedings of MTS/IEEE Oceans 01, Honolulu, USA.

Prior, D. B., and J. M. Coleman (1979), Submarine landslides - geometry and nomenclature, *Zeitschrift für Geomorphologie N.F.*, *23*, 415-426.

Prior, D. B., J. M. Coleman, and B. D. Bornhold (1982), Results of a known seafloor instability event, *Geo-Marine Letters*, *2*, 117-122.

Raghavan, V., K. Wadatsumi, and S. Masumuto (1993), Automatic extraction of lineament information of satellite images using digital elevation data, *Nonrenewable Resources*, *2*, 148-155.

Raghavan, V., S. Masumoto, K. Koike, and S. Nagano (1995), Automatic lineament extraction from digital images using a segment tracing and rotation transformation approach, *Computers and Geosciences*, *21*, 555-591.

Rauch, A. F., and J. R. Martin (2000), EPOLLS model for predicting average displacements on lateral spreads, *Journal of Geotechnical and Geoenvironmental Engineering*, *126*, 360-371.

Riazanoff, S., B. Cervelle, and J. Chorowicz (1988), Ridge and valley line extraction from digital terrain models, *International Journal of Remote Sensing*, *9*, 1175-1183.

Richards, J. A. (1986), *Remote Sensing Digital Image Analysis: An Introduction*, Springer-Verlag, New York.

Richards, K. S. (1982), *Rivers: Form and process in alluvial channels*, Methuen, London.

Richardson, L. F. (1961), The problem of contiguity: An appendix to "Statistics of Deadly Quarrels", *General Systems Yearbook*, *6*, 139-187.

Riedel, M., I. Novosel, G. D. Spence, R. D. Hyndman, N. R. Chapman, and T. Lewis (2006), Geophysical and geochemical signatures associated with gas hydrated-related venting in the northern Cascadia margin, *Geological Society of America Bulletin*, *118*, 23-38.

Rigon, R., A. Rinaldo, and I. Rodríguez-Iturbe (1994), On landscape self-organization *Journal of Geophysical Research*, *99*, 11971-11993.

Rigon, R., I. Rodríguez-Iturbe, A. Maritan, A. Giacometti, D. G. Tarboton, and A. Rinaldo (1996), On Hack's Law, *Water Resources Research*, *32*, 3367-3374.

Riis, F., K. Berg, J. Cartwright, T. Eidvin, and K. Hansch (2005), Formation of large crater-like evacuation structures in ooze sediments in the Norwegian Sea, *Marine and Petroleum Geology*, *22*, 257-273.

Rinaldo, A., I. Rodríguez-Iturbe, R. Rigon, E. Ijjasz-Vasquez, and R. L. Bras (1993), Self-organized fractal river networks, *Physical Review Letters*, *70*, 822-835.

Rise, L., D. Ottensen, K. Berg, and E. Lundin (2005), Large-scale development of the mid-Norwegian margin during the last 3 million years, *Marine and Petroleum Geology*, *22*, 33-44.

Roekoengen, K., L. Rise, P. Bryn, B. Fregnstad, B. Gustavsen, A. Nygärd, and J. Sættem (1995), Upper Cenozoic stratigraphy on the mid-Norwegian continental shelf, *Norsk Geografisk Tidsskrift*, *75*, 88-104.

Roering, J. J., J. W. Kirchner, and W. E. Dietrich (2005), Characterizing structural and lithological controls on deep-seated landsliding: Implications for topographic relief and landscape evolution in the Oregon Coast Range, USA, *Geological Society of America Bulletin*, *117*, 654-668.

Rohn, J., M. Resch, H. Schneider, T. M. Fernandez-Steeger, and K. Czurda (2004), Large-scale lateral spreading and related mass movements in the Northern Calcareous Alps, *Bullettin of Engineering Geology and the Environment*, *63*, 71-75.

Romstad, B. (2001), Improving relief classification with contextual merging, paper presented at 8th ScanGIS'2001 Scandinavian Research Conference on Geographical Information Science Norway.

Rouai, M., and E. B. Jaaidi (2003), Scaling properties of landslides in the Rif mountains of Morocco, *Engineering Geology*, *68*, 353-359.

Rowbotham, D. N., and D. Dudycha (1998), GIS modelling of slope stability in Phewa Tal watershed, Nepal, *Geomorphology*, *26*, 151-170.

Sagar, B. S. D., M. B. R. Murthy, C. B. Rao, and R. B. (2003), Morphological approach to extract ridge and valley connectivity networks from Digital Elevation Models, *International Journal of Remote Sensing*, *24*, 573-581.

Sapozhnikov, V. B., and E. Foufoula-Georgiou (1996), Do the current landscape evolution models show self-organized criticality?, *Water Resources Research*, *32*, 1109-1112.

Sasaki, Y., K. Tokida, H. Matsumoto, and S. Saya (1991), Shake table tests on lateral ground flow induced by soil liquefaction, 371-385 pp.

Saunders, A. D., J. G. Fitton, A. C. Kerr, M. J. Norry, and R. W. Kent (1997), The North Atlantic Igneous Province, in *Large Igneous Provinces: Continental, Oceanic and Planetary Flood Basal Volcanism*, edited by J. J. Mahoney and M. F. Coffin, pp. 45-93, American Geophysical Union.

Schertzer, D., and S. Lovejoy (Eds.) (1991), *Nonlinear Variability in Geophysics*, Kluwer Academic Publishers, Dordrecht.

Schumm, S. A., and R. W. Lichty (1965), Time, space and causality in geomorphology, *American Journal of Science*, *263*, 110-119.

Schuster, R. L. (1978), Introduction, 1-10 pp, Transport Research Board, National Research Council, Washington D.C.

Sejrup, H. P., E. Larsen, J. Landvik, E. L. King, H. Haflidason, and A. Nesje (2000), Quaternary glaciations in southern Fennoscandia: evidence from southwestern Norway and the northern North Sea region, *Quaternary Science Reviews*, *19*, 667-685.

Sejrup, H. P., H. Haflidason, B. O. Hjelstuen, A. Nygärd, P. Bryn, and R. Lien (2004), Pleistocene development of the SE Nordic Seas margin, *Marine Geology*, *213*, 169-200.

Shamoto, Y., J. M. Zhang, and M. Sato (1998), Methods for evaluating residual post-liquefaction ground settlement and horizontal displacement, *Soils and Foundations*, *2*, 69-83.

Sharp, M. K., R. Dobry, and T. Abdoun (2003), Liquefaction centrifuge modeling of sands of different permeability, *Journal of Geotechnical and Geoenvironmental Engineering*, *129*, 1083-1091.

Shary, P. A., Sharaya, L.S. and Mitusov, A.V., L. S. Sharaya, and A. V. Mitusov (2002), Fundamental quantitative methods of land surface analysis, *Geoderma*, *107*, 1-32.

Shepard, F. P. (1963), *Submarine Geology (2nd edition)*, Harper and Row, London.

Shih, T. Y., J. T. Hwang, and T. J. Tsai (1999), The fractal properties of sea surface topography derived from TOPEX/POSEIDON (1992-1996), *Computers and Geosciences*, *25*, 1051-1058.

Sloan, E. D. (Ed.) (1998), *Physical/chemical properties of gas hydrates and their application to world margin instability and climatic change* 20 pp., Geological Society Special Publication.

Smith, D. K., and P. R. Shaw (1989), Using topographic slope distributions to infer seafloor patterns, *IEEE Journal of Oceanic Engineering*, *14*, 338-347.

Solheim, A., K. Berg, C. F. Forsberg, and P. Bryn (2005a), The Storegga Slide complex: repetitive large scale sliding with similar cause and development, *Marine and Petroleum Geology*, *22*, 97-107.

Solheim, A., P. Bryn, H. P. Sejrup, J. Mienert, and K. Berg (2005b), Ormen Lange - an integrated study for the safe development of a deep-water gas field within the Storegga Slide Complex, NE Atlantic continental margin; executive summary, *Marine and Petroleum Geology*, *22*, 1-9.

Sorriso-Valvo, M., G. Gullà, L. Antronico, C. Tansi, and M. Amelio (1999), Mass-movement, geologic structure and morphologic evolution of the Pizzotto-Greci slope (Calabria, Italy), *Geomorphology*, *30*, 147-163.

Southgate, H. N., and N. K. Möller (2000), Fractal properties of coastal profile evolution at Duck, North Carolina, *Journal of Geophysical Research*, *105*, 11489-11507.

Speight, J. G. (1974), A parametric approach to landform regions, in *Progress in Geomorphology*, edited by Institute of British Geographers Special Publication, pp. 213-230, Alden Press, Oxford.

Stark, C. P., and N. Hovius (2001), The characterization of landslide size distributions, *Geophysical Research Letters*, *28*, 1091-1094.

Stark, T. D., and G. Mesri (1992), Undrained shear strength of liquefied sands for stability analysis, *Journal of Geotechnical Engineering*, *118*, 1727-1747.

Steinhaus, H. (1960), *Mathematical Snapshots*, Oxford University Press, London.

Stretch, R. C., N. C. Mitchell, and R. A. Portaro (2006), A morphometric analysis of the submarine volcanic ridge south-east of Pico Island, Azores, *Journal of Volcanology and Geothermal Research*, *156*, 35-54.

Strout, J. M., and T. I. Tjelta (2005), In situ pore pressures: What is their significance and how can they be reliably measured?, *Marine and Petroleum Geology*, *22*, 275-285.

Sugai, T., H. Ohmori, and M. Hirano (1994), Rock control on magnitude-frequency distribution of landslides, *Transactions of the Japanese Geomorphological Union*, *15*, 233-251.

Sulebak, J. R., B. Etzelmüller, and J. L. Sollid (1997), Landscape regionalization by automatic classification of landform elements, *Norsk Geografisk Tidsskrift*, *51*, 35-45.

Sulebak, J. R., L. M. Tallaksen, and B. Erichsen (2000), Estimation of areal soil moisture by use of terrain data, *Geografiska Annaler*, *82A*, 89-105.

Sultan, N., P. Cochonat, M. Canals, A. Cattaneo, B. Dennielou, H. Haflidason, J. S. Laberg, D. Long, J. Mienert, F. Trincardi, R. Urgeles, T. O. Vorren, and C. Wilson (2004a), Triggering mechanisms of slope instability processes and sediment failures on continental margins: a geotechnical approach, *Marine Geology*, *213*, 291-321.

Sultan, N., P. Cochonat, J. P. Foucher, and J. Mienert (2004b), Effect of gas hydrates melting on seafloor slope instability, *Marine Geology*, *213*, 379-401.

Summerfield, M. (1991), *Global Geomorphology: An Introduction to the Study of Landforms*, Longman, London.

Sung, Q. C., and Y. C. Chen (2004), Self-affinity dimensions of topography and its implications in morphotectonics: an example from Taiwan, *Geomorphology*, *62*, 181-198.

Székely, B., and D. Karátson (2004), DEM-based morphometry as a tool for reconstructing primary volcanic landforms: examples from the Börzsöny Mountains, Hungary, *Geomorphology*, *63*, 25-37.

Taboada, V., and R. Dobry (1998), Centrifuge modeling of earthquake-induced lateral spreading in sand, *Journal of Geotechnical and Geoenvironmental Engineering*, *120*, 1195-1206.

Tate, N. J. (1998a), Maximum entropy spectral analysis for the estimation of fractals in topography, *Earth Surface Processes and Landforms*, *23*, 1197-1217.

Tate, N. J. (1998b), Estimating the fractal dimension of synthetic topographic surfaces, *Computers and Geosciences*, *24*, 325-334.

Teide Group (1997), Morphometric interpretation of the northwest and southeast slopes of Tenerife, Canary Islands, *Journal of Geophysical Research*, *102*, 20325-20342.

ten Brink, U. S., E. L. Geist, and B. D. Andrews (2006a), Size distribution of submarine landslides and its implication to tsunami hazard in Puerto Rico, *Geophysical Research Letters*, *33*, L11307-11311.

ten Brink, U. S., E. L. Geist, P. Lynett, and B. Andrews (2006b), Submarine slides north of Puerto Rico and their tsunami potential, in *Caribbean Tsunami Hazard*, edited by A. Mercado and P. L. F. Liu.

Terzaghi, K., and R. B. Peck (1967), *Soil Mechanics in Engineering Practice*, 2nd. ed., John Wiley and Sons, New York.

Tokida, K., H. Matsumoto, T. Azuma, and I. Towhata (1993), Simplified procedure to esimate lateral ground flow by soil liquefaction, in *Soil Dynamics and Earthquake Engineering VI*, edited by A. S. Cakmak and C. A. Brebbia, Elsevier Applied Science, New York.

Towhata, I., K. Yamada, H. Kubo, and M. Kikuta (1989), Analytical solution of permanent displacement of ground caused by liquefaction, 131-144 pp.

Towhata, I., K. Tokida, Y. Tamari, H. Matsumoto, and K. Yamada (1991), Prediction of permanent lateral displacement of liquefied ground by means of variational principle, 237-251 pp.

Toyota, H., and I. Towhata (1994), Post-liquefaction ground flow in shaking table tests, 315-330 pp.

Tribe, A. (1991), Automated recognition of valley heads from digital elevation models, *Earth Surface Processes and Landforms*, *16*, 33-49.

Tricot, C. (1995), *Curves and Fractal Dimension*, Springer-Verlag, New York.

Turcotte, D. L. (1992), *Fractals and Chaos in Geology and Geophysics*, Cambridge University Press, Cambridge.

Turcotte, D. L. (1999), Self-organized criticality, *Reports on Progress in Physics*, *62*, 1377-1429.

Turcotte, D. L., B. D. Malamud, G. Morein, and W. I. Newman (1999), An inverse-cascade model for self-organized critical behavior, *Physica A*, *268*, 629-643.

Turcotte, D. L. (2001), Self-organized criticality: Does it have anything to do with criticality and is it useful?, *Nonlinear Processes in Geophysics*, *8*, 193-196.

Turcotte, D. L., B. D. Malamud, F. Guzzetti, and P. Reichenbach (2006), Self-organization, the cascade model and natural hazards, *Proceedings of the National Academy of Sciences of the United States of America*, *99*, 2530-2537.

Vågnes, E., P. Gabrielsen, and P. Haremo (1998), Late Cretaceous-Cenozoic intraplate contractional deformation at the Norwegian continental shelf: Timing, magnitude and regional implications, *Tectonophysics*, *12*, 29-46.

Van Den Eeckhaut, M., J. Poesen, G. Govers, G. Verstraeten, and A. Demoulin (2007), Characteristics of the size distribution of recent and historical landslides in a populated hilly region, *Earth and Planetary Science Letters*, *256*, 588-603.

Vanneste, M., J. Mienert, and S. Bünz (2006), The Hinlopen Slide: A giant, submarine slope failure on the northern Svalbard margin, Arctic Ocean, *Earth and Planetary Science Letters*, *245*, 373-388.

Varnes, D. J. (1978), Slope movement types and processes, 11-33 pp, National Academy of Sciences, Transportation Research Board, Special Report 176.

Vogt, P. R., and W. Y. Jung (2002), Holocene mass wasting on upper non-Polar continental slopes - due to post-Glacial ocean warming and hydrate dissociation?, *Geophysical Research Letters*, *29*, 1341.

Wadge, G., and A. M. Cross (1989), Identification and analysis of alignments of point-like features in remotely-sensed imagery: volcanic cones in Pinacate volcanic field, Mexico, *International Journal of Remote Sensing*, *10*, 455-474.

Walsh, J., D. R. Butler, and G. P. Malanson (1998), An overview of scale, pattern, process relationships in geomorphology: a remote sensing and GIS perspective, *Geomorphology*, *21*, 183-205.

Ward, A. W., T. W. Ward, A. B. McBratney, and J. J. De Gruijter (1992), *MacFuzzy: A Program for Data Analysis by Fuzzy k-Means*, CSIRO Division of Soils, Glen Osmond.

Weaver, P. P. E., R. B. Wynn, N. H. Kenyon, and J. Evans (2000), Continental margin sedimentation, with special reference to the north-east Atlantic margin, *Sedimentology*, *47*, 239-256.

Weibel, R., and J. L. DeLotto (1988), Automated terrain classification for GIS modelling, Virginia.

Wessel, P., and W. H. F. Smith (1991), Free software helps map and display data, *EOS Transactions of the American Geophysical Union*, *72*, 445-446.

Whitehouse, I. E., and G. A. Griffiths (1983), Frequency and hazard of large rock avalanches in the central Southern Alps, New Zealand, *Geology*, *11*, 331-334.

Wolinsky, M. A., and L. F. Pratson (2005), Constraints on landscape evolution from slope histograms, *Geology*, *33*, 477-480.

Wolman, M. G., and J. P. Miller (1960), Magnitude and frequency of forces in geomorphic processes, *Journal of Geology*, *68*, 54-74.

Wood, J. (1996), The Geomorphological Characterisation of Digital Elevation Models, PhD thesis, University of Leicester, Leicester.

Xia, Z. G., and K. C. Clarke (1997), Approaches to scaling of geo-spatial data, in *Scale in remote sensing and GIS*, edited by D. A. Quattrochi and M. F. Goodchild, pp. 309-360, Lewis Publishing (CRC), New York.

Xu, T., I. D. Moore, and J. C. Gallant (1993), Fractals, fractal dimensions and landscapes - a review, *Geomorphology*, *8*, 245-262.

Yasuda, S., H. Nagase, H. Kiku, and Y. Uchida (1992), The mechanism and a simplified procedure for the analysis of permanent ground displacement due to liquefaction, *Soils and Foundations*, *32*, 149-160.

Yokoi, Y., J. R. Carr, and R. J. Watters (1995), Fractal character of landslides, *Environmental and Engineering Geology*, *1*, 75-81.

Youd, T. L., and S. N. Hoose (1976), Liquefaction during 1906 San Francisco earthquake, *Journal of Geotechnical Engineering*, *12*, 425-439.

Youd, T. L., and D. M. Perkins (1987), Mapping of liquefaction severity index, *Journal of Geotechnical Engineering*, *113*, 1374-1392.

Youd, T. L., and S. J. Kiehl (1996), Distribution of ground displacements and strains induced by lateral spread during the 1964 Niigata earthquake, paper presented at 6th Japan-U.S. Workshop on Earthquake Resistant Design for Lifeline Facilities and Countermeasures Against Soil Liquefaction, September 11.

Youd, T. L., C. M. Hansen, and S. F. Bartlett (2002), Revised multilinear regression equations for prediction of lateral spread displacement, *Journal of Geotechnical and Geoenvironmental Engineering*, *128*, 1007-1017.

Zadeh, L. A. (1965), Fuzzy sets, *Information Control*, *8*, 338-353.